SLAC-R-471

INTERNATIONAL LINEAR COLLIDER TECHNICAL REVIEW COMMITTEE REPORT 1995

Stanford Linear Accelerator Center, Menlo Park, CA 94025
Work supported in part by US Department of Energy contract DE-AC03-76SF00515.

This report was produced on behalf of the International Linear Collider Technical Review Committee by the Stanford Linear Accelerator Center under contract DE-AC03-76SF00515 with the U.S. Department of Energy. Copies may be obtained by requesting SLAC-R-95-471 from the:

Stanford Linear Accelerator Center
Technical Publications Department
Stanford University
P.O. Box 4349
Stanford, CA 94309, USA
E-mail address: techpub@slac.stanford.edu

Foreword

This 1995 report of the International Linear Collider Technical Review Committee is the first attempt to gather in one document the current status of all major e^+e^- linear collider projects in the world. The report is the result of a collaborative effort of scientists from many laboratories working together over a period of about one year. A short description of the organization, origins and history of the report is given below.

To get an idea of the organization, the reader should first refer to the Table of Contents. Chapter 1 is an introduction and general overview of the respective 500 GeV c.m. energy machines. In contrast, Chapter 2, cutting across individual machine boundaries, gives a comparative description and discussion of all the major machine sub-systems as well as particle physics experimentation, showing where these subjects stand today and what additional work needs to be done in the next few years to reach the point where complete design reports can be prepared. Chapter 3 describes the various paths to energy upgrades, and other experimental options ($\gamma\gamma$, e^-e^-, etc.). Chapter 4 gives a short status report of the machine experiments and test facilities being built in the world. Chapter 5 outlines current and other possible areas of collaboration and finally, Chapter 6 summarizes our principal conclusions.

The reader should note that the idea of generating this report was not born overnight but rather, was the result of a protracted series of events and observations. To quote David Burke from SLAC,

> *"The accelerators and colliders needed to explore particle physics at high energies have become increasingly expensive and complex. The successful integration of the resources and efforts of scientists from differing countries in the completion of the HERA electron-proton collider and ongoing international cooperation in the design and building of accelerators at CERN have demonstrated the feasibility of international collaborations to realize the instruments required to explore further the high energy physics frontier. In contrast, the failure of the SSC has emphasized the necessity of such collaborations.*
>
> *The LHC, now approved for construction at CERN, has garnered considerable interest amongst scientists from all over the globe, and the project is moving forward to perhaps be the first scientific instrument built by a truly world-wide collaboration. There is also great interest in the world in the future of electron-positron colliders. The successful use of the SLC to study the physics of the Z^0 has demonstrated the feasibility of linear colliders as tools for exploration of the TeV energy scale, and research at many laboratories around the world is directed at several different approaches to the design and construction of such a collider. In anticipation of the need for international collaboration to realize a TeV-scale linear collider, these laboratories have joined together in the Interlaboratory Collaboration for R&D on TeV-scale Linear Colliders. This Collaboration is intended to provide a more formal arrangement for the discussion and evaluation of the various technical options for future linear colliders, and to set a point of reference for those laboratories wishing to participate in the research on related accelerator physics and technologies."*

A first and preliminary organizational meeting of the Interlaboratory Collaboration was held on October 18, 1993, during LC93 at SLAC. At that time, DESY, KEK and SLAC presented drafts of proposals for Memoranda of Understanding, and various discussions took place on how this international collaboration might be orchestrated. The first official meeting of the Collaboration Council was held in June 1994 at EPAC 94 in London. A membership list of the Council is shown on page *iv*. The Council, as one of its first missions, decided to create a Technical Review Committee and asked its members to prepare a report, in accordance with the following charge:

> *"The Technical Review Committee is to consider the goal to design, build, and operate a TeV-scale linear electron-positron collider capable of satisfying the need to explore the particle physics of this energy range. Specifically, the Committee is to examine accelerator designs and technologies suitable for a collider that will initially have center-of-mass energy of 500 GeV and luminosity in excess of $10^{33} cm^{-2} s^{-1}$, and be built so that it can be expanded in energy and luminosity to reach 1 TeV center-of-mass energy with luminosity of $10^{34} cm^{-2} s^{-1}$. The Committee should consider construction and operation of both the initial facility and the upgrade path to 1 TeV. The Committee is also asked to comment on the potential of technologies to reach higher energies and luminosities, and to provide alternative physics capabilities, for example gamma-gamma collisions.*
>
> *The Technical Review Committee is to identify the accelerator physics and technological requirements for each approach to provide particle physics opportunities at the energy and luminosity goals stated above. The report of the Committee should contain a brief commentary of the status of and expected progress toward understanding and achieving the most important of these requirements. The Committee should attempt to identify areas of possible further collaboration in the world-wide linear collider R&D program.*
>
> *A draft of the Committee report should be submitted to the Collaboration Council shortly after the LC95 meeting scheduled for March 1995 in Japan."*

The membership of the Technical Review Committee was gathered gradually via telephone and e-mail during the summer and fall of 1994. Following some rather lengthy discussions on both content and format, and on how best to communicate with all its members, the committee began substantive work in November 1994. Partial encounters and meetings took place in winter 1995, and some first drafts were delivered at LC95, in March 1995 in Tsukuba. At that point, we collectively realized that much coordination and editing work was left to do. Some fundamental disagreements on content were cleared up and the final table of contents could then be firmed up. We agreed that the body of the report would be focused on the 500 GeV c.m. machines and that upgrades to 1 TeV c.m. and other options ($e^-e^-, \gamma\gamma, e^-\gamma$) would be treated in a separate chapter. We also agreed that in this first report we would stay away from cost estimates and any discussions of specific sites. Wherever possible, lists of references would be avoided.

A first progress report was given at the second meeting of the Collaboration Council at PAC95 in Dallas on May 2, 1995. A second progress report was given on September 8, 1995, at the LCWS95 held in Morioka-Appi, Iwate, Japan. The current structure and membership list of the Technical Review Committee is shown on page *v*.

While the material which the reader will find here is the result of a considerable amount of work, we are collectively aware that much remains to be done and improved. The designs are all progressing nicely but they are still in a state of flux. While this state of affairs may give the impression of an unfinished symphony, it also testifies to the competitiveness and vitality of the field.

G.A. Loew
Chairman

T. Weiland
Secretary

December 1995

Acknowledgements

As pointed out above, the scientists who put this report together met a few times in groups or sub-groups, in various places in the world. However, most of the exchanges, discussions, arguments and cross-checks took place via innumerable e-mail messages. All chapters, not without some difficulty, were transmitted around the world in LaTeX. The entire communications process would have been impossible without the dedication and enormous effort made by Eleanor Mitchell at SLAC who lived through and helped us with the preparation of the entire report. She was also assisted at SLAC by Scott Berg from the Accelerator Theory and Special Projects Department, and Evelyn Eldridge-Diaz and Terry Anderson from the Publications Department.

Interlaboratory Collaboration for R&D Towards TeV-scale Electron-Positron Linear Colliders

July 1995

Asia

IHEP	S. Wang	E-Mail: WANGSHbepc2.ihep.ac.cn
KEK	K. Takata	E-Mail: TAKATA@jpnkekvx
POSTECH	W. Namkung	E-Mail: NAMKUNG@vision.postech.ac.kr

FSU

BINP	V. Balakin	E-Mail: BALAKIN@VLEPP.Serpukhov.su
JINR	A. Sissakian	E-Mail: SISAKIAN@jinr.dubna.su

Europe

Aachen	K. Lubelsmeyer	E-Mail: LUEBELSMEYER@acphyz.hep.rwth-aachen.de
Berlin	H. Henke	E-Mail: HENKE@tu-berlin.de
CEA	J. Haissinski	E-Mail: JHAISS@saclay.cea.fr
CERN	K. Hübner	E-Mail: HUBNER@cernvm.cern.ch
Darmstadt	T. Weiland	E-Mail: DD2E@temf00.temf.e-technik.th-darmstadt.de
DESY	B. Wiik	E-Mail: F35BLU@dhhdesy3
Frankfurt	H. Klein	E-Mail: UF14@ddags13
Frascati	S. Tazzari	E-Mail: TAZZARI@irmlnf
LAL (Orsay)	J. Lefrancois	E-Mail: LEFRANCOIS@lalcls.cern.ch
SEFT	R. Orava	E-Mail: SEFT@phcu.helsinki.fi

America

BNL	R. Palmer	E-Mail: PALMER@bnl
CEBAF	Ch. Leeman	E-Mail: SOLTYS@cebaf.gov
Cornell	H. Padamsee	E-Mail: HSP@cesr10.lns.cornell.edu
Fermilab	S. Holmes	E-Mail: HOLMES@fnal
LBNL	W. Barletta	E-Mail: BARLETTA@lbl.gov
Maryland	A. Dragt	E-Mail: DRAGT@quark.umd.edu
SLAC	D. Burke	E-Mail: DAVEB@slac.stanford.edu
UCLA	C. Pellegrini	E-Mail: PELLEGRINI@uclahep

Ex officio

ICFA	J. Peoples	E-Mail: PEOP@fnalv.fnal.gov

Structure and Members of the Technical Review Committee

Steering Group:

G. Loew, Chairman
T. Weiland, Secretariat

Reading Committee:

B. Aune, V. Balakin, H. Edwards, K. Hübner, E. Paterson,
A. Sessler, K. Takata, G. Vignola, G. Voss, B. Wiik

Working Groups:

1) Injection Systems and Pre-Accelerators

M. Yoshioka, Chair
A. Mikhailichenko, Deputy Chair
H. Braun, J.P. Delahaye (CLIC), K. Flöttmann, J. Frisch, R. Miller, C. Pagani, L. Rinolfi,
J. Rosenzweig, H. Tang, C. Travier, D.A. Yeremian

2) Damping and Compression Systems

J. Rossbach (SBLC), Chair
J. Urakawa,Deputy Chair
S. Chattopadyhay, A. Mikhailichenko, J.P. Potier, T. Raubenheimer

3) Linac Technology

P. Wilson (NLC),Chair
D. Proch, Deputy Chair
N. Holtkamp, Deputy Chair
G. Caryotakis, T. Higo, H. Mizuno, W. Namkung, H. Padamsee, R. Palmer,
N. Solyak (VLEPP), G. Westenskow, I. Wilson

4) Beam Dynamics

K. Yokoya (JLC), Chair
A. Mosnier, Deputy Chair
G. Guignard, R. Ruth, R. Wanzenberg

5) Beam Delivery

R. Brinkmann (TESLA),Chair
V. Telnov, Deputy Chair
A. Dragt, J. Irwin, O. Napoly, K. Oide, A. Sery, B. Zotter

6) Experimentation

R. Settles, Chair
T. Markiewicz, Deputy Chair
S. Bertolucci, S. Kawabata, D. Miller, R. Orava, F. Richard, T. Tauchi, A. Wagner

Contents

LIST OF FIGURES

LIST OF TABLES

1 INTRODUCTION and GENERAL OVERVIEW of 500 GeV c.m. MACHINES

The purpose of this first chapter is to provide the reader with an overview of all the major e^+e^- linear colliders currently under consideration in the world at a center-of-mass energy of 500 GeV with a luminosity of at least $10^{33}\ cm^{-2}\ s^{-1}$. These colliders include TESLA (coordinated by DESY), the S-band Linear Collider or SBLC (also coordinated by DESY), the JLC with its S-band, C-band and X-band variations for the main linac (coordinated by KEK), the NLC (coordinated by SLAC), VLEPP (coordinated by BINP) and CLIC (coordinated by CERN). The term "coordinated" is used here because all these projects, in one way or another, are collaborative efforts (see Chapter 5).

Information on these projects is first presented in tabular form for ease of comparison. Table 1.1 summarizes the overall and final focus parameters and Table 1.2 summarizes the pre-linac, damping ring and main-linac parameters. All the symbols, nomenclature, etc. follow the standard definitions used in current accelerator physics literature. The nominal luminosity, for the sake of uniformity, is simply defined as $N^2/4\pi\,\sigma_x^*\sigma_y^*$ multiplied by the number of crossings per second, where N is the number of particles per bunch and starred symbols are those measured at the final focus. For the nominal luminosity calculation, collisions are assumed to be head-on, and hour-glass and pinch effect are neglected. The actual luminosity includes all the effects relevant to each specific design. The background numbers appearing at the bottom of Table 1.1 have all been calculated by P. Chen at SLAC. They differ somewhat from those appearing in Section 2.6 because of slightly different methodologies and assumptions. In both Tables 1.1 and 1.2, the unloaded gradient is the average gradient per section and the loaded gradient includes the effect of single-bunch and multibunch beam loading, assuming the bunches ride on crest. The main linac active length is defined as that length which is needed to reach 500 GeV in the center-of- mass, including off-crest running and a reserve for klystron population management. The total linac length includes the extra length needed for beam line components, cryostats, etc. The total length for "beam delivery" is the distance between the ends of the e^- and e^+ main linacs, which is required for collimation, bends and final foci. The total AC power needed to make rf power for the main linacs does not include power for water cooling, magnets and instruments. All other parameters are listed and discussed in subsequent chapters.

General descriptions with machine and tunnel layouts are given in sections 1.1 through 1.6 below. The material used for these descriptions has been supplied by:

R. Brinkmann (TESLA)
J. Rossbach/N. Holtkamp (SBLC)
K. Yokoya (JLC)
T. Raubenheimer (NLC)
N. Solyak (VLEPP)
J.P. Delahaye (CLIC)

The reader should bear in mind that all these machine designs are in a dynamic state of evolution and that ideas and parameters change frequently. Thus, it is likely that in the next few months and certainly years, many changes, improvements and refinements will appear.

This state of affairs is the inevitable result of active, productive and competitive R&D. Upgrades to center-of-mass energies higher than 500 GeV and other physics opportunities are described in Chapter 3.

Table 1.1

Linear Colliders: Overall and Final Focus Parameters – 500 GeV (c.m.)

	TESLA*	SBLC	JLC (S)	JLC (C)	JLC (X)	NLC	VLEPP	CLIC
Initial energy (c.of .m.) (GeV)	500	500	500	500	500	500	500	500
RF frequency of main linac (GHz)	1.3	3	2.8	5.7	11.4	11.4	14	30
Nominal Luminosity (10^{33} cm^{-2}s^{-2})†	2.6	2.2	5.2	7.3	5.1	5.3	12.3	0.7-3.4
Actual luminosity (10^{33} cm^{-2}s^{-2})†	6.1	3.75	4.3	6.1	5.2	7.1	9.3	1.07-4.8
Linac repetition rate (Hz)	10	50	50	100	150	180	300	2530-1210
No. of particles/bunch at IP (10^{10})	5.15	2.9	1.44	1.0	.63	.65	20	.8
No. of bunches/pulse	800	125	50	72	85	90	1	1-10
Bunch separation (nsec)	1000	16.0	5.6	2.8	1.4	1.4	–	.67
Beam power/beam (MW)	16.5	7.26	1.3	2.9	3.2	4.2	2.4	.8-3.9
Damping ring energy (GeV)	4.0	3.15	2.0	2.0	2.0	2.0	3.0	2.15
Main linac gradient, unloaded/loaded††(MV/m)	25/25	21/17	31/–	40/32	73/58	50/37	100/91	80/78
Total two-linac length (km)	29	33	22.1	18.8	10.4	15.6	7	8.8
Total beam delivery length (km)	3	3	3.6	3.6	3.6	4.4	3	2.4
$\gamma\epsilon_x/\gamma\epsilon_y$ (m-$rad \times 10^{-8}$)	2000/100	1000/50	330/4.8	330/4.8	330/4.8	500/5	2000/7.5	300/15
β_x^*/β_y^* (mm)	25/2	22/0.8	10/0.1	10/0.1	10/0.1	10/0.1	100/0.1	10/0.18
σ_x^*/σ_y^* (nm) before pinch	1000/64	670/28	260/3.0	260/3.0	260/3.0	320/3.2	2000/4	247/7.4
σ_z^* (μm)	1000	500	120	120	90	100	750	200
Crossing Angle at IP (mrad)	0	3	6.4	6.0	6.1	20	6	1
Disruptions D_x/D_y	0.56/8.7	.36/8.5	.29/25	.20/18	.096/8.3	.07/7.3	.4/215	0.29/9.8
H_D	2.3	1.8	1.6	1.4	1.4	1.34	2.0	1.42
Upsilon sub-zero	.02	.037	.20	.14	.12	.089	.059	0.07
Upsilon effective	.03	.042	.22	.144	.12	.090	.074	.075
δ_B (%)	3.3	3.2	12.7	6.5	3.5	2.4	13.3	3.6
n_γ (no. of γ's per e)	2.7	1.9	2.2	1.5	.94	.8	5.0	1.35
N_{pairs}(p_T^{min}=20 MeV/c,θ_{min}=0.15)	19.0	8.8	31.6	10.3	2.9	2.0	1700	3.0
$N_{hadrons}$/crossing	0.17	0.10	0.98	0.23	0.05	0.03	45.9	0.05
$N_{jets} \times 10^{-2}$ (p_T^{min}=3.2 GeV/c)	0.16	0.14	3.4	0.66	0.14	0.08	56.4	0.10

* Refer to Section 1.1 regarding possible TESLA parameter changes.

† For the sake of uniformity, the nominal luminosity is simply defined as $N^2/4\pi\,\sigma_x^*\,\sigma_y^*$ times the number of crossings per second, and in all cases assumes head-on collisions, no hour-glass effect and no pinch. The actual luminosity incorporates all these effects, including crossing angle where applicable. NLC calculations assume crab-crossing.

†† The loaded gradient includes the effect of single-bunch (all modes) and multibunch beam loading, assuming that the bunches ride on crest. Beam loading is based on bunch charges in the linacs, which are slightly higher than at the IP.

Table 1.2
Pre-linacs, Damping Rings and Main Linac Parameters – 500 GeV (c.m.)

	TESLA*	SBLC	JLC (S)	JLC (C)	JLC (X)	NLC	VLEPP	CLIC
Pre-linacs								
First stage $e\pm$ energy (GeV)	4	3.15	1.98	1.98	1.98	2	3.0	2.15
Second stage $e\pm$ energy (GeV)	-	-	-	20	10-20	10	–	9.0
Beam energy to make e^+ (GeV)	250	250	10	10	10	3-6	150	2.15
Damping Rings								
e^+ pre-damping ring energy (GeV)	-	-	1.98	1.98	1.98	2.0	–	2.15
$e\pm$ damping ring energy (GeV)	4	3.15	1.98	1.98	1.98	2.0	3.0	2.15
Ring circumference (m)	20,000	650	222	321	277	223	160	283
Damping times (ms) (τ_x/τ_y)	20/20	3.8/3.8	6.1/8.0	3.5/4.3	4.0/5.2	4.1/4.6	1.8/2.9	10.5/10.5
Number of bunches per ring	800	125	100	288	340	360	3	48×10
Bunch length (mm)	10	3.6	4.8	5.0	5.0	4.1	9.8	1.8
Extr. beam emittance, $\gamma\epsilon_x/\gamma\epsilon_y$ 10^{-6}	20/1	10/.5	3/0.03	3/0.03	3/0.03	2.5/0.03	45.5/0.45	2.5/0.04
Main Linacs								
RF frequency (GHz)	1.3	3.0	2.8	5.7	11.4	11.4	14	30
Unloaded/loaded†† gradient (MV/m)	25/25	21/17	31/–	40/32	73/58	50/37	100/91	80/78
Active two-linac length (km)	20	30.2	19.8	15.7	8.7	14.2	5.8	6.3
Total two-linac length (km)	29	33	22.1	18.8	10.4	15.6	7.0	8.8
Total number of klystrons	604	2517	2560	4356	3320	3936	1400	2
Total number of modulators	604	2517	2560	2178	3320	1970	140	NA
Klystron peak power (MW)	8	150	135	48	135	50	150	NA
Klystron repetition rate (Hz)	10	50	50	100	150	180	300	2530/1210
Klystron pulse length (μsec)	1315	2.8	4.5	2.4	.5	1.2	.5	.0116/.00176
Pulse compression ratio	-	-	3.75	5	2	5	4.55	-
Pulse compression gain	-	-	~2	3.5	1.96	3.83	3.2	-
RF pulse length at linac (μsec)	1315	2.8	1.2	.480	.230	.240	.110	.0116/.00176
Number of sections	19328	5034	5120	8712	6640	7872	5600	22466
Section length (m)	1.04	6	3.6	1.8	1.31	1.8	1.0	0.280
a/λ (range if applicable)	.15	.16/.11	.14/.10	.16/.12	.20/.14	.22/.15	.14	.20
Total AC power to make rf (MW)	164	139	118	139	114	103	57	100
Wall plug → beam efficiency (%)	20	10.4	3.0	4.6	5.6	8.2	8.4	1.6/7.8

* Refer to Section 1.1 regarding possible TESLA parameter changes.

†† The loaded gradient includes the effect of single-bunch (all modes) and multibunch beam loading, assuming that the bunches ride on crest. Beam loading is based on bunch charges in the linacs, which are slightly higher than at the IP.

1.1 TESLA

The TESLA approach towards a next generation linear collider of 500 GeV center-of-mass energy uses superconducting accelerating structures operating at a frequency of 1.3 GHz and a gradient of 25 MV/m. To realize such a large scale superconducting rf system, to operate it stably at the required gradient and to build it within reasonable cost limits represents a considerable technological challenge. It is the goal of the TESLA Test Facility (TTF) to demonstrate that this challenge can be met. The TTF is presently under construction at DESY and full tests with beam will be performed by 1997. The justification for this technological effort is given by the following essential advantages of the TESLA approach:

- The comparatively low rf frequency results in small transverse and longitudinal wake-fields in the accelerating structures, enabling one to loosen the tolerances required for emittance preservation in the linac.

- The high rf-to-beam power transfer efficiency of the superconducting rf system allows for a high average beam power, while keeping the AC power consumption within acceptable limits. A high luminosity can thus be achieved without the need for an excessively small spot size at the IP, again contributing to looser tolerances.

- In contrast to conventional approaches, the klystron peak power is low and the beam in TESLA is accelerated in very long rf pulses ($800\mu s$). This feature leads to a large spacing between bunches ($\Delta t_b = 1\mu s$) which is advantageous from the point of view of experimentation because it makes it easy to resolve individual bunch crossings. The bunch spacing is also large enough to use the first in the train of 800 bunches as a pilot bunch, measure its orbit deviation and correct for the other 799 bunches with a kicker. The problem of pulse-to-pulse orbit vibrations is therefore practically eliminated for TESLA. Furthermore, coupled bunch oscillations driven by transverse HOM's in the accelerating structures are very effectively suppressed with the large bunch spacing.

Given below is a brief description of the overall TESLA layout, as sketched in Fig.1.1. For the electron part of the injection system, two options are being considered. With the relatively large beam emittance of TESLA, it may be possible to generate the required beam quality directly from a laser-driven rf gun. In this case, a damping ring for the electron beam would not be required. The alternative solution (and also a possible upgrade of the machine towards smaller emittance) would require a damping ring similar to the one inevitably required for the positron injection system (although with somewhat relaxed requirements for the damping time and injection acceptance).

The positron part of the injection system has to provide an average charge of 4×10^{13} e^+ per pulse, which does not seem feasible with a conventional source. Instead, the alternative that is being considered is to produce the positrons from γ-conversion in a thin target. The photons are produced by passing the spent e^- beam after the interaction through a wiggler. The captured positrons are pre-accelerated to 4 GeV and injected into the damping ring. The ring has to accommodate the bunch train in a compressed mode, i.e. reduced bunch spacing. Two options for the damping ring are being investigated. One version uses a 20 km-long dogbone-shaped ring which, except for the short arcs, is almost entirely housed in the same tunnel as the main linac, thus eliminating the need for a costly long additional

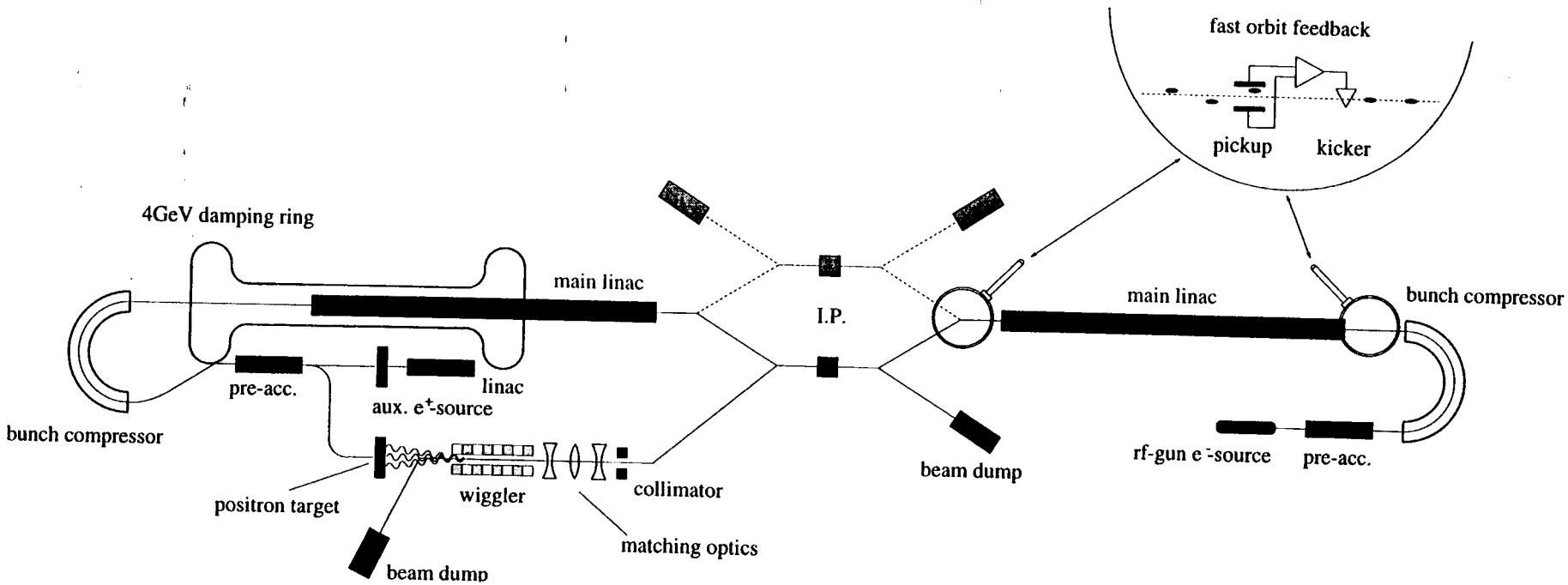

Fig.1.1 Overall TESLA layout.

tunnel. The second version assumes that TESLA is to be built at a site where a ring tunnel of sufficient size (TEVATRON, HERA) is already available. Whereas this version is preferable from the cost point of view (in particular if there is already an electron ring suitable as a damping ring, i.e. HERA-e), the dogbone, being about three times longer, has the advantage of relaxed requirements concerning coherent multibunch instability suppression and injection/extraction hardware. For both approaches, a single bunch compressor will be sufficient to yield the design bunch length of 1mm. In order to be able to commission the e^+ linac without having to run the e^- linac, an auxiliary low-intensity e^+ source is planned.

The basic module of the TESLA main linac consists of an 8 MW klystron powering 32 1m-long 9-cell superconducting cavities (see cryostat layout in Fig. 1.2). Assuming an average packing factor of 0.70, the total length of the two main linacs amounts to 29 km (including 2% reserve for energy management). A sketch of the linac tunnel layout is shown in Fig.1.3. The AC power specified in the parameter table to produce the rf power includes a 9.5 MW reserve for the control of phase errors caused by mechanical vibrations of the cavities. Beam focussing in the linac is achieved by superconducting quadrupoles so that no significant additional power for their excitation is needed.

The beam transport between the linac and the IP (the so-called beam delivery section) consists of collimation, beamline separation (for two separate IP's) and final focus sections. In the interaction region no crossing angle is needed since the beams can be separated well before the first parasitic collision (150m from the IP) by an electrostatic separator. This makes it possible to use large aperture superconducting quads for the final doublet before the IP. One consequence of this is that collimation requirements upstream are very relaxed. Backgrounds from muons originating at the collimators are unlikely to be a problem for TESLA. An additional advantage of the large bunch spacing is the possibility of deflecting the beam into a dump in case the loss rate at the collimator exceeds a tolerable limit.

The TESLA interaction parameters are chosen for good energy resolution and low background in the experiment. The beamstrahlung photons and the disrupted beams are safely extracted from the IR through the large aperture superconducting quads. This design has the additional advantage that a compensating solenoid to shield the quads from the detector field is not required.

Note on TESLA Parameters

Given the small wakefield effects in the TESLA linac, the design value for the vertical beam emittance is very conservative. The TESLA linac is therefore ideally suited to deliver a smaller ϵ_y. The TESLA collaboration is currently investigating the implications of parameter changes towards a smaller vertical emittance for the 500 GeV c.m. machine. This opens up the potential of increasing the luminosity or, alternatively, decreasing the operating cost by reducing the repetition rate at constant luminosity. With a moderate reduction of ϵ_y by a factor of 4 and a repetition rate of 5 instead of 10 Hz, TESLA can deliver the same luminosity as quoted in Table 1.1 at a two-linac AC power of 88 MW (+ 5 MW for 10% control reserve). While the vertical spot size at the IP in this case decreases to 19 nm, disruption and beamstrahlung parameters are kept essentially constant for this new parameter set. No concurrent changes need to be made in the design of the linac components (i.e. number of klystrons, klystron power and rf pulse length).

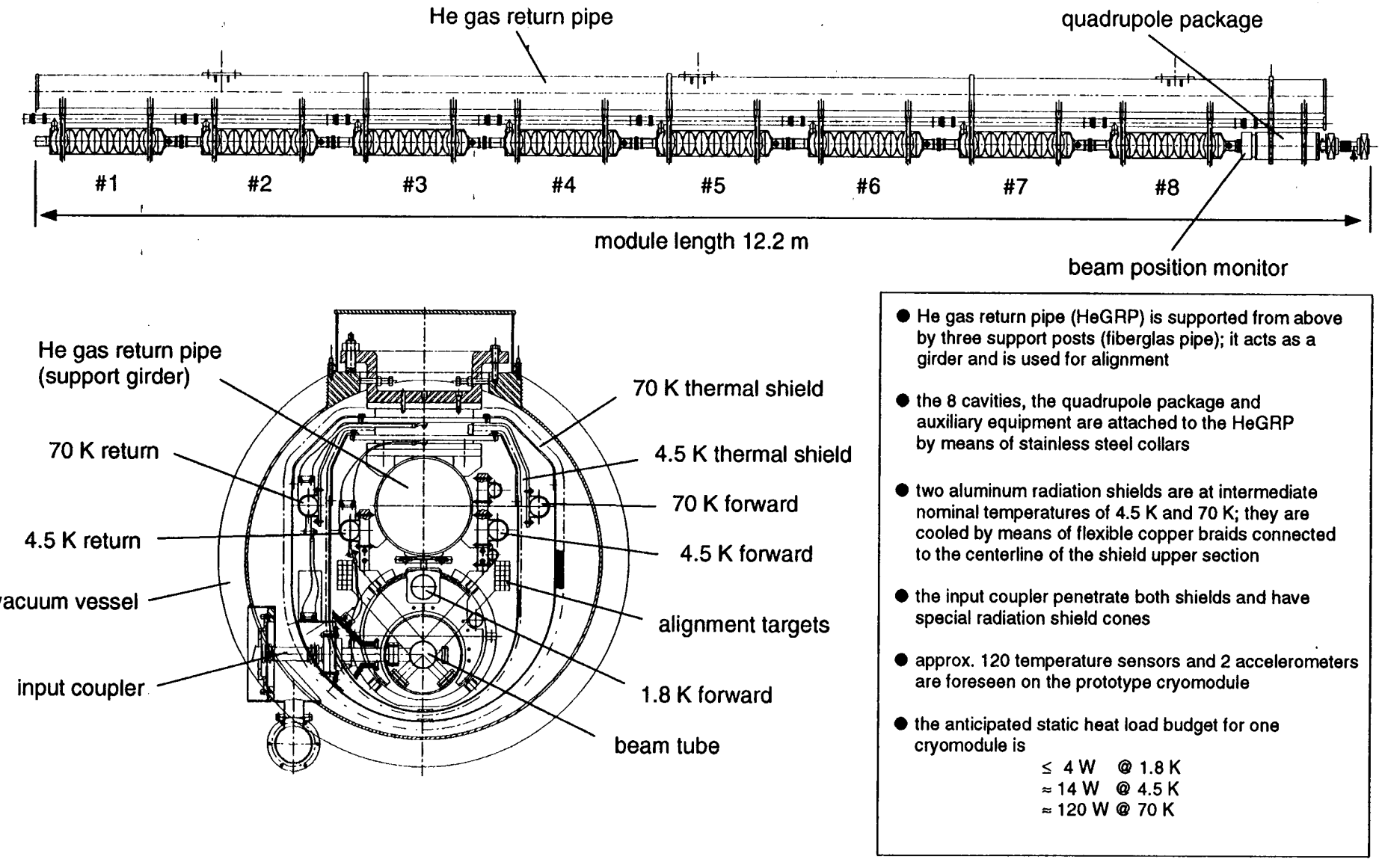

Fig.1.2 Basic module of the TESLA main linac.

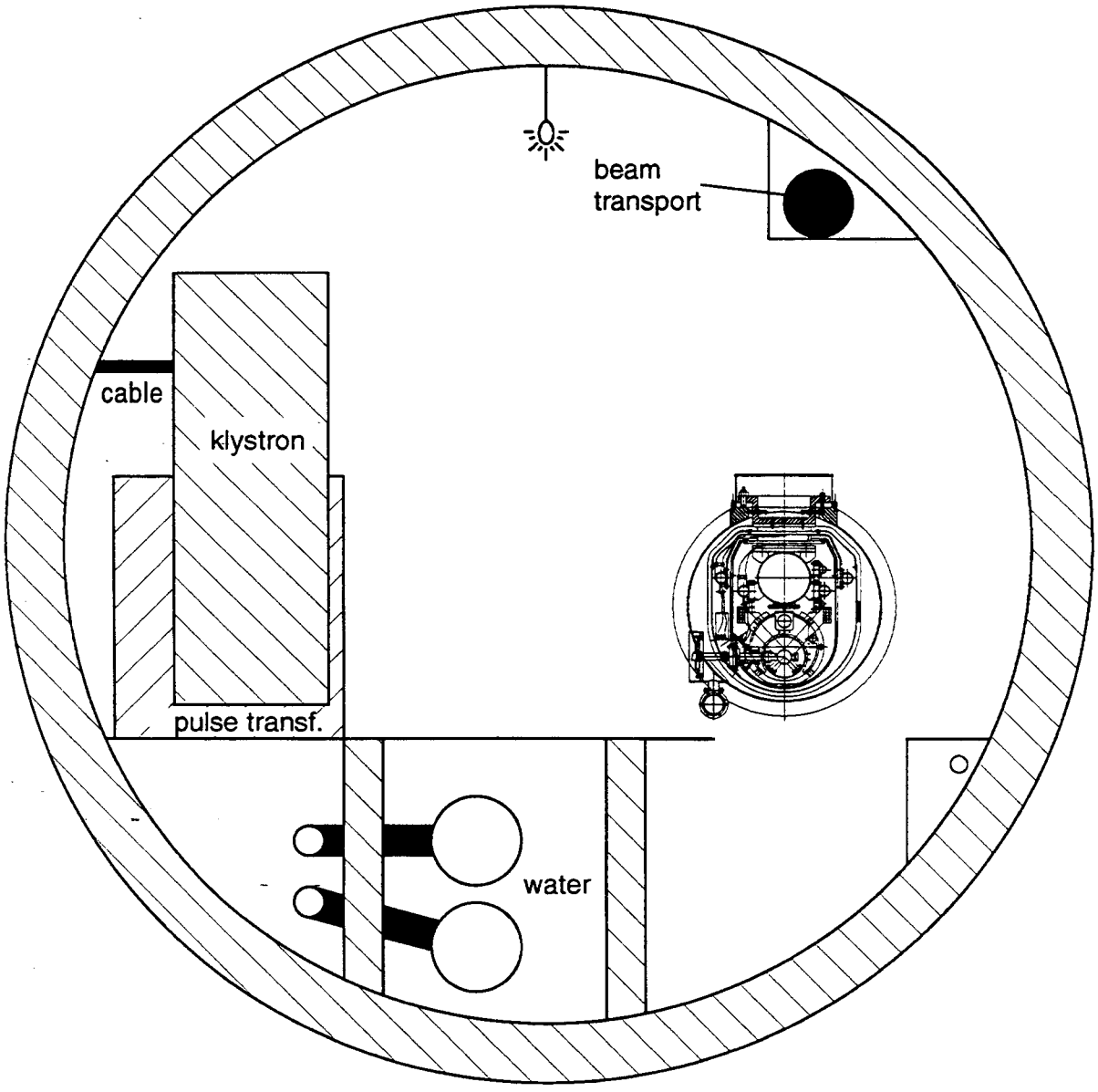

Fig.1.3 TESLA cross-section at mid-point of a cryostat.

1.2 SBLC

The S-band Linear Collider (SBLC) approach is based on the widespread experience with 3 GHz technology. Compared to all other designs, it benefits most directly from the S-band technology, beam diagnostics tools and tuning procedures developed at the only existing linear collider, namely the SLC at Stanford (USA), and therefore seems to be a natural extension of that machine. In addition, comparatively small wakefields and looser tolerances as well as high power conversion efficiency make the SBLC design a feasible choice.

The relatively low rf frequency and a moderate accelerating gradient allow for a high overall efficiency by accelerating a 2.0 μs long bunch train in a 2.8 μs long rf pulse with a repetition rate of only 50 Hz. The proposed 3 GHz (S-band) accelerating structures are conventional traveling-wave sections with a loaded gradient of 17 MV/m, considered to be a good choice to balance estimated linear costs and rf power costs.

The overall SBLC machine layout is shown in Fig 1.4. The electron part of the injection system starts with a standard thermionic gun, or optionally a polarized laser-driven gun. The desired small emittance is produced in a 650 m circumference, 3.15 GeV damping ring which stores one bunch train per pulse. Longitudinal bunch compression can be achieved in a one-stage system since a compression factor of only about 8 is required.

The positron part of the injection system has to provide 3.6×10^{12} e^+ per pulse, which does not seem feasible with a conventional positron source using known technology. The alternative being considered is to produce the positrons from a γ-beam converted in a thin target. The photons are produced by passing the spent e^- beam after the interaction point through a wiggler. The captured positrons are pre-accelerated to 3.15 GeV and injected into the e^+ damping ring which is very similar to the e^- damping ring. In order to be able to commission the positron linac without having to run the entire e^- linac, an auxiliary low-intensity e^+ source is planned.

The basic module of the SBLC linac consists of a 150 MW klystron which directly feeds two 6 m-long accelerating structures. A pulse compression scheme is not considered necessary for the 500 GeV c.m. design; it will be added later to increase the machine energy without increasing the machine length but by shortening the effective rf pulse. The klystron is powered by a 2.8 μs pulse length modulator. In total, 2518 of these basic modules are needed for the two 250 GeV linacs, including overhead for klystron population management and off-crest running for BNS damping. Assuming a packing factor of 90 % and the above overhead, the total length of the two linacs amounts to 33 km. To overcome the multibunch instability, a scheme for the suppression of HOM modes has been proposed recently, which reduces the quality factor of the higher order modes by approximately a factor of 8. At the same time the fundamental mode dissipation is only increased by less than 5 %. This is done by coating the lips of some of the accelerator irises with a high loss material. In addition, pulse-to-pulse orbit stabilization of the multibunch train is foreseen at different positions along the linac to increase the beam breakup threshold even further. Measuring quadrupole vibrations and using feedback to stabilize their position has been tested and proven to be possible, even in a noise-contaminated environment. It is assumed that all linac components are installed in one tunnel and that access to the tunnel during machine operation is possible for klystron replacement and general maintenance by having sufficient shielding between the accelerator beam line and the klystrons (see Fig. 1.5).

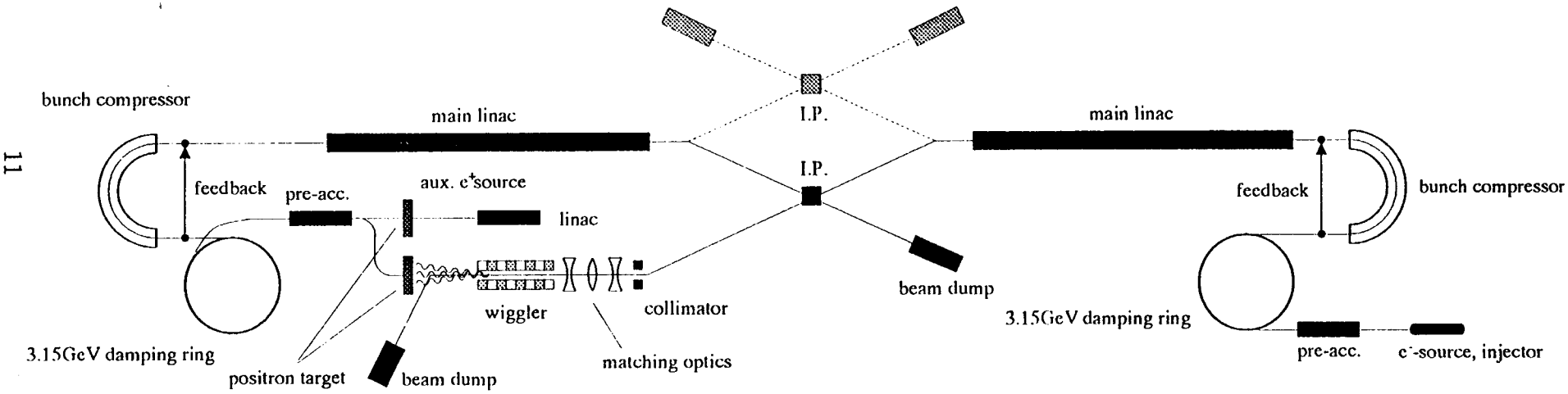

Fig.1.4 Overall SBLC machine layout.

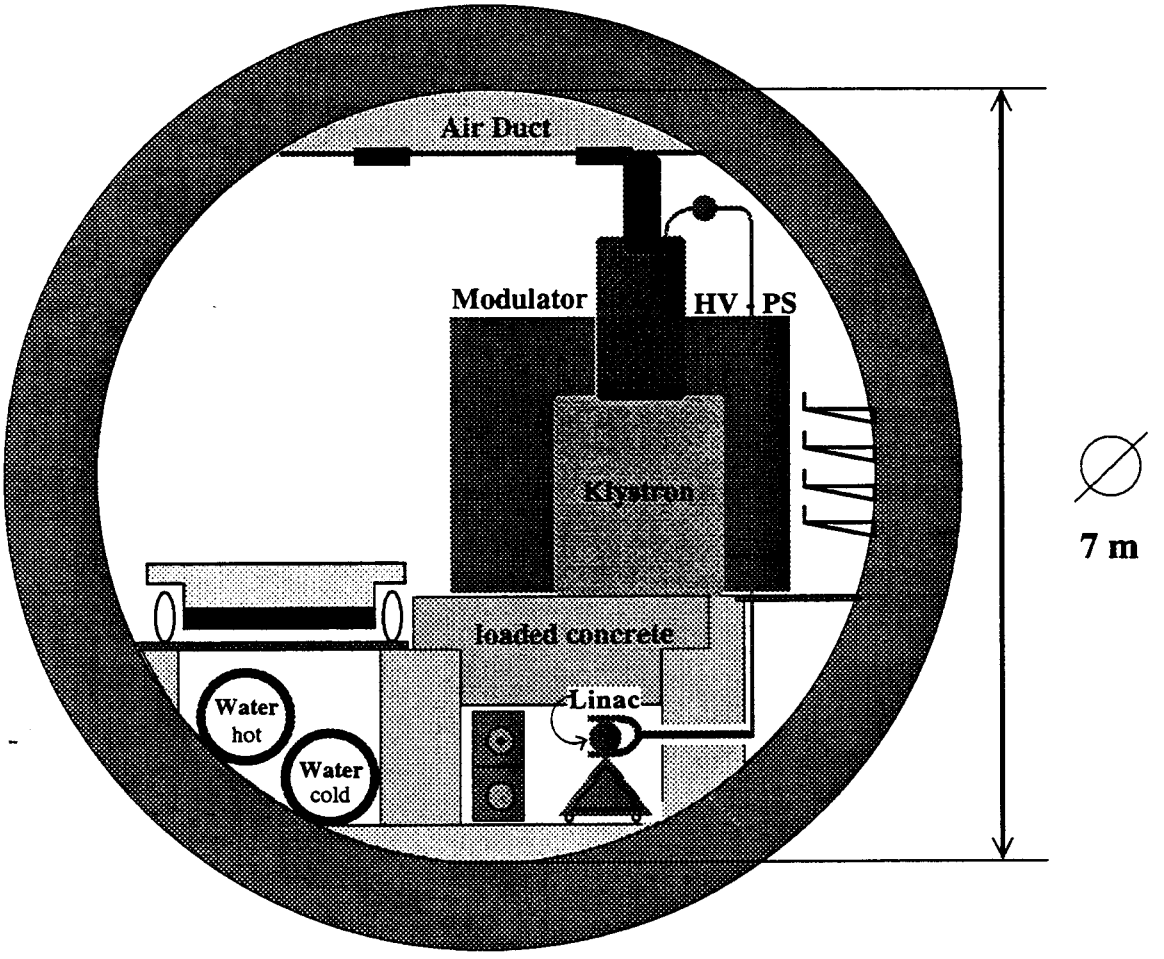

Fig.1.5 SBLC linac tunnel layout.

The beam transport between the linac and the IP (the so-called beam delivery system) consists of collimation, beam line separation (for two separated IP's) and final focus sections. This brings the total length of the SBLC to 36 km. In the interaction region, a crossing angle of 3 mrad provides separation of the incoming and outgoing beams. Non-zero dispersion at the IP makes use of the correlated single bunch energy spread and provides crab crossing without using crab cavities. The design value for the vertical spot size at the IP is 28 nm and thus only about a factor of two smaller than already achieved at the FFTB experiment. The interaction parameters are chosen for a small energy spread due to beamstrahlung and manageable backgrounds from e^+e^- pairs as well as hadronic events.

1.3 JLC

R&D on the Japan Linear Collider (JLC) started officially in 1986 as a result of a recommendation by the Japanese High Energy Physics Committee. Until that time, a couple of possible options were being considered for the main acceleration mechanism of the linear collider, but after some discussions it was decided to select the conventional rf linac approach using beam pulses with multiple bunches. The desired center-of-mass energy was around 1 TeV, and an rf system at 11.4 GHz (X-band) was chosen for the main linacs to reach this goal. Starting in 1992, as the Japanese physics community also became increasingly interested in lower center-of-mass energies, two alternate lower rf frequencies for the main linac, namely 2.9 GHz (S-band) and 5.7 GHz (C-band), were also chosen for consideration. As a few more years of research are needed to decide which frequency to adopt, some of the parameters for all three frequencies are presented in this report (see Table 1.1), although the optimization of S and C-band is still in a primitive stage.

As shown in Fig. 1.6, the electron beam is created by either a thermionic gun, an rf gun or a laser-driven photocathode gun which can produce polarized electrons. The positron beam is produced from a 10 GeV electron beam accelerated by an S-band linac and impinging on a target somewhat larger than that of the SLC positron source. The electron beam is injected directly into a damping ring, whereas the positron beam, having a larger emittance, must first be "cooled down" to an invariant emittance of $\gamma\epsilon_x \sim 0.001$ m-rad in a pre-damping ring.

The beam energy of the damping rings is chosen to be 1.98 GeV and the equilibrium emittances are respectively $\gamma\epsilon_x = 3 \times 10^{-6}$ and $\gamma\epsilon_y = 3 \times 10^{-8}$ m-rad The damping is provided mainly by a long wiggler section and the small emittance by the arcs with a FOOF lattice. The 5 mm-long bunch from the damping ring is compressed to 90-120 μm by a single-stage bunch compressor consisting of an rf section and a chicane. The beam energy spread after the compressor is more than 5%. The pre-acclerator linac parameters (rf frequency, energy, etc.) have not yet been studied in detail. After acceleration up to an energy such that the fractional energy spread becomes small enough, the beam is injected into the main linac.

To make the total linac length reasonably short, the unloaded gradient in the main linacs is set to relatively high values for all three bands under consideration: 31, 40, 73 MV/m for S, C, and X-band respectively. The beam loading ranges from 20 to 27%. Constant-gradient structures would be adopted for S-band and C-band and detuned structures for X-band. Pulse compression would be achieved by three alternate schemes, namely two-port

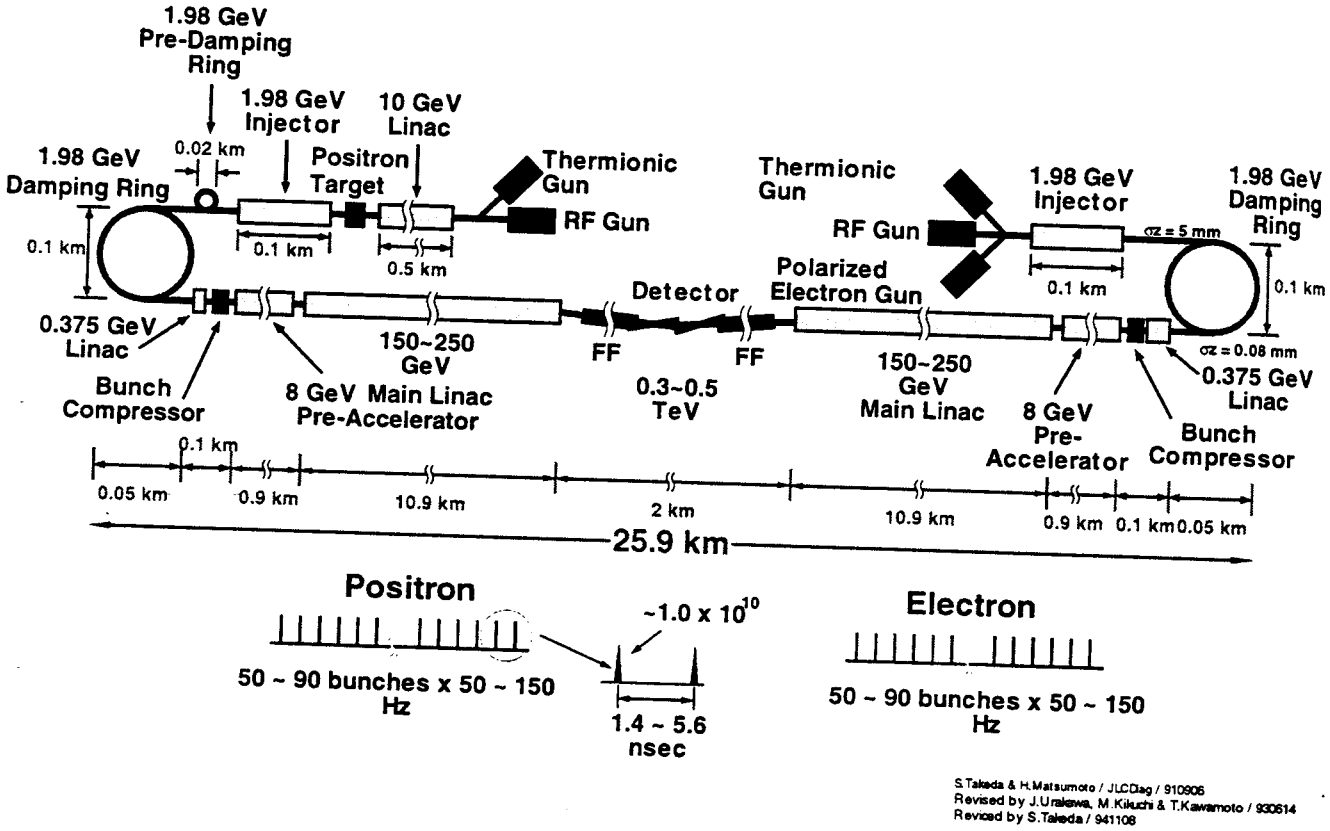

Fig.1.6 JLC schematic layout.

SLED, disk-loaded SLED II, and DLDS (see section 2.3.2), respectively. The transient beam loading would be compensated by structures using frequency-shifted cavities for S-band, or stagger-timed triggering of klystrons for C-band and X-band. A possible cross-section of the linac is shown in Fig. 1.7.

The beam delivery system consists of so-called "big bends," collimators and the final focus system. The first two are inserted in order to suppress backgrounds at the experiments. The "big bends" also make it possible to have two collision points, one of which may be used for collisions other than e^+-e^-, such as γ-e and γ-γ. The final focus system is based on a two-family non-interleaved sextupole scheme and is designed to give a final spot size ($\sigma_x^* \times \sigma_y^*$) as small as $\sim 300 \times 3$ nm.

1.4 NLC

The SLAC NLC linear collider design is based on linear accelerators using normal conducting traveling-wave structures and powered with 11.424 GHz (X-band) rf. The required X-band rf power is generated in modules consisting of klystrons and modulators producing pulses of about 1 μs length. These pulses are compressed to roughly 200 ns, a process which increases the peak power to produce the required gradient along the accelerator sections. The choice of the X-band frequency for the main linacs has been considered very carefully because it requires developing a new technology, but X-band has the major advantage that it can more easily supply and sustain the higher gradients necessary for the final center-of-mass energy desired for the collider. Most of this new technology is being developed at the present time and will be tested in the form of a complete system during the next few years at the NLC Test Accelerator (NLCTA).

The SLAC NLC is being designed to start at an initial center-of-mass energy of 500 GeV capable of being decreased to about 350 GeV for study of the top quark, and upgradable to the TeV level at a later time. One of the main advantages of the X-band rf is the capability for high accelerating gradients up to ~100 MV/m with low dark current. The required power will be supplied by conventional klystrons that are being developed in the rf R&D program at SLAC. The main parameters of the 500 GeV design are listed in Table 1.1 while a schematic of the layout is illustrated in Fig. 1.8. If one simply considers the components necessary for the 500 GeV design, the overall physical length is about 20 km including the space necessary for the linacs and the beam delivery sections (see below) which transport the beams from the ends of the linacs to the IP. However, the planned design has an overall length of roughly 26 km to allow for the adiabatic energy increase to 1 TeV.

The electron injector system for the collider is based upon a polarized photocathode electron gun with a sub-harmonic bunching system. This system is very similar to that operating reliably at the SLC. The beams from the injector are accelerated in an S-band linac to 2 GeV, where they are injected into a damping ring that decreases the beam emittances to $\gamma\epsilon_x = 3 \times 10^{-6}$ m-rad and $\gamma\epsilon_y = 3 \times 10^{-8}$ m-rad.

The positron injector system is based upon a conventional source using an electromagnetic shower. The parameters are scaled from the operating SLC positron system. A drive electron beam, accelerated in an S-band linac to an energy between 3 and 6 GeV, collides with a rotating target and produces a shower. To improve the positron capture efficiency, the positrons are accelerated in a large aperture L-band linac and then injected into a large

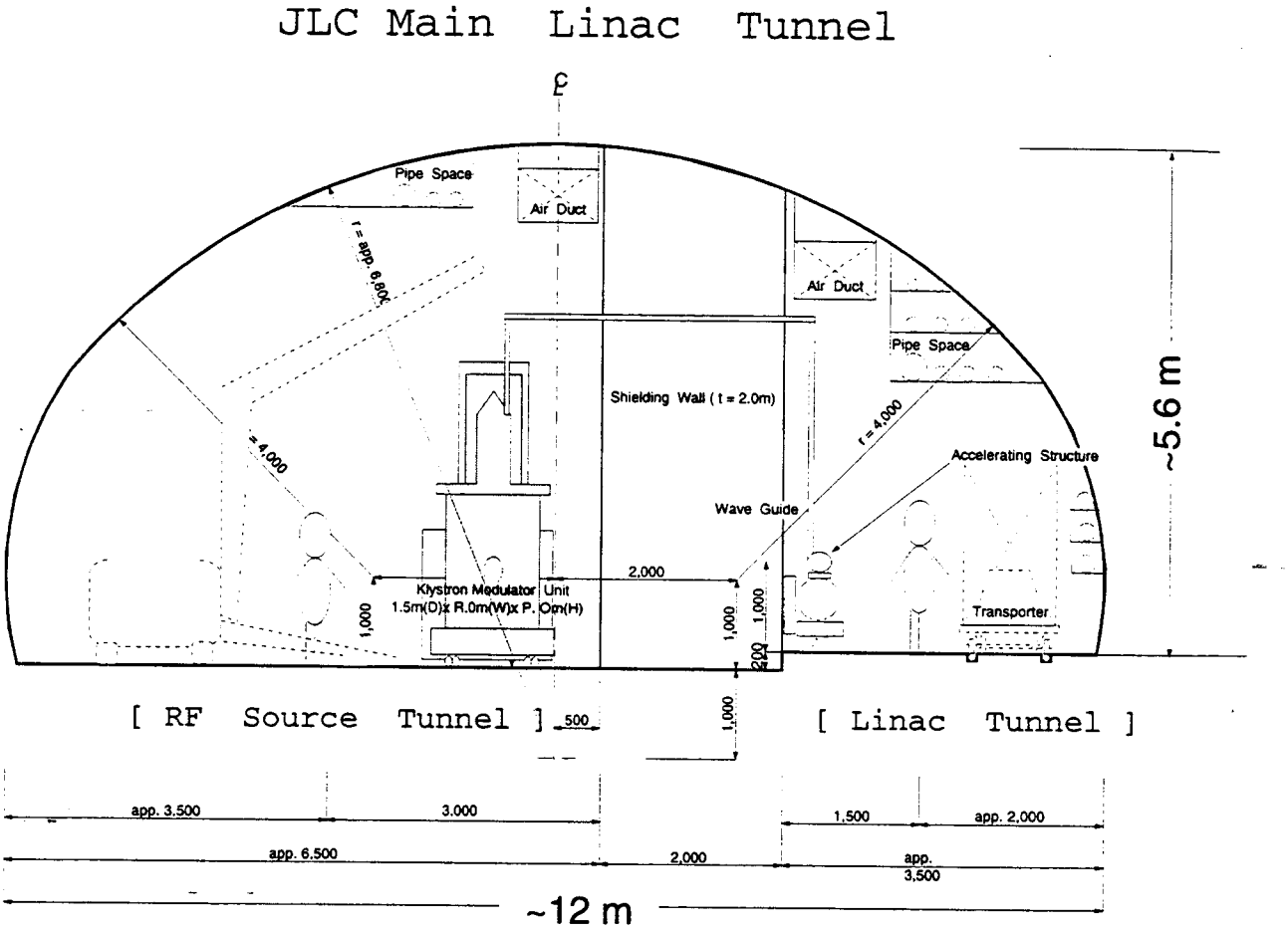

Fig.1.7 JLC linac cross-section.

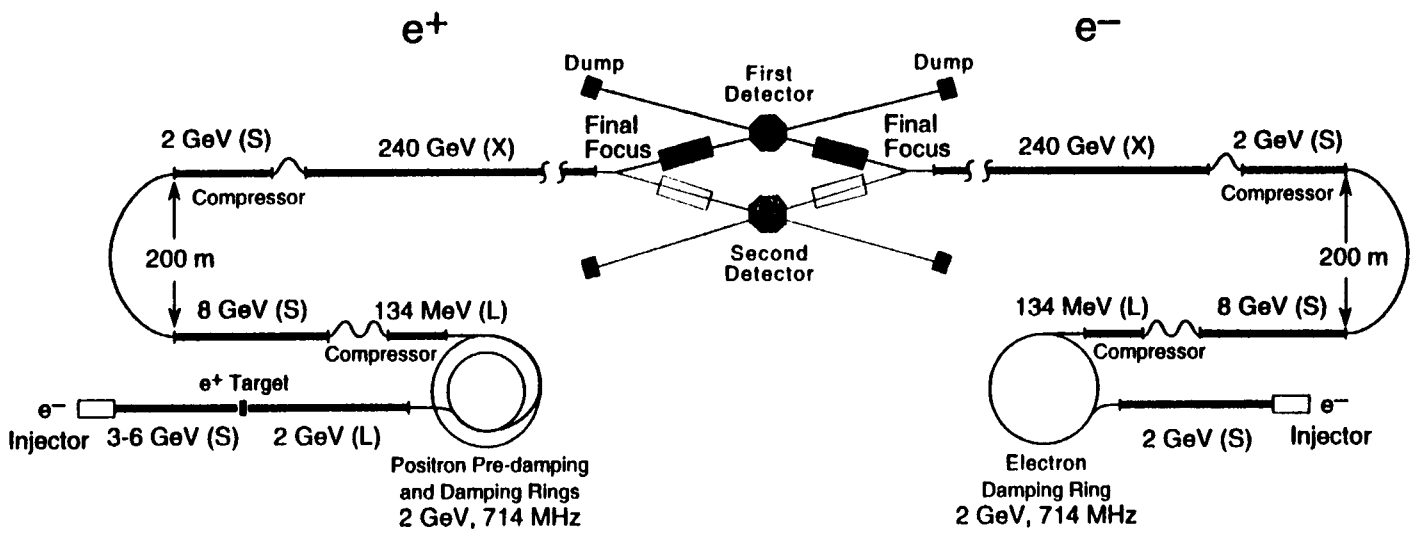

Fig.1.8 NLC schematic layout.

aperture pre-damping ring at 2 GeV. After the pre-damping, the positrons are injected into a main damping ring, identical to the electron main damping ring.

After the damping rings, the electron and positron bunches are compressed in two bunch compressors. The first compressor, located immediately after the damping rings, compresses the bunches from 4 mm to 500 μm for injection into an S-band pre-linac that accelerates the beams to 10 GeV. At this point, the bunch lengths are further compressed to 100 μm in a two-stage compressor that also reverses the direction of travel; this allows for further upgrades of the main linac length and also permits feedforward corrections using the extracted beams from the damping rings.

The beams are then injected into the X-band linacs, where they are accelerated to a final energy of 250 GeV. The linac focusing lattice is designed to allow the center-of-mass energy to vary from 350 GeV to 1 TeV. Diagnostic stations are located at five positions along each linac. These stations include laser wire scanners to measure the transverse phase space, beam-based feedbacks to correct for centroid shifts of the bunch train, multibunch BPMs and high-frequency kickers to measure and correct bunch-to-bunch position errors, and magnetic chicanes to provide non-invasive energy and energy spread measurements. Possible tunnel layout schematics for the NLC are shown in Figs.1.9 and 1.10.

After the linacs, the beams enter the beam delivery sections which start with arrays of collimators where the beam energy spread and transverse phase space are collimated. Collimation is performed for both the x and y planes at both the IP phase and the final-doublet phase. This primary collimation is then followed by a secondary collimation, again in both planes and both phases, to remove additional scattered particles.

At this point, the beams pass a dc deflecting magnet which can be used to switch the beams from one IP collision point to the other. Two separate IP's are needed to allow for other experiments. The IP switch is followed by short arcs that provide a deflection of 10 mrad, leading to a total crossing angle of 20 mrad.

Finally, the beams enter the final focus systems. At this point the e^+ and e^- flat beams follow the design of the FFTB beamline at SLAC. It consists of a matching section with beam phase space diagnostics, horizontal and vertical chromatic correction sections, a final transformer, a final doublet, and a diagnostic/dump line for the exiting beam. The final doublets are mounted in a single barrel and require active stabilization to insure beam collisions. The spot size tuning is to be performed by using an advanced laser fringe monitor and the beam-beam deflections. The IP parameters are chosen to minimize the backgrounds.

1.5 VLEPP

A general layout of VLEPP is shown in Fig.1.11. The VLEPP machine is entirely symmetrical with respect to the interaction point. The halls for beam preparation (injectors, pre-accelerators, damping rings, etc.) and the detector hall are situated at the symmetry point. The main linacs (left and right) are housed in 5.1 m diameter tunnels.

VLEPP is designed as a machine with a single bunch per rf pulse. The intense 2×10^{11} single bunches $e\pm$ are accelerated in room-temperature traveling-wave rf linacs powered by klystrons. To keep the cost down, a high gradient (100 MV/m) and a high rf frequency (14 GHz) have been chosen. The single bunch regime simplifies the design of the accelerating structure.

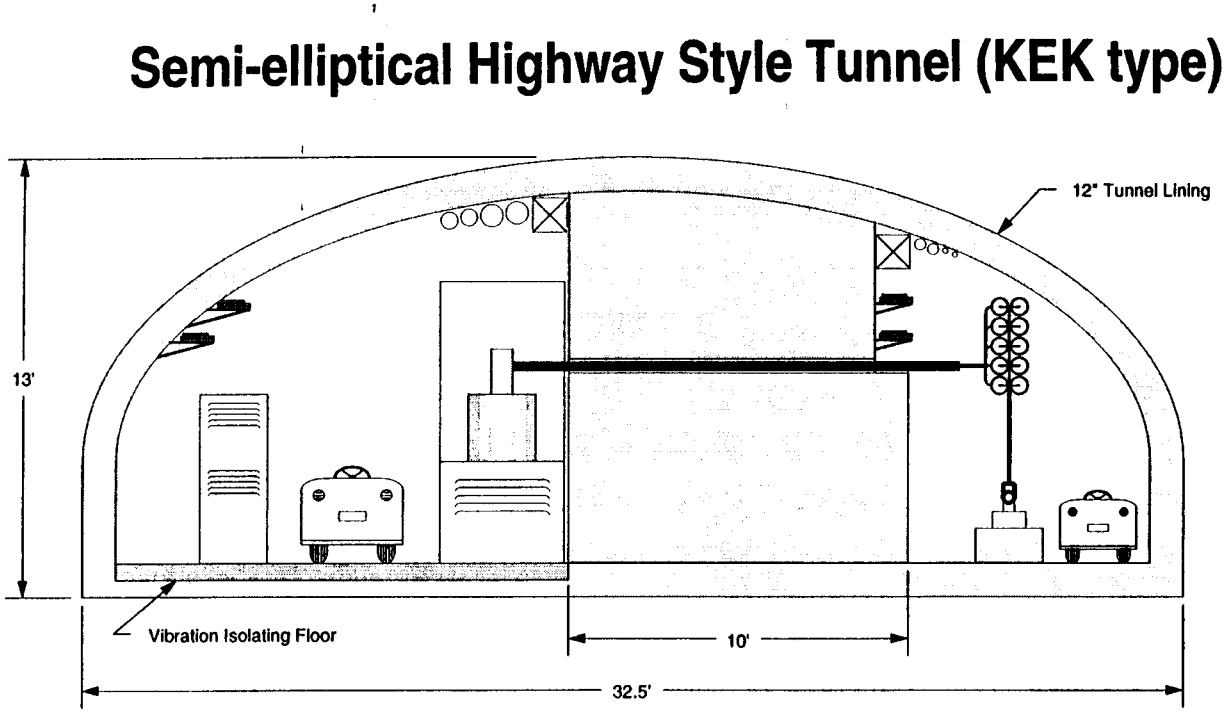

Fig.1.9 NLC possible tunnel layout.

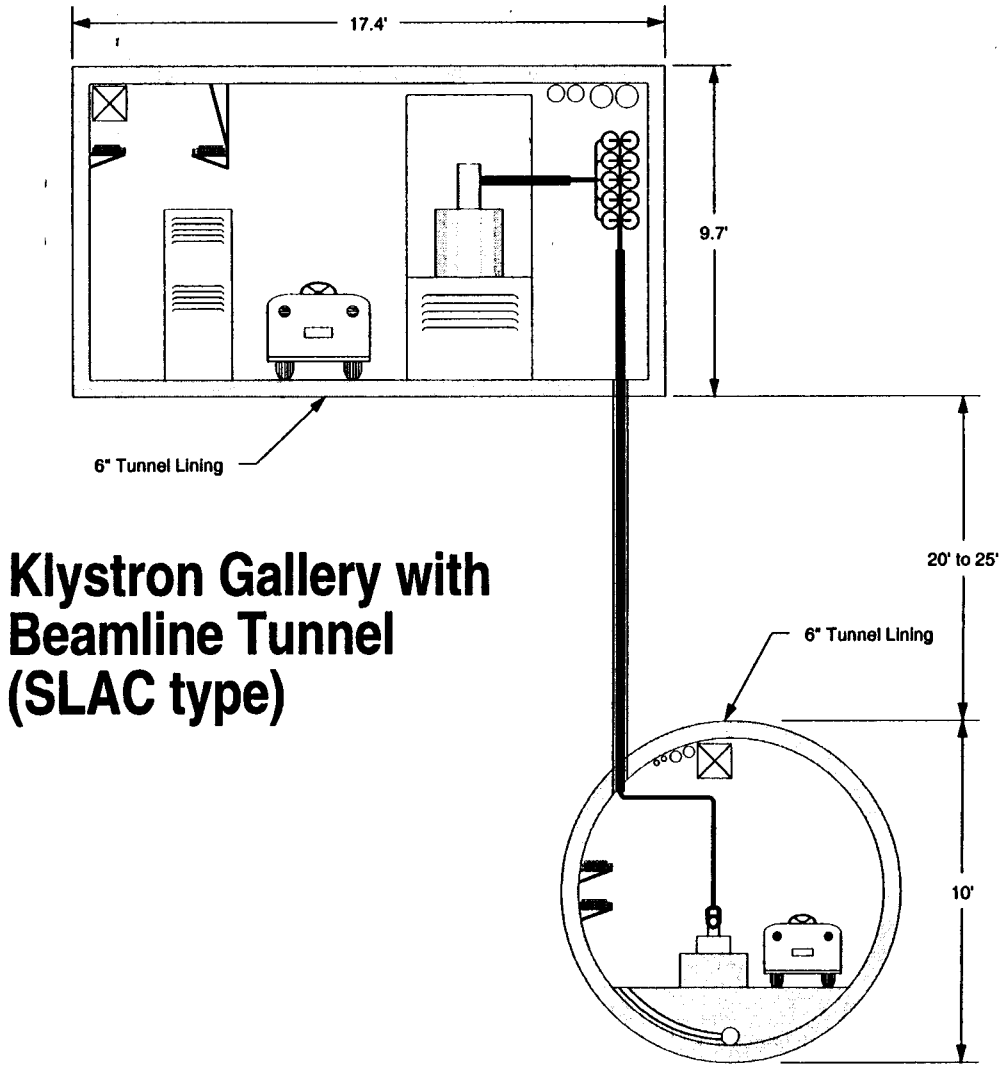

Fig.1.10 Another possible NLC tunnel layout.

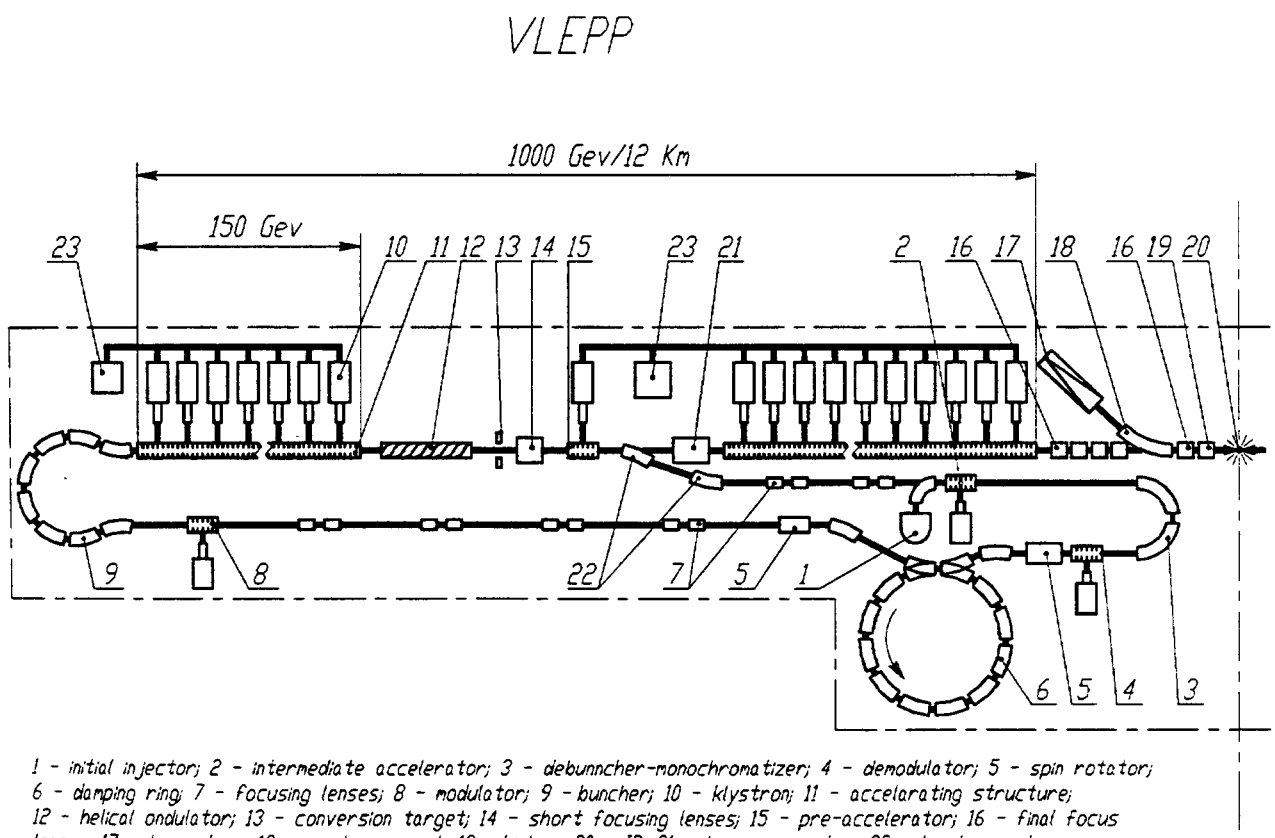

Fig.1.11 VLEPP general layout.

The problem of single bunch transverse wakefields can be solved by using the so-called "autophasing" regime together with an adaptive feedback alignment system. The one-meter long accelerator sections are of the standard $2\pi/3$ mode, constant-impedance type with a relatively large aperture-to-wavelength ratio. Four sections are powered by one 150 MW X-band klystron. The peak power from each klystron is increased by a factor of 3.2 by a pulse compression system. The VLEPP klystron is somewhat different from more conventional tubes: it is a DC high voltage powered (1 MV), grid-controlled, PPM focused, high gain klystron with a traveling-wave output structure. Without a modulator, the power supply system consists of DC HV sources (HVS) feeding the capacitances of pulse forming lines (PFL).

The linacs consist of identical modules and have a two-level architecture. On the first level there are large 50 m-long modules (supermodules) that include one HVS feeding a 50 m-long PFL and 10 klystrons. A general layout of a supermodule in the tunnel is shown in Fig.1.12. On the second level, the basic 5 m-long units consist of 4 accelerating sections, quads, BPM's, pumping and cooling systems, etc., assembled on a support table and powered by one klystron through two pulse compressors. Hence, one supermodule includes 10 basic units. All this equipment can be easily housed in a 5.1 m diameter tunnel (see Fig.1.13).

The polarized electron and positron bunches are produced from gamma conversion in a thin target. The polarized photons are produced by a 150 GeV beam from the main linac, passing through a helical undulator. The bunches are captured, pre-accelerated to 3 GeV, decompressed and injected and "cooled" in a damping ring. To conserve beam polarization during transport, spin rotators are used. Unpolarized electrons are used from the injector only during the first pulse.

The VLEPP final focus and interaction parameters are chosen to give low backgrounds and maximum luminosity. The use of a "traveling focus" regime at the IP decreases the requirement on the vertical emittance. After interaction, the photons and beams are extracted and dumped, using a 6 mrad angle between the colliding e^+ and e^- beams.

1.6 CLIC

In the multidimentional space of possible parameters for linear colliders, the CLIC study explores the technical feasibility of beam acceleration by traveling-wave structures at room temperature and high frequency (30 GHz), powered by a superconducting drive linac, the so-called two-beam-acceleration scheme. The two main advantages of high frequency accelerating structures are their relatively low rf energy requirements for filling because of their reduced volume and their capability of sustaining high accelerating fields with a negligible dark current. As a consequence, the specified luminosity of $10^{33}\ cm^{-2}s^{-1}$ at a c.m. energy of 500 GeV is reached with collisions of single bunches at a repetition frequency of 2.5 kHz and a reasonable wall-plug power consumption of 100 MW for rf power generation. The luminosity is further increased to almost $5 \times 10^{33}\ cm^{-2}s^{-1}$ by a possible operation with ten bunches per pulse which is now under study. In both modes, good conditions for physics experimentation are fulfilled, in particular an average energy loss in the bunches at collision limited to 3.5%. Based on accelerating fields of 80 MeV/m, the overall physical dimension of 11.2 km for the whole complex, including 2.4 km for the final focus and detectors, is rather compact as illustrated in the general layout in Fig. 1.14. The main drawback of the high

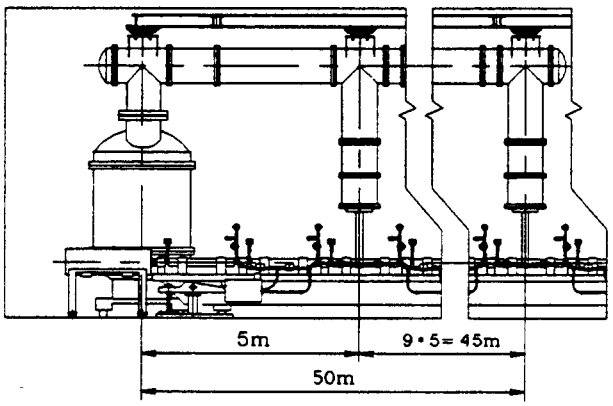

Fig.1.12 VLEPP linac. Schematic of a 50 m supermodule in the tunnel.

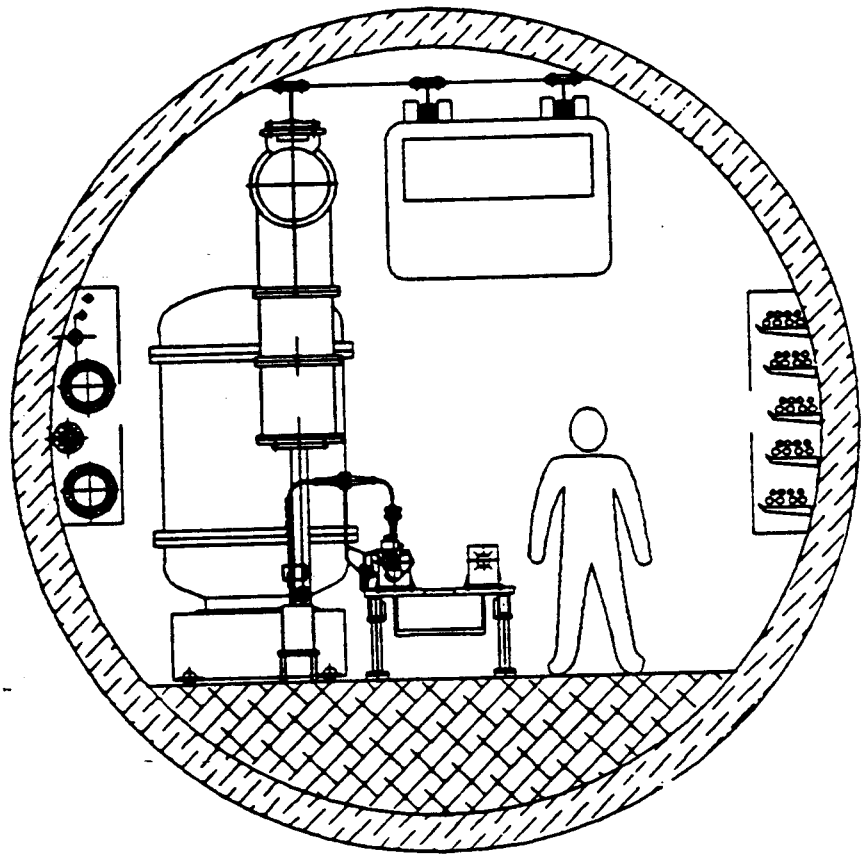

11 km

Fig.1.13 VLEPP tunnel cross-section.

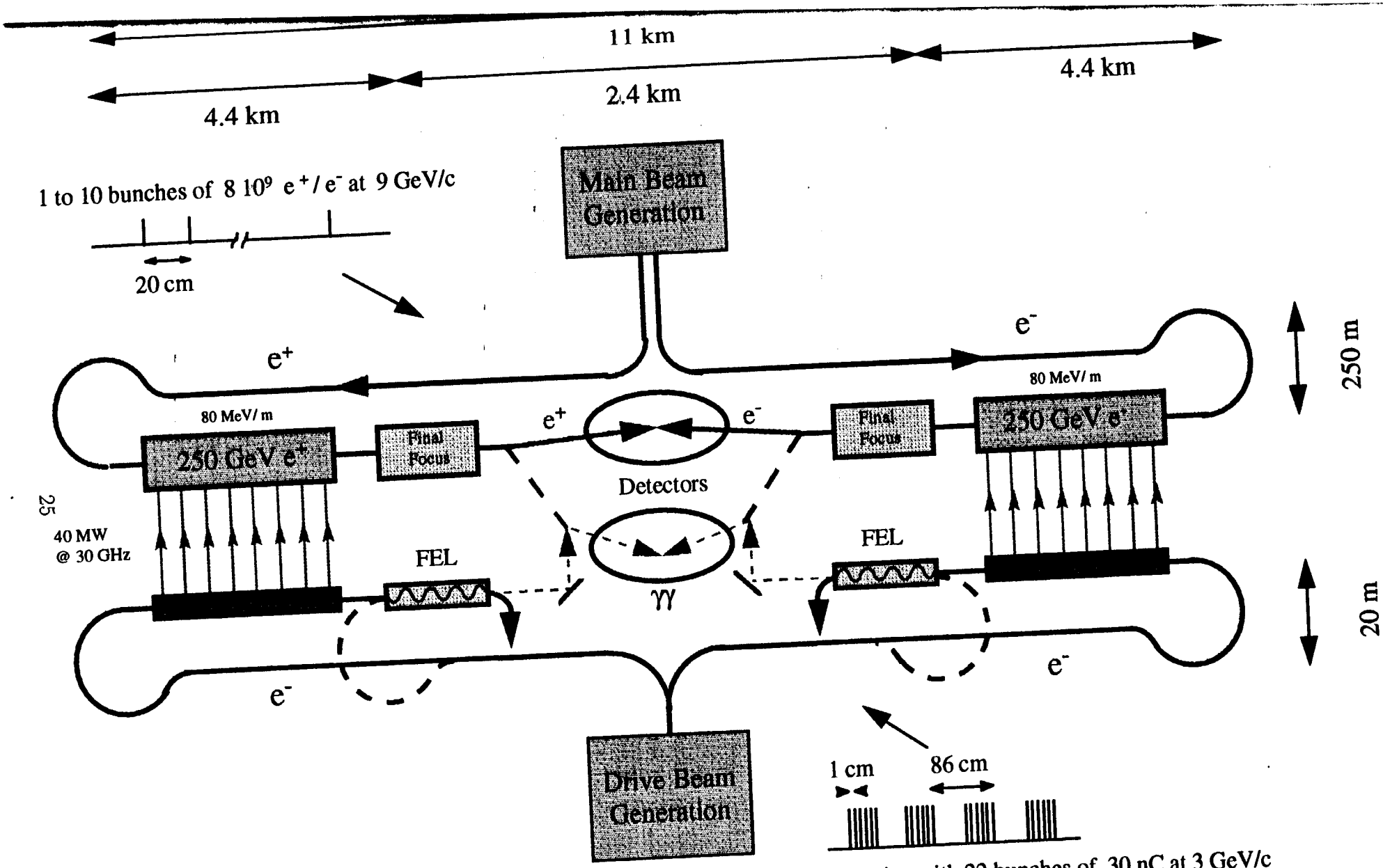

Fig.1.14 CLIC general layout.

frequency comes from the small accelerator iris aperture which leads to the generation of strong wakefields and potential emittance dilution. To control these effects, one needs sophisticated methods of beam trajectory correction and structure alignment within a ± 10 μm r.m.s. precision for beam emittance preservation. Such tight tolerances over long distances are achieved with state-of-the-art technology on structure fabrication, precise pre-alignment of the elements on their girders via an automatic stretched-wire system and active beam-based alignment optimizing the position of the quadrupoles to minimize beam emittance blow-up. Bunches of 8×10^9 electrons or positrons are accelerated to the specified energy of 250 GeV with 11233 accelerating sections of length 28 cm in each linac. About 10% of these sections are used as microwave quadrupoles with simultaneous acceleration and time-dependent transverse focusing for single bunch wakefield stabilization. Beam focusing with a total of 532 quadrupoles arranged in 6 sectors with constant lattice in each sector and a scaling to the beam energy from sector to sector is specially adapted for strong wakefields. This extends the length of each main linac from 3.1 km for active acceleration to 4.4 km when taking into account the necessary space for magnetic elements, beam instrumentation and drifts for flanges, bellows, vacuum system, etc. One particularly challenging aspect of the CLIC scheme is the rf power generation at a frequency at which high power klystrons are not feasible. Accelerating structures are fed, via standard waveguides, with 30 GHz rf power extracted from a drive beam with a 2.6 μC charge and an initial energy of 3 GeV. The drive beam, running all along the linac, is progressively decelerated in transfer structures and finally dumped after conversion of up to 75% of its energy into rf power. This results in a particularly simple arrangement of the structures in a single tunnel without any active rf element, as illustrated in Figs. 1.15 and 1.16.

The two injector complexes for the e^+ and e^- main beams (Fig. 1.17) as well as for the drive beams (Fig. 1.18) are both located in a central area close to the detector, centralizing the main activities and anticipating further extension of the facility to higher energies. The beams are then transported at 9 GeV for the main beams and at 3 GeV for the drive beams to the injection point of the linac via simple transport lines in the main tunnel and isochronous loops. Both complexes are based on superconducting structures filled with power in a continuous mode for their excellent beam power efficiency and compatibility with operation at a high repetition frequency. As a consequence, transfer efficiencies as high as 26% from wall plug to rf power and about 8% from wall plug to beam power in ten bunch operation mode, are expected.

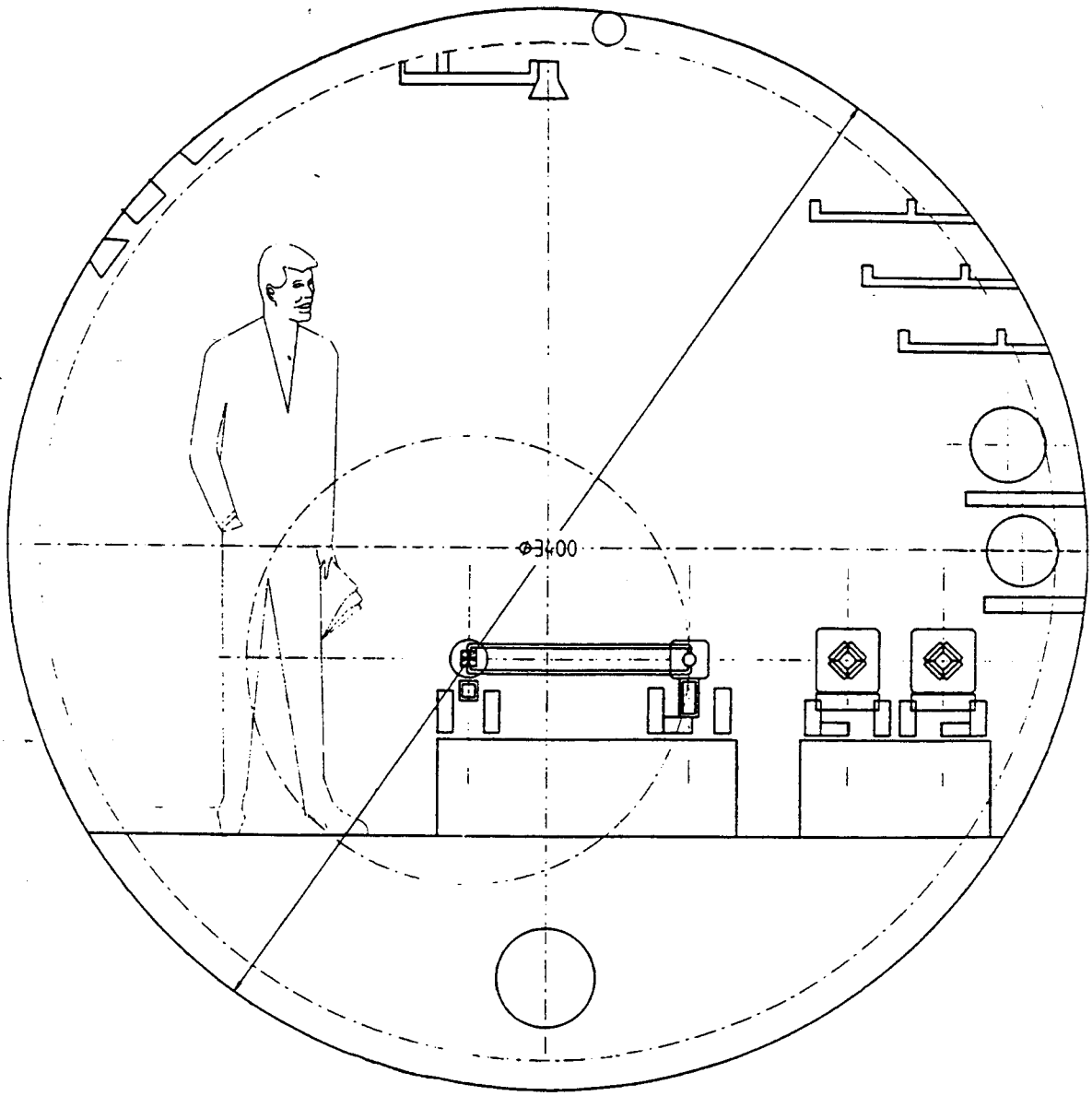

Fig.1.15 CLIC tunnel layout.

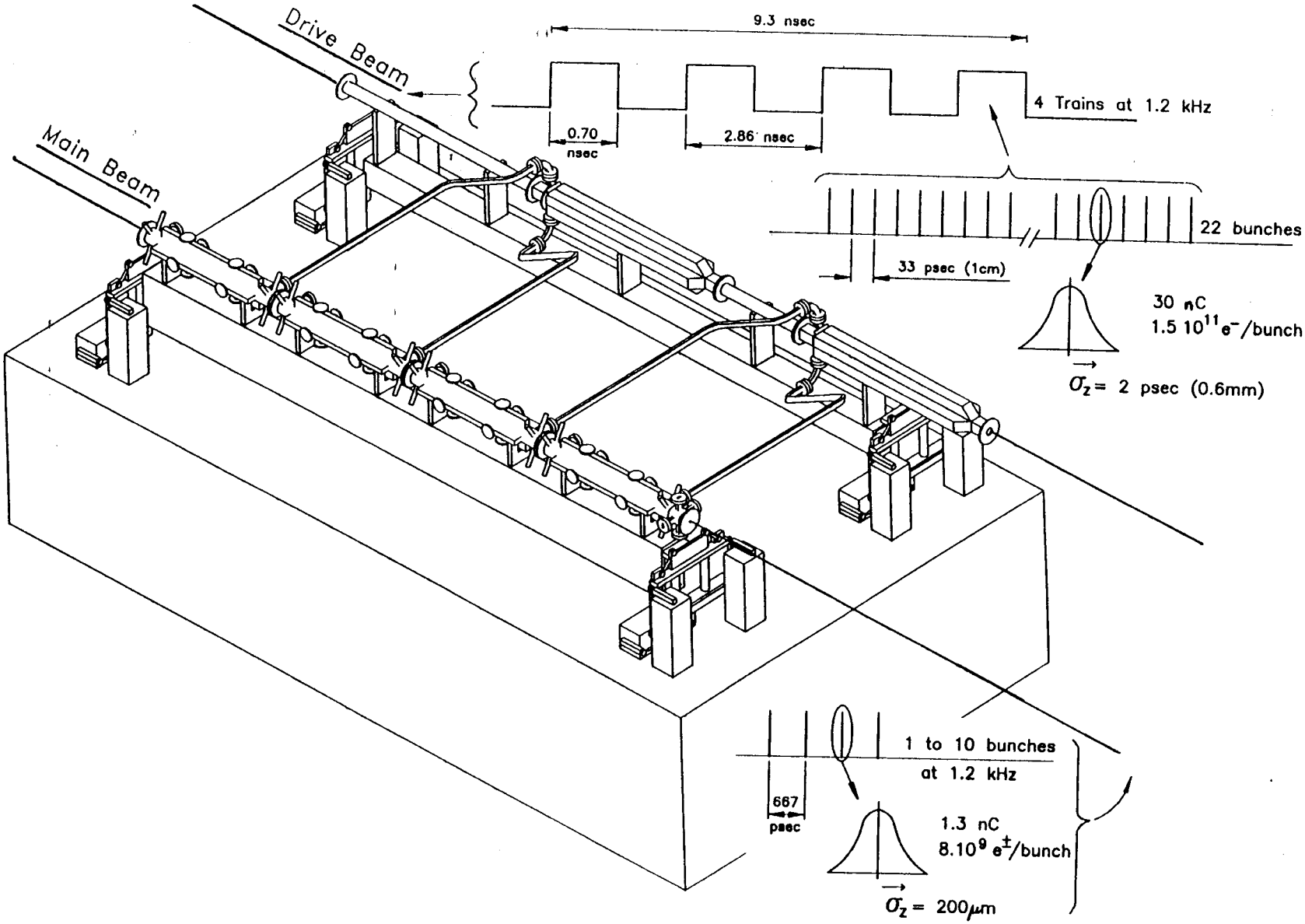

Fig.1.16 CLIC two-beam accelerator layout (drive beam parameters for single bunch operation).

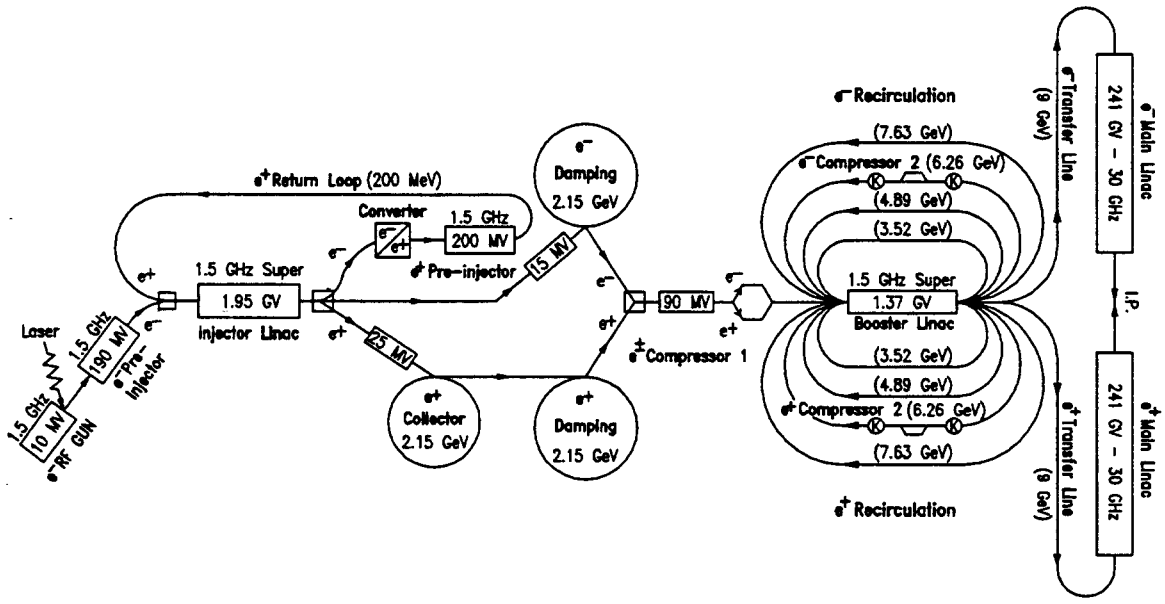

Fig.1.17 CLIC injector complex for the e^+ and e^- sources.

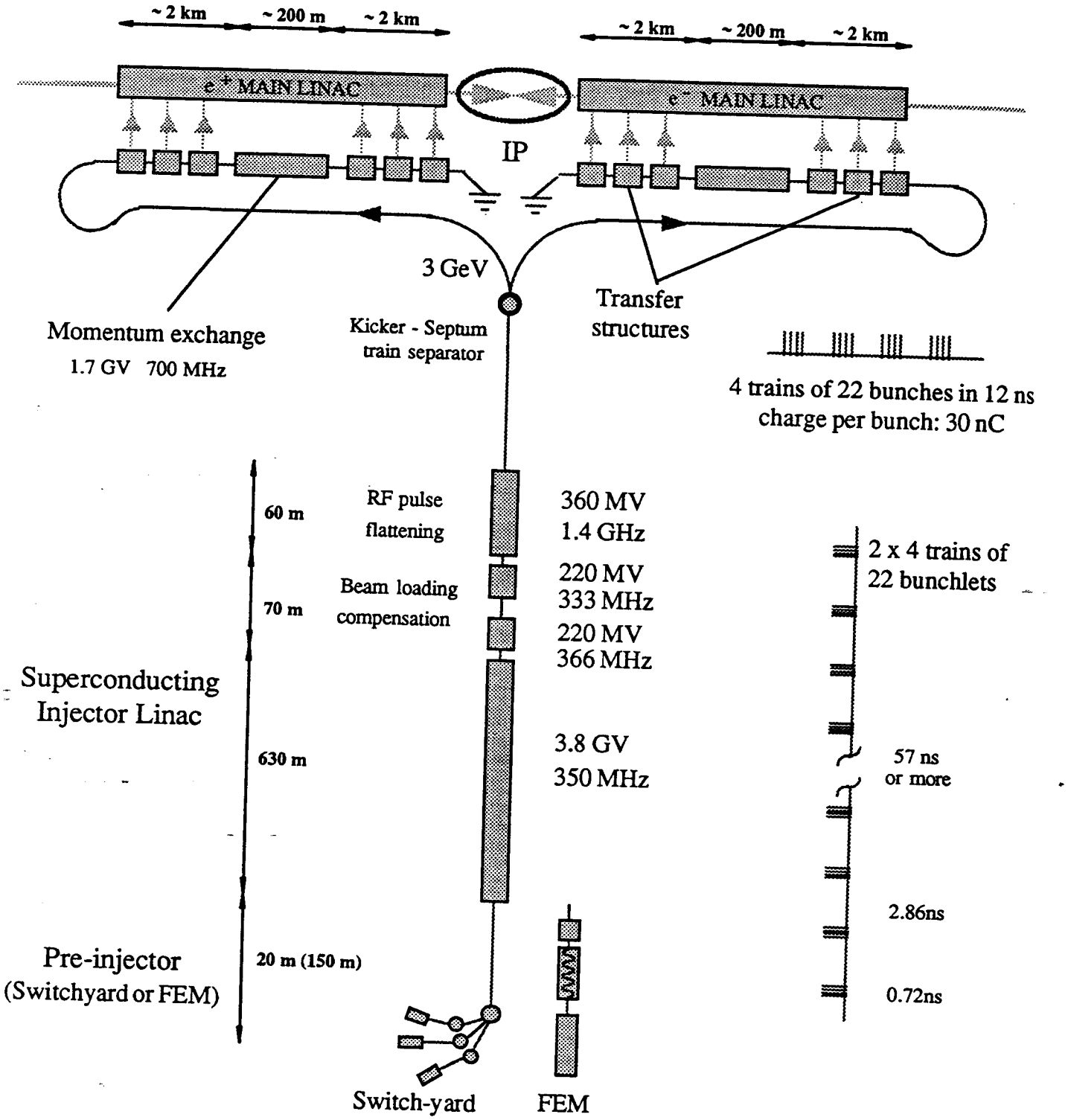

Fig.1.18 CLIC drive beam generation reference scheme for single bunch operation.

2 WORKING GROUPS

2.1 INJECTOR SYSTEMS

2.1.1 The Group

M. Yoshioka (Chairman)
Physics Department, KEK, 1-1 Oho, Tsukuba-Shi, Ibaraki-Ken 305, Japan. E-mail: YOSHIOKA@jpnkekvx
A. Mikhailichenko (Deputy Chairman)
BINP, Pr. Lavrentyeva 11, 630090 Novosibirsk, Russia. Present address: Cornell University.
E-mail:MIKHAIL@lns62.lns.cornell.edu
H. Braun
CERN, PS/LP, CH-1211, Geneva 23, Switzerland. E-mail: HBRAUN@vxcern.cern.ch
K. Flöttmann
DESY, Notkestrasse 85, 22603 Hamburg, Germany. E-mail: MPYFLO@dsyibm.desy.de
J. Frisch
SLAC, Mail Stop 66, P.O.Box 4349, Stanford, CA 94309. E-mail: FRISCH@slac.stanford.edu
R. Miller
SLAC, Mail Stop 26, P.O.Box 4349, Stanford, CA 94309. E-mail: RHM@slac.stanford.edu
C. Pagani
INFN MILANO - LASA, Via F.lli Cervi 201, 20090 Segrate (Milano), Italy. E-mail: PAGANI@mvlasa.mi.infn.it
L. Rinolfi
CERN, PS/LP, CH-1211, Geneva 23, Switzerland. E-mail: RINOLFI@cernvm.cern.ch
J. Rosenzweig
UCLA, Dept. of Physics, 405 Hilgard Av. Los Angeles, CA 90024. E-mail: ROSEN@uclahep.physics.ucla.edu
H. Tang
SLAC, Mail Stop 66, P.O.Box 4349, Stanford, CA 94309. E-mail:TANG@slac.stanford.edu
C. Travier
LAL Orsay, Bat. 200, Centre d'Orsay, 91405 Orsay Cedex, France. E-mail: TRAVIER@lalcls.in2p3.fr
D. Yeremian
SLAC, Mail Stop 26, P.O.Box 4349, Stanford, CA 94309. E-mail: ANAHID@slac.stanford.edu

2.1.2 Overview

This chapter describes the electron and positron sources for the various linear colliders discussed in this report. While not all the machine designs include plans for polarized electrons, it is expected that most if not all of them will switch to a polarized electron gun in the future. Some of them may also have polarized positrons. The specific parameters relevant to the sources are dictated by the bunch charges, time structures and tolerances of the various machines. Table 2.1.1 summarizes these parameters. Note that this table does not yet include the actual bunch charges and emittances needed at the exit of the sources. These depend on derating factors for known and unknown beam losses and other assumptions that are not yet available.

Table 2.1.1
Parameters relevant to e^- and e^+ Sources

	TESLA	SBLC	JLC-S	JLC-C	JLC-X	NLC	VLEPP	CLIC
No. of particles/bunch at IP (10^{10})	5.15	2.9	1.44	1.0	0.63	.65–1.25	20	.8
Repetition rate (Hz)	10	50	50	150	150	180	300	2530–1210
No. of bunches/pulse	800	125	50	72	85	90	1	1–10
Beam pulse length (μsec)	800	2	.280	.202	.119	.126	NA	.006
Bunch separation (nsec)	1000	16	5.6	2.8	1.4	1.4	NA	.667

2.1.3 Where We are Today

Electron Sources

Many of the electron injectors required for the future linear colliders described here will benefit from technology that is already quite mature today. Production of short high peak intensity bunches has been successfully demonstrated by machines in many institutions all over the world. Much progress has been made in developing and operating various injector systems such as conventional subharmonic bunchers with thermionic and polarized DC guns, as well as rf guns. Much work has also been done in developing accelerating systems for injectors and in controlling effects such as beam loading, emittance growth and wakefields.

Thermionic guns and bunching systems

The conventional subharmonic bunching system pioneered at SLAC has been successfully used on the SLC for almost 15 years. The SLC injector is currently capable of producing two 20 ps long bunches with a charge as high as 9 nC each at the entrance of the damping ring, and routine operation with 7 nC. Most of the injectors proposed for future linear colliders plan to use this type of bunching scheme. The relatively new issues to be addressed for this scheme are the production of the bunch train, the bunch-to-bunch intensity stability, the overall intensity stability from pulse to pulse and beam loading.

The cleanest way to produce the desired bunch train is to do it right at the gun by using a gridded gun, and pulsing the grid at the required rate. Such pulsers have been developed at KEK in Japan for the ATF, and also for the DESY SBLC in Germany. The ATF goal is to produce a train of bunches 1.4 ns apart. Currently, the KEK team is able to produce a train with 2.8 ns bunch spacing, and development continues for the 1.4 ns spacing. The DESY pulser is able to meet the full requirements of the SBLC injector of producing bunches with three options of bunch separations, i.e., 8, 16, and 24 ns.

The SBLC and JLC test accelerator facilities use injectors which are identical to those planned for their future colliders. For budget and schedule reasons, the NLCTA injector at turn-on will not have the ultimate subharmonic buncher systems to be used on the NLC. The early injector will operate at X-band and the multibunch issues will be addressed by making the average current in the pulse equal to that of the eventual NLC system. A subharmonic system will be added later.

Polarized guns and bunching systems

In the past 5 years the use of a polarized electron gun together with a conventional subharmonic bunching system has become the routine method of operating the SLC injector, producing as much as 5.5 nC in a single bunch at the IP, with 80% polarization. This

polarized source has operated with over 99% up-time when the rest of the SLC was on. Routine maintenance of the polarized source is minimal. It includes cesiation every 4 or 5 days, which takes 20 minutes, and laser flash lamp replacement every 2 months which takes about 4 hours. This quick cesiation has been made possible through the use of the SLC control system. Furthermore, extensive use of feedback systems helped to reduce the laser intensity jitter at the cathode to less than 2%. The electron beam intensity jitter was less than 1% as a result of the so-called "surface charge limit" phenomenon of the cathode. Much has been learned about this phenomenon and appropriate techniques to assure the survivability of these cathodes in the accelerator environment have been established at SLAC. In addition, successful photocathode development programs are ongoing in Japan, Germany, Russia, and at other institutions in the US, promising improved charge and polarization performance.

RF guns

In the past 10 years, much progress has been made in the development of low emittance photocathode rf guns, and TESLA and CLIC in particular plan to use these devices. While as mentioned earlier, most of the other proposed machine injector designs are based on conventional bunching systems for their baseline approach, it is clear that if rf guns, particularly polarized source rf guns, could be used reliably, many of them would also adopt this scheme. Indeed, producing a low (1 to 3 mm-mrad rms) normalized emittance from the injector would greatly simplify the operation of the electron damping rings. In the case of TESLA, the damping ring could be eliminated altogether.

Work is in progress at CERN, LAL, LANL, BNL, KEK, SLAC, UCLA and other institutions on various aspects of making an rf gun work, but even so, additional support may be needed to accelerate progress in this area.

LANL, where the photocathode rf gun concept was pioneered, has had several successful rf guns operating with a cesium-potassium antimonide cathode and an L-band structure. They have successfully used one of their rf guns as an injector for FEL experiments. BNL has been successful in using metallic cathodes with a UV laser system in an S-band structure, while CERN has developed a high quantum efficiency and robust cesium telluride cathode which works with a UV laser. The promising Ti:Sapphire laser that can produce very short optical pulses (0.1-10 ps) has been successfully used at the LAL (Orsay) rf gun to illuminate metallic and dispenser cathodes. The high pressure ultra pure water rinsing technique, originally developed at CERN, is a critical step towards the survivability of polarized electron cathodes in an rf gun.

While various laser systems have been constructed to be used with rf gun development programs, a reliable laser with the appropriate bunch train structure and stability required by the various linear colliders is not yet in existence. The subsection below spells out the requirements for these various lasers.

Laser requirements

Most linear collider designs use a photocathode gun for the electron source, and therefore require a photocathode drive laser. The type of laser required will depend on the type of electron gun used: polarized, unpolarized, DC or RF. While none of the proposed linear collider source designs push the current state of the art in lasers in any one parameter, they do require a combination of parameters which will require some laser development. For example, the wavelengths, peak, and average powers needed for these sources are readily

achieved but the specific pulse structures and intensity are not.

SLAC has used a laser system driving a polarized photocathode DC gun as the electron source for the main linac for several years. This system, based on Nd:YAG pumped Ti:Sapphire (Titanium doped Sapphire) has operated successfully, but the pulse structure used is considerably different from that required by most future linear collider designs.

The TTF laser, under development at the Max Born Institute, and the University of Rochester/Fermilab R&D laser more closely resemble linear collider source lasers. These systems deliver beams appropriate for the TESLA rf gun. The current systems are based on Nd:YLF, and are appropriate for UV photocathode guns. If a decision is made to use polarized electrons from a semiconductor photocathode, a different laser material will be required to obtain the required wavelength.

As many of the linear collider sources require either electron polarization (and therefore tunable laser wavelengths) or very short ($\approx$ 1 picosecond) pulses, high bandwidth tunable laser materials may be used. At the present time Ti:Sapphire is the most commonly used tunable laser material. It provides high gain and good thermal properties. Unfortunately, it is difficult to flashlamp pump, and is usually pumped with either frequency doubled YAG, or CW Argon ion lasers. This will make it somewhat difficult to obtain the pulse structures required for some designs.

Newer materials, most notable LICAF and LISAF, can produce short pulses with tunable wavelengths. They are easily pumped by flashlamps or diodes, and should be able to produce the required time structures. Unfortunately, their thermal properties are poor, and some development will be required to reach the repetition rates and average powers required by linear colliders. Development of new laser materials is ongoing, and may yield better solutions for source lasers.

There do not seem to be any serious obstacles to the development of source lasers appropriate to any of the linear collider designs. The required laser systems will, however, be quite complex, and some time to develop them is to be expected.

Positron Sources

The basic process for positron production on which all of proposed linear collider positron sources rely is $e^{\pm}$ pair production from electromagnetic interaction of a high energy photon with the Coulomb field of a nucleus. Depending on how the high energy photons are generated, the proposed positron sources may be classified into two categories: conventional SLC-type sources and wiggler-based sources. The use of a helical undulator also offers the unique possibility of polarized positrons. The JLC, NLC and CLIC positron sources fall in the first category, whereas the TESLA, SBLC and VLEPP sources belong to the second. In an SLC-type source, a thick high-Z (such as tungsten) target is used both for the generation of high-energy photons (via bremsstrahlung radiation) and for their conversion into $e^{\pm}$ pairs. In a wiggler-based source the high-energy photons are generated in a wiggler or undulator using a primary electron beam with an energy in excess of 150 GeV, and positron production is then accomplished in a thin target. In an SLC-type source, thermal stress in the conversion target due to the impact of a single drive beam pulse imposes a practical limit on the obtainable positron beam pulse intensity. This difficulty is greatly mitigated in a wiggler-based positron source.

In addition, R&D is in progress to develop a new type of positron source using 2 to 10 GeV electrons channeling through a thin single crystal to produce the high-energy photons.

Regardless of the positron source type, the phase space of the positrons generated at the target is in general characterized by broad transverse and longitudinal momentum distributions but narrow phase and transverse position distributions. On the other hand, the optics of the positron capture system, i.e., a high-gradient accelerating section embedded in a uniform solenoidal field, is characterized by a large transverse position acceptance but a small transverse momentum acceptance. For optimum capture efficiency, therefore, a phase space matching device must be used to match the phase space of the positron beam emerging from the target to the acceptance of the capture optics. Both the positron yield and the energy spread of the captured beam are strongly dependent on the phase space transformer. The broad-band Adiabatic Matching Device (AMD) is the design of choice among the various proposals, with the exception of VLEPP for which a lithium lens design has been proposed. A lithium lens has been in operation at BINP since 1970.

Conventional positron sources similar to the SLC source

The SLC positron source has operated very reliably since 1991 over extended periods of physics runs. As the most intense positron source in the world, it may be used as a basis for positron source design for future linear colliders. The SLC source uses a 30 GeV single-bunch drive electron beam with an intensity of 3-5$\times 10^{10}$ electrons/bunch to produce positrons from a $W_{75}Re_{25}$ target with a thickness of 6 radiation lengths (X_0). Its capture system includes an adiabatic matching device and a high-gradient S-band section with an aperture of 18 mm diameter embedded in a 0.5 T uniform-field solenoid. The positron yield after capture downstream of the target is typically 4 per drive electron. After 180° turn-around and energy analysis, it is reduced to 2.5 positrons at 200 MeV within a $\pm 5\%$ energy spread. SLC-type positron sources have been proposed for JLC, NLC and CLIC.

In the proposals for these three linear colliders, the energy of the drive electron beam ranges from a few GeV to 10 GeV, while the target thickness ranges from 4 to 6 radiation lengths. In order to meet the positron beam intensity requirements for the respective linear colliders, which are more than an order of magnitude higher than that of the SLC, both the drive beam power and the capture efficiency must be increased over those of the SLC positron source. Since excessive thermal stress in the target caused by single-pulse beam heating may lead to target failure, the size of the drive beam incident on the target must be sufficiently large to keep the single-pulse beam energy density below the material failure threshold. For a $W_{75}Re_{25}$ target, the failure threshold has been determined at SLAC to be about

$$\rho_{th} = \frac{N_{e^-} E_{e^-}}{\pi \sigma^2} = 2.0 \times 10^{12} \quad \frac{\text{GeV}}{\text{mm}^2}$$

with about 20% of the beam energy deposited in the target. In practice, as stated in the various designs, it is wise to keep the deposited energy density in the target comfortably below this threshold, e.g., $\sim 60\%$. To satisfy this criterion, the rms spot size of the drive beam on the target for the proposed SLC-type sources ranges from 3 to 8 mm^2. The cumulative effect of thermal stress build-up due to successive multiple beam pulse impacts is minimized by adopting a rotating target design such that the areas of successive beam pulse impacts are adequately separated.

The AMD used for transverse phase space matching is comprised of a pulsed flux concentrator embedded in a DC tapered-field solenoid. The ideal profile of the longitudinal field profile along the axis in the AMD should be

$$B(z) = \frac{B_i}{1 + g \cdot z}$$

where B_i is the initial (maximum) field and g is the taper parameter, typically in the range of 30-60 m^{-1}. Strictly speaking, the condition for adiabatic transformation only holds for particles of energies below ≈10 MeV. Particles with higher energies experience a non-adiabatic field, leading to a decrease in the transverse momentum acceptance for such high energy particles and hence particle losses. Further beam losses also occur as a result of bunch lengthening due to path length differences in the AMD and the capture accelerator, and velocity differences for positrons of varying transverse and longitudinal momenta. Increased capture efficiency may be achieved by increasing the aperture of the high-gradient section and by increasing the magnetic field in the AMD and in the capture section. The NLC positron source design uses an L-band capture accelerator with a 40 mm diameter aperture, more than twice that of the SLC source, yielding an invariant transverse phase-space acceptance of 0.06 m-rad. On the other hand, the proposed JLC source retains the S-band design but with an enlarged aperture and increased magnetic fields. The designs for the JLC, NLC and CLIC sources have allowed at least a factor of 2 safety margin in the positron beam intensity after the capture section to make up for unforseeable downstream beam losses.

In the SLC-type positron sources, by limiting the drive beam pulse energy density on the target below the material failure threshold, increased positron production can be realized only by increasing the drive beam size, which results in a proportional increase of the transverse phase space volume of the emerging positrons. This leads to a captured high intensity positron beam with a larger transverse emittance. The optics of a damping ring designed to yield an invariant equilibrium vertical emittance of about 5×10^{-8} m-rad within the time limit given by the repetition frequency of the collider and the number of simultaneously stored beam pulses dictates that the dynamic acceptance of the ring be typically limited to $\sim$ 0.01 m-rad. The emittance of the positron beam produced by the SLC-type sources is then simply too large for such a damping ring. Therefore, the use of a pre-damping ring to reduce the tranverse beam emittance of the positron beam prior to its injection into the main damping ring has been proposed. The pre-damping ring is characterized by a large dynamic aperture, a short damping time, and an intermediate equilibrium emittance. In this scheme, the total time for emittance damping is also doubled.

Positron sources based on radiation from wigglers or crystal channeling

The SLC-type approach to positron production is characterized by a high-powered drive beam impacting a thick target which must absorb a significant fraction of the beam power. If the requirement on the positron beam intensity is of an order of magnitude higher than for JLC and NLC, i.e., TESLA or SBLC, this approach becomes unfeasible because of the engineering difficulty of cooling the target and the difficulty of efficiently collecting positrons from a large-size drive beam. Thus, positron sources based on wiggler radiation have been proposed instead for TESLA and SBLC. In the wiggler scheme, photons generated from a high-energy electron beam, typically ≥150 GeV, passing through an undulator, produce

positrons by pair production in a thin target. The use of a helical undulator also provides the possibility for producing polarized positrons as well as electrons.

In the channeling scheme, photons generated from electrons with energies in the range of 2 to 10 GeV traveling through an appropriate crystal produce positrons in a thin amorphous target. This scheme could be applied to JLC, NLC or CLIC.

Wigglers and Undulators

The basic principle is to use a wiggler to generate an intense photon beam from a high-energy ($\geq$150 GeV) electron beam. The beam of the main linac can be used before or after collisions for the production of photons in a wiggler section. After collision, the emittance of the primary beam is distorted because of beamstrahlung and a special matching optics is required to capture a high fraction of particles ($\sim$ 70 %). This problem is avoided if the beam is used before interaction. However, the effect of the wiggler on the emittance of the primary beam has to be investigated in more detail. In the wiggler, photons with a mean energy of $\sim$ 20 MeV are emitted in a cone of angle $1/\gamma$ along the forward direction. The photons are then converted into $e^{\pm}$ pairs inside a very thin target (<1 X_0), while the primary electrons leaving the wiggler are deflected by a dipole magnet. Thus, thermal stress problems in the conversion target are reduced. In addition, since the conversion efficiency is to first order independent of the material, it is possible to use low Z materials which in general have a higher heat capacity (Dulong-Petit rule). The positron yield of titanium is only about 16% lower than tungsten if a target of 0.4 X_0 is considered. The maximum allowable beam energy density inside the target is, however, up to an order of magnitude higher for a titanium alloy than for a tungsten alloy. An additional advantage of the thin target is the reduction of multiple-scattering inside the target. As a result of the narrower transverse momentum distribution, the phase-space density of the emerging positrons is higher in the case of a thin target source. Finally the mean power deposition and the neutron production are also reduced in a source based on wiggler radiation.

For the capture and matching optics, TESLA and SBLC use an AMD phase space transformer. Because of the higher phase space density, the positron capture efficiency is increased by a factor of $\sim$ 5 compared to an SLC-type source with the same acceptance of the capture optics. The designs for TESLA and SBLC allow a factor of two safety margin in positron beam intensity after the capture section. Because of the relatively small emittance of the captured positron beam, a pre-damping ring is generally not required. For VLEPP, a lithium lens has been proposed to serve as the matching device.

Polarized positron sources

The physics potential of polarized positron beams is discussed in section 2.6. A polarized positron source is proposed for VLEPP, while TESLA and SBLC regard the polarized source as an option. For polarized positrons, a helical undulator has to be used to produce circularly polarized photons which are converted into longitudinally polarized positrons in the target. In order to take care of all processes, polarization states have been included into the Monte Carlo code EGS4. The emittance requirements of the incoming electron beam are much tighter than in the case of unpolarized sources. Hence the electron beam has to be used before the interaction point. Simulations show that a polarization of up to 70% can be achieved with a helical undulator of about 1 cm period length and 1T field strength. The total length of the undulator has to be about 150m. However, if polarization is not required,

the undulator may be shorter and the angular separation is less stringent. The technical and operational feasability of a helical undulator with these parameters has to be proven.

Crystal channeling

In this scheme the high energy photons are produced by electrons (with energies on the order of 2 to 10 GeV) channeling through a single crystal: the photons are generated by the existence of periodic atomic potentials in the crystal. Both the crystal and the conversion target are thin, ensuring that the thermal loads are minimum. The emerging positron beam retains the characteristics of a narrow transverse momentum distribution and hence a high phase-space density. For this approach to work, the angle of incidence, or the angle between the beam direction and the direction of the atomic rows in the crystal along which electron channeling is expected to occur, must be smaller than a critical angle given by:

$$\theta_e = \sqrt{\frac{2V_0}{E_0}}$$

where E_0 is the particle energy and V_0 is the depth of the potential well. In addition, the electron beam divergence also needs to be smaller than θ_e. Coherent pair production in crystals using high energy photon beams (150 GeV) has already been measured at CERN with a Germanium crystal orientated on its $\ll 110 \gamma\gamma$ axis. However, more R&D is necessary to establish the feasibility of this approach and the survivability of the crystal over a reasonable period of use.

Current status

The important parameters for the positron sources are summarized in Table 2.1.2. As a reference, the parameters of the existing SLC positron source are also included.

The present status of the positron production for the various linear colliders is given below.

TESLA

The positron source is based on radiation from a wiggler. The primary beam is the high energy electron beam emerging after the collision point.[1] The emittances are therefore distorted because of beamstrahlung, and special optics are required to capture ≈70% of the particles. The primary beam power is the highest among the various linear colliders. A fast rotating e^+ target will be built to increase the impact area on the target within each rf pulse. The required beam pulse is 800 μs and it will provide the greatest number of positrons per pulse of all the proposed machines. However, an rf multipulse SLED-system should be built in order to increase the gradient and reduce the Joule losses in the structure of the capture accelerator. No pre-damping ring is required for TESLA because of the assumed better source performance and the large acceptance of the damping ring. Positron polarization is regarded as an option. An auxilary positron source based on a conventional target and capture section is planned to test the system before the electron beam is available to make the positrons.

[1] Since the yield depends on the energy of the wiggled beam producing the photons, it should be noted that this yield will be quite low for energies below 100 GeV.

Table 2.1.2
Positron source parameters for various linear collider projects. SLC parameters are given as a reference.

	Unit	SLC	TESLA	SBLC	JLC-X	NLC	VLEPP	CLIC
Positron Source Type			wiggler/ undulator based	wiggler/ undulator based	SLC-type	SLC-type	wiggler/ undulator based	SLC-type
General Parameters								
Ne^+/pulse at IP	10^{10}	3–5	4120	362.5	53.6	58.5	20	0.8–8
No. of bunches per pulse		1	800	125	85	90	1	1–10
Pulse duration	μ s	$3 \cdot 10^{-6}$	800	2	0.119	0.126	NA	0.006
Bunch spacing	ns	–	1000	16	1.4	1.4	–	0.66
Repetition frequency	Hz	120	10	50	150	180	~ 150	2530-1210
Primary Beam								
Energy	GeV	30	≥ 150	≥ 150	10	3.11	150	2.15
Ne^-/pulse	10^{10}	3–5	4000	360	35	135	20	3.8–38
Beam power	kW	17–29	≥ 9613	≥ 4326	84	121	721	33–158
Linac frequency	MHz	2856	1300	2998	2856	2856	14000	1500
Wiggler length	m	–	35(≥ 150)	35(≥ 150)	–	–	~ 150	–
Wiggler period	cm	–	3.6(~ 1.2)	3.6(~ 1.2)	–	–	~ 1.0	–
Peak field	T	–	1.7(~ 0.9)	1.7(~ 0.9)	–	–	0.5	–
No. of photons per electron		–	~ 350	~ 350	–	–	100	–
Conversion Target								
Material		$W_{75}Re_{25}$	Ti alloy	Ti alloy	$W_{75}Re_{25}$	$W_{75}Re_{25}$	W, Hg	$W_{75}Re_{25}$
Thickness	χ_0	6.0	0.4	0.4	6.0	4	0.5	4.5
RMS spot size of drive beam	mm	0.8	0.7	0.7	1.2	1.6	1.0	1.0
Temperature rise per pulse	K	200–300	~ 800	~ 800	~ 220	~ 200	~ 200	~ 200
Mean deposited power	kW	4.2–6.0	14	5.9	~ 30	~ 10	0.2	9.9–47
Ne^+/pulse at exit	10^{10}	180–300	43700	3930	750	~ 800	60	20–200
Capture System								
Matching device		AMD*	AMD*	AMD*	AMD*	AMD*	Li-Lens	AMD*
Initial field	T	7.0	10	10	8.0	7.0	–	7.0
Taper parameter	m^{-1}	–	30	30	50	–	–	–
End field	T	0.5	0.62	0.62	0.8	0.5	–	0.5
Length	m	0.15	0.5	0.5	0.18	0.2	0.01	0.15
Wavelength of accel. RF	m	0.1	0.1	0.1	0.105	0.21	0.01	0.2
Minimum iris radius	mm	9.0	9.0	9.0	13	20	–	18.0
Gradient	MV/m	30	15	30	30	20	–	12
Pre-damping ring required		No	No	No	Yes	Yes	No	Yes
Ne^+/pulse at entrance of pre-damping ring	10^{10}	4.5–7.5	8000	720	108	144	50	0.9–9
Efficiency incl. dephasing	%	4	18	18	14	17	–	20
γA of pre-damping ring§	πm	0.01	0.012	0.012	0.027	0.09	0.1	0.34
Energy of pre-damping ring	GeV	1.15	4.0	3.15	1.98	2.0	3.0	2.15
Energy accept. of match. device	MeV	20	± 30	± 30	40	30	–	20
Polarization								
Degree of polarization	%	–	(70)	(70)	–	–	~ 75	–
Power consumption (up to DR)	MW		option	option				25

* adiabatic matching device
§ γA = normalized acceptance

SBLC

The positron source is based on wiggler radiation. Similarly to TESLA, the primary beam is the spent electron beam after the collision point[1] and therefore has the same constraints and advantages regarding energy. Polarized positrons with the use of a helical undulator are regarded as an option.

JLC

The positron source is of the SLC type. A dedicated 10 GeV e^- S-band linac to produce the positrons uses either a thermionic gun or an rf gun as a source. This is the only design that uses an S-band capture section and pre-accelerator among the SLC-type sources.

NLC

The positron source is of the SLC type. The primary beam comes from a dedicated 3–6 GeV S-band linac and the e^+ beam is accelerated in an L-band linac. In order to increase the reliability and maintainability of the positron source, two parallel positron production and capture systems are being proposed, which are set side-by-side in separate rooms adequately shielded from each other.

VLEPP

The positron source uses a helical undulator before the collision point. The design is made, from the beginning, for polarized positrons and electrons. It is the only linear collider designed to use a W or perhaps Hg target to produce positrons and a lithium lens, which is simply a lithium rod of about 1 cm in length, as the matching device. A field gradient of up to 1600 T/m and 100 kA current can be generated in the lithium rod, corresponding to a focal length of 0.4 cm for 20 MeV positrons. Electrons are defocused and hence the separation of positrons and electrons starts already in the lens. The small energy acceptance of the lithium lens is used for preliminary energy selection, which is essential for collecting highly polarized positrons. The primary beam is accelerated with an rf frequency of 14 GHz.

CLIC

The positron production is of the SLC type. However, the SLC yield must be improved by a factor 3. This seems achievable if the transverse acceptances of the capture optics are doubled and the longitudinal acceptance is increased by 50%. The use of an L-band capture linac and a pre-damping ring meet the increased acceptance requirements. The charge of $3.8 \times 10^{10} e^-$ per bunch at an energy of 2.15 GeV provides an energy density on the target of 1×10^{11} GeV/mm^2 which is well below the failure threshold. This assumption is made for a beam radius of σ=1 mm. In the case of multibunches, one can increase the beam size on the target.

2.1.4 The Steps to be Taken in the Next Three Years

Electron Sources

As we have seen earlier, there are still a number of problems that must be solved to upgrade today's sources to meet the full requirements of future linear colliders. These problems are considered below.

Thermionic guns and bunching systems

Most of the single bunch problems that come up with conventional thermionic guns and subharmonic bunching-type injectors have already been solved. The issues that must be

addressed in the next few years are mainly those related to the bunch train production at the gun and beam loading in the bunchers. DESY plans to address these issues in the SBLC injector this year as they near the completion of the test accelerator injector. At SLAC these issues will be addressed when the NLCTA is upgraded with a subharmonic bunching system identical to that proposed for the NLC. The beam loading issues in an S-band buncher will not be directly addressed by the NLCTA until later but lessons learned from the X-band accelerator and the DESY injector will be used to design the S-band buncher for the NLC. KEK plans to address the beam loading issues in the ATF injector during the next year or so.

Polarized electron guns and bunching systems

Except for TESLA which has a wide bunch spacing, one of the main issues to be addressed in the next few years is the problem of charge limitation in polarized electron cathodes. For example, for the NLC 500 GeV c.m. case, a 5 A bunch current will have to be generated in a train of 90 bunches with 1.4 ns spacing. The polarization will need to be at least 80%. Tests will include improving cathode quantum efficiency and lifetime by using a protective Arsenic coating, and exploring graduated doping techniques which might reduce relaxation times from 100 ns to 5 to 10 ns for the 80% polarized electron cathode.

The laser bunch train structure, the tunability of this train structure, and the stability of the intensity are also very important issues to be addressed.

RF guns

Entire rf gun systems are currently under development, be it with an unpolarized electron photocathode or, even more difficult, with a polarized photocathode. The issues to be explored are beam dynamics (including space charge, rf effects, beam loading and wakefields) to produce the low emittance beams possible with photocathode rf guns, treatment of the gun environment to produce the ultra-high vacuum environment necessary for the photocathodes and high gradients, the lifetime of photocathodes (polarized and unpolarized) in a high gradient environment, and reliable laser systems with less than 1% intensity fluctuations and flexible train structures. One of the interesting features that is currently being investigated at UCLA and Fermilab is the possibility of producing flat beams at the gun. A collaboration between SLAC and CERN is also beginning to test GaAs cathodes inside an rf gun.

Laser requirements

While none of the proposed linear collider injectors push the current state of the art in laser technology in any one parameter, they do call for a combination of parameters which will require some laser development. Wavelengths, peak and average powers needed for these sources are readily available, but the specific and sometimes elaborate pulse timing requirements will result in fairly complex systems. Intensity and mode structure issues will have to be addressed. Most linear collider guns require a current stability of less than 1% RMS, and clean Gaussian or "top hat" transverse profiles. These features will place additional demands on the associated laser systems.

An additional issue is the required reliability of the laser systems. A linear collider laser should operate with $> 99\%$ of scheduled uptime. Some simple commercial lasers can meet this requirement, but it is difficult for complex lasers. The SLAC source lasers (which are somewhat less complex than most of the designs here) have met this goal, but only after

considerable development time. It may be desirable to have two independent source laser systems in order to provide the required system uptime.

It is difficult to estimate the cost and development time required for these systems without a detailed design. A rough guess would be that these systems will all have hardware costs within a factor of 2 of a million US dollars, and require three to five years of development time.

Future developments in laser technology may have some impact on these systems. In particular, the pump lasers may be replaced by diode-pumped solid state lasers, resulting in a significant reduction in system size, and possibly cost. At the present time, however, commercial diode pumped systems are more expensive than conventional lasers. New laser materials could also simplify the laser designs. At the present time, however, there are no promising alternatives to Ti:Sapphire for high repetition rate, tunable or short pulse operation.

Although the source laser probably represents a modest technological challenge, in comparison to the rest of a linear collider laser system designers should expect a significant development time.

Positron Sources

Most of the parameters listed in Table 2.1.2 are based on judicial choices or extensive numerical simulations. A guiding principle behind all these designs is that the parameters should all be achievable using existing technologies. R&D efforts in the areas outlined in the following paragraphs should greatly enhance the current designs.

- Conventional positron sources similar to the SLC source.

  The SLAC test on target material failure due to single beam pulse impact was conducted for a single target thickness ($\sim 5.4X_0$) and a single drive beam energy ($\sim$ 22 GeV). The JLC, NLC and CLIC positron source designs all rely on extrapolating from this one data point in a large two-dimensional parameter space constituted by beam energy and target thickness, which ranges from 2 to 10 GeV and from 4 to 6 X_0, respectively. Since the reliability of such an extrapolation is questionable, it is highly desirable to perform a more exhaustive target failure test within the parameter range of the various designs.

  For NLC, high-power L-band klystrons and a mechanism to seal the rotating target shaft need to be developed, the latter also applicable to JLC. For JLC, NLC and CLIC, positron source maintenance, which directly affects operating efficiency, is a challenging problem because of the very high radiation levels in the positron production area and capture section. The two-source design for NLC should significantly improve the serviceability of each source. Compared with the electron beam, the intensity jitter of the positron beam is likely to be much more difficult to control. A careful analysis of this problem is needed. Engineering experience will be gained from the ATF positron source which is under construction at KEK.

- Positron sources based on radiation from wigglers/undulators.

The technical and operational feasibility of long helical undulators is one of the major questions for polarized positron sources. The beam transport through the undulator and emittances at the undulator exit need careful investigation through simulations and experiments. Also, the stability of a source driven by the spent electron beam has to be investigated in more detail, since in this case the drive beam intensity is affected by the quality of the beam-beam interaction. Finally, the target material failure for a low Z titanium alloy target has not been determined experimentally. Even if a high safety margin on this limit has been included in the designs for TESLA and SBLC, it would be highly desirable to perform failure tests with low Z materials in order to determine the stress limit more accurately. This would also be useful for the design of other linear collider components like scrapers and dumps. Operational issues will be adressed in the various high energy accelerator laboratories.

The principles of polarized positron sources will be investigated by a Compton backscattering experiment at KEK.

The realization of a single crystal capable of withstanding the high power beam without damage to the crystalline structure will be investigated at SLAC. The performances of positron production with such crystals will be evaluated at SLAC and at CERN.

Pre-Accelerators

All the machines have pre-accelerators or so-called pre-linacs, generally located between their sources and their damping rings, and in some cases between their damping rings and their main linacs. The energies of these pre-accelerators are between roughly 2 and 10 GeV. Their designs are just being developed. In most cases, they operate at L-band ($\approx$1.4 GHz) or at S-band ($\approx$3 GHz) and they have bunch compressors of the same rf frequency located just upstream or downstream of them (see machine schematic diagrams in Chapter 1).

It is too early to describe these pre-accelerators in detail but a few generic issues can be brought up here. For example, the NLC complex has six S-band linacs and 3 L-band linacs (see Fig. 1.8). The main L-band linac accelerates the positron beam from the positron target to 2 GeV where it enters the predamping ring. In addition there are two 134 MeV L-band linacs associated with the electron and positron first-stage compressors at the output of the two damping rings. These linacs are run in phase quadrature with the beam to introduce the linear correlation between time and energy within each bunch which is required for compression. The six S-band linacs are the following:

1. The positron drive linac which accelerates the electrons which strike the positron target;

2. The electron booster linac which accelerates the electron beam to 2 GeV where it enters the electron damping ring;

3. and 4. The electron and positron pre-accelerators which accelerate the beams from the damping rings to 10 GeV where the second bunch compression occurs;

5. and 6. The 2 GeV S-band linacs to produce the linear energy correlation required for each of the second-stage compressors.

These linacs share enough common characteristics and design problems that it is appropriate to discuss their rf design together in this section. The principal design issues are beam loading and dipole wakefields. Except for the first 200 MeV portion of the positron L-band linac which is inside a 0.5 T solenoid, all of these linacs must be capable of accelerating about 2-ampere beams with about 100 ns macropulse length. The part of the positron L-band linac inside the solenoid needs to accelerate a total effective current of about 5.5 amperes since both electrons and positrons get captured and drift on to their respective accelerating crests, $\lambda/2$ apart. Because the electrons are produced by ionization as well as by pair production, there are about 25% more electrons than positrons.

All of these linacs are fairly heavily loaded by a beam with a pulse length much shorter than the filling times of the structures which in turn are shorter than the ringing time, $2Q/\omega$, of the structures. In this situation, the energy of the beam will drop approximately linearly with time during the pulse as a result of beam loading. For this case, there are two natural choices for beam loading compensation: 1. Δ-t (or early injection), i.e., injecting the beam into the structure before the structure is full; 2. Δ-f, i.e., having one or more accelerator structures running at a frequency 1 to 2 MHz above or below the nominal frequency and roughly in phase quadrature with the accelerating phase. Thus the beginning of the pulse can be decelerated by the off-frequency-section(s), while the end of the pulse is accelerated. The advantage of Δ-t compensation is that the compensation occurs in every accelerator section, so that the energy spread can be narrow throughout the linac, thus minimizing emittance growth from dispersion and chromatic effects. The disadvantage of early injection is that the compensation requires a particular structure filling time which is typically shorter than would be chosen for optimizing the use of rf power, and so in general it can require more rf power than the Δ-f technique. The disadvantage of the Δ-f technique is that two more types of accelerator structures need to be designed and constructed, one tuned for $^{-}\Delta$-f and one for $^{+}\Delta$-f.

The S-band accelerator sections will be detuned by about 10% in a Gaussian density distribution to diminish the effect of dipole wakefields. This will cause the structure to be what might be called "over constant-gradient," i.e., the gradient rises from the input to the output. Damping will also be desirable.

The JLC(X) pre-accelerators will be comprised of 3 m long S-band accelerator sections driven in pairs by 85 MW x 4.5 microsecond klystrons with 2-iris SLED pulse compression. This combination will achieve 50 MeV/m unloaded gradient, 40 MeV/m loaded in 3 m-long Shintake choke-mode structures. Beam loading compensation will use the Δ-f technique. The linacs will be about 300 m long and will have 34 klystrons each.

Finally, it should also be mentioned that between the pre-accelerators and damping rings, it may be desirable to install rf debunchers which improve the injection process into the rings by decreasing the incoming bunch energy spread and by lengthening the bunch length. Such a device was installed in the SLC injection line to the positron damping ring with some measure of success.

2.1.5 Summary and Comparisons

Electron sources

Unpolarized electrons

For unpolarized electrons, conventional thermionic guns with appropriate bunching systems are available at the present time. RF guns with relatively robust cathodes are planned for the TESLA and CLIC colliders.

SBLC will use a DC gridded gun with the desired time structure. The pulser for this gun has already been constructed. JLC is working towards achieving the 714 MHz bunch separation with their gun pulser.

Polarized electrons

For polarized electrons, photocathodes with conventional DC guns are proposed for JLC and NLC. Many of the polarized source problems have been solved and reliable operation has been established at SLAC. The main difficulty in using polarized sources for NLC and JLC is the ability to sustain the 4 to 6 Ampere peak current from the cathodes for a bunch train of duration greater than 100 ns. Present cathode development shows that we are about a factor of 5 away from producing the required charge for the NLC gun because of the charge limiting phenomenon observed on the GaAs cathodes. A further challenge will be to operate rf guns with polarized cathodes. Aggressive R&D programs are required to develop all these sources and to show that they can be operated reliably.

Lasers

The lasers to drive the polarized or unpolarized sources use conventional components available with today's technology. However, these laser systems tend to be complex, requiring feedback and feedforward systems to attain the required intensity stability and operational reliability. In addition, the lasers for rf guns have to meet extra requirements for their broadband pulse trains. The most difficult problem for the lasers for most linear collider designs is the less than 1% RMS intensity jitter tolerance which is at the limit of today's technology.

Positron sources

Conventional positron sources similar to the SLC source

JLC, NLC and CLIC will have SLC-type positron sources driven by dedicated electron beams from linacs. The JLC positrons will be captured with a similar S-band linac whereas the NLC and CLIC positrons will be captured by L-band linacs for increased acceptance and capture efficiency. These positron sources require further study and development, in particular in the area of target technology.

Positron sources based on radiation from wigglers or undulators

TESLA and SBLC plan to pass their spent beams (i.e., at the exit of their IR's) through wigglers or undulators to produce γ's which in turn will generate the proper trains of positrons through interaction with a thin target. TESLA may obtain polarized positrons, as a possible option. VLEPP will use a helical undulator before the collision point to produce polarized positrons. These sources are based on a promising scheme which, however, has not yet been demonstrated for collider operation.

2.2 DAMPING and COMPRESSION SYSTEMS

2.2.1 The Group

J. Rossbach,(Chairman)
DESY, Notkestrasse 85, 22603 Hamburg, Germany. E-mail: H02ROB@dsyibm.desy.de
J. Urakawa,(Deputy Chairman)
KEK, 1-1 Oho, Tsukuba-Shi, Ibaraki-ken 305, Japan. E-mail: URAKAWA@kekvax.kek.jp
S. Chattopadhyay
LBL, 1 Cyclotron Rd., MS 71-259, Berkeley, CA 94720, USA. E-mail: CHAPON@csa2.lbl.gov
A. Mikhailichenko
BINP, Pr. Lavrentyeva 11, 630090 Novosibirsk-90, Russia. E-mail: MIKHAIL@lns62.lns.cornell.edu
J.P. Potier
CERN, PS/LP, 1211 Geneva 23, Switzerland. E-mail: POTIER@cernvm.cern.ch
T. Raubenheimer
SLAC, 2575 Sand Hill Rd., Menlo Park, CA 94025, USA. E-mail: TOR@slac.stanford.edu

2.2.2 Overview

To achieve the desired luminosity, all the linear collider schemes need very small transverse and longitudinal beam emittances. Presently, there is no experimentally verified method of producing the desired (normalized) phase space densities directly at the electron or positron source. For electrons, it is conceivable that with vigorous R&D on laser driven photocathode rf guns, one may begin to reach the required phase space density, but the chances of success and required time scales are currently both uncertain. Thus, a mechanism is required that overcomes Liouville's Theorem. This theorem states that the normalized phase space density cannot be increased in isolated, non-interacting Hamiltonian systems. The solution proposed by all the collider schemes is to use radiation damping in a storage ring. In a damping ring, the two primary parameters are the equilibrium emittance and the damping times. These are determined by the ring energy, the magnet lattice, and the mechanical tolerances. Beyond an energy of 1 GeV or so, the various scattering mechanisms within a high density beam lead to negligible emittance blow up. However, some schemes come close to these limits. The typical emittance values are comparable to those attained in the third generation synchrotron light sources but the required damping times are considerably shorter.

There is agreement that, in order to stay within reasonable beam-beam interaction parameters, all schemes need flat beams, i.e. $\varepsilon_y << \varepsilon_x$. Since decreasing the vertical emittance ε_y is one of the few ways to increase luminosity without increasing beamstrahlung energy losses, one should, at least in principle, reduce ε_y until it is limited by intra-beam scattering, by the natural opening angle of synchrotron radiation, or by vertical disruption during beam-beam interaction. Actually, in the 500 GeV c.m. collider designs, tolerance considerations in both the main linac and damping rings lead to considerably larger values of ε_y.

While it is likely that the required transverse emittance values can be achieved with storage ring designs at least comparable with existing machines, the equilibrium bunch length has to be further compressed after extraction from the damping ring. The reason is that generation of a bunch length below a few millimeters in a storage ring would require installation

of extremely high rf voltages and would ultimately be limited by the microwave instability.

The proposed bunch compressors consist of an rf system that generates a correlated energy distribution along the bunch and a subsequent bending section with a nonzero momentum compaction described by the R_{56} matrix element. In a compressor, the bunch length is compressed while the uncorrelated energy width is increased, according to Liouville's Theorem applied to longitudinal phase space. Transverse and longitudinal emittance growth occurs because of higher order dispersion and nonlinear chromaticity if the energy spread after the bunch compressor exceeds a few percent. Thus, the large compression factor, needed for those collider designs with bunch lengths in the 100 micron range, would be difficult if not impossible to achieve just after the damping ring. One proposed solution is a two-stage compressor: after a moderate compression at the exit of the damping rings, the beam is accelerated to above 10 GeV, thereby reducing the fractional energy width. At this point, the final compression is performed. The inherent complication with this solution is that the emittance growth due to synchrotron radiation increases rapidly with beam energy. To avoid this problem, the compressor length must be increased.

Another problem that must be addressed is the compensation of bunch-to-bunch phase offsets induced by beam loading in the damping rings and the compressor rf sections. If not corrected, these phase errors become energy errors at the end of the linac. Ideally, a "90°" compressor (i.e. $R_{55} = 0, R_{56} \neq 0$) provides this compensation, although the nonlinearities degrade the performance for large compression factors. A second-stage compressor of the same type, however, again transforms momentum errors into phase errors. Thus, a second-stage compressor must provide $R_{55} \neq 0, R_{56} = 0$ (i.e. a longitudinal telescope) which is technically more difficult.

It is obvious that the phase offset compensation becomes more demanding with both increasing rf frequency and decreasing bunch length in the main linac. It is helpful, however, that the phase offsets are demagnified along with the bunch length.

2.2.3 Where We are Today

Damping Rings

Parameter lists of the present damping ring designs are given in Table 2.2.1. Electron and positron rings are assumed to be identical in the respective designs. Therefore, they are represented only once ($e^{\pm}$) in the table. Since the acceptance and damping requirements in the positron system will always be more demanding, it is possible that the parameters of the electron damping rings may be relaxed compared to the values quoted in the table. In addition, the requirements on the electron rings could be further relaxed if an rf gun (giving polarized electrons when necessary) could be used as the electron source.

It should be noted that none of the existing storage rings operate at present at the normalized phase space densities quoted in Table 2.2.1. To achieve both the horizontal emittance values and the short damping times simultaneously, very strong focusing is required. Consequently, the rings tend to have severe dynamical acceptance limitations. Similarly, in the vertical plane, very tight mechanical tolerances are required to minimize coupling and spurious dispersion. While it is true that emittance ratios ($\varepsilon_y/\varepsilon_x$) below 1% have routinely been achieved in several storage rings, one should be aware that at very small ε_y values, the critical parameter which matters is not the coupling nor the emittance ratio, but the

absolute level of alignment.

Because of high bunch charge and small beam dimensions, single bunch instabilities are an issue for damping rings. As a figure of merit, a longitudinal impedance threshold $(Z/n)_{thresh}$ given by

$$(Z/n)_{thresh} = \frac{(2\pi)^{3/2} E \sigma_\epsilon^2 \sigma_z \alpha}{N e^2 c} \mathcal{F}$$

has been included in the parameter list.

As a conservative assumption for the form factor, $\mathcal{F} = 1$ has been used. While the validity of this formula may be doubted by many experts, it might at least serve as a conservative first estimate until more detailed investigations are performed. Of course, using the value (Z/n) to compare rings with very different circumferences could be misleading since a large ring would have a larger vacuum chamber and fewer obstacles (contributing to the impedance) per meter length (see LEP experience).

In Table 2.2.1 on the damping rings we have included the Touschek lifetime. Although this lifetime is much longer than the envisaged beam storage time in the damping ring, it may impose constraints on the commissioning procedure.

Because of its comparatively large design emittances, TESLA is the only LC scheme which might use direct injection from an rf gun instead of an electron damping ring. However, an appropriate rf gun which can produce polarized electrons has not yet been designed. For the TESLA damping ring, the main challenge is to compress the 240 km long bunch train, to accommodate as many as 800 bunches in the damping ring and, after damping, to expand the train again. Two damping ring alternatives are considered: an unconventional "ring" fitting into the main linac tunnel (except for small loops at the ends) called the "dog-bone" ring, and a big circular ring of the size of HERA.

At this time, for the dog-bone ring, a magnet lattice design is available. For that lattice, linear optics and dynamic acceptance values meet the requirements. The vertical emittance is smaller than required even in the presence of substantial misalignment errors.

A rough estimate shows that the required parameters for the big circular ring solution can also be met. The primary problem stems from the need for very fast injection/extraction kickers (<25 ns rise time) that must operate at 1 MHz. A system similar to the one proposed for CLIC might be useful. In addition, the big ring seems to be more expensive than the dog-bone scheme, if a circular tunnel of appropriate size is not already available; the size is comparable to the HERA or TEVATRON tunnels.

The SBLC damping ring has been investigated in some detail. It was shown that using a modified Chasman-Green (C-G) lattice, the dynamic acceptance is sufficient, even in the presence of substantial misalignment errors, and the vertical emittance is still ten times smaller than required. No intensity limiting effects have been studied yet. However, since the design σ_z^* at the IP is 0.5 mm and the rf frequency is low, one could tolerate a longer bunch in the damping ring than indicated in Table 2.2.1 (e.g., $\sigma_z > 10$ mm).

Since a conventional positron source needs a large damping ring acceptance compared to that of a wiggler based source, NLC, JLC and CLIC need a "pre-damping ring" (see section 2.2.1). This ring has large acceptance to collect the positron "cone" and provides some initial damping – typically damping the injected positron emittance to the level of the corresponding injected electron emittance and thereby allowing identical electron and positron main damping rings. Because of moderate focusing, a larger dynamic acceptance is achieved at

the expense of larger equilibrium emittances. Damping is nevertheless sufficient to result in emittances that can easily be injected into the main damping ring. Most limitations in the pre-damping rings are less important than in the main damping rings. The three primary issues are the dynamic aperture, which must be very large, the injection/extraction kickers, which must provide large deflections (although the stability tolerances are looser than in the main rings), and the extra costs for installation and operation.

As seen in Table 2.2.1, the NLC and JLC main damping rings are quite similar. Optics designs are fairly advanced for both of them. As very small vertical emittance values are mandatory for NLC and JLC, techniques for alignment, control, and compensation of magnet misalignments will be essential. The respective tolerances are close to the present state of the art and will be reached using beam-based techniques. Therefore, the results of the Accelerator Test Facility (ATF), currently under construction at KEK, will supply invaluable information on the feasibility of these parameters. In addition, since the ATF parameters are very close to the required NLC and JLC parameters, a careful investigation of the ATF longitudinal impedance threshold can be used to verify the vacuum chamber design. For the JLC and NLC damping rings, the Intra-Beam Scattering (IBS) has been investigated in detail and the effects are not thought to be severe.

For VLEPP-type single bunch colliders, only three (however intense) bunches have to be stored, and a long bunch length would be tolerable. Tolerances and instability considerations have not yet been worked out. The choice of the vertical emittance is based on the limits given by IBS considerations. In view of the resulting design parameters, the vertical magnet alignment tolerance is expected to be severe.

The CLIC scheme is very special because it has to serve a very high linac repetition rate, *and* very small emittances (see Fig. 1.17). The proposed solution is to damp simultaneously 50 or 150 bunch trains where each train consists of 10 bunches or a single bunch, respectively. These trains must be injected and extracted by a very fast kicker system involving a pair of rf transverse deflectors (effective rise time <6.5 ns). In order to cope with the multibunch scheme with bunch-to-bunch spacing as small as 20 cm, the rf frequency is chosen to be 1.5 GHz. It appears that this makes the goal of achieving the ambitiously low longitudinal impedance even more difficult. For short bunches, it is expected that the bunch spectrum samples the high frequency capacitive component of the ring impedance significantly, thus compensating bunch lengthening effects caused by the low frequency inductive impedance component. This needs further investigation.

The damping ring lattice providing the very small desired emittance is sensitive to sextupole misalignments as in the JLC and NLC rings. The normalized horizontal emittance $\gamma\varepsilon_x$ is 20 % below the design value at the IP in order to take into account dilution in the main linac due to strong wakefields. Whether this is adequate should be addressed in section 2.4 .

Multibunch instabilities will be an issue for *all* damping rings (even for those serving single bunch linacs). Numerical simulations involving higher order mode (HOM) damped cavities have been performed for NLC and JLC. Preliminary measurements of HOM damping in both a novel "choke mode" cavity (JLC) and the single-mode PEP-II cavities have shown good damping characteristics. Because of the small interbunch spacing, active feedback systems need wider bandwidth than existing systems, although the NLC and JLC requirements are close to the systems designed for PEP-II and the ALS. Only SBLC, TESLA and VLEPP

parameters are close to values of the operating HERA feedback. The HERA feedback, however, would not tolerate the enormous beam loading from a full bunch train injected within one turn.

Bunch Compressors

The main parameters of the bunch compressors for the various collider schemes are collected in Table 2.2.2.

Neither the TESLA nor the SBLC bunch compressor has been considered in detail. Because of the long design bunch length at the IP, both could use single stage compressors with comparatively moderate parameters. Also, as the linac rf frequency is not very much larger than the damping ring rf frequency, beam loading phase offsets might be comparatively easy to compensate.

For NLC a two-stage system has been designed and investigated in detail. The first stage provides zero net bending and can be driven either by an S-band or by an L-band linac. The second stage (the longitudinal telescope, mentioned in section 2.2.2) consists of a 180° arc plus another linac section followed by a chicane. For the second-stage linac section, both X-band and S-band versions have been investigated. Table 2.2.2 presents only the lower frequency versions. They will be somewhat more expensive but allow looser tolerances. Alignment tolerances for quadrupoles and accelerating structures are still demanding. RF phase tolerances have not yet been specified. A scheme to compensate the beam loading of compressor cavities (necessary for JLC, NLC and, maybe, SBLC) has been discussed but needs further study. Emittance dilution from systematic effects (higher order dispersion, chromaticity) is small.

For JLC, a system similar to that for the NLC has been investigated, but the present design favors a single stage scheme. It is considered less complicated and less expensive. Since it does not comprise any net bend, a feedforward system stabilizing bunch-to-bunch offsets cannot be installed. Emittance dilution due to the large energy spread and large space charge forces at the exit of the compressor will be severe. This problem has not yet been investigated.

A VLEPP bunch compressor scheme is still under consideration. Space charge may require that the final compression be done at higher than 3 GeV beam energy. The main complication might arise from cavity alignment tolerances on a account of high bunch charge.

Because of its high repetition rate, CLIC proposes to use superconducting linacs in the injector complex. To save cost, a tricky system has been devised that allows to use the same linacs for both electrons and positrons. Tolerances on alignment, field stability and phase errors have not yet been specified. They may be very tight because of the many bends and optics involved (i.e., four isochronous recirculations) and because of the very high frequency in the main linac.

2.2.4 The Steps to be Taken in the Next Three Years

The following list of tasks focuses on those issues which might be critical for the respective linear collider schemes. Of course, many more details have to be considered for any realistic design. Potential trapped ions and vacuum issues are generic to all damping rings and require attention. Some of these problems will be studied at the ATF at KEK and the ALS at LBL.

Table 2.2.1

Parameters for Damping Rings

		TESLA		SBLC	JLC		NLC		VLEPP	CLIC	
		dog-bone	big ring	$e^{\pm}$ d.r.	e^{+}pre-d.r.	$e^{\pm}$ main d.r.	e^{+}pre-d.r.	$e^{\pm}$ main d.r.	$e^{\pm}$ d.r.	e^{+}coll.d.r.	$e^{\pm}$ main d.r.
Energy	GeV	4.0	6	3.15	1.98	1.98	2.	2.	3.	2.15	2.15
Circumference	m	18600	6336	650	63.	222.5	114	223	160.	112***	283***
<I>	mA	103	303	268	726	410	410	410	180	260	226-758**
ν_x, ν_y		54.86,54.71	61.16,62.28	43.18, 27.29	11.6, 5.2	24.7,13.6	10.18, 4.18	23.81, 8.62	15.74, 15.68	11.4,3.2	31.2, 13.4
$\gamma\epsilon_x$, $\gamma\epsilon_y$	$10^{-6}\pi$m	14., < 0.8	20, 1*	4.1,0.05	48., 48.	2.7,0.04	25, 25	2.9, 0.02	45.5, 0.05 ?	64,1.5	2.5,0.04*
L_{Wigg}	m	380	90	84	0	100	0	26	0 ?	0	0
σ_ϵ	10^{-3}	1.1	1.4	1.15	0.72	0.91	1.	0.9	1.6	0.98	0.83
σ_z	mm	9	11	3.7	11.	4.8	7.0	4.1	9.8	4.6	1.8
τ_x, τ_y	ms	19.1, 19.1	20, 20	3.83, 3.83	2.4	6.1, 8.0	3.4, 3.4	4.1, 4.6	1.8, 2.9	2.7,2.7	10.5,10.5
$\mathcal{J}_x$		1	1	1	1.	1.3 ?	1.34	1.15	1.6 ?	1.	1.
α		0.00029	0.0003	0.00017	0.011	0.00098	0.005	0.0005	0.0013 ?	0.0043	0.00022
V_{rf}	MV	40	20	5	2.0	1.1	1.5	1.0	1.5	1.5	1.
f_{rf}	MHz	500	500	500	714	714	714	714	700	1500	1500
Momentum aperture		0.012	0.012	0.028	0.017	0.019	0.015	0.02	0.011	0.01	0.021
Lattice Type		FODO	FODO	C-G	FODO	FOBDO	FOOF	TME	FOBDO	FDBDF	FDBDF
p	nTorr	1 ?	1 ?	1 ?	1	1 ?	10	1	1 ?	1 ?	1 ?
γA_{dyn}	πm	0.03	0.05	>0.01	0.027	0.003	>0.1	>0.009	0.003	0.33*	0.016
σ_{BPM}	mm	0.1	?	0.1	0.1	0.1	0.1	0.1	?	0.025	0.025
$\sigma_{misalign.}$	mm	0.1	0.2	0.1	0.2	0.05	0.1	0.05	?	?	0.050
$\sigma_{stab.}$	mm	0.01	?	?	0.02	0.01	?	?	?	?	?
$(Z/n)_{thresh}$	Ω	0.045	0.14	0.028	2.34	0.145	2.8	0.14	0.16	1.5	0.02
$\tau_{Touschek}$	s	800	1300	160	2600	41	71000	400	30	71000	155
Total power per d.r.	MVA	≈ 15	≈ 10	≈ 10	3	5	?	8(?)	?	≈ 1.5	≈ 5

Table 2.2.1 Parameters for the damping rings. Normalized dynamic acceptance γA_{dyn} values and normalized vertical emittance $\gamma\epsilon_y$ refer to the rms sextupole misalignment $\sigma_{misalign.}$ quoted (orbit correction assumed) and to the respective rms quadrupole stability $\sigma_{stab.}$ over one day. Intra-Beam Scattering has not been included. The average currents <I> quoted in this table are based on the approximate assumption that there are no significant beam losses between the damping rings and the IP in any of these machines. $\tau_{Touschek}$ is a crude estimate of the Touschek lifetime.

For the JLC, there are three versions of the damping ring under discussion, depending on the choice of the linac frequency. We present only the S-band version because it might be the most demanding one with respect to Touschek lifetime and longitudinal impedance, and because differences are not very big.

* Indicates that tolerances have not yet been specified to achieve the respective value.

** Refers to 1 and 10 bunches, respectively.

*** Indicates that straight sections for cavities and injection/extraction are not included.

Table 2.2.2

Parameters for Bunch Compressors

		TESLA		SBLC	JLC	NLC		VLEPP	CLIC	
		dog-bone	big ring			1st stage	2nd stage		1st stage	2nd stage
Energy	GeV	4.	6.	3.15	2.	2.	10.	?	2.15	6.26
RF voltage	MV	200.	400.	150.	600.	134.	1300.	?	150.	1370.
RF frequency	GHz	1.3	1.3	3.	3.	1.4	2.8	?	1.5	1.5
Length	m	?	?	?	400	100.	300., 200.*	?	18.7	32.3
Bending field	T	?	?	?	0.89	1.4	0.4	?	0.29	0.33
Bending radius	m	?	?	?	7.4	4.8	80 m	?	25.	62.5
R_{56}	m	0.8	0.6	0.35	0.089	0.5	0.5, 0.1*	?	0.43	0.12
Entrance bunch length	mm	9.	11.	4.	5	6.	0.5	10.	1.8	0.48
Compression factor		9.	11.	8.	62.5	12.	5.	13.3	4.07	2.45
σ_ϵ at entrance	10^{-3}	1.1	1.4	1.2	0.9	1.	2.5	1.6	1.0	1.5
σ_ϵ at exit	10^{-3}	≈ 10	< 20	10.	56.	12.	12.5	22	4.1	3.6
δy_{mag}	μm	?	?	?	10.	17.	20.	?	?	?
δy_{acc}	μm	?	?	?	≈ 10	100.	4.	?	?	?
$\delta\phi$	deg	?	?	?	0.8	?	?	?	?	?
$\delta(\gamma\epsilon_x)$, $\delta(\gamma\epsilon_y)$	$10^{-6}\pi$m	?	?	?	0.03, 0.003	0.03, 0.0002	0.02, 0.0002	?, ?	0.0017	0.026,?

Table 2.2.2 Parameters for the bunch compressors. Note that the two-stage system for CLIC is foreseen to allow longitudinal bunch shaping in order to ease wakefield effects in the main linac.

δy_{mag}, δy_{acc}, and $\delta\phi$ represent the tolerances on vertical magnet alignment, accelerating structure alignment and rf phase stability, respectively. $\delta(\gamma\epsilon)$ is the normalized emittance growth in the compressor.

* Designates values for the arc and chicane components, respectively.

TESLA

- Optimization of damping ring lattices including tracking and alignment tolerances
- Detailed design of injection/extraction regions
- Development of rf gun to eliminate electron damping ring
- R&D on fast kickers operating at 1 MHz
- Studies of multibunch instabilities in the presence of transient beam loading and feedback
- Longitudinal impedance budget
- Investigation of intra-beam scattering
- Detailed design of bunch compressor, including tolerances
- Specification of commissioning and correction procedures

SBLC

- Detailed design of injection/extraction regions
- Studies of multibunch instabilities in the presence of transient beam loading and feedback
- Longitudinal impedance budget
- Investigation of intra-beam scattering
- Detailed design of bunch compressor, including tolerances
- Specification of commissioning and correction procedures

JLC

- Detailed design of injection/extraction regions
- Studies of multibunch instabilities in the presence of transient beam loading and feedback
- Specification of rf tolerances for compressor
- R&D on compensation of static phase offsets due to beam loading in the rings
- R&D to achieve tight alignment tolerances
- Studies of emittance dilution by a single-stage compressor
- Specification of commissioning and correction procedures

- *Results from the ATF under construction at KEK will provide answers to many of these questions*

NLC

- Detailed design of injection/extraction regions
- R&D on broad-band ring impedance to determine longitudinal microwave threshold
- Studies of multibunch instabilities in the presence of transient beam loading and feedback
- Specification of rf tolerances for compressor
- R&D on compensation of static phase offsets due to beam loading in the rings
- R&D to achieve tight alignment tolerances
- Study of required magnet stability
- Specification of commissioning and correction procedures
- *Results from the ATF under construction at KEK and the ALS at Berkeley will provide answers to many of these questions*

VLEPP

- Design of damping ring lattices including tracking and alignment tolerances
- Design of bunch compressor lattices including tracking and alignment tolerances, and space charge
- Studies on multibunch instabilities in the presence of transient beam loading and feedback
- Longitudinal impedance budget
- Specification of commissioning and correction procedures

CLIC

- Detailed design of injection/extraction regions
- R&D on very fast kickers and rf transverse deflectors
- Studies of multibunch instabilities in the presence of transient beam loading and feedback
- Longitudinal impedance budget
- Detailed investigation of intra-beam scattering
- Specification of commissioning and correction procedures
- Simulation of compressor including alignment, stability tolerances and rf phase errors

2.2.5 Summary and Comparisons

In the previous section we compiled a number of important topics which must be examined in the next few years in order to complete the designs of the respective damping and compression systems. In contrast, in this summary we attempt to tabulate the intrinsic challenges and difficulties associated with each machine. This is not easy because all linear collider designs are in varying stages of development and a number of issues have not yet been investigated, specially when straightforward solutions appeared to be available.

On the other hand, for this comparison to be fair, we cannot ignore a serious problem simply because it has not yet been considered. In any case, it is clear that the comparisons compiled in Table 2.2.3 are on a less solid basis than the information in the previous sections.

Since all damping rings have unusually small momentum compaction factors as a result of using low emittance lattices, it is possible that we may be entering a new regime of single bunch instability parameters. This problem needs careful attention and further work. Experiments at the ATF at KEK should be able to provide answers to these questions.

Table 2.2.3

Comparison of Damping Ring and Bunch Compression Issues, Challenges and Difficulties in the Respective Machines

Name	Description of Issue	Challenges and Difficulties
TESLA	Ring size	Large circumference: implications need to be studied
	Injection/extraction	Fast kickers at 1 MHz (especially for big circular ring)
	Vertical emittance	Alignment tolerances (to be checked)
	Multibunch instability	Broadband feedback, transient beam loading
SBLC	Multibunch instability	Broadband feedback, transient beam loading
	Microwave instability	Longitudinal impedance
JLC	Vertical emittance	Alignment tolerances, for single stage bunch compression: Large energy spread and space charge
	Longitudinal position	RF phase tolerances, beam loading compensation
	Multibunch instability	Broadband feedback, transient beam loading
	Microwave instability	Longitudinal impedance
NLC	Vertical emittance	Alignment tolerances
	Longitudinal position	RF phase tolerances, beam loading compensation
	Multibunch instability	Broadband feedback, transient beam loading
	Microwave instability	Longitudinal impedance
VLEPP	Vertical emittance	Magnet alignment tolerances
	Vertical emittance vs. wakes	Cavity alignment tolerances
CLIC	Vertical emittance	Alignment tolerances
	Injection/extraction	RF kickers
	Multibunch instability	Broadband feedback, transient beam loading
	Longitudinal position	Very tight rf phase tolerances, Beam loading compensation
	Microwave instability	Longitudinal impedance, high rf frequency
	Recirculation	Field stability, tolerances

2.3 LINAC TECHNOLOGY

2.3.1 The Group

P. Wilson, (Chairman)
SLAC/MS-26, P. O. Box 4349, Stanford, CA 94309. E-mail: PWILSON@slac.stanford.edu
N. Holtkamp, (Deputy Chairman)
DESY, Notkestr.85, D-22603 Hamburg, Germany. E-mail: MPYHOL@dsyibm.desy.de
D. Proch, (Deputy Chairman)
DESY, Notkestr. 85, D-22603 Hamburg, Germany. E-mail: PROCH@proch.desy.de
G. Caryotakis
SLAC/MS-33, P. O. Box 4349, Stanford, CA 94309. E-mail: CARYO@slac.stanford.edu
T. Higo
KEK, 1-1 Oho, Tsukuba-shi, Ibaraki-ken, 305 Japan. E-mail: HIGO@jpnkekvx.bitnet
H. Mizuno
KEK, 1-1 Oho, Tsukuba-shi, Ibaraki-ken, 305 Japan. E-mail: MIZUNO@jpnkekvx.bitnet
W. Namkung
Pohang Inst. of Sci. & Technology,P. O. Box 125, Pohang, Korea. E-mail: MHCHO@vision.postech.ac.kr
H. Padamsee
Laboratory of Nuclear Studies, Cornell University, Ithaca, NY 14853. E-mail: HSP@lns62.lns.cornell.edu
R. Palmer
Brookhaven National Laboratory, Upton, NY 11973. E-mail: PALMER@bnl.bitnet
N. Solyak
Branch Institute of Nuclear Physics, Protvino, Russia. E-mail: SOLYAK@vlepp.serpukov.su
G. Westenskow
Lawrence Livermore Laboratory, Livermore, CA 94550. E-mail: GW@llnl.gov
I. Wilson
CERN, CH-1211 Geneva 23, Switzerland. E-mail: WILSON@cernvm.bitnet

2.3.2 Overview

All of the linear collider designs under discussion here are based on the production and manipulation of rf power in the frequency range 1.3-30 GHz. The rf system itself must convert power from the ac mains (wall plug) to rf power at the input of the accelerating structure with the greatest possible efficiency. The design of the accelerating structure involves two factors: first, to establish the desired accelerating gradient with some fraction of the input rf power; and second, to transfer a reasonable fraction of this power to the beam.

In general, it is easier to attain a high accelerating gradient at a higher rf frequency. Breakdown field strengths increase with frequency, and the capture of so-called "dark current" has a threshold which also increases with rf frequency. The theoretical threshold gradients for the various collider projects are approximately: TESLA, 7 MV/m; SLC, 15 MV/m; SBLC, 16 MV/m; NLC and JLC X-Band, 61 MV/m; VLEPP, 75 MV/m; CLIC, 160 MV/m. Dark current, whether captured or not, originates from field-emitted electrons, secondary-emitted electrons and possibly others. Field emission is a steep function of surface electric field and depends on surface conditions (flatness, cleanliness, crystal boundaries, etc.). It can be decreased by careful rf conditioning. The potentially deleterious effects of

these electrons are that they can produce radiation and undesirable noise in instruments (e.g., BPM's), and if transmitted to the end of the accelerator, can generate backgrounds. There is also a concern that asymmetries in these currents may produce transverse wakefields. Noise in instruments and current at the end of the machine are observed at SLAC where the SLC linac runs at an average accelerating gradient of 21 MV/m with a few sections at 30 MV/m. An S-band accelerator section recently built by KEK using Hot Isostatic Pressed (HIP) copper for the disks, along with high standards of cleanliness, showed only 300 μA of peak current for a maximum accelerating field of about 50 MV/m. The same technique has been used for the KEK ATF linac. As this report goes to press, this linac has reached an accelerating gradient of 26 MV/m without any measureable dark current on intercepting screens. For superconducting cavities, TESLA results are encouraging and it appears that field emission can be minimized at 25 MV/m. Considerable and very interesting research is underway in all these areas, and all the test facilities coming on line in the near future will no doubt elucidate many of these questions.

Although a higher frequency in general allows a higher accelerating gradient for copper structures, nature imposes other limitations on the rf system. The energy stored per unit length in the accelerating structure will scale roughly as $G^2\lambda_{rf}^2$. If one chooses a gradient which scales with the dark current threshold gradient (admittedly not a unique choice), then the stored energy per unit length remains roughly constant, independent of frequency. However, the time allowed for this energy to be collected in the accelerating structure depends on the decrement time, $2Q/\omega \sim \omega^{-3/2}$. Thus the rf pulse length will also tend to scale as $\omega^{-3/2}$, and since the stored energy per meter is roughly constant under the above scaling assumptions, the peak power required per meter will scale as $\omega^{3/2}$. Unfortunately, the maximum output power available from a klystron tends to decrease rather than increase as frequency increases. Thus high frequency rf systems using klystrons to generate the rf power (NLC, JLC X-Band, VLEPP) require some sort of pulse compression to enhance the peak klystron output. The additional loss associated with the compression process tends to lower the overall efficiency of the rf system. The two-beam accelerator concept (TBNLC, CLIC) bypasses the limitations imposed by conventional klystrons in producing high frequency, high peak power rf at short pulse lengths. The drive beam in a two-beam accelerator is, in fact, equivalent to the beam in a klystron, and the TBA scheme is also called a "relativistic klystron". A collider using a superconducting accelerator structure (TESLA) increases the $2Q/\omega$ limitation on energy collection time by a very large factor over that of copper, allowing a long pulse, low peak power, efficient rf system with low ohmic losses in the structure. As will be discussed later, both klystron and modulators which operate at a long pulse length tend to be more efficient than klystrons and modulators which must produce short, very high peak power pulses. However, the additional power required by the refrigeration systems must be included in calculating the overall efficiency of the rf system. Note that this report does not include a description of the cryogenics systems required for TESLA and CLIC.

General RF Design Parameters and Brief System Descriptions

Table 2.3.1 gives general design parameters for the main linac rf systems of the various machines. The active length is computed by the expression in footnote (1) of this table, except that in the case of CLIC there is no allowance for energy management, and for TESLA

there is no factor for BNS damping or energy management. By "energy management" we mean a provision for additional active linac length to allow for klystron failures, either from end-of-life or from missing pulses due to modulator, vacuum or reflected power faults. Also included in energy management is an overhead for feedback systems (for example to smooth out modulator amplitude ripple). In the case of TESLA, a "regulation reserve" is needed to provide for feedback against cavity detuning as a function of field amplitude due to the Lorentz force acting on the cavity walls. The total linac length is taken to be 1.1 times the active length for SBLC, JLC, NLC and the NLC/TBA option. For VLEPP the total linac length is based on the number of supermodules, each 5.0 m in length (1.2 times the active length). For TESLA and CLIC special considerations (cryostat length, etc.) lead to the numbers shown. A Power Unit is defined differently for each of the machines (see Fig. 2.3.1.) . For TESLA it is one klystron with modulator feeding 32 accelerating sections. For the SBLC it is one klystron with modulator feeding 2 accelerating sections. For the X-band approach of the JLC it is two klystrons and two modulators driving one pulse compression unit which feeds four accelerating sections. Note that the JLC(S) and JLC(C) variations which also appear in Fig. 2.3.1 are not described in this section and are shown here only for reference. For NLC it is one modulator for two klystrons, which together drive one pulse compression unit feeding four accelerating sections. For the TBNLC it is one transfer structure per NLC accelerating section. For VLEPP it is one grid-modulated klystron driving two pulse compression units which together feed four accelerating sections. For CLIC it is one transfer structure driving two accelerating sections.

Following are some brief descriptions of the rf systems for the various machine proposals at 500 GeV c.m. energy. Upgrades to 1 TeV are described in Chapter 3.

TESLA

The linac consists of superconducting cavities with a frequency of 1.3 GHz. The L-band frequency is a compromise between arguments for small wakes, low higher-order-mode power and low BCS resistance (in favor of low frequencies) vs. high r/Q values, low stored energy and cost (in favor of high frequencies). The actual frequency of 1.3 GHz is chosen because of availability of klystrons. The 9-cell superconducting cavities (structures) have an active length of 1.035 m and operate at a design gradient of 25 MV/m. The beam pulse consists of 800 bunches of 8 nC each, separated by 1 μs. The klystron pulse is 1.3 ms long, including a 515 μs cavity filling time. The output power of 7.1 MW per klystron is equally split to feed 32 cavities. During the beam pulse the cavities are matched, and a power of 213 kW per cavity is transferred to the beam. The cavities operate at 1.8 °K. The cooling power is supplied by 16 cryoplants operating with cold compressors. The AC power required for refrigeration is 58 MW. The AC power for producing RF, not including a regulation reserve, is 96 MW. A 10% ($\approx$ 10 MW) regulation reserve is planned.

SBLC

The rf accelerating system for the S-band linear collider (SBLC) consists of modulators, klystrons and travelling-wave accelerating sections operating at a frequency close to 3.0 GHz and at a beam-loaded gradient of 17 MV/m. One klystron and one modulator, together with two accelerating sections and the quadrupoles, correction coils and beam diagnostics installed in between, define a module of the collider. This module is repeated in the tunnel approximately 1260 times for each linac.

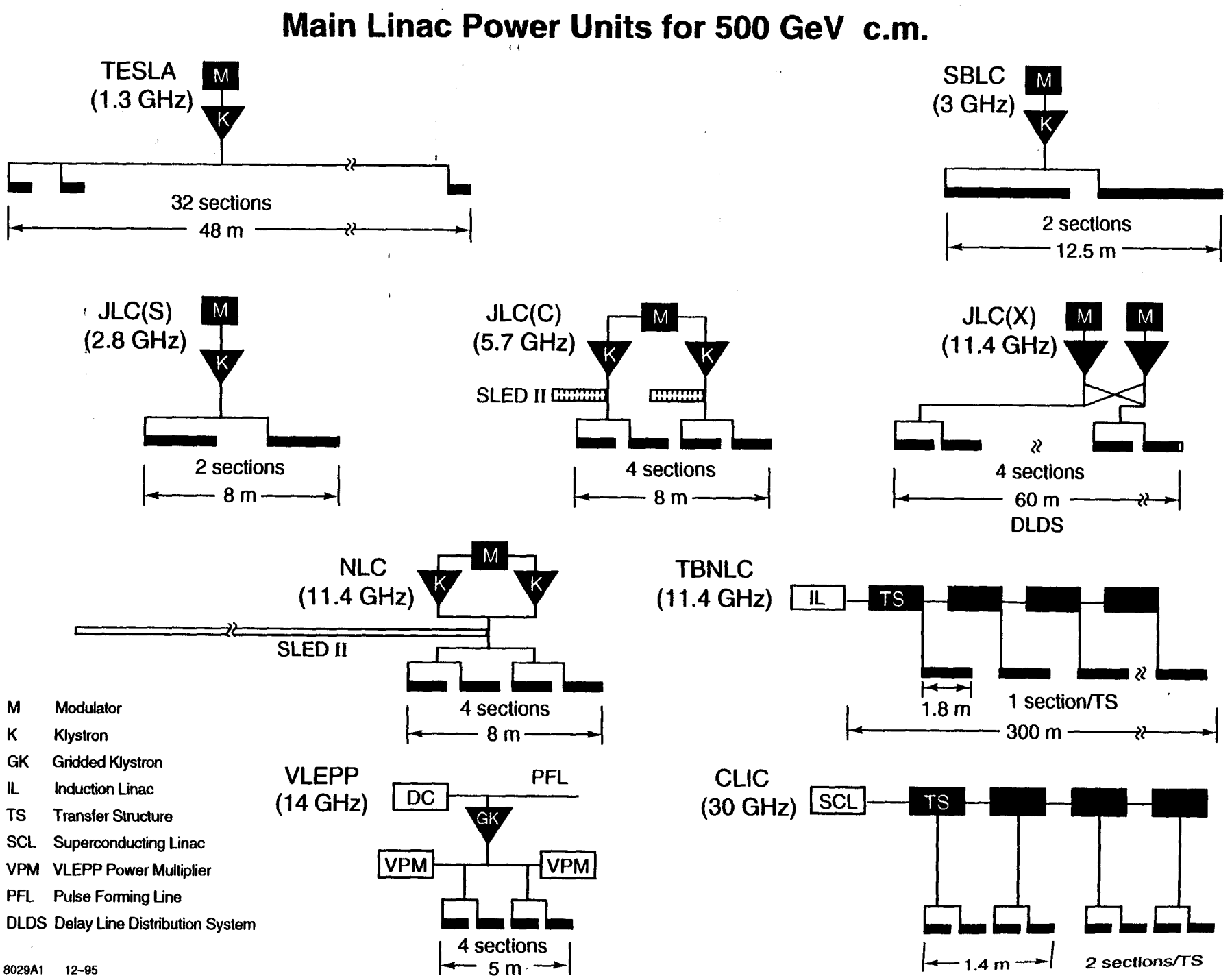

Fig.2.3.1 Main Linac Power Units for 500 GeV c.m.

An S-band frequency was chosen for a number of reasons. A strong base of technology already exists at this frequency (in particular, at the SLC collider at SLAC). The relatively low rf frequency also implies lower wakefield strengths and looser tolerances on the fabrication and alignment of the accelerating sections.

A pulse compression system is not required for the 500 GeV c.m. design, but will be considered for the second stage in upgrading the c.m. energy to 1 TeV.

JLC

Since the choice was made to study an X-band rf system for the main linac of the JLC, most of the R&D to date on klystrons, accelerating sections, etc., have been carried out at X-band (see discussion in Sec. 1.3.1). A schematic layout of the JLC/X-band rf system is shown in Fig. 2.3.2. A unique feature of this design is a novel rf pulse compression method, termed the Delay Line Distribution System (DLDS). In this scheme, the time for power to flow to the upstream pair of accelerating sections, plus the time for the electron beam to propagate back to the downstream pair, is adjusted to be one-half the klystron output pulse length. The power from two klystrons is combined in a 3db coupler and is directed upstream during the first half of the pulse. A 180° phase shift at the input to one of the klystrons switches the combined power to the downstream pair of structures half way through the pulse. There is one modulator for each of the 130 MW klystrons.

NLC

The primary reason for choosing the NLC frequency of 11.4 GHz is to achieve a higher accelerating gradient with a reasonable wall plug power, and to allow an eventual upgrade to 1.0 or 1.5 TeV. It was also chosen to be an integer multiple of the SLC frequency, and to stay within the X-band frequency range where rf components are readily available and a base in industrial accelerator technology presently exists. As mentioned previously, the major disadvantages of a higher rf frequency are stronger wakefields, tighter tolerances, the difficulty in producing klystrons with the required peak power, and the need for an rf pulse compression system.

A schematic layout of an NLC module is given in Fig. 2.3.3. Note that one modulator drives two 50 MW klystrons. The power from the klystrons is combined to drive a SLED-II pulse compression system. The output of the pulse compression system is split four ways to drive four 1.8 m accelerating sections at a loaded gradient of 37 MV/m.

TBNLC

The TBNLC describes a relativistic klystron two-beam accelerator point design which could serve, in the more distant future, as an alternative rf power source for the main linac of the NLC (see Section 3.1.5). A five-year R&D program to explore this technology is now underway. The peak rf power provided by the TBNLC is higher (200 MW/m in TBNLC vs. 50 MW/m in NLC), producing a higher unloaded gradient (100 MV/m vs. 50 MV/m). At the higher gradient, and for the same beam loading factor, twice the charge per bunch can be accelerated. The rf pulse length provided by the TBNLC is longer (100 ns rise time with a 200 ns flattop) than in the NLC design allowing a longer bunch train to be accelerated (140 bunches vs. 90 bunches); however the repetition rate is lower (120 Hz vs. 180 Hz). The combination of these factors provides a luminosity which is several times higher than that of the NLC design. One disadvantage of the TBNLC scheme is that there is less flexibility to adjust the phase (for BNS damping), or to time-modulate the phase (for fine-tuning

Fig.2.3.1 Main Linac Power Units for 500 GeV c.m.

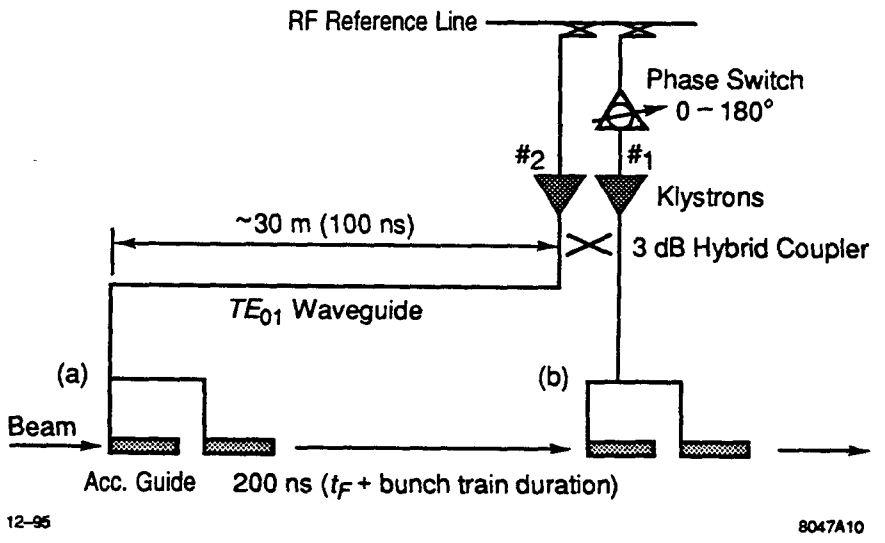

Fig.2.3.2 Schematic diagram of the Delay Line Distribution System (DLDS) for the JLC.

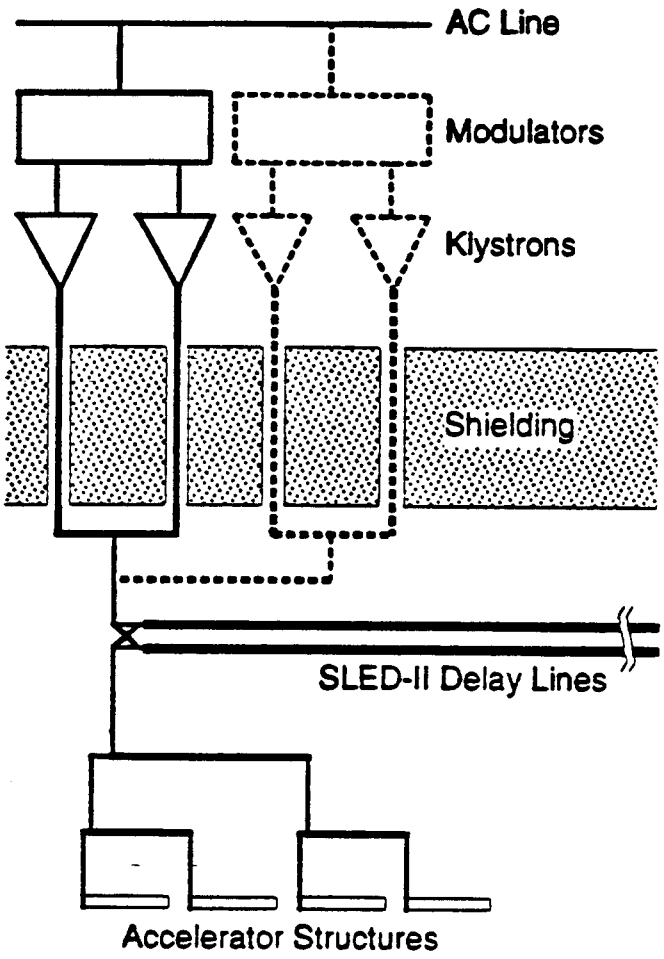

Fig.2.3.3 Schematic layout of the NLC RF system. Dashed lines show upgrade to 1 TeV.

beam loading compensation) at the individual transfer structures. Some adjustment could, however, be implemented in quantized steps of 300 m (the length of an individual TBNLC drive beam) by adjusting the phase of the drive beam bunches with respect to the main beam, and by time-modulating the bunch charge in the drive beam.

Figure 2.3.4 shows a schematic diagram of a TBNLC unit. The TBNLC collider would use 26 of these units for a 0.5 TeV c.m. collider. BBU concerns limit the extraction length of the drive beam in each unit to 300 meters. The front end of each TBNLC unit consists of a 1.2 kA injector, followed by an rf chopper at 2.5 MeV, and an "adiabatic capture" unit in which the chopped beam (average current 600 A) is accelerated to 10 MeV and further bunched with idler cavities in preparation for injection into the main TBA. To enhance the efficiency of the TBNLC system, an "afterburner" at the end of the main TBA continues to extract rf power through 12 successive output cavities before depositing the spent beam (average beam energy about 3 MeV) at the beam dump. The overall efficiency (drive-beam to rf) of each TBNLC unit is calculated to be about 90%. The wall-plug to rf efficiency is about 40%.

The technical challenges for making the TBNLC into a realizable power source lie in the dynamics of the drive-beam, which must propagate over long distances. In particular, the beam breakup (BBU) instability through a long multi-cavity TBNLC is known to be severe. While BBU suppression techniques have been successfully demonstrated for a few cavities, a demonstration of beam control over many traveling-wave cavities will require experimental verification of the BBU suppression scheme proposed for TBNLC where all the rf extraction cavities are located at betatron nodes. Similarly, the longitudinal stability of the rf bunches over a multi-cavity TBA must be able to be demonstrated. Because of uncertainty with the construction of a full scale linear collider based on the relativistic klystron two-beam accelerator concept, we envision that the first large scale demonstration could be incorporated into NLC as an upgrade for a 1 TeV system.

VLEPP

The VLEPP frequency of 14 GHz was chosen to allow a high gradient (100 MV/m unloaded), and hence a shorter linac with, what the proponents believe, a lower total cost. The linac rf system consists of identical modules having a two-level architecture. On the first level are supermodules 50 m long, each of which includes one DC high voltage supply which charges the capacity of a pulse forming line (PFL) up to 1.15 MV. The PFL is assembled from identical 5-m pieces, each of which serves to pulse the grid of one klystron. Each klystron drives two VPM (VLEPP Power Multiplier) pulse compression cavities, and each cavity in turn powers two accelerating structures. Thus a 5-m submodule (one klystron) powers four accelerating sections (4.0 m active length). A schematic diagram of a VLEPP rf module is shown in Fig. 2.3.5.

CLIC

The rf linac consists of normal conducting disk-loaded waveguide structures operating at a frequency of 30 GHz and a gradient of 80 MV/m. The rf power is supplied by transfer structures which extract energy from a 3 GeV high-intensity electron drive linac running parallel to the main linac in the same tunnel. The transfer structure consists of an 11.5mm diameter circular beam tube coupled by two diametrically-opposite 4.5 mm wide slots to the broad side of two periodically-loaded rectangular waveguides. It is designed to have a

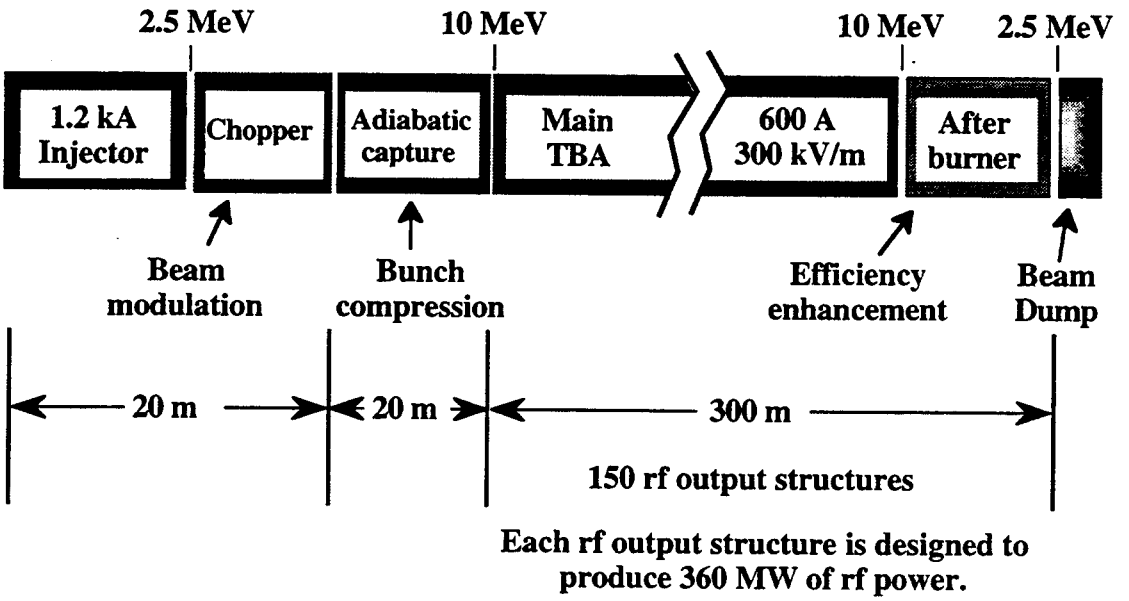

Fig.2.3.4a Layout of a TBLNC unit. Each unit would provide the rf power for 300 meters of the high gradient accelerator; 64 of the units would be used to provide the rf power for a 1 TeV c.m. collider.

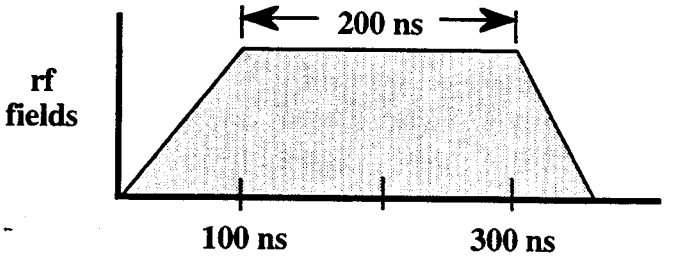

Fig.2.3.4b Desired waveform of the rf fields in the high gradient accelerator for the TBLNC design. With 1.3×10^{10} electrons per bunch and 143 bunches per train the loaded gradient would be 74 MV/m. The active length of the accelerator would be 2×7.1 km.

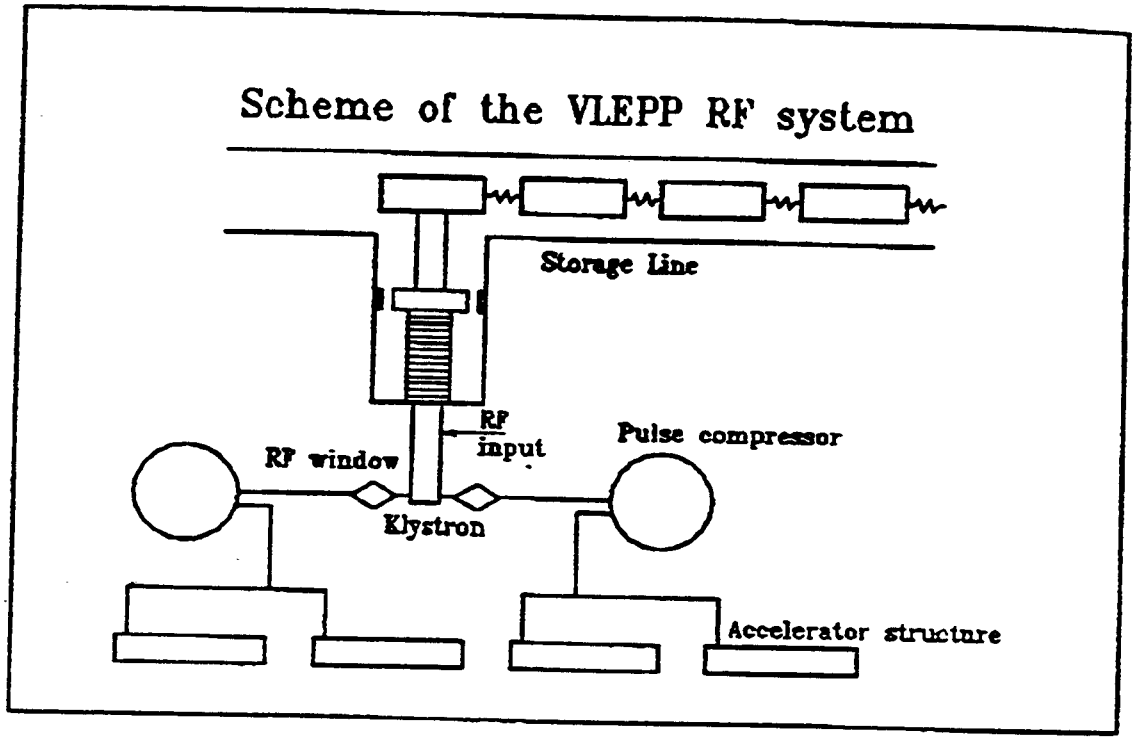

Fig.2.3.5 Schematic layout of the VLEPP RF system.

low fundamental mode shunt impedance (r/Q=45 ohms/m) and to have a low transverse impedance. The section has a drain time of 2.84 ns and a Q value of 3420 (0.9 theoretical Q). Each 35 cm long section produces two 11.6 ns long 44.6 MW power pulses which drive two accelerating structures. This output power is extracted from the beam with an efficiency of 95%. The total drive beam charge of 2.58μC is contained in four trains of 22 bunches per train (29 nC/bunch) with a space between bunches of 1 cm and an rms bunch length of 0.6 mm.

A schematic layout of the drive beam generation and acceleration scheme is shown in Fig. 1.18. The 88 bunches of the drive beam are produced by a battery of 11 S-band photoinjector linacs. Each linac provides 8 bunches which occupy the 1, 2, 12, 13, 23, 24 and 34, 35 rf buckets. Each photoinjector linac consists of a laser-illuminated (262 nm) photocathode (Cs_2Te) in an S-band rf gun (100 MV/m) followed by an S-band rf booster. The energies of the 11 linacs are slightly different (25-50 MeV) allowing the 11 outputs which are timed relative to each other by 1 cm to be merged in a magnetic combiner to lie along a single trajectory. The resulting 12 ns long bunch train is accelerated to 3 GeV using 3.8 GV of 350 MHz (6 MV/m) SC cavities combined with 0.36 GV of 1400 MHz (10 MV/m) SC cavities for pulse flattening. Short sections (each 220 MV) of SC cavities operating at 333 and 366 MHz compensate the effects of beam loading. The net beam loading of each train is zero in the 4th harmonic cavities because the train duration covers exactly one period. No re-acceleration of the drive beam is necessary in the tunnel but a "momentum rotation" section using 700 MHz SC cavities is foreseen to maximize energy extraction efficiency. The drive beam is finally dumped at about 350 MeV.

RF System Efficiency and AC Power Budget

Design goals for rf system efficiencies and ac power requirements are summarized in Table 2.3.2. Details concerning the efficiencies of the various subsystems — klystron, modulator, rf pulse compression and power transmission — are given in the following sections. Note that net efficiencies for production of rf power all fall in the range 30-40%, while the total ac power requirements fall in the range 60-160 MW. The machines differ over a wider range in the efficiency of converting ac power to beam power.

2.3.3 Where We are Today and R&D Needed over the Next Three Years

Klystrons

Table 2.3.3 shows design and achieved klystron parameters for those machines employing pulsed klystrons as an rf source to drive the main linac. For application to a linear collider, klystron efficiency is of obvious importance. It is well known that klystron efficiency depends on the microperveance, defined as $K_\mu = (I_b/V_b^{3/2}) \times 10^6$, where I_b and V_b are the beam current and voltage. On a plot of efficiency vs. microperveance, points representing the performance of both measured and simulated tubes all fall below a line given by $\eta = 0.80 - 0.15 K_\mu$. CW and long pulse klystrons sometimes approach this line; high peak power, short pulse klystrons tend to fall further below it. Although this maximum efficiency is not a rigid physical barrier, the gap between it and the design efficiency is a measure of the technological difficulty in achieving the design efficiency. Values for this limiting efficiency are listed as

"scaled maximum efficiency" in the table. A short summary of the status of each of the klystron designs begins on the following page.

TESLA

In total 604 10 MW diode klystrons are foreseen to operate at 1.315 msec with a rep rate of 10 Hz. The high voltage pulse of 110 kV is produced by a GTO switch discharging a 1.4 mF capacitor (which is in series with a bouncer circuit) into a pulse transformer. The droop of the high voltage pulse during 1.315 msec is less than 1%. The rf power is distributed via a central circulator, WR 650 waveguides and directional couplers. The loss in the waveguide system is estimated to be 4%. The vector sum of 32 cavities is kept constant by phase and amplitude controls. An amount of 10% additional rf power for regulation reserve increases the wall plug power of 96.6 MW by another 9.5 MW. Klystrons with TESLA specifications are available at the power level of 5 MW. The efficiency, however, is below 45%. Therefore, contact with industry has been established to develop a 10 MW high efficiency klystron. Simulations show that a multi-beam klystron with reduced perveance and efficiency above 70% is possible. A development contract has been signed to develop a prototype within the time frame of two years.

SBLC

In order to satisfy the rf power requirements for the S-band linear collider, a separate R&D program together with SLAC was started in 1993. Following an earlier development done in 1986 when a 150 MW, 1 μsec-klystron with an efficiency of more than 50% was built, the goal was to construct and operate a 150 MW klystron with a pulse length of 3 μsec and a repetition rate of 50 Hz, following the general parameters for the SBLC. By 1994, 1-1/2 years later, the klystron was tested and met these specifications. The operating parameters achieved with the first of at least two different klystrons being constructed so far, are given in Table 2.3.3.

The main aims for further R&D are to reduce investment costs and improve the klystron efficiency, lifetime, and power gain. To achieve these ends, several efforts may be pursued:

- (i) the klystron focusing, which takes around 10 kW of average power with a solenoid optimized for this klystron. Superconducting solenoids or periodic permanent magnetic (PPM) focusing have to be investigated.
- (ii) the electronic efficiency of the klystron should be increased. Therefore, the micro-perveance should be decreased and the beam voltage increased, although this seems not to be desirable for a number of reasons. Installing two klystrons per modulator with a lower peak power each and very low microperveance could be considered, comparing investment (more klystrons) and operating costs (higher efficiency).
- (iii) the lifetime should be increased, which requires conservative values for the cathode loading and probably new developments on cathodes.
- (iv) the gain should be increased to decrease the drive power to a value which could easily be met with solid state amplifiers (probably less than 200 W).

In terms of investment costs, two aspects are investigated already. With four windows, although being conservative in the power level transmitted through one window (40 MW), the klystron is more expensive, mechanically very large and difficult to handle around the output cavity region.

In general new designs of klystrons have to be tested, which could combine the advantage of a switch tube modulator with the efficiency requirement of the klystron by using a gridded gun. In addition, a solution to eliminate the room temperature focusing solenoid of the klystron would be highly desirable. If superconducting solenoids could be used, the general design of the klystron would not have to be changed. For PPM focusing, lower perveance and therefore higher beam voltage is desirable. This would be the optimum solution for a linear collider in terms of investment and operating costs. Nevertheless it is still an open question whether an efficiency larger than 50% can be achieved. However, if none of these desirable developments come through, the SBLC klystron is (apart from TESLA) the only tube which could tolerate standard focusing at an acceptable consumption limit for AC power; the increase would be 18% if a 10 kW solenoid is used.

JLC

KEK together with Toshiba has tested a 100 MW class klystron named XB72k. Two tubes have achieved 340 MW DC beam power with a longer pulse length than the design value. A maximum efficiency of 33% was obtained. The power output of the present design with a single output gap is limited by rf breakdown in the output gap. A multi-gap output circuit version, which has a lower surface field, is under design study in collaboration with VLEPP.

NLC

All experimental results to date at X-band are based on solenoid-focused tubes. At the beginning of the program, the objective was to achieve 100 MW of peak power in a high perveance (microperveance = 1.8) design. The experience gained from building a series of eight of these tubes (XC series) narrowed the choice of rf output circuits suitable for achieving the required peak power and pulse length, and led also to gun and rf window improvements. In the interest of a more conservative and more efficient design, the microperveance was dropped to 1.2 and the design power to 50 MW (XL series). Two tubes in this series have achieved the design power and pulse length (50 MW at 1.2 μs or more), with an efficiency of about 40%. Of the various technological development efforts associated with the X-band klystron, rf window development and refinement is the farthest along toward meeting the final design requirement. In resonant ring tests traveling-wave TE_{01} windows have demonstrated the capability of transmitting over 100 MW at 1.5 μs pulse length.

To achieve the NLC design goals, a PPM-focused tube with a microperveance of 0.6 is under design. Two PPM-focused test vehicles will be completed in calendar year 1995. The first is a beam stick, to test gun design and dc beam transmission. The second is a 50 MW tube with a projected efficiency from computer simulations of 66%, although the actual design goal is 60%. One additional XL-series klystron is also being built to supply the NLC Test Accelerator (NLCTA) and to provide additional comparisons of measured rf efficiency with computer simulations. An efficiency of 54% is predicted for this more advanced XL tube with a four-cell, disk-loaded output circuit and a computed output of 84 MW.

For eventual upgrades, a PPM-focused klystron is also under design with a microperveance of 0.75 and an output power of 72 MW at an efficiency greater than 60%.

VLEPP

The VLEPP klystron has several features which contrast with those of conventional klystrons: a gridded gun with a honeycomb 120 mm diameter oxide multicell cathode, a

high voltage segmented insulator with 15 intermediate electrodes, a PPM focusing system, eight gain cavities within the beam drift tube, and a 14-cell travelling-wave output structure. A few units of these klystrons have been produced and tested in two high voltage regimes: pulsed (HV pulse length about 100 μsec) and at DC voltage. The obtained beam transmission efficiency in the PPM beam transport system is $\geq 95\%$ and can be improved by careful tuning of the magnetic system and beam steering. An output power of 60 MW was obtained in a 0.7 μsec pulse. A very high gain ($\approx$ 90 dB; the design gain was 75 dB) was demonstrated for a power level of 50 MW. The achieved power was limited by a dipole-mode instability in the klystron, which can be suppressed by additional losses in the drift tubes. This has been demonstrated experimentally.

In Dubna, the large aperture klystron studies will be continued, using a 1 MV $\times$ 300 A $\times$ 0.25μsec beam from an induction linac, to reach a design 100 MW power level. In Novosibirsk (INP), another klystron will be studied by using a pulsed HV generator (ELIT) with 1 MV $\times$ 200 A $\times$ 0.8μsec. Power from the klystron will be used for tests of high power components of the rf system in a resonant ring (rf windows, directional couplers, pumping ports, etc.).

Modulators

The rise time of a modulator is an important parameter in determining the modulator efficiency. In a conventional modulator, the pulse forming network (PFN) capacitance is charged by a dc power supply to a voltage V_{PFN}. The PFN is then (completely) discharged by a switching device, usually a thyratron, through the primary of a pulse transformer with a turns ratio n. The output of the pulse transformer produces a voltage $n \cdot V_{PFN}/2$ (single stage PFN), or $n \cdot V_{PFN}$ (two stage or Blumlein PFN). In the case of the TESLA modulator, an energy storage capacitor is partially discharged through the primary of the pulse transformer. The switching is done by solid state devices (GTO's, or thyristors).

The energy efficiency, η_E, of the pulse transformer is defined as the useful energy in the flat-top portion of the pulse divided by the total energy in the pulse. The energy in the fall-time portion of the pulse tends to scale in proportion to the rise time, so that the energy efficiency can be written as:

$$\eta_E = \frac{T_K}{T_E} = \frac{T_K}{T_K + \alpha \cdot T_R}$$

where T_K is the flat top portion of the pulse, T_E is the energy width and α is a coefficient between about 1.0 and 1.2 which depends on the pulse shape and the definition of rise time. In turn, a simple physical argument leads to the scaling $T_R \sim n \cdot (T_E)^{1/2}$. Combined with the preceding relation, this gives

$$T_E = \left(\frac{\beta \cdot n + (\beta^2 \cdot n^2 + 4T_K)^{1/2}}{2} \right)^2$$

where β is a constant that can be obtained by fitting to existing pulse transformer designs. For the pulse transformer driving the 5045 klystron at SLAC, $\beta = 0.0333$. It is found that the above expression then gives a good fit to a number of the other pulse transformers measured

at SLAC having a variety of turn ratios and pulse lengths. Along with T_K and n, values of η_E are listed in Table 2.3.4 for the various modulator designs as the "scaled energy efficiency". An accurate simulation of energy efficiency must also include the effect of the load (klystron) capacitance and the series inductances of the thyratron and high current leads on the rise time. As shown in Table 2.3.4, core losses in the pulse transformer and resistive losses in the thyratron and high current leads also dissipate several percent of the energy. An additional 5-10% is lost in the dc power supply. Of course, the best efficiency is obtained by eliminating the modulator entirely, i.e. using a gridded klystron as proposed for VLEPP. Brief comments follow on the modulator designs for the various proposed machines.

TESLA

The TESLA modulator consists essentially of a 1.4 mF capacitor bank, a bouncer circuit, a GTO switch and a pulse transformer. The output pulse is started by turning on the GTO switch, which connects the capacitor bank to the pulse transformer primary. During the pulse, the capacitor bank discharges by 20% of its initial voltage, putting an intolerable 20% slope on the output pulse. To decrease the slope to the 1% level without resorting to a 20 mF capacitor, the slope is corrected with a bouncer circuit. This is a resonant LC circuit, which creates a single sine wave with a period of 7 ms. The bouncer is triggered slightly before the main pulse so that the linear, bipolar portion of the cycle is in progress during the main pulse. The bouncer waveform reduces the 20% slope to less than 1%. The pulse is terminated after 2.3 ms by turning the GTO off. The primary pulse level is 9.6 kV/1.14 kA, and is stepped up to the klystron operating level by the 13: 1 pulse transformer. The pulse rise time is less than 100 microseconds. The power fluctuations seen by the mains are reduced to 15% by a 3 H choke.

Installation at DESY and successful final commissioning took place in April, 1994. Since then the modulator has been in regular use without any problem. The modulator is described in more detail in: "A Long Pulse Modulator for Reduced Size and Cost", H. Pfeffer *et al.*, to be published in the Proceedings of the 21st Power Modulator Conference, Costa Mesa, CA, June 20-23, 1994. Two more such modulators are presently being built at FNAL.

SBLC

The modulator being considered to drive the 150 MW klystron is a PFN type modulator with the pulse forming network connected to a pulse transformer. Such a modulator has already been constructed at SLAC to test the klystron at full power and a maximum repetition rate of 60 Hz. Two further modulators are under construction at DESY for the S-band test facility. The modulators are designed for a maximum voltage and current of 550 kV and 700 A. The main aim for further R&D has to be the reduction of investment and operating costs, which means that new components have to be developed and the power consumption has to be reduced.

To address these points, several improvements have to be made:

- (i) The rise and fall time of the modulator pulse have to be decreased.
- (ii) Instead of operating the modulator with two thyratrons in parallel, a reliable thyratron capable of operating at 70 kV and 10 kA has to be developed.
- (iii) The size of the modulator has to be minimized for installation in the tunnel.

Reduction of investment cost is difficult to quantify, because the result depends strongly on the detailed assumptions made for cost reductions for large quantities. In parallel, a switch tube modulator has been designed and tested up to 150 kV at DESY to investigate the possiblity of direct switching of the high voltage pulse to the klystron, which should increase the efficiency and decrease investment costs at the same time.

JLC

The first Blumlein-type modulator assembled in the same oil tank with a 1:7 pulse transformer is now under low voltage tests. Preliminary operation with a transistor switch instead of a thyratron showed a 200 ns rise time. For the JLC design version, all parts such as a high voltage capacitor, a thyratron, etc. are available commercially. As the next step, some changes will be made in the parts and the design specifications, and these have to be tested.

NLC

The NLC modulator is designed to drive two NLC klystrons at beam voltages up to 500 kV. It utilizes a pulse transformer with a low turns ratio (1:7) in order to minimize leakage inductance and obtain a fast rise time of the output pulse. A Blumlein pulse forming line is used to reduce the voltage on the thyratron switch and energy storage lines to a nominal value of about 70 kV. Previous modulators built at SLAC have had risetime problems due in part to the poor quality of the capacitors used in lumped-element PFN's. The currently planned modulator uses a distributed line designed around a Heliax triaxial cable, which is filled with a high dielectric constant liquid ($e_r = 7$) to reduce the length. The pulse transformer is built with two bifilar secondary windings to allow each of the klystron heaters to be independently controlled. The distributed line is charged directly from an efficient 80 kV switching power supply, which also provides the necessary voltage regulation and control. Detailed simulations on this modulator design are in progress. A full-scale prototype will be constructed and tested over the next two years. In the meantime, construction of three modulators of conventional design (single stage PFN with 1:21 pulse transformer) for the NLCTA is now nearing completion. Tests on these modulators will provide useful information on measured vs. simulated performance.

An additional prototype modulator, with a 3-stage PFN ($V_{\text{out}} = 1.5nV_{\text{PFN}}$) and a 1:5 pulse transformer is now ready to begin full power tests. Measured results will validate the design procedures and simulations for a modulator based on a low turns ratio, fast rise time pulse transformer.

VLEPP

The DC high voltage system consists of a high voltage source and a coaxial pulse forming line (PFL), which is pressurized with SF_6 up to 12 atm in order to increase the electric field strength within the PFL. The design operating DC voltage is 1 MV. A 5-meter piece of the PFL was tested in the VLEPP Test Facility (VTF) in Protvino, and 960 kV has been achieved. Also, the high voltage source has now been produced and tested. Testing and study of the DC High Voltage components will be continued at the VTF. The main goal in the next three years is to test standard 5-meter accelerating modules, designed for the linac.

RF Pulse Compression Systems

RF pulse compression is a method of enhancing the klystron output power at the expense of pulse width. Although some energy is lost in the compression process, the efficiency can in principle be quite high. High Q energy storage elements, either resonant cavities or delay lines, are required to achieve efficient pulse compression. As an example, a Q on the order 10^6 is readily obtained at X-band using a TE_{01}-mode delay line with a diameter of 14 cm. However, such a compression system can be awkward in overall length, and in addition is highly overmoded, which implies certain technological complexities. Using resonant cavities, a more manageable size can be gained at the expense of lower efficiency. As a final introductory comment, it should be noted that getting rid of the rf pulse compression system does not necessarily lead to a higher overall rf system efficiency. A certain total amount of energy compression must be carried out between the ac line and the rf pulse at the input to the accelerating structure. If there is less rf pulse compression, then more dc pulse compression is needed in the modulator in order to produce a shorter output pulse at higher peak power, with a consequent lower modulator efficiency. For the low frequency machines like SBLC (500 GeV c.m.), no pulse compression will be required because the gradients and the required peak power per meter are relatively low. Therefore, the overall complexity of the rf system is reduced. In the case of TESLA, the superconducting structure itself is in essence an rf pulse compressor, since it can collect energy at low peak power over a long period of time.

RF pulse compression is used in three of the 500 GeV c.m. designs. VLEPP and NLC use a SLED-type scheme (SBLC plans to use a SLED system only for the energy upgrade). In a SLED compression system, energy builds up in a storage element (resonant cavity for SLED-I or resonant length of delay line for SLED-II) over the major part of the klystron output pulse. During the final part of the pulse (equal to the desired output pulse length), a phase reversal triggers a discharge of the stored energy, which adds to the energy coming directly from the klystron. During the filling time of the storage device, there is an unavoidable power reflection. In addition some energy is left behind after the output pulse. Together, these factors lead to a maximum intrinsic efficiency for a SLED system on the order of 80%, even assuming lossless components. Taking losses into account gives a net efficiency of approximately 75%. On the other hand, the JLC uses a compression method (DLDS) which is inherently 100% efficient. Although related to Binary Pulse Compression, the DLDS uses less delay line pipe by feeding power in the up-stream beam direction, thus taking advantage of the beam transit time to achieve a factor of two reduction in the required delay line length.

Both the DLDS and the SLED-II compression schemes have the advantage of producing a flat output pulse. The VPM scheme uses a single traveling wave resonator, and is therefore very compact. SLED-I and VPM output pulses are not inherently flat, which is of no consequence for single bunch acceleration. In fact, methods have been proposed and tested to fit the rf output pulse of a SLED pulse compressor to compensate for transient beam loading in a multibunch linac; this compensation must be done for all designs in any case. Parameters for the three pulse compression systems are given in Table 2.3.5; a brief discussion of these systems follows.

JLC

Since the DLDS (Delay Line Distribution System) was recently proposed at KEK, only

preliminary design work has been done. This scheme will be simple to implement since the main rf components such as a mode converter, 3-dB coupler etc. exist already. The first DLDS, which is equivalent to a factor of two rf compression scheme, is to be assembled in 1995 under close collaboration with the VLEPP group.

NLC

The SLED-II rf pulse compression system proposed for the NLC has a compression ratio of five and an intrinsic efficiency of 80.4%. In addition, there are copper losses in the SLED-II components (3 db coupler, reflective irises, tapers, flower petal mode converters, and overmoded delay lines), and potential mode conversion losses in the delay lines. A design efficiency of 95%, based on measured efficiencies for individual components, takes account of these losses. An efficiency of about 91% for these losses has been measured on a prototype system. The additional loss is thought to be due largely to mode conversion associated with the flower petal mode converters, which couples to parasitic resonances in the delay lines. A re-designed mode converter which includes mode suppression chokes will be tested soon. The design efficiency for power transmission from klystron to compression system, and from compression system to accelerating section input, is 94%. Transmission efficiencies measured in practice have been significantly lower than this, again because of resonant mode conversion problems. It is expected that work over the next year will push these efficiencies toward the design values.

The peak power at the output of the SLED-II 3 db coupler reaches 380 MW for the 500 GeV design parameters. In high power tests on a prototype system, a peak power of 205 MW (150 ns pulse length) has been reached at this location. Within the next six months, it is planned to combine the output of two klystrons in the ASTA test area to drive a prototype compression system to the full design power level.

VLEPP

The compact VLEPP pulse compression system (VPM), which uses as a storage element a barrel-like open cavity, has been successfully tested at KEK in 1994. The 150 MW peak obtained so far was limited by the klystron. The gain and efficiency are close to the design values (see Table 2.3.5). It has also be shown experimentally at low power that pulse shape and efficiency can be improved by using two or more of these cavities in series.

Accelerator Sections

The primary function of the accelerating section is to transform input rf power into accelerated beam in the most efficient manner possible. Copper sections designed for multibunch acceleration carry an additional burden — that of suppressing frequency dipole-mode wakefields, which would otherwise lead to unacceptable emittance growth over the length of the bunch train. The most difficult part of this task is to decouple the wakes from the individual cells in the structure on a time scale equal to the bunch spacing, Δt. This is accomplished by tuning each cell to a different dipole mode frequency, while maintaining the accelerating mode frequency by appropriate perturbations in cell geometry. The total frequency spread which is required is on the order of $\Delta\omega \approx \pi/\Delta t$. A standard constant gradient section design provides the required frequency spread in the case of SBLC, which has a comparatively large bunch spacing. The section for an X-band collider requires stronger detuning. In addition, the JLC and NLC designs propose a detuning in which the dipole mode density is Gaussian

as a function of frequency. This leads to a time- domain wake which is also Gaussian, with a sigma less than the time between bunches. In a structure with a finite number of cells, N, the wakefield recoheres on a time scale on the order of $t \approx N/\Delta\omega$. This can be avoided by introducing some additional light damping, where $(2Q_d/\omega) \approx (N/\Delta\omega)$. In the NLC this is accomplished by running four damping manifolds along the structure, with a small coupling to every cell. In the SBLC, stainless steel sputtered on the tips of the irises will decrease the Q sufficiently. In the case of TESLA, damping couplers are used to lower the Q's of both dipole and longitudinal modes. Longitudinal mode resonances are also dangerous for TESLA because they can extract power from the beam and produce excessive dissipation at the 2°K level.

Manufacturing tolerances are also an important consideration in accelerating structure design. They are obtained from simulations of emittance growth in the presence of rms offset errors on a scale ranging from one accelerating cell to many accelerating sections, as discussed in the Beam Dynamics section of this report. Errors on a scale longer than the length of one section are alignment tolerances. Errors on a scale less than the length of one section impose a straightness tolerance on the section. The tightest of these tolerances, with the corresponding scale lengths, are listed in Table 2.3.6. Comments follow on the design of the accelerating sections for the various machines.

TESLA

The accelerating structure consists of 9-cell standing-wave superconducting cavities at 1.8°K. The coaxial input coupler is placed at one end of the resonator; two HOM couplers are used, one at each end of the structure. The input coupler matches the beam power demand of 214 kW by adjusting the external Q-value to $3 \cdot 10^6$. The HOM couplers load the dominant longitudinal and transverse higher order modes to Q-values around 10^4. A broadband absorber is placed every 8 cavities in the beam pipe to dump the propagating power of the very high frequency part of the spectrum at 70°K. Slow tuning of the resonant frequency is accomplished by a motor and gear box placed at cryogenic temperatures. For a frequency change of +30 KHz the length of the cavity is enlarged by 0.1 mm.

The cavity is filled with rf energy during the first 0.515 msec. A stiffening ring around the iris of the cavity reduces the shift of the cavity resonance due to the Lorentz force to about one bandwidth (429 Hz). During filling the generator tracks the resonance frequency. At beam arrival, the frequency is locked and the phase slip during the 800 msec pulse is kept below 1° by the feedback system of the vector sum control. The cavities are fabricated from niobium sheet material by forming and welding techniques. Production techniques to fabricate seamless cavities are under investigation. Careful cleaning and handling procedures (automated chemistry, furnace treatment, high pressure water cleaning, dust free handling, high power processing) are essential to reach the design gradient of 25 MV/m without quench or field emission loading. The main difficulties in achieving a gradient of 25 MV/m are the phenomena of thermal breakdown and field emission. To overcome thermal breakdown, the thermal conductivity of the niobium has to be raised. This can be done by starting with sheet metal with a higher thermal conductivity, or by a later solid-state gettering process. To reduce field emission, improved cleaning techniques have been successfully applied. Finally a technique called High Pulsed Power (HPP) processing has been proven to destroy field emitters and substantially improve gradients. A new infrastructure has been set up at DESY

(site of the Tesla Test Facility or TTF), where all the required facilities, such as automated chemistry, high pressure water rinsing, UHV high temperature furnace, and HPP processing have been installed. By late 1994, 6 prototype cavities had been fabricated by industry and 12 more will be delivered in 1995. Two pre-series cavities were used to commission the infrastructure. The first complete treatment of one of these cavities resulted in an accelerating gradient of 20 MV/m under continuous wave conditions. The first production cavity reached 25 MV/m under pulsed conditions. The beam loading was simulated by shaping the klystron power so that a flat top of 800 msec at high gradient was established. Within the coming next two years (1995/96) sufficient experimental evidence is expected to qualify procedures to fabricate high gradient cavities.

Mechanical vibrations might produce a substantial challenge to the amplitude and phase control system. The loaded Q of the superconducting cavities is 3.0×10^6, the equivalent bandwidth is 429 Hz. Therefore the cavity transforms small vibration amplitudes into large phase and amplitude modulations. Experience with vibrations in cryogenic systems shows that external noise sources, like rotating pumps, can be decoupled by damping or detuning techniques in the connecting lines. The internal cryostat construction is carefully designed to avoid mechanical resonances or to shift them so they are not close to a harmonic of the 10 Hz repetition rate. Furthermore, an overlap of resonance frequencies of the cavity structure, the cold support system and the vacuum vessel is avoided by careful attention to mechanical design. A residual fluctuation in phase or amplitude can be compensated by the vector sum control of 32 cavities per klystron. In spite of all theoretical predictions, the vibration problem must be investigated by experiments. Here the TTF activity is expected to deliver the appropriate experimental data.

Field emitted current will be captured above 10 MV/m and will be accelerated through the adjacent cavities. Simulations show that this current will be deflected out of the beam aperture at the next quadrupole, but additional cryogenic loading and potential errors in beam monitor readings due to dark current must still be avoided. Thorough cleaning (high pressure water rinse) and in situ cleaning (high peak power processing) are applied to minimize the number of possible field emitting sites. In total, 40 cavities (or 80 cavities for an upgraded TTF program) will be treated at the TTF installation. It has to be demonstrated that high gradients at low field emission loading can be established.

SBLC

The section is a standard $2\pi/3$ mode constant gradient section designed to have a continuous taper from the beginning to the end. The final required straightness of the section is determined by the maximum HOM excitation that can be tolerated. Assuming an average Q value of the HOM's of 2500 (accelerating-mode $Q \approx 13{,}000$) with a bunch charge of 3×10^{10}, the tolerance calculated so far is 30μm rms over the full six meter length. The first section has been measured after brazing, and maximum deviations from the axis on the order of one millimeter were found. After correction, the rms value was on the order of 100 micrometers; nevertheless, this deviation is still too large by almost a factor of 4.

Other major technical developments in progress so far are the collinear load and a very compact symmetric high power input coupler. The collinear load absorbs the remaining rf power over the last eight cells of the section while still accelerating the beam. Such a load avoids a second high power coupler (thereby reducing costs), is perfectly symmetric (no

transverse kick) and also absorbs higher-order modes touching the downstream end.

Due to the high conversion efficiency of rf to beam power at 300 mA average current, the extracted power is almost 40%, resulting in a variation of the heat load along the section by the same amount. Without feedback/feedforward, this results in a temperature dependent, intolerable energy spread and must be compensated with a fast-regulating cooling system reacting immediately to average current or average power changes in the section.

To control HOM excitation and the resulting emittance growth, each section will be equipped with two HOM dampers. One will be located near the front end, and one almost at the 2/3 point of the section length. Two couplers are definitely not sufficient for damping all the modes in the first HEM_{11} passband because about 2/3 of the severe modes in this passband are trapped at different locations of the section. The HOM couplers, in combination with a set of micromovers, will have to control the beam induced HOM power. While the HOM couplers are used to couple out as much HOM power as possible, the amplitude of the extracted power can in addition be processed to produce a control signal for the micromovers. A second method for internal damping is under development. Sputtering a 20μm stainless steel layer onto the iris lip strongly damps trapped higher order modes, but only reduces the shunt impedance of the fundamental mode by a very small and tolerable amount. The combination of these two methods will provide the required overall damping and HOM control.

In addition, a second R&D program has been set up with the MEPhI in Moscow to develop symmetric high power couplers which can couple out the HEM_{11} modes which are trapped close to the input end.

JLC

By utilizing the capability of the precision machining shop at KEK, the efforts have been focused on the feasibility study of a purely detuned structure (or a slightly damped one with $Q_{ex} \approx 2000$) aiming at controlling the cell frequencies within $\delta f/f = 10^{-4}$ and obtaining a cell alignment tolerance on the order of a few microns. By a diffusion bonding technique, KEK has obtained the required frequency control in a short structure 30 cm long, and an alignment tolerance of 40 microns along a 1.2 m structure. The high field capability for a full size structure has not been tested yet, although the 20 cm structure made by CERN with precision machining and brazing techniques was tested up to 100 MV/m without serious problems.

NLC

The design of the NLC detuned structure is well documented (SLAC-PUB-6032). The necessary detuning is achieved by varying the iris thickness in addition to the iris aperture. This serves to give additional detuning to the higher-order dipole modes, which could otherwise produce unacceptable emittance growth. Dipole mode wakefield suppression has been measured with a beam on a full-scale 1.8 m prototype structure in the ASSET test area of the SLC; measured results are in good agreement with theory. Recently, it has been decided to achieve damping of the long-range resurgence wake (arising, as mentioned above, from the limited number of cells available in a single section to model the Gaussian distribution) by means of damping manifolds, rather than by interleaving the distributions for several structures. The four damping manifolds also serve as beam position monitors, and can possibly provide information on structure straightness. Test stacks are now being prepared for veri-

fying cell dimensions. A full-scale 1.8 m section with damping manifolds will be completed and ready for ASSET wakefield measurements by Spring 1996. In the meantime, two 0.9 m injector sections and a second 1.8 m section (detuned but without damping manifolds) will have been constructed and installed in the NLCTA. Later in 1996 and in 1997 additional refinements will be made in section design, with beam tests in ASSET and NLCTA, and high-gradient tests up to 100 MV/m in the ASTA area in the SLAC Test Laboratory building. The design effort will focus on developing construction techniques for achieving tighter tolerances at reduced cost.

A full-scale 1.8 m detuned section (without damping manifold) has been tested to 65 MV/m (150 MW input power at a pulse length of 150 ns). During 1995, using combined output from two klystrons to drive the 150 ns prototype pulse compression system in ASTA, the same section will be tested to a gradient approaching 100 MV/m. Shorter test sections have already been tested at high gradients. A 75 cm constant impedance section reached an average accelerating gradient of 79 MV/m and a 26 cm section reached an average gradient of 101 MV/m; in both cases the gradient was limited by the available rf power. A 6 cm standing-wave structure was limited by rf breakdown at a peak surface field of 500 MV/m (corresponding to about 210 MV/m accelerating field in a 1.8 m traveling-wave section).

VLEPP

The required 2 μm rms machining precision for the cell and iris diameters is achieved in practice with a specially designed lathe, which can produce cells with a 1 MHz rms frequency error. A specially designed technology for brazing 1-meter long sections avoids the need for any tuning on single cells after brazing. The section is brazed from two 1/2-meter pieces with a few correction cells. Tuning the section to the final operating frequency is achieved by individual temperature regulation within a range of (40 ± 5)°C for each section. At present, ten full scale sections have been produced for technology studies and power tests.

CLIC

The main emphasis of CLIC structure studies has until now been oriented towards the development of constant impedance (CI) sections. The following information therefore concerns only the CI structures. For multibunch operation, damped and/or detuned structures will be required and these are being studied.

The 30 GHz CI accelerating sections have an external diameter of 35 mm, have 84 cells, are 28 cm long and operate at 80 MV/m. 30 GHz was chosen to minimize stored energy without creating excessive wakefields. Working at such a high frequency essentially eliminates all dark current problems. The 35 mm outer diameter, which is machined to a precision and concentricity with the beam aperture of $\ll 1$ μm, serves as the reference for alignment. Individual cells are pumped by four vacuum manifolds through radial holes. The internal geometry of the cavity cells is machined by single-point diamond turning to an accuracy of 1μm and to a surface finish of 20 nm. The unit cost of mass-producing the cups for these sections has been estimated by a recent in-depth cost estimate study carried out by four independent firms to be about \$12. The individual cups are brazed together by a special copper-copper diffusion/brazing technique developed at CERN for this specific application. Microwave quadrupoles are used for single-bunch wakefield stabilization–they focus the tail more strongly than the head. These quadrupoles, featuring simultaneous acceleration and time-dependent transverse focusing, are obtained by giving 10% of the accelerating sections

a circular aperture in a flat (quasi-rectangular) cell. Two full-length accelerating sections have been fabricated and tested with the CLIC nominal pulse length of 12 ns to 94 MV/m (the nominal CLIC gradient is 80 MV/m) without breakdown (no conditioning was needed).

Status of TBNLC

Demonstration of rf power extraction from an intense relativistic electron beam has been performed. Also, the concept of the reacceleration of a bunched beam and later rf power extraction has been shown experimentally and theoretically. Construction of a partial TBNLC unit is planned to start this year at LBNL and to be completed within a five-year period. This test facility will investigate issues of beam dynamics, efficiency, and operational control. Physics and engineering support will explore beam dynamics that would be seen in a full scale TBNLC unit and refine cost estimates. The test unit could also provide the rf power for a 100 MV/m test at the NLCTA at SLAC.

Status of CLIC

The present status is that: (i) a 95 MeV drive beam consisting of a train of 24 bunches spaced at 10 cm with a charge per bunch of 4.2 nC and an rms bunch length of 1.3 mm has been generated using a photoinjector linac consisting of a laser-illuminated (262 nm) photocathode (Cs_2Te) in an S-band rf gun (100 MV/m) followed by an S-band rf booster; (ii) 76 MW of 30 GHz power has been generated by the 95 MeV drive linac — this power has been transmitted to a CLIC accelerating section in a two-beam configuration and has been used to accelerate a low intensity electron beam; (iii) the output waveguide of the transfer structure has transmitted 60 MW of 30 GHz power without breakdown (nominal waveguide power 45 MW) but has not yet been tested with a bunched beam.

The work remaining to be done includes:

- (i) further studies of beam dynamics of the drive beam to substantiate the assumed minimum energy level, to design a realistic segmented focusing layout, to check velocity dephasing/debunching, and to study wakefields and energy spread effects on beam size in SC cavities.
- (ii) further studies of momentum rotation section.
- (iii) studies of an alternative scheme based on beam stacking in an isochronous ring for improved power efficiency and lower cost.

2.3.4 Summary and Comparisons

The present status of linac technology for the various machine proposals is summarized in the four tables on klystrons, modulators, pulse compression and accelerating structures. The gaps between design goals and the results that have been achieved to date is apparent in these tables; details as to how these gaps will be overcome by further R&D during the next few years have been given in the preceding text. The tables themselves provide the best summary of linac technology status, and only a few brief comments will be added here.

Klystrons

As discussed above, all of the klystron development programs have made major progress and several of them have reached their design power output goals (SBLC, NLC). Measured efficiencies still fall short of the design values, but a comparison in each case between the design efficiency and the maximum scaled efficiency shows that the design efficiencies are reasonably conservative. If properly funded, R&D over the next three years has a good chance in most cases of closing the gap between overall klystron design goals and achieved performances.

All of the proposals appear to have a window design which is adequate at present power levels; in the case of the JLC and NLC klystrons, the windows have been tested at full design power in a resonant ring. In three of the designs (SBLC, JLC, NLC), focusing solenoids must be replaced by PPM focusing, or by a superconducting solenoid, to reduce average power. There remain issues of lifetime and reliability, which cannot be accurately predicted until a relatively large number of operational tubes of the final design have been built. One predictor of cathode life time is the cathode loading; this seems somewhat high in the case of the JLC klystron.

Modulators

The technology of modulators of conventional design is quite mature. Efficiency and reliability can be well predicted if the design does not depart radically from standard designs (e.g., the SLAC modulator, which has had 240 units operational for almost three decades). The most important predictor of modulator efficiency is the turns ratio of the output pulse transformer. To reduce this ratio, two of the designs (JLC, NLC) propose a Blumlein type of pulse forming network. Reliability issues must be carefully considered for this and other major departures from conventional modulator design. Two of the designs (SBLC and JLC) have efficiency design goals which are greater than that predicted on the basis of pulse length and transformer turns ratio. The R&D program in these cases must show that the proposed efficiency can, in fact, be achieved.

RF Pulse Compression Systems

RF pulse compression is a new technology where both system efficiency and peak power capability must be demonstrated in prototype systems. NLC and VLEPP have carried out high power tests which have reached roughly half of the design peak power. For both NLC and VLEPP, compression efficiencies which are close to the design goal have been demonstrated. Neither proposal has demonstrated the design efficiency for power transmission and rf distribution on a full-scale prototype. In the case of the NLC, the required transmission efficiency has been demonstrated for individual components, but falls short when these components are assembled into test systems. It is expected that this efficiency problem for power transmission can be overcome; if so, by 1996 the NLCTA will have provided a convincing demonstration of the effectiveness of the solution in a full-scale system. The JLC compression system (the DLDS) is in the design stage only; system tests will be carried out later this year in collaboration with the VLEPP group.

Accelerator Sections

TESLA, SBLC, NLC and CLIC have met or exceeded their design goals for unloaded gradient in tests on full-scale section prototypes [for details see footnote 1), Table 2.3.6]. For copper structures, tests on short sections in fact indicate that breakdown limits are well

above the design gradients for all of the machine proposals. The real problem has been obtaining sufficient rf power to drive a full-scale structure to the design gradient. The major potential problem is not so much breakdown in the accelerating sections at the operating gradient, but the magnitude and effects of dark current (on beam position monitors for example). Tests on dark current effects will be an important goal for the multi-section test facilities which are planned for TESLA, SBLC and NLC.

The second major component of accelerating structure design is wakefield suppression. For all of the proposed section designs, theory and simulation indicate that the suppression is adequate to prevent unacceptable emittance growth. The NLC detuned section has been tested with a beam (ASSET studies in the SLC), and good agreement was found between the measurements and theory. It is fully expected that further beam tests in the S-band Test Facility (DESY) and the NLCTA (SLAC) will verify the adequacy of wakefield suppression in the design of the SBLC and NLC sections. TESLA has additional problems due to the superconducting nature of the structure: microphonics, detuning due to the electromagnetic forces acting on the metallic surface, and enhanced cryogenic losses due to beam-induced higher-order-mode power dissipation. These effects will be fully measured in the TTF at DESY.

The biggest problem facing all of the structure designs is not a scientific problem but an equally difficult practical one: how to manufacture the accelerating sections to the required tolerances at a reasonable cost. All of the groups will be working hard on this as part of their R&D programs for the next three years.

Table 2.3.1
General RF Design Parameters for Main Linac

	TESLA	SBLC	JLC	NLC	TBNLC	VLEPP	CLIC
RF frequency (GHz)	1.3	3.0	11.4	11.4	11.4	14	30
Accelerating Gradient							
Unloaded/Loaded[1] (MV/m)	25/25	21/17	73/58	50/37	100/74	100/91	80/78
Overhead Factor,[2] F_{OH}	1.00	1.05	1.09	1.09	1.10	1.07	1.02
Active Linac Length[3] (km)	20	30.2	8.7	14.2	7.1	5.8	6.3
Total Linac Length[4] (km)	29	33	10.4	15.6	7.8	7.0	8.8
Peak Power per Meter (MW/m)	0.206	12.2	100	50	200	120	144
Structures per Power Unit (PU)	32	2	4	4	1	4	2
Structure length per PU (m)	33.2	12	5.2	7.2	1.8	4.0	0.56
Total Number of Power Units[5]	604	2517	1660	1968	3938	1400	11233
Total Number of Klystrons	604	2517	3320	3936	—	1400	—
Total Number of Modulators[6]	604	2517	3320	1968	26	140	2
Repetition Rate (Hz)	10	50	150	180	120	300	2530/1210[9]
RF Pulse Length at Structure (μs)	1315	2.8	0.23	0.240	0.242[7]	0.11	.0116
Peak Beam Current[8] (A)	.0083	0.30	0.80	0.74	1.49	SB	SB/1.92[9]
Total Ave. RF Pwr. at Str. (MW)	54	51.6	32.4	30.6	41	22	26.4

1) On-crest beam loaded gradient, taking into account both single-bunch and multibunch beam loading.
2) Includes allowance for: off-crest operation for BNS damping; feedback overhead; inactive accelerating sections (repair margin), feedback overhead and repair margin not included for TESLA and CLIC.
3) Active length = [(500 GeV − 2 × injection energy)/(loaded gradient)] × F_{OH}.
4) Total linac length = Active length plus allowance for beam line components, including cryostat where applicable.
5) Number of power units = number of klystrons for TESLA, SBLC and VLEPP, = number of pulse compression units for JLC and NLC, = number of transfer structures for TBA and CLIC. For VLEPP there are two pulse compressors per power unit.
6) Number of drive beams for TBA and CLIC and number of high voltage sources (supermodules) for VLEPP.
7) Equivalent length for a rectangular pulse.
8) SB=single bunch acceleration.
9) For acceleration of 1/10 bunches.

Table 2.3.2
RF System Efficiencies and AC Power Requirement: Design Goals

	TESLA	SBLC	JLC	NLC	TBNLC	VLEPP	CLIC
Klystron Electronic Efficiency [1](%)	70	50	45	60	92	60	75
Klystron Auxiliary Power[2] (MW)	2.7	2.5	7	1.5	—	1.4	—
Pulse Compression Efficiency (%)	—	—	98	77	—	74	—
Power Transmission Efficiency (%)	96	97	95	94	98	95	90
Modulator Efficiency[3] (%)	86	80	82	72	44	95	52
Modulator Auxiliary Power [4] (MW)	—	3.5	5	3	3	0.4	1
Cryogenic Power (MW)	58	—	—	—	—	—	24
Total Aux. plus Cryo. Power (MW)	61	6	12	4	3	2	25
RF System Efficiency Excluding Auxiliary & Cryogenic Power (%)	58	38	34	31	40	40	35
AC Power Excluding Auxiliary and Cryogenic Power (MW)	94[5]	133	102	98	103	55	75
Total AC Power (MW)	154[5]	139	114	103	106	57	100
Net Efficiency for Production of RF Power[6] (%)	35	37	30	30	39	39	26
Efficiency for Conversion of AC Power to Beam Power (%)	21	10.4	5.6	8.2	16.7	8.4	1.6/7.8

1) For TBNLC/CLIC: efficiency for conversion of drive beam power to rf.
2) Cathode heater plus solenoid power.
3) Drive beam production efficiency for TBNLC/CLIC.
4) Thyratron cathode and reservoir heater power (drive beam focusing for CLIC).
5) Does not include regulation reserve.
6) Including cryogenic power for TESLA and CLIC.

Table 2.3.3
Klystron Parameters: Design Goals and Achieved to Date

	TESLA		SBLC		JLC		NLC		VLEPP	
	Design	Ach.'d	Design	Ach.'d	Design	Ach.'d	Design	Ach.'d	Design	Ach.'d
RF Frequency (GHz)	1.3	1.3	3.0	3.0	11.4	11.4	11.4	11.4	14	14
Peak Output Power (MW)	7.1	5.0	150	150	135	96/50	50	67/55	150	60
Pulse Length (μs)	1314	2010	2.8	3	0.5	0.1/0.2	1.2	0.05/1.5	0.50	0.7
Repetition Rate (Hz)	10	10	50	60	150	100	180	60	300	2
Ave. Output Power (kW)	93	100	21	27	10		11	0.2/5	24	
Microperveance	0.5[1]	2.0	1.2	1.8	1.2	1.2	0.6	1.2	0.25	0.15
Electronic Efficiency (%)	70	45	50	42	45	33	60	44/38	60	40
Scaled Max. Efficiency[2] (%)	73	50	62	53	62	62	71	62	76	78
Beam Voltage (kV)	110	130	575	528	600	620	455	444/430	1000	1000
Beam Energy per Pulse[3] (J)	13,300	10,100	840	1070	150	170	100	8/215	125	100
Cathode Loading (A/cm^2)		3.1	6	6	13.5	13.5	7.4	7.6	5	5
Cathode Heater Pwr. (kW)		0.5	1	2	0.5	0.5	0.4	0.4	1.0	1.0
Focusing Type	Sol.	Sol.	PPM	Sol.	SCM	Sol.	PPM	Sol.	PPM	PPM
Solenoid Power (kW)	4	4	—	15	1	40	—	$\approx$ 20	—	—
Output Window Type	Coax.	Pillbox	Pillbox	Pillbox	TE_{11} TW	TE_{11} $\lambda/2$	TE_{01} TW	TE_{01} SW	TE_{11} TW	TE_{11}
No. of Windows/Klystron	1	1	2	4	2	2	1	1	2	2
Overall Length (m)		2.0	2.5	2.5	1.5	1.5	1.3	1.3	1.46	1.46

1) Perveance per beam in multibeam klystron.
2) η (Max) $\approx$ 0.80 - (0.15 $\times$ Microperveance).
3) In flat-top portion of pulse.

Table 2.3.4
Modulator Parameters: Design Goals and Achieved to Date

Modulator Type[1]	TESLA		SBLC		JLC		NLC		VLEPP	
	Storage cap. with bouncer		PFN		Blumlein PFN		Blumlein PFL		Gridded Gun	
	Design	Ach.'d	Design	Ach.'d	Design	Ach.'d	Design	Ach.'d[5]	Design	Ach.'d
Flat Top Pulse Length, $T_k(\mu s)$	1314	2010	2.8	3.0	0.5	0.7	1.2	1.5	0.50	0.50
Output Voltage (kV)	110	130	575	528	600	620	455	455	1000	960
Transformer Ratio n	1:12	1:13	1:18	1:23	1:5	1:7	1:7	1:20	—	—
PFN Voltage (kV)	9	10	65	46	120	80	66	46	1000	960
Rise/Fall Energy Efficiency (%)	89	89	86.5	≈ 65	89	70	80	≈ 60	—	—
Scaled Energy Efficiency[2] (%)	99	99	70	65	79	70	81	58	—	—
I^2R/Thy./Core Loss Efficiency (%)			97	95	97		97		—	—
Energy Stored on PFN[3] (J)	15000	22000	1000	1650	174		258			
Power Supply Efficiency (%)	97	97	95	90	95		93	≈ 90		
Mod. Eff. without Aux. Power (%)			79.5	≈ 60	82		72	≈ 52	95	
Auxiliary Power[4] (kW)			1.5	3	1.5		1.5	1.5	0.3	
Net Modulator Efficiency (%)	86	86	77.5	59	80		70		92.5	
Ave. AC Input Power (kW) (Including Auxiliary Power)	155	260	54.2	88	29		51.5		40.5	

1) PFN = lumped element pulse forming network; PFL = pulse forming line (transmission line).
2) See text.
3) Energy switched per pulse from storage element for TESLA and VLEPP.
4) Includes thyratron cathode heater, reservoir heater and other control power.
5) Standard (not Blumblein) PFN.

Table 2.3.5
RF Pulse Compression and Power Transmission: Design Goals and Achieved to Date

Table 2.3.5
***RF Pulse Compression and Power Transmission:* Design Goals and Achieved to Date**

	JLC		NLC		VLEPP	
Type of Pulse Compression System [1]	DLDS		SLED-II		VPM	
	Design	Ach.'d	Design	Ach.'d	Design	Ach.'d
Compression Ratio	2		5	6	4.55	4.55
Input/Output Pulse Length (ns)	500/250		1200/240	900/150	500/110	500/110
Compression Efficiency (%)	98		76.5	73	74	72
Power Gain	1.96		3.83	3.7	3.37	3.3
Power Transmission Efficiency (%)	95		94	84	95	95
Power Gain Including Transmission Loss	1.86		3.60	3.0	3.20	3.1
Length of Structure per Power Unit (m)	5.24		7.20		4.00	
Power at Structure per Power Unit (MW)	524		360	150	480	
Maximum Power in P.C. System (MW)	282		380	205	250	150
Required Klystron Power (MW)	2 × 141		2 × 50		2 × 75	

1) DLDS = Delay line distribution system; VPM = VLEPP Power Multiplier.

Table 2.3.6
Accelerating Structures: Design Goals and Demonstrated Accelerating Gradient

Demonstrated	TESLA	SBLC	JLC	NLC	VLEPP	CLIC
Accelerating Mode	π SW	$2\pi/3$ TW	$2\pi/3$ TW	$2\pi/3$ TW	$2\pi/3$ TW	$2\pi/3$ TW
Structure Type and	SW	const. grad.	gauss. det.	gauss. det.	const. imp.	const. imp.
Wakefield Control	2 HOM couplers	2 damping cells, μ-movers	damping cells ?	damping manifold	—	RF quads
Damping (Q_e)	$\approx 1 \times 10^4$	$\approx$2000	?	1×10^3	—	—
Length L (m)	1.035	6.0	1.31	1.80	1.00	0.280
Number of Cells (N)	9	180	150	206	142	84
Filling Time (ns)	515 μs	790	110	100	110	11.6
Attenuation Parameter (nepers)	—	0.55	0.58	0.53	0.79	0.25
Iris Aperture (a/λ)	0.30	0.16-0.11	0.20-0.14	0.22-0.15	0.14	0.20
Group Velocity (% c)	—	4.2-1.4	10-2	11.9-3.0	3.1	8.2
Q_1 to Q_N (or Q_0/Q_L for SW)	$5\times10^9/3 \times 10^6$	13.5×10^3	$7.2\text{-}6.4 \times 10^3$	$7.4\text{-}6.7 \times 10^3$	6.0×10^3	4.2×10^3
R/LQ (kΩ/m)	1.00	3.6-4.7	10.2-13.6	9.1-13.2	17.7	26.2
Unloaded Gradient (MV/m)	25	21	73	50	100	80
Gradient Achieved[1] (MV/m)	25	21		65		94
Input Power (MW)	0.213	73	130	150	120	40.2
Power Diss. per Meter (kW/m)	.002@1.8°K	1.1	2.6[3]	1.6[3]	3.0	2.1
RMS Straightness Tol. (μm/N)[2]	500μm/9	30μm/20		10μm/10	2μm/1 10 μm/142	SB/?

1) In high-power tests on full-scale, near-prototype structure. Except: the NLC structure was tested without damping manifold; the TESLA structure was a "fully dressed" production cavity with a somewhat different input coupler, but tested in a vertical cryostat.
2) Tightest tolerance on structure straightness over N cells. SB=single bunch acceleration with loose tolerance.
3) At unloaded gradient.

2.4 BEAM DYNAMICS

2.4.1 The Group

K. Yokoya (Chairman)
Physics Department, KEK, 1-1 Oho, Tsukuba-Shi, Ibaraki-Ken 305,Japan. E-mail: YOKOYA@jpnkekvx
A. Mosnier (Deputy Chairman)
CEA Saclay, DAPNIA/SEA, CE Saclay, 91191 GIF-sur-Yvette, France. E-mail: MOSNIER@hep.saclay.cea.fr
G. Guignard
CERN, SL/AP, CH-1211, Geneva 23, Switzerland. E-mail: GUIGNARD@cernvm.cern.ch
R. Ruth
SLAC, SLAC, PO Box 4349, Stanford, CA 94309, U.S. E-mail: RRUTH@slac.stanford.edu
R. Wanzenberg
DESY, Notkestrasse 85, 22603 Hamburg, Germany. E-mail: MPYWAR@dsyibm.desy.de

2.4.2 Overview

The main linac is the largest component in a linear collider complex. Its purpose is to accelerate the beam to the desired energy. The major concern of the beam dynamics group, however, is not the acceleration itself but preserving the high beam quality to the final focus system. This must be done both longitudinally and transversely.

The longitudinal quality is defined by the spread and stability in the beam energy, and by the bunch length and stability of the arrival time. Except for the special case when the physics demands an extremely sharp energy distribution, like in t-$\bar{t}$ physics, the direct requirements on the energy spread/stability come from the energy acceptance of the final focus system. The energy spread itself is not hard to achieve; however, it has an important effect on the transverse beam quality via chromatic effects. The bunch length is determined by the bunch compressor system and is frozen once the beam enters the linac because of the high beam energy. The bunch length affects the energy spread because of the curvature of the rf accelerating field and the induced longitudinal wakefield. The arrival time of the bunch at the final focus is only important relative to the arrival time of the opposing bunch. This relative time depends upon the phase locking of the electron and positron systems and sets tight tolerances on the stability of the timing system.

The transverse quality is defined by the emittance and the stability of the beam center. Recent designs of all the linear collider systems adopt very flat beams at the collision point in order to minimize the beamstrahlung. Flat beams are obtained by using a small vertical beta function at the collision point and by using a small vertical emittance. Because this small emittance must be generated in the damping ring or source and then preserved through the acceleration of the beam, the major problems in the linacs are related to the *vertical* beam dynamics.

The transverse degradation of the beam ultimately comes from the misalignments or vibrations of the linac components, i.e, accelerator structures, focusing magnets and beam position monitors (BPM). The physical mechanism of the emittance blowup from the misalignment/vibration includes the optical effects of the focusing system and the transverse wake effects in the accelerator structures. If one assumed a very low intensity, and if the beam were strictly monochromatic, the optical effect would be to shift the beam center,

which could easily be compensated by a simple one-to-one correction method, even pulse-to-pulse using a feedback system, unless the vibration were too fast. However, the actual situation is much more complicated because of the chromatic/dispersive effects which call for more sophisticated correction methods. The wakefield can also cause different trajectories from particle to particle depending on their longitudinal position in the bunch. The relative weights of these two effects depend on the design. In VLEPP and CLIC, wakefield effects are clearly more important, whereas the two effects are comparable in JLC and NLC.

All the existing designs, except VLEPP, adopt multiple bunches in each rf pulse in order to raise the luminosity with only modest added power consumption. By somewhat decreasing the bunch charge of each bunch, it is also possible to decrease the backgrounds due to beam-beam effects at the IP. On the other hand, the multibunch scheme introduces another complication to each item above. The transient beam loading due to the bunch train is roughly 20% in SBLC, JLC and NLC. Thus the bunch-to-bunch energy compensation is very important. The energy spread due to the long-range higher-order longitudinal wakefields is not significant. However, cumulative beam breakup due to the long-range transverse wake can cause a severe problem and must be reduced by a careful design of the accelerator structures.

2.4.3 Where We are Today

Longitudinal Dynamics

Single-bunch energy spread

The short-range wake effects on the single-bunch energy spread have been studied extensively in the SLC. The bunch is placed off the rf crest so that the slope of the rf compensates the variation of the induced single bunch beam loading. This technique will also work for NLC, JLC, SBLC and CLIC. VLEPP, where the bunches are longer and more intense, must also rely on a cancelation of higher order loading effects.

In addition to the above energy spread, a correlated energy spread is added in many designs to compensate the transverse wakefield (NLC, JLC, SBLC, VLEPP). This technique, called BNS damping, takes advantage of the increased focusing on the lower energy tail of the bunch to compensate the deflecting wake due to offsets. This energy correlation can be added and removed by varying the phase of the rf along the linac. It can be left in to pass through the Final Focus provided that the bandwidth is sufficient. These shifts in phase require energy overhead. In the CLIC design the correlation in focusing strength is produced by rf quadrupoles which decouple the BNS compensation and the energy overhead. In TESLA, since the single bunch wakes are small, BNS damping is probably not needed. The bunch can be placed at the optimal phase for minimum energy spread. In VLEPP, energy spread can be controlled by adjusting bunch length as a function of total bunch charge.

Inter-bunch energy spread

The problem of the bunch-to-bunch energy spread is more severe because the uncompensated energy spread due to the transient beam-loading is one order of magnitude larger than that due to the short-range wake. In the TESLA design, the loading is the largest and is compensated by matching the power extracted by the beam to the rf power supplied by the generator during the beam pulse. The residual variations due to Lorentz forces or

microphonic detuning, rf mismatch, beam current fluctuations and power source ripple must be compensated by a feedback system.

The JLC and SBLC design use the "staggered timing" method. By varying the trigger timing from power unit to power unit, one can reduce bunch-to-bunch energy fluctuations to a few parts per thousand. The NLC design achieves the same effect by ramping the input rf power to match the transient of the beam loading. This method will be tested in the NLCTA. Both methods are flexible enough to allow for changes in parameters such as bunch population or accelerating gradient. The staggered timing method is simple but has the disadvantage that the compensation is not done locally but over several rf system modules, allowing the beam to travel through some distance along the focusing system before the bunch energies are fully equalized. This effect has implications for the transverse beam dynamics.

The staggered timing method cannot be applied to the two-beam machine CLIC where the timing is determined by the single driving beam. CLIC will solve this problem by modulating the rf power by varying the charge of the drive beam bunchlets.

Another method to compensate beam loading is to add structures and klystrons, with small frequency shifts from the fundamental frequency. This method is proposed for the JLC(S) and will be tested in the S-band injector linac of the ATF at KEK. The required number of frequency-shifted structures in JLC(S) is about 3% and the residual bunch-to-bunch energy spread will be a few parts per thousand. Again, this technique has the disadvantage that it is not local.

Because of the large loading, the tolerance on the pulse-to-pulse fluctuation of total population of a bunch train is quite tight. This problem is due to dispersive effects in the linac, energy bandwidth of the final focus and in some cases requirements for physics experiments. Since the total energy spread due to the uncorrected loading is about 20% (SBLC, JLC, NLC), a 1% fluctuation of the train population will cause an energy change of 0.2%. The tolerance on the random variation among bunches is much less severe. TESLA plans to allow a 10% fluctuation in current; however, this requires that the rf field feedback system reduce the resultant loading variation by more than a factor of 100; without compensation the 10% change would lead to a 4% energy variation.

Transverse Single-Bunch Dynamics

Since the normalized vertical emittance in all the designs is considerably smaller than that in existing linacs, the emittance preservation is a critical issue even in the absence of the wakefields.

Choice of optics

Apart from details, the linac optics can be characterized by the energy scaling of the beta function and the phase advance per FODO cell. SBLC, JLC and NLC adopt the scaling $\beta \propto E^{\alpha}$ with $\alpha = 1/2$, and use a phase advance of about 90 degrees. This scaling makes the required BNS energy spread constant. In the case of TESLA where the wakefields are weak, the beta function is larger and scales weakly with energy, $\alpha = 0$ to 0.2. The CLIC design, because of strong wakefields, allows the phase advance to vary from 90 degrees at the entrance to 60 degrees at the exit of the linac with $\alpha = 0.35$. In all cases, the vertical and

horizontal phase advances should be separated by about 5-10% to decouple the two planes.

Vibration and centroid feedback

The alignment of a linear collider varies in time because of microseismic activity. If we look in the frequency domain, the motion can be quite large at low frequencies of about .2 Hz, but it falls off dramatically at higher frequencies. In addition, the differential motion between any two points can be correlated. For example, at very low frequency the entire linear collider site simply moves as a unit. At low frequency the beam can be used in a feedback loop to keep the bunches colliding by using steering magnets. This technique is used routinely at the SLC. At a frequency greater than about $f_{rep}/20$ this becomes very difficult to do, and one must rely on the reduced motion at high frequency, correlations of neighboring magnets or some local damping of supports to reduce the motion of quadrupoles. This fast motion (called jitter) has the tightest tolerance which ranges from 10nm to 100nm from JLC/NLC to TESLA (see Table 2.4.1).

Table 2.4.1
Linac Parameters Related to Beam Dynamics for 500 GeV c.m.

			TESLA	SBLC	JLC-X	NLC	VLEPP	CLIC
Accelerating frequency	f_{acc}	GHz	1.3	3.0	11.424	11.424	14	30
Bunch population	N	10^{10}	5	2.9	0.70	0.65	20	0.8
Number of bunches	n_b		800	125	85	90	1	1(10)
Distance between bunches	t_b	ns	1000	16	1.4	1.4	-	0.66
Repetition rate	f_{rep}	Hz	10	50	150	180	300	2530
								(1210)
Normalized emittance	ϵ_x	10^{-6} m.rad	20	10	3	5	20	3.0
	ϵ_y	10^{-6} m.rad	1.0	0.5	0.03	0.05	0.075	0.15
R.M.S. bunch length	σ_z	mm	1.0	0.5	0.090	0.10	0.75	0.2
Total length per linac		km	14.5	16.5	5.2	7.8	3.5	4.4
Unloaded gradient		MV/m	25	21	73	50	108	80
Loaded gradient		MV/m	25	17	53	37	91	78
Normalized iris radius	a/λ		0.15	0.16-0.11	0.20-0.14	0.14	0.2	0.2
Structure length		m	1.04	6	1.31	1.8	1.01	0.280
Number of structures per linac			9664	2517	3320	3936	2800	11233
Phase advance per FODO cell	μ_y	deg	90	90	90	90		90-60
Beta function scaling $\beta \propto E^{\alpha}$	α		(0.2)	0.5	0.5	~ 0.5		0.35
Number of betatron oscillations			52	73	90	80		85
BNS energy spread		%	none	0.9	0.6	0.6		5.5
Jitter tolerance of quad position[1)]		nm	100[2)]	75	10	9	24	30
Pre-alignment tolerance								
for quadrupoles		μm	500	100	100	100		50
for acc. structures		μm	500	100	100	100		10
for BPM's		μm	100	100	100	100		10
required BPM resolution[3)]		μm	10	3-4	1	1-2	0.1	0.1
Total emittance growth[4)]		%	10	30	60	20-25		200

1) The allowance of emittance increase differs from machine to machine.
2) Applies to extremely rapid vibration only. It is 2μm owing to bunch centroid feedback, if slower than $\sim$MHz.
3) For beam based alignment.
4) The respective emittance growths quoted here are calculated for the tolerances attained after applying the beam-based alignment techniques described in the text.

If the local motion is too large compared to the tolerances, it can be reduced by an active stabilization of the magnets using a geophone. Recent tests from the SBLC test facility yielded a reduction by a factor of 3 (20nm in their case). The repetition rate f_{rep} sets the scale for the magnitude of the problem in a particular design. The advantage of looser tolerances in the SBLC design is partly balanced by larger vibration amplitudes at lower frequencies which are more relevant because of the low repetion rate, while machines such as JLC, NLC and CLIC with tighter tolerances will have smaller motions to deal with due to the higher repetition rate.

The exception to this is TESLA which has a very low repetition rate. In TESLA, where the bunches within a train have very large spacing, one can apply feedback on the bunch centroid within the train rather than from pulse to pulse. In this case the first several bunches would be used at the end of each linac to learn the new trajectory and fast correctors would be adjusted to cause the remaining bunches to collide. If the motion is too large pulse-to-pulse, then a local correction technique must be used to avoid filamentation.

Correction techniques

For the large displacements due to the "fixed" quadrupole misalignments of the system, one must use dipole correctors or quadrupole movers to correct the trajectory. A common technique that is used extensively in the SLC is a one-to-one (or one-to-few) correction that uses the nearby position at BPMs to determine the settings of corrector magnets. For TESLA, the one-to-one correction is sufficient, though a more sophisticated correction can relax the tolerances. For the other designs, the quad and BPM alignment tolerance for one-to-one correction is much tighter, a few μm to 20μm over a length smaller than the betatron wavelength in the linac. For larger misalignments, a one-to-one correction causes emittance dilution in the case of SBLC, JLC and NLC, because of dispersive effects and comparable wake effects. In the case of CLIC, the one-to-few correction allows re-centering the initially prealigned quadrupoles (50 μm r.m.s. or more) to within the position tolerance (10 μm) of the position monitors, provided that the BPMs are aligned to this accuracy.

If the BPM centers can be located in the quadrupoles to high accuracy, the beam can be used to align the quadrupoles to about that same accuracy. This can be accomplished to the level of the BPM resolution by varying the quadrupole strength and observing beam motion on BPM's downstream. This method has been used extensively for quadrupole alignment in the SLC where the alignment is about a factor of 8 worse than the BPM resolution. This technique has the disadvantage that it is time consuming. If the dilutions are primarily caused by dispersive effects, one can use a similar technique called DF (Dispersion Free) steering that reduces the dispersion locally. This technique works quite well with weak wakefields and can loosen quadrupole tolerances to the 100 μm (NLC, JLC) and 500 μm (TESLA) levels respectively. This technique also depends upon the BPM resolution which ranges from 1 μm to 10 μm in the above examples. VLEPP has developed a different correction scheme called "adaptive alignment." It consists of measuring the beam position for a single pulse or averaged over several pulses in all quadrupoles simultaneously, by using the data from three adjacent BPM's for each quadrupole. This correction can be applied for the entire linac on the order of ten times per second, and used continuously during a physics run. By this method, the short wavelength components of the misalignment can gradually be smeared out and the vibrations of linac elements with frequencies on the order of 1 Hz can

be compensated. The corrections can be achieved by moving the quadrupoles or by using special dipole coils on the quadrupoles.

Wakefield effects

The next step is to include the effects of the wakefields. It has been known for more than ten years that the effects of the short-range transverse wake can be reduced by BNS damping. This technique has been tested extensively at the SLC. BNS damping is essential for all the designs except for TESLA. The variation in the betatron frequency from head to tail of the bunch is less than 1% for SBLC, JLC and NLC. In these three designs, the frequency change is produced by the negative energy slope obtained from the longitudinal wake and the rf phase. The energy spread is eventually eliminated at the end of the linac by a compensating change in the rf phase. In case the IP is designed with a small crossing angle, this energy slope can be kept for crab crossing using the dispersion function (SBLC), provided that high luminosity is more important than energy spread.

The required spread for BNS damping in CLIC is very large (5%) because of the strong wakefields. In this case the BNS damping is made by modulating the transverse focusing strength along the bunch by using a time dependent (rf) quadrupole field generated by oval-bodied accelerating cavities. These rf quads work at a phase where the acceleration and the slope of the transverse focusing are maximum since only this slope is relevant for BNS damping. VLEPP, for which the required spread exceeds 10%, may have a more sophisticated mechanism called "autophasing."

When considering an alternating gradient system, BNS damping only takes place in the average. To avoid enhancing wake effects in this case, the above DF correction should be replaced by a so-called WF (Wake-Free) correction, in which the strengths of focusing and defocusing quads are changed differently. In the ideal case this technique causes wake effects as well as dispersive effects to cancel locally.

Several other methods of correction have also been proposed. In one of them the bunch population and/or bunch length are changed instead of changing quadrupole settings. Alternatively (and more simply) the accelerator structure misalignments can be eliminated by moving the structure to reduce the HOM signals induced in the structure. This technique is planned for the SBLC, NLC and VLEPP. For VLEPP, special movers with a few nanometers accuracy and a frequency response up to 30 Hz have been designed and tested to move accelerator structures. Also, wakefield effects can be canceled nonlocally by using nondispersive bumps (except in CLIC where the wakefields are too high). In this way, wakefield tails can be compensated without introducing extra dispersion.

The strategy of including all these correction techniques, fast to slow, small to large amplitudes, will be discussed in the section on alignment.

Transverse Multibunch Dynamics

Assuming that the bunch-to-bunch energy spread is well compensated, the major problem of the transverse multibunch dynamics is cumulative beam breakup. Again, the problem is similar in SBLC, JLC and NLC. For TESLA, a slight damping of the higher order modes is needed in addition to the natural frequency spread due to the fabrication errors.

For SBLC, JLC and NLC, various types of accelerating structures have been investigated as a cure for the beam breakup problem. These can be classified into two categories, damped structures and detuned structures. In addition, damped structures can be divided into

strongly damped structures (i.e. $Q \sim 20$) and lightly damped structures ($Q \sim 1000$).

Although many different types of strongly damped structures have been considered, the most promising is the choke mode cavity. This structure is a combination of a radial line which damps all modes by letting them leak out, and a choke that just reflects back the accelerating mode. The required Q-value of the dominant TM_{11} mode for the JLC is less than 20, whereas the expected Q in the design is much less than 10. Details are discussed in the section on linac technology. An S-band model was constructed at KEK for high power experiments and has revealed excellent properties as expected from the design.

Constant-gradient structures, which in some sense are already detuned structures, have been studied for SBLC, JLC and NLC. The constant-gradient structures are known to be far better than constant-impedance structures with respect to the beam break-up problem because of the spread in the deflecting mode frequencies. The idea of the detuned structure is to enhance this effect by intentionally distributing the frequencies in a smooth distribution. This has been considered for the JLC(X) and NLC. The required spread is determined by the bunch-to-bunch distance, and in the case of JLC and NLC is about 10%. This spread is created by changing the iris aperture from cell to cell. In the NLC design, the disk thickness is also varied in order to have a large spread in the higher deflecting mode frequencies. A full scale detuned structure has been tested at SLAC with a satisfactory agreement with theory if one takes into account the fabrication errors. However, the cancellation of the long-range tail is still marginal. To cure this problem, JLC may have an interleaved distribution of cell frequencies between two structure families. The NLC design will use the detuned structure but add additional damping by means of four symmetrically placed waveguides running parallel to the structure and closely coupled to each cell. These damping manifolds result in Q's $\simeq$ 1000 for the deflecting modes and leave the fundamental essentially unchanged. The manifolds can also be used as monitors for beam position in the structure for alignment. In the case of SBLC, the conventional constant-gradient structure has a smaller relative frequency spread, but the bunch-to-bunch distance is 48 fundamental rf buckets as compared to 16 buckets in JLC and NLC. The increased spacing and larger number of bunches cause the long range tail of the wake to be more important in SBLC. The beam breakup cure adopted for SBLC is to prepare ten types of constant-gradient structures with the HOM frequency shifted by 36MHz in total. In addition, the higher order modes are damped down to $Q < 4000$ via two damping ports per plane and lossy material covering the tips of a number of irises. The HOM signal detection is also planned for monitoring the structure position, and moving the structure with respect to that signal by means of a mover.

If after this effort, there remain some orbit differences between bunches, the residual difference can be corrected by several pairs of fast position monitors and kickers which can be adjusted for each bunch, or at least for groups of bunches. The measurement and correction need not be pulse-to-pulse and one may accumulate information over many pulses.

Alignment Techniques

Recent experimental and theoretical studies have resulted in the development of a number of beam-based alignment techniques. With these techniques, the initial or pre-alignment tolerance is looser than the available survey accuracy. This kind of prealignment is similar for all machines. A value of 100μm over a distance of a betatron wavelength is already

within the present level of technology. The pre-alignment tolerances (or the assumed survey accuracy) for the different machines are given in Table 2.4.1.

The ground motion has been investigated in various locations in the world. What is important for linear colliders is how the relative displacement between two points varies in time. Apart from some systematic motions (due to, for example, the electric power lines and the ocean tides, etc.), the so-called "ATL-law", which was first suggested by the VLEPP group, seems to apply at relatively long time scales. The law states that if one measures the change Δy of the relative position of two points separated by L, the expectation value after a time T will be expressed as $\langle \Delta y^2 \rangle = A \times T \times L$, where the coefficient A depends on the site and ranges from 10^{-19}m/s in quiet places to 10^{-16}m/s in noisy places. Although every motion cannot be described by this law, it is a good model for simulation studies. Assuming the coefficient, one can estimate how often each correction has to be repeated.

Every linear collider design uses a somewhat different beam-based alignment technique. The accepted total emittance growth together with the required resolution of the BPM's is also given in the table. The orbit correction and alignment philosophies for each machine are discussed below.

TESLA

In TESLA, the initial rms misalignment resulting from a standard survey will be on the order of 500 microns for the cavity and quadrupole components. The quadrupole and BPM errors must then be located to the 100 micron level by a beam-based alignment procedure. This level has been achieved at the SLC with BPM resolutions of about 15 microns. The TESLA BPM resolution must be of that order also. An alternative method that avoids linac modeling is to vary the quadrupole strengths one by one to determine the location of the quadrupole magnetic centers. The beam is then steered with the one-to-one correction. With a cavity misalignment tolerance of 500 microns, the combined effects - dispersive and wakefield effects - give an emittance growth of about 10 %, including the initial and correlated energy spreads. Both effects have been balanced by a proper optimization of the lattice. No cavity movers are needed to align the structures to the beam. Thanks to three combined effects: structure damping ($Q \simeq 10^4$ to 10^5), natural cavity-to-cavity detuning due to fabrication errors (0.5 to 1 MHz) and the large bunch spacing, the multibunch emittance dilution is much smaller (about 10 times) than the single-bunch dilution. For that reason, combined single and multibunch simulations give very similar results to the single-bunch ones. In addition, the non-dispersive bump technique is very efficient for all the individual bunches of the train and can increase the cavity misalignment tolerance.

Because of the large bunch spacing, a kicker located at the linac exit could be used to re-align the centroids of the later bunches in the train. The jitter tolerance on quadrupole motion, which is then determined by the single bunch emittance dilution, amounts to a few microns. For slow ground motions, a feedback is needed to re-steer the beam periodically. According to the ATL law, the feedback has to be faster than 40 to 400 seconds, depending on the A factor. When the quadrupole displacement becomes too large, on the order of 100 microns, the quad and BPM errors have to be determined again through a beam based alignment. The re-alignment procedure should be repeated every 4 to 40 days. The step-by-step correction would be applied if the periodicity is of a few weeks, whereas a "dispersion/wakefree" type correction would be preferable for a shorter time.

SBLC

The SBLC design study considers the following alignment approach. All components will have to be pre-aligned within a 100 μm (rms) tolerance over a distance of about 500 m. After an initial one-to-one steering with a low intensity single bunch, a beam based orbit correction will be performed using the DF and WF algorithms. Then the accelerator structures will be moved on the basis of the signals from the HOM dampers. As a result of this, a final alignment tolerance of 30 μm (rms) for the accelerating structures will have to be achieved with respect to the orbit. This should limit the emittance growth to 25 %. Non-dispersive bumps may be used for a fine tuning of the emittance preservation.

NLC

In the NLC correction procedure, the initial linac alignment of quadrupoles and structures will be done with conventional techniques to the level of about 100 μm. Then the error between the BPM centers and quad centers will be determined to a few microns by varying the quadrupole strengths. After this, the trajectory will be steered through the centers of the quadrupoles, a process which establishes a "gold" trajectory. Using HOM detection on each structure, the accelerator structures will be aligned to this trajectory with movers to the level of about 10 μm. Higher intensity bunches will be used to confirm alignment. If there are residual bunch-to-bunch effects, these will be corrected with bunch-to-bunch kickers that will realign the train. The beam will be frequently resteered back to the gold trajectory. If necessary, the gold trajectory may be quickly updated with WF steering. Centroid feedback will be used to stabilize the bunch train for motions below 10 Hz. For higher frequency ground motion due to background and cultural noise, the size will have to be (and is expected to be) small enough to keep resultant beam motion to less than $\sigma/4$.

CLIC

For CLIC, the accelerator will have to be pre-aligned so that the beam passes through the available aperture along a fraction of the linac. It is foreseen to do this by using signals from a stretched-wire system; the relative positions of two adjacent support girders (1.4 m long) will thus be maintained within a few microns transversely, while excursions from a straigth line of about 0.2 mm will be allowed over longer distances of say 100 m. The quadrupoles will be supported and activated independently of the string of girders, and the BPM signals will be used to optimize their positions. First using a one-to-few algorithm with approximately 3 monitors for 1 quadrupole, correction will be effected by moving the quadrupoles which are thus re-centered toward the ideal line within the position tolerances of the monitors (i.e. 10 μm). Next will come corrections based on trajectory difference measurements and on the observation of the emittance at 10 or 12 positions along the linac. These may be either the DF and WF algorithms or a correction method which uses difference measurements while simultanously varying the bunch intensity as well as the quadrupole setting in order to minimize the wakefield effect and the dispersion. The high resolution of the 30 GHz resonant cavity BPM (0.1 μm) makes these methods very efficient, and the vertical emittance growth may be maintained below the CLIC design value even in the presence of strong wakefields. Corrections may be iterated and the high repetition rate will offer the possibility of fast feedback.

2.4.4 Status and Future Plans for Each Machine Design

The beam dynamics parameters of all linear collider design studies can be found in Table 2.4.1.

TESLA

For TESLA, the short-range and long-range wakefield effects are small because the rf frequency is low and the iris aperture is large. Nevertheless, the magnitude of these longitudinal and transverse wakefields can and will be carefully checked in the TESLA Test Facility by injecting the bunches on and off-axis. The single bunch energy spread can be kept small (on the order of 5×10^{-4}) because the longitudinal wakefield is small and no BNS is needed, and the multibunch beam-loading in the ideal case is compensated by the rf generator along the entire bunch train. The different energy spread sources will also be carefully studied in the facility. Although the alignment tolerances are rather loose, the alignment errors of the components inside the cryostat must also be measured before and after cooldown. Apart from these checks, no new developments concerning the beam dynamics are required because all the components already exist: the BPM resolution is reasonable, no micromovers are needed, there are no stringent mechanical tolerances in the cavity fabrication and quadrupole stabilizers are not required.

SBLC

For the SBLC design study, it is worthwhile to mention that the invariant emittance in the SLC linac at SLAC is, even for the vertical plane, only a factor 10-20 higher than assumed for the SBLC design. Furthermore, the bunch population of 2.9×10^{10} is lower than the values already achieved at SLAC. However, the alignment tolerances of structures and quadrupoles are tighter than those in the SLC.

To avoid single bunch emittance growth and multibunch beam breakup, the following diagnostics and cures are considered for the SBLC: beam-based alignment techniques, higher order mode dampers at each accelerating structure and lossy irises, accelerating structure movers, nondispersive trajectory bumps (tuned by emittance measurements), fast kickers, and active stabilization of quadrupole supports, which have already been experimentally studied at the test facility.

To preserve the small single bunch emittance in the SBLC, a BPM resolution of 3 to 4 μm is required as indicated by computer simulations. For the FFTB at SLAC an even better BPM resolution has been achieved. The mechanical prealignment tolerances of the quadrupoles and the BPM's are much looser ($\sim$ 100 μm). HOM dampers are necessary to damp the dipole modes, which drive the cumulative multibunch beam breakup. Furthermore, the accelerator structures can be moved on the basis of the HOM signals. The usefulness of the HOM signals as a diagnostic tool will be investigated at the DESY S-band test facility. Once the multibunch beam break-up is cured by HOM dampers and structure movers, the single bunch effects determine the alignment tolerances.

JLC

For the JLC, there are still many items to be studied, in particular for the S-band and C-band designs. All three designs are based on the same emittance and have the same final focus system which was originally intended for the X-band design. If the small emittance design for X-band is feasible, there is no strong reason against adopting the same small emittance for the lower frequency bands. The small emittance allows low beam power which is advantageous in designing the particle sources and the damping rings. One disadvantage of the tight focusing at the IP for low rf frequencies is the need for a short bunch length. However, as a problem in linac dynamics for a given emittance, the lower bands should show different features mainly because of the reduced wakefields. In fact, the structure misalignment tolerance in the present design is considerably looser for S- and C-band (e.g., a factor of 4 greater in C-band than in X-band). Therefore, further studies in the direction of looser focusing in the linac should be carried out.

NLC

For the NLC, most of the beam dynamics issues have been modeled in detail, and where possible, experience from the SLC and FFTB has been used to develop the design. The beam-based alignment of quads is well established in the SLC and FFTB. With the achieved BPM resolution in the FFTB, the NLC linac can be aligned to the required level using beam-based techniques. BNS damping is well understood, both theoretically and experimentally. The detuned structure performs as expected, and the damped detuned structure will further decrease the wakefields to eliminate beam breakup. The tolerances on the structure construction are about 10μm and are achievable with care. The damping manifolds will allow alignment of the structure by providing a structure-to-beam position. Calculations indicate that at 180 Hz, with expected correlations, beam motions resulting from observed intrinsic ground vibrations in model sites remain within acceptably low limits.

CLIC

For CLIC, development work is being carried out on micron-displacement systems, submicron resolution BPM's and active pre-alignment schemes. The work is based on the principle of mounting four accelerator structures on a support girder, the positions of which can be adjusted by micro-movers. These movers with a resolution of 0.1 μm and an absolute accuracy of 1 μm over ± 4 mm provide both large displacements for initial alignment and micron movements for correction. The structures are fixed to the girder via V-supports with a precision of 3 μm. The ends of two adjacent girders are on a common platform which assures continuity of position between units. This system maintains the tolerances but allows the movement of groups of 4 structures in a continous path. The present simulation model uses the actual dimensions (coming from the test bench) for the girders, the drift spaces and the structures; it also includes a more realistic layout divided into 6 sectors of increasing length, with constant lattice in each sector, but different focusing characteristics corresponding to the energy scaling.

The parameters of Table 2.4.1 suggest that the following points for CLIC also be considered. The high resolution of the BPM's which is inherent to the design (resonant cavity) but not an actual requirement for the corrections, would work as well with a value on the order of 1 to 2 μm, i.e., small with respect to the position tolerances (10 μm). The prealignment tolerances of the quadrupoles reflect a beam transmission condition applied to the whole 250

GeV linac; they could easily be increased to say 100 μm, by applying this condition to only a fraction of the linac. Up to now in CLIC, the possibility of using HOM measurements and of moving groups of four stuctures on girders was not yet considered and will be the subject of investigations. Such a correction would allow to relax the pre-alignment tolerances given in Table 2.4.1 for the cavities, which presently represent the bare values required for emittance control. For these reasons, they should be compared to the positioning tolerances aimed at in other designs after beam-based corrections, that range between 10 and 30 μm for non-superconducting linacs. In CLIC however, the correction efficiency relies on the good prealignment of the BPMs that are not linked to the quadrupoles but rather to the cavity girders, for the beam must be well centered in the cavities.

CLIC offers the substantial advantage that the single bunch mode of operation already provides a significant and useful luminosity ($> 10^{33} cm^{-2} s^{-1}$). However, reaching higher values implies running CLIC in the multibunch mode (10 bunches). The multibunch option requires studies of damped/detuned accelerator structures for the roll-off of the wakefields between consecutive bunches, and beam dynamics studies to figure out by how much the long range wakefield has to be attenuated.

2.5 BEAM DELIVERY

2.5.1 The Group

R. Brinkmann,(Chairman)
DESY, Notkestrasse 85, 22603 Hamburg, Germany. E-mail: BRINKMANN@desy.de
V. Telnov, (Deputy Chairman)
BINP, Pr. Lavrentyeva 11, 630090 Novosibirsk-90, Russia. E-mail: TELNOV@inp.nsk.su
A. Dragt
University of Maryland, High Energy Laboratory, College Park, MD 20742. E-mail: DRAGT@quark.umd.edu
J. Irwin
SLAC, 2575 Sand Hill Road, MS 26, Menlo Park, CA 94025, USA. E-mail: IRWIN@slac.stanford.edu
K. Oide
KEK, 1-1 Oho, Tsukuba-Shi, Ibaraki-ken 305, Japan. E-mail: OIDE@jpnkekvx
O. Napoly
CEA Saclay; DAPNIA, F-91191 Gif-sur-Yvette CEDEX, France. E-Mail: NAPOLY@hep.saclay.cea.fr
A. Sery
IHEP, RU-142284 Protvino Moscow Region, Russia. E-Mail: SERY@hep.saclay.cea.fr
B. Zotter
CERN, PS/LP, 1211 Geneva 23, Switzerland. E-mail: ZOTTER@cernvm.bitnet

2.5.2 Overview

The beam delivery system for a linear collider is defined as the section between the main linac and the interaction point (IP). It has to provide:

- Demagnification of the transverse beam dimensions to the required spot size at the IP,
- Correction of the strong chromatic aberrations inevitably induced by the demagnifying beam optics,
- Protection of the interaction region (IR) from background caused by electrons (positrons) with large deviations from the central orbit and/or energy,
- Removal of the disrupted beams after the IP and the beamstrahlung from the IR, and separation of the outgoing from the incoming beam.

The first two requirements are fulfilled by a suitable beam-optical system, the Final Focus System (FFS). Issues critical to the design of the FFS are the energy bandwidth which has to accomodate the total energy spread of the incoming beam, and the tolerances regarding magnet positions and strengths which lead to a degradation of luminosity due to partial transverse separation of the colliding beams and/or blow-up of the spot size at the IP.

The third condition requires a beam collimation system (BCS) between the linac and the FFS which restricts the particle betatron amplitudes and energy deviation to limits set by the properties of the FFS and the IR layout. Issues critical to the BCS are wakefields from the small-aperture collimators which may spoil the emittance, machine safety problems in case of beam loss in the collimators, and the overall collimation efficiency (one minus the probability that large amplitude halo particles escape from the BCS and reach the IR).

Furthermore, muons originating from the collimators/absorbers are a source of experimental background and must be kept under control.

The last condition concerns the geometry of the IR, in particular the crossing angle at the IP and the aperture of the final quadrupoles. The opening angles of the disrupted beams and the hard γ beamstrahlung require a layout which safely guides the debris out from the IR. For the designs which use more than one bunch per rf pulse, a sufficiently large beam separation at the positions of parasitic crossings must be provided. The disposal of the spent beams has to be effected safely and methods to use them for diagnostic purposes must be developed. Specific use of the spent electron beam for positron production is briefly discussed below, and in Section 2.1.

There is general agreement (also see Section 2.6) that the beam delivery system should provide two separate IR's. Therefore, additional bending sections have to be included which provide separation of the two beam lines and yield the geometrical matching of the IR's to the main linacs.

2.5.3 Where We are Today

Overall Layout

A complete detailed layout of the entire system exists for TESLA, SBLC, JLC and NLC. The SBLC layout (very similar to the TESLA layout, except for the zero crossing angle for TESLA) is sketched in Fig. 2.5.1 as an example. It is assumed that the beam lines are split up after a common collimation section, thereby saving tunnel and beam line costs. The same approach is foreseen for NLC. The JLC design assumes separate beamlines after the bending section following the linac.

The total length of the system from linac to IP (two identical lattices for the e^- and e^+ beams are assumed) is about 1.5 km for SBLC and TESLA, 1.8 km for JLC, and 2.2 km for NLC, the differences resulting mainly from the length of the collimation section lattice (see page after next), and in the case of NLC, from an additional 400 m long section for 4D bunch size diagnostics and betatron coupling correction (similar additional sections will most probably have to be added to the other designs as well). All designs assume that the main linacs lie on parallel lines so that the required crossing angle at the IP results from the net bend angle of the respective beam delivery systems.

Interaction Region

The interaction parameters for the various designs are listed in Table 2.5.1. The beam sizes at the IP include aberrations in the FFS (see page after next), but do not include the beam-beam pinch effect, the crossing angle, and the hourglass effect. An effective luminosity enhancement factor which represents a combination of these effects is included in Table 2.5.2. With respect to the hourglass effect, which becomes substantial if the beta-function is smaller than the bunch length σ_z, VLEPP is an exception. It is assumed for VLEPP that the condition $\beta_y^* < \sigma_z$ can exist without luminosity reduction by employing the so-called travelling focus scheme. This scheme uses the coherent energy spread ($\sigma_{E,coh} = 1\%$) in the bunch together with a partially uncompensated chromaticity of the final quad to obtain a z-dependent focal point, which together with the pinch reduces the hourglass effect. The

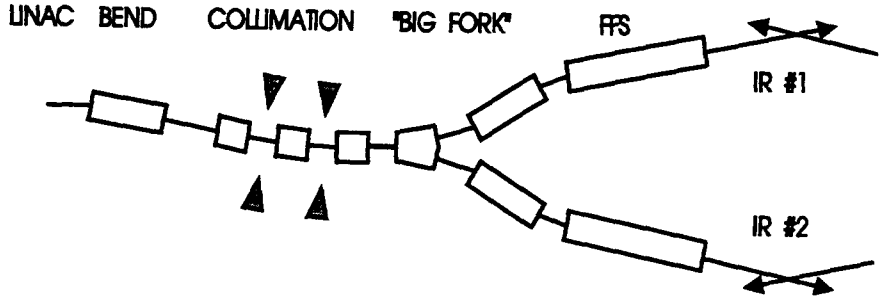

Fig.2.5.1 Sketch of a beam delivery system.

travelling focus leads to an enhanced sensitivity of the luminosity with respect to beam separation at the IP. The luminosity loss due to beam offsets is about a factor of 5 larger than for the other designs. The coherent intra-bunch energy spread is also used for SBLC, where the effect of the crossing angle on luminosity is compensated by introducing a finite dispersion function at the IP: crab-crossing is obtained without the need for rf devices but $\sigma_{E,coh} = 0.5\%$ is required.

	TESLA	SBLC	JLC(X)	NLC	VLEPP	CLIC
$N_e(10^{10})$	5.1	2.9	.65	.65	.63	0.8
$\gamma\epsilon_x/\gamma\epsilon_y$ (m-$rad \times 10^{-6}$)	20/1	10/.5	3.3/.045	5/.05	20/.06	3/.15
β_x^*/β_y^* (mm)	25/2	22/.8	10/.1	10/.1	100/.2	10/.18
σ_x^*/σ_y^* (nm) before pinch	1000/63	678/30	280/3.5	320/3.2	2000/6	250/7.5
σ_z^* (mm)	1	.5	.07	.1	.75	.2
θ_c (mrad)	0	3	7.2	20	5	1
l^* (m)	3	2	2.5	2	1.25	1.25
a_Q (mm)†	24	4	6.8	5	6	3.5

† Final quad aperture.

Table 2.5.1 Basic IR parameters. The spot sizes include aberrations in the FFS.

	TESLA	SBLC	JLC(X)	NLC	VLEPP	CLIC
$<\Upsilon>_{av.}$	.029	.041	.096	.16	.074	.075
$<\Delta E/E>_{bm.}(\%)$	3.1	2.8	4.5	3.0	10.8	3.5
$<\Delta E/E>_{c.m.}(\%)$	1.8	1.5	2.5	1.8	4.0	1.8
N_γ/N_e	2.7	1.8	.95	.85	5	1.35
Disr. Param. D_x/D_y	.5/8.5	.4/8.5	.1/6	.1/8.	.4/170	.3/9.8
Enh. Fct. H_D	2.3	1.7	1.2	1.4	1.0	1.42
$L_{bunch}(10^{29}cm^{-2})$	3.29	3.30	3.87	4.60	324.8	4
$L(10^{33}cm^{-2}s^{-1})$	6.04	3.51	5.22	7.40	7.8	1.00

Table 2.5.2 Parameters related to beam-beam effects. The machine luminosity has been included for consistency with other sections of the report. In the case of CLIC, the luminosity is given for single bunch operation . For operation with 10 bunches (option under study) the CLIC luminosity would be $4.8 \times 10^{33}cm^{-2}s^{-1}$. For VLEPP, the effective enhancement factor including the crossing angle has been estimated according to simulation results obtained with R. Brinkmann's computer code.

For the crossing angle θ_c, two criteria must be considered. The first sets a lower limit in order to avoid the multibunch kink instability arising from parasitic long-range beam-beam interactions between the bunch trains travelling in opposite directions. VLEPP, being a single bunch machine, and TESLA, with the first parasitic interaction 150 m from the IP, are exceptions here. The criterion is fulfilled for all designs. However, for CLIC with the multibunch option, a 1 mrad crossing angle would be close to the limit.

The second criterion in the choice of θ_c concerns the exit of the debris from the IP through the final quad. Beamstrahlung and particles from the disrupted beam must not hit the quad aperture. A larger θ_c is desirable here (JLC, VLEPP), but even for SBLC (3 mrad) simulations have shown that the specified quad aperture a_Q and crossing angle are also sufficient to fulfill this criterion. For CLIC this is yet an open question: the detailed IR

layout is still under discussion and the use of large aperture superconducting quads might provide a solution.

NLC favors an even larger crossing angle and requires crab crossing using special rf cavities. This allows the use of permanent magnet final quads (with advantages concerning field and position stability) accompanied in series by superconducting quads (outside of the detector) for energy tunability.

Transmitting the spent beams outside the final quads is also considered advantageous from the point of view of using them for diagnostic purposes. The tolerance for the crab rf phase is 0.2 degrees, but it concerns only the relative phase difference between the cavities for the e^+ and the e^- beams. Powering both cavities from one klystron will help achieve this phase stability.

TESLA will have head-on collisions with a separation scheme using electrostatic separators (compensated by a magnetic field for zero deflection of the incoming beam) outside the IR and the use of large aperture superconducting quads close to the IP, through which the spent beam can safely exit. With iron-free superconducting quads, TESLA does not need a compensating solenoid to shield the quads in the IR. The resulting coupling effect due to the superposition of the quadrupole with the longitudinal field of the detector solenoid can be compensated by a small skew quad close to the final doublet.

The properties of the various designs in relation to the beam-beam interaction are summarized in Table 2.5.2. Background issues are discussed in Section 2.6. Most results quoted here have been obtained with the ABEL simulation code. A difficult case is VLEPP, where the extremely large vertical disruption parameter makes the calculation of the pinch effect difficult with ABEL (the result obtained by A. Sery is quoted in the table). The quoted effective luminosity enhancement factor includes the pinch effect due to the beam-beam interaction according to the simulation, the hourglass effect and the crossing angle.

Final Focus System

The lattice and optics for all FFS's are based on the same concept. The large chromaticity from the final lens is compensated by two non-interleaved pairs of sextupoles separated by a betatron phase difference of 180°. The designs differ in the method that is applied to increase the momentum acceptance of the FFS. SBLC, NLC and VLEPP employ additional sextupoles to minimize higher order chromatic aberrations. JLC achieves a higher bandwidth by introducing a deliberate asymmetry in the dispersion function at the sextupoles. TESLA does not need a large bandwidth, and CLIC has so far not investigated further optimization. All FFS systems provide a bandwidth in excess of the peak-to-peak beam energy spread (see Table 2.5.3). The remaining higher order aberrations and synchrotron radiation in dipoles and quadrupoles cause a dilution of the beam emittance. The effective spot size growth due to these effects (not including tolerances) is included in Table 2.5.3 and also taken into account in the design luminosity quoted in Table 2.5.2.

Concerning tolerances, the sensitivity of the luminosity to various classes of errors is specified in two categories. First, a pulse-to-pulse jitter of transverse quadrupole positions causes a reduction in luminosity due to offsets of the beams at the IP. These tolerances for a luminosity decrease of 2% are specified in the first part of Table 2.5.4, assuming uncorrelated simultaneous position errors for all quads in the FFS (without the final doublet), and

	TESLA	SBLC	JLC(X)	NLC	VLEPP	CLIC
Length (m)	400	450	590	760	?	680
Bend angle (mrad)	-4.8	-9	-7	5.3	?	4.8
Bandwidth (%)	±.8	±1.8	±.8	±.8	±2	±.7
$(\Delta E/E)_{beam,pp}$ (%)	±.1	±1	±.8	±.4	±2	±.5
Aberr. of $\sigma_x^*\sigma_y^*$ (%)	1	6	30	10	20	1

Table 2.5.3 Parameters of the final focus systems.

separately for the final doublet. The pulse-to-pulse beam jitter tolerance must be viewed in relation to the repetition frequency, since the mechanical magnet vibration amplitude decreases with frequency, and orbit feedback can only operate at a fraction (about 1/10) of the linac repetition frequency f_{rep}. This makes it easier for the designs with high f_{rep} (see Table 2.5.4) to stabilize the orbit (TESLA is an exception here, see below).

Second, drifts in magnet position and strength cause an increase in the spot size at the IP, an effect related to a longer time scale than the former one. These tolerances, again assuming uncorrelated errors and 2% luminosity reduction, are summarized in the last three rows of Table 2.5.4. Various correction and optimization procedures have to be applied continuously in order to keep the spot size at the IP close to its design value. Orbit correction, beam based alignment and tuning algorithms have been investigated for JLC, NLC and VLEPP. It is found that a BPM resolution of 1μm with a stability of 0.1μm is required.

A detailed description of the complex spot size stabilization procedure is beyond the scope of this summary. In general, one may say that the ability to achieve nanometer tolerances depends on details of (a) the ground motion spectrum from cultural and seismic sources coupled together with magnet support systems, (b) the resolution of beam-based and element-based diagnostics, and (c) the spectral performance of beam based feedback systems. For example, specification of ground motion requires knowledge of a spectral function P(k,ω). The integral of this function over k gives the well-known spectral power distribution of the motion of a single point. However, the k dependence at a given ω is less well known. Since the beam will follow the contours of long wavelength lattice motions, they are less important than short wavelength motions, making knowledge of the k-dependence of P(k,ω) essential. Diffusive ground motion measurements (also known as the "ATL law") suggest a spectrum that has short wavelengths at all frequencies, whereas wave-like phenomena would have only long wavelengths associated with the large-amplitude low frequency ground motion. Measurements to determine P(k,ω) for frequencies between 1 and 1/100 Hz are underway at several laboratories.

The requirements for TESLA are substantially different from those for the other designs since, on account of the large separation between bunches, there exists the possibility of a fast orbit feedback responding within the passage of a pulse train. The position of the first bunches in the train can be measured, and the remainder of the pulse steered so as to insure collision of the large majority of the bunches in the train.

Collimation section

The collimation system has to assure that in (x,x',y,y',dp/p) phase space, the coordinates are restricted so that (a) the beam is well confined within the aperture of the final quads in

	TESLA	SBLC	JLC(X)	NLC	VLEPP	CLIC
FFS jitter x/y (nm)	186/48	184/28	15/1.5	15/4	300/?	61/10
F.D. jitter x/y (nm)	74/10	51/5	15/.5	15/1	260/.6	19/1.5
$f_{rep}(Hz)$	10	50	150	180	300	2500
FFS pos. x/y (μm)	1/.5	.33/.14	.2/.07	.22/.04	.15/.016	.6/.05
FFS strength (10^{-4})	8	1	.2	.1	(?)	1
F.D. strength (10^{-4})	.6	.3	.08	.06	.05	.2
Bend strength (10^{-4})	.8	.3	.06	.06	?	.1

Table 2.5.4 Jitter and drift tolerances for the FFS (see text for definitions).

front of the IP, and (b) synchrotron radiation generated in the final quads does not hit the face of the first quad on the other side of the IP. The latter condition is the more restrictive one (except for NLC because of the very large crossing angle) and is used to define the acceptance of the collimation section. Since the offset of a trajectory at the final doublet is essentially defined by its slope at the IP, the required restriction in phase space concerns the sine-like (w.r.t. the IP) part of the trajectory much more than the cosine-like part. This argument has been used for the design of the TESLA and SBLC collimation systems, where it is assumed that collimation at the IP-phase (i.e. for cosine-like trajectories) is much more relaxed than at the doublet-phase (i.e. for sine-like trajectories). The prerequisite for such a simplified collimation system to be sufficient is that not too much "mixing" occurs between the two phases between the collimation system and the IP, i.e., an initially large amplitude with the IP-phase must not couple too strongly into the quad-phase because of aberrations in the bending section and the FFS.

Preliminary results from tracking calculations for SBLC and TESLA indicate that this is indeed not the case and that an asymmetric collimation scheme is conceivable, although questions like rescattering of particles from the spoilers and absorbers, and synchrotron radiation in quadrupoles along the beam line have not yet been studied in full detail. The JLC and NLC approaches are less optimistic in this respect and assume that collimation for both phases has to be equally tight. No detailed investigations of collimation have been performed so far for VLEPP and CLIC.

The parameters of the TESLA, SBLC, NLC and JLC collimation systems are shown in Table 2.5.5. All systems are based on ideas originally developed for NLC. The essential idea

	TESLA	SBLC	NLC	JLC	VLEPP	CLIC
Length (m)	310	400	2000	800	?	?
Accept. $A_x/A_y(10^{-9}\mathrm{m})$	4/2	1/.05	.3/.07	.3/.07	?	?
No. of σ's $(A_x/\epsilon_x)^{1/2}/(A_y/\epsilon_y)^{1/2}$	10/35	7/7	9/40	6/35	?	?
Accept. dE/E (%)	± 3	± 3	± 4	± 1.5	?	?
Half gap $_{x/y}$ (mm)	2/4	2.4/1	.7/.5	.3/.3	?	?

Table 2.5.5 Parameters of the beam collimation systems.

is to intercept large amplitude trajectories by short spoilers (2 R.L. of pyrolitic graphite or Ti for SBLC and TESLA, .25 R.L. of graphite for NLC) which create a large spread in particle energy and/or trajectory angle. At suitable positions downstream of the spoilers, these trajectories are then stopped in absorber blocks. Although conceptually similar in

principle, the approaches are different in detail. TESLA, SBLC and NLC assume a so-called conventional approach where the spoilers are placed at lattice positions with large beta-functions to provide a sufficiently large beam spot size on the spoiler so as to avoid damage in case of excessive beam loss due to mis-steering, etc. The JLC design employs a strong sextupole upstream of the spoilers which creates the required blow-up of beam size, and removes the nonlinear distortion after the spoiler by a second sextupole placed 180 degrees downstream of the first one.

The above mentioned difference regarding single-phase vs. two-phase collimation results in considerable differences in the length of the collimation systems. For TESLA and SBLC it is assumed that no additional lattice is required for IP-phase collimation, which is simply provided by introducing a sextupole at a suitable (IP-phase) position upstream of the first spoiler so that the trajectory acquires a large angle and is intercepted by the quad-phase spoiler. In addition, energy collimation is done simultaneously with transverse collimation (separate for JLC). The tolerances concerning magnet position errors for SBLC, TESLA and JLC are relaxed compared to the ones in the FFS, whereas the NLC system has jitter tolerances comparable to the FFS.

A critical issue concerns wakefields induced by the small-aperture spoilers which can dilute the emittance in case of a beam offset. Tapers are planned in order to reduce the discontinuity introduced in the vacuum pipe, and gold-plating of the graphite (or Ti) is proposed to minimize the resistive wall component of the wakefield. These effects do not play an essential role in TESLA.

The required efficiency of the collimation system is directly connected with the fraction of the beam that lies outside the accepted phase space area. This number is difficult to estimate since it requires detailed knowledge of all effects which populate tails in the phase space distribution, as for example gas scattering, wakefields and dark current in the main linac.

For NLC and JLC it is assumed that 10^{10} particles per pulse (about 1% of the total intensity) have to be scraped off the beam by the collimation system. SBLC designers consider that this number is likely to be too pessimistic, but a definite estimate has not yet been made. For TESLA it is believed that scraping of beam halo is much less of an issue since the acceptance is large and the population of tails is expected to be small due to the small wakefields in the superconducting linac (it is assumed in that case that the beam is properly collimated before the entrance into the main linac).

The efficiency of the collimation system is mainly limited by edge scattering effects. It is likely that a small fraction of large-amplitude particles can escape from the system. In order to stop these trajectories as well, post-collimation in the bending section between the collimators and the FFS, and/or in the FFS, are foreseen for all designs. For NLC and JLC the system is designed to yield an efficiency of 10^{-7}, for SBLC and TESLA 10^{-5}.

Bending and matching sections

To complete the overall design of the beam delivery system, additional bending sections to provide the required beam line geometry are included. These sections are placed between the linac and the BCS, and between the BCS and the FFS. All existing designs (TESLA, SBLC, NLC and JLC) use simple FODO lattice structures, the main boundary condition being that

emittance growth due to synchrotron radiation is tolerable (typically on the order of a few %). An additional advantage of the bend between the BCS and the FFS is a reduction in muon background at the IP (muons originate from the spoilers/absorbers of the BCS). The reduction factor is found to be about 20 for all designs. Further reduction is possible by installing a system of magnetized toroid spoilers at strategic positions between the BCS and the IR, and/or by introducing offsets in the tunnel.

For NLC, a beam size diagnostic and coupling correction section, inserted between the big bend and the FFS, has been worked out in detail. As mentioned before, such a lattice insertion will be required for all designs and will add length to the delivery systems (about 400 m in case of NLC).

A special feature of the TESLA design arises from the large spacing between bunches in a train (1 μs). This allows the installation of a beam dump system at the entrance of the BCS which can be triggered between bunch passages if the loss rate at a spoiler exceeds tolerable limits (there is sufficient drift space available in the BCS for this purpose). Furthermore, as has been mentioned earlier, it is possible to measure the transverse position of the first bunch in a train and correct for the orbit of all other bunches with kicker magnets, thus compensating pulse-to-pulse orbit variations originating from quad vibrations in the main linac.

Beam line after the IP

In addition to the requirement that the disrupted beams must be extracted from the IR safely without hitting any aperture limitation, the possibility of continuous monitoring of their properties such as energy distribution, angular distribution and polarization can be of great value. So far, little work has been done in this area for any of the designs. As mentioned above, NLC designers consider it advantageous to use a large crossing angle and pass the beams outside the final quads, whereas for SBLC, JLC, VLEPP and CLIC the spent beams go through the final doublets with an offset. One possible problem with this approach comes from the nonlinearity of the quad fields at large offsets which can considerably distort the phase space distribution. For TESLA, the beams exit through the center of the doublets and thus remain in the region of good (linear) field. In this case, as well as for SBLC, the properties of the spent electron beam are important because it is planned to be used for positron production (see Section 2.1). An optics has been designed which is capable of capturing about 70 % of the spent TESLA beam with an effective emittance of $\epsilon_x = 2 \times 10^{-9} m, \epsilon_y = 10^{-11} m$. The layout also includes methods for separating the outgoing from the incoming beam line, and for collimation of beamstrahlung and the low energy tail of the disrupted beam. Preliminary results for SBLC indicate that the effective emittance of the captured beam will be larger than for TESLA but still sufficiently small for the production of unpolarized positrons. Production of polarized positrons seems to be excluded for SBLC, whereas for TESLA with a somewhat tighter energy cut (i.e. less than 70 % of the spent beam) it might just be possible.

2.5.4 The Steps to be Taken in the Next Three Years

TESLA

Concerning the spot size at the IP and the FFS optics, the TESLA design is safe in view of the FFTB experiment which has demonstrated the feasibility of a vertical beam size very close to the TESLA design value. It is nevertheless necessary to investigate tuning and correction procedures in order to determine the requirements for instrumentation (e.g. BPM resolution), to check for the necessity of additional matching and diagnostic lattice sections, etc. The jitter tolerances of the superconducting final quads may be more difficult to achieve than for conventional designs and they need special attention.

In addition, the method of eliminating orbit offsets of the colliding beams by measuring the deflection at the IP for the first bunch and correcting for the trailing ones should be investigated in more detail. Asymmetric collimation should be carefully reviewed and the efficiency of the collimation system checked in more detail.

SBLC

Concerning spot size stabilization, the requirements are similar to those for TESLA but more critical because of the smaller beam size and the larger beam energy spread. Collimation issues should be reviewed in more detail and an estimate of the number of halo particles should be made. The solution for the capture of the spent beam has to be optimized.

NLC, JLC

Feedback systems for spot size stabilization operating at various time scales are vital for the few-nm vertical beam size. The instrumentation required for spot size stabilization has to be developed (e.g. high resolution BPM's). Benefits/difficulties of mechanical vs. nonlinear collimation will be reviewed.

VLEPP

More work is necessary on the overall layout of the complete delivery system. In particular, a solution for collimation must be found that takes into account the strong wakefield effects due to the high bunch charge. Requirements concerning spot size stabilization are similar to NLC/JLC. Additional tightening of tolerances for the travelling focus scheme should be investigated.

CLIC

Optimization of the IR layout for multibunch operation must be studied. Overall design of the delivery system has to be completed. Spot size stabilization is required as for NLC/JLC.

2.5.5 Summary and Comparisons

Since the most important issue in the beam delivery system is to provide and maintain the IP spot size required for high luminosity, one may divide the different designs into two categories. Whereas TESLA and SBLC aim for a vertical beam size comparable to or about a factor of two smaller than that achieved at the FFTB experiment, the other designs demand a beam size smaller by about an order of magnitude. This translates into a difference in the tolerances of also about an order of magnitude between the two categories. When the different linac repetition frequencies are taken into account, the differences concerning vibration tolerances become less pronounced because at a higher frequency a better orbit

stability can be achieved. TESLA has the special advantage here of allowing for a fast orbit correction within about $1\mu s$.

The other designs must stabilize their systems by using either beam-based feedback based on their higher repetition rate, or observe and compensate element motion directly for a small number of critical elements, or a combination of both.

Concerning the important and challenging issue of beam collimation, the somewhat different approaches of SBLC and TESLA, NLC, and JLC do not seem to be fundamentally related to the basic differences between these linear collider designs. Instead, a particularly good solution found for one machine is likely also to be beneficial for the other machines.

We would like to conclude that during recent years good progress has been made on the design of all beam delivery systems, and sophisticated solutions for the different choices of linear collider designs are available. There are still many details to be looked at carefully, and it is strongly recommended that the different design groups continue to cooperate both theoretically and experimentally in this field of accelerator physics and technology.

2.6 EXPERIMENTATION

2.6.1 The Group

R. Settles (Chairman)
Max-Planck-Institut für Physik, Föhringer Ring 6, D-80805 München, Germany.
E-mail: RON@dmumpiwh.bitnet
T. Markiewicz (Deputy Chairman)
Stanford Linear Accelerator Center, P.O. Box 4349, Stanford, CA 94309, USA.
E-mail: TWMARK@slac.stanford.edu
S. Bertolucci
INFN, Laboratori Nazionali di Frascati LNF, CP 13, I-00044 Frascati, Italy.
E-mail: BERTOLUCCI@irmlnf.bitnet
S. Kawabata
Physics Department, KEK, 1-1 Oho, Tsukuba-Shi, Ibaraki-Ken 305, Japan.
E-mail: KAWABATA@jpnkekvx.bitnet
D. Miller
Physics and Astronomy, Univ. College London, Gower St., GB-London, W.C.1E 6BT, England.
E-mail: DJM@hep.ucl.ac.uk
R. Orava
U. Helsinki, Res.Inst.for Hi.En.Phys. SEFT, Siltavuorenpenger 20C, SF-00170 Helsinki, Finland.
E-mail: ORAVA@finuhcb.bitnet
F. Richard
Université de Paris-Sud, Inst. Nat. de Phys. Nucléaire, LAL, F-91405 Orsay Cedex, France.
E-mail: RICHARD@lalcls.cern.ch
T. Tauchi
Physics Department, KEK, 1-1 Oho, Tsukuba-Shi, Ibaraki-Ken 305, Japan.
E-mail: TTAT@jpnkektr.bitnet
A. Wagner
DESY, Deutsches Elektronen-Synchrotron, Notkestraße 85, D-22603 Hamburg, Germany.
E-mail: F11WAG@dhhdesy3.bitnet

2.6.2 Introduction

The purposes of this subgroup are to summarize:
(1) the important physics goals and their demands on the machine and detector,
(2) issues relating to the experimental programme,
(3) the effect of machine parameters on detector and experiment,
(4) generic detector possibilities,
(5) the areas of R&D which need close teamwork between machine and detector.

2.6.3 Physics

The physics discussion here and in the next subsection will be brief, in form of an executive summary. More details and references may be found in the Appendices.

The e^+e^- physics topics and examples of experiments with requirements on machine and detector are listed in Tables 2.6.1 and 2.6.2, which reflect the results of recent international workshops [1]-[16]. Three facets of the physics potential of the e^+e^- collider are:
(1) a programme of new physics, Table 2.6.1 – search for the Higgs boson and for physics beyond the standard model ($\mathcal{SM}$), for example supersymmetry ($\mathcal{SUSY}$);
(2) a rich programme of standard physics, Table 2.6.2 – measurements in hitherto poorly mapped regions of the $\mathcal{SM}$, such as top quark properties and trilinear gauge couplings, and measurements in familiar regions such as QCD;
(3) a potential, the second topic of Table 2.6.1, for understanding the mechanism for the spontaneous breaking of electroweak symmetry even in the heavy, strongly-interacting Higgs scenario, which involves precision measurements of gauge boson production at the highest energy.

Further options are discussed below. Complementary theoretical predictions will be confronted in the e^-e^-, $\gamma\gamma$, and $e^-\gamma$ collider modes. Running on the Z^0 peak with polarized beams could measure $\sin^2\theta_W$ to greater accuracy than at LEP/SLC and provide the indirect M_{Higgs} determination to test the $\mathcal{SM}$ framework .

The main goal of next-generation colliders is to understand the origin of electroweak symmetry breaking ($\mathcal{ESB}$). The mechanism for $\mathcal{ESB}$ is most probably operating in the energy regime [11] of $\sqrt{s} \simeq \mathcal{O}(1$ TeV) or below, which will be accessed in complementary ways by the hadron colliders and the e^+e^- colliders.

2.6.4 Experimentation Aspects

Issues relating to the experimental programme are addressed here.

Experimentation phases

$\odot$ – At the international workshops the first-stage energy has been clearly demonstrated to be $\sqrt{s} \simeq 0.5$ TeV, which yields a healthy physics programme complementary to that of LHC.

If it would turn out to be advantagous to commission the machine at a lower energy, the following energies could be possible milestones, according to present knowledge:
–At $\sqrt{s} \simeq 0.3$ TeV with 1fb^{-1} of data, any measurement gap that might exist between LEP2 and LHC could be closed, a definitive test of the $\mathcal{SUSY}$-Higgs scenarios could be performed since in those models the lightest Higgs has $M_h \leq 150$ GeV/c^2 and would be discovered, and many standard analyses could be performed, for example the trilinear gauge couplings ($WWV, V{=}\gamma, Z^0$) measured about twice as precisely as at LEP2. Already at $\sqrt{s} \simeq 0.3$ TeV, the e^+e^- linear collider is unique in being able to cover all presently known $\mathcal{SUSY}$ Higgs models and, more generally, theories involving multi-Higgs doublets and singlets.
–At $\sqrt{s} \simeq 0.4$ TeV, the top threshold could be found with a binary scan involving 0.5fb^{-1}of data at each of ~6 energies, or with a 2-3fb^{-1} run above threshold, to yield M_{top} to about ± 2 GeV/c^2. The trilinear-gauge-coupling precision would improve by a factor of four relative to LEP2. The top threshold scan with 1fb^{-1}per point at 10 energy points, which could follow straight away or be delayed until later, would determine M_{top} to ± 0.5 GeV/c^2. Now that the indirect knowledge (from LEP and SLC operation with e^+e^-) of the top quark has been confirmed by the direct discovery (at the Tevatron), $\sqrt{s} \simeq 0.4$ TeV would also be viable as

Table 2.6.1 Some e^+e^- physics topics and the corresponding performance quality needed for machine and detector. Quality key: from "-" not important, to "$\star\star\star$" very important (LEP/SLC detectors $\sim \star\star$).

PHYSICS	MACHINE[a]				DETECTOR[b]						
	$\int \mathcal{L}dt$	$\sqrt{s}$	Narrow	Pol.	Herme-	Track-	Calor-	3-Dim.	Lepton	Vertex	pi/K
	fb^{-1}/y	TeV	$\mathcal{L}(\sqrt{s})$	beams	ticity	ing	imetry	Granul.	I.D.	Tag	I.D.
•HIGGS											
Light Higgs	1-10	.2									
Higgs spin-parity	20	to	$\star\star$[c]		$\star\star$	$\star\star\star$	$\star\star$	$\star\star$	$\star\star$	$\star\star\star$	$\star$
SM/Susy B.R.	100	$\sim$.5									
Interm. Higgs	200	$\sim$1									
•HEAVY, STRONGLY-INTERACTING HIGGS											
W_LW_L-scatt.	200	$\sim$1.5			$\star\star\star$	$\star\star\star$	$\star\star$	$\star\star\star$	$\star\star$	-	-
•SUSY											
Light $\tilde{t}$	10	.2									
$\tilde{\chi}_j^{\pm}, \tilde{\chi}_i^0, \tilde{\ell}$	10										
Susy spectroscopy	20	to		$\star$[d]	$\star\star\star$	$\star\star$	$\star\star$	$\star\star$[d]	$\star\star$	-	-
Susy parameters	100										
$\tilde{q}, \tilde{g}$	100	$\sim$1-2									
•EXTENDED GAUGE											
New particles	200	$\sim$2			$\star\star\star$	$\star\star\star$	$\star\star$	$\star\star\star$	$\star\star$	$\star\star$	
Overall from Tables 2.6.1, 2.6.2	-		$\star\star\star$	$\star\star$[d]	$\star\star\star$	$\star\star\star$	$\star\star$	$\star\star\star$	$\star\star$	$\star\star\star$	$\star\star$

[a] Narrow c.m.s. energy spread arising from machine and beamstrahlung effects. $\star\star\star$ means the energy spread from the machine must be small ($\sigma \simeq \mathcal{O}(0.2\%)$); the luminosity spectrum must be well-measured (to the $\pm 0.1\%$ level); the last row of Table 2.6.2 describes the performance quality of the detector for measuring the luminosity spectrum.

[b] By "Tracking" and "Calorimetry" is meant the measuring accuracy for momentum and energy, respectively.

[c] If $M_{Higgs} \simeq M_{Z^0}$, upgrade to $\star\star\star$.

[d] If supersymmetry is discovered, upgrade to $\star\star\star$.

Table 2.6.2 Some e^+e^- physics topics related to known $\mathcal{SM}$ processes and the corresponding performance quality needed for machine and detector. Quality key: from "-" not important, to "$\star\star\star$" very important (LEP/SLC detectors $\sim \star\star$).

PHYSICS	MACHINE[a]				DETECTOR[b]						
	$\int \mathcal{L}dt$ fb^{-1}/y	$\sqrt{s}$ TeV	Narrow $\mathcal{L}(\sqrt{s})$	Pol. beams	Herme-ticity	Track-ing	Calor-imetry	3-Dim. Granul.	Lepton I.D.	Vertex Tag	pi/K I.D.
●ELECTROWEAK GAUGE BOSONS											
WWV-coupl.	10	.3									
Unfoldγ, Z-coupl.	50	to	$\star\star\star$	$\star\star$	$\star\star\star$	$\star\star\star$	$\star\star$	$\star\star$	$\star\star\star$	-	-
WWVV-coupl.	100	1									
●TOP QUARK											
Thr. scan	10	$\sim$.35	$\star\star\star$		$\star\star$	$\star\star$	$\star\star$	$\star\star$	$\star\star$	$\star\star\star$	$\star$
g-2,hel.anal.,V+A	50	.4									
Rare decays	50	to		$\star\star$	$\star\star\star$	$\star\star$	$\star\star$	$\star\star$	$\star\star$	$\star\star\star$	$\star\star$
Yukawa coupl.	100	1									
●QCD											
Hadronization	1	For									
Heavy flavors	10	all			$\star\star$	$\star\star$	$\star\star$	$\star$	$\star$	$\star\star$	$\star$
$\alpha_s(s)$	10	$\sqrt{s}$									
●(Virtual)$\gamma\gamma$											
Minijets	1										
$F_2^\gamma(x, Q^2)$	10		$\star$		$\star\star\star$[c]	$\star\star$	$\star\star$	$\star\star$	$\star\star$	$\star$	$\star$
Heavy flavors	10										
$\mathcal{L}(\sqrt{s})$ Det.[a]					$\star\star$	$\star\star\star$	$\star\star$	$\star\star$	$\star\star$	-	-

[a]Narrow c.m.s. energy spread arising from machine and beamstrahlung effects. $\star\star\star$ means the energy spread from the machine must be small ($\sigma \simeq \mathcal{O}(0.2\%)$); the luminosity spectrum must be well-measured (to the $\pm 0.1\%$ level); the last row of the table describes the performance quality of the detector for measuring the luminosity spectrum.

[b]By "Tracking" and "Calorimetry" is meant the measuring accuracy for momentum and energy, respectively.

[c]Small angle tagger would allow low-x studies and high Q^2.

first-stage energy of the machine.
-At the design goal of the first stage, with 10-100fb^{-1} of data at $\sqrt{s} \simeq 0.5$ TeV, many properties of the enigmatic top quark would be measured, M_{top} again to $< \pm 0.5$ GeV/c^2, the trilinear gauge couplings to about $\pm 0.2\%$, and the Higgs bosons with masses up to $\sim$350 GeV/c^2 could be discovered. If light supersymmetry exists, depending on how it is realized in nature, this first stage could find some of the lighter supersymmetric particles ($\tilde{\chi}_j^{\pm}$, $\tilde{\chi}_i^0$, $\tilde{\ell}$).

$\odot$ – The second stage uncovers the new physics that lies at higher energies along with standard physics at those energies. The machine energy could be increased to successively higher values, with $\sim$100-200fb^{-1} of data to be taken at appropriate energies up to $\sqrt{s} \simeq$ 1-2 TeV. The goal would be to search for heavier Higgses and/or supersymmetric particles. The $\mathcal{SM}$ Higgs H_{SM} could be discovered up to a mass of $M_{\phi^0} \simeq 800$ GeV/c^2. If $\mathcal{SUSY}$ has been found earlier, the search for the heavier Higgs states (H^0 and A^0, produced in association, and $H^{\pm}$, produced in pairs) and the colored superpartners ($\tilde{g}$, $\tilde{q}$), which are heavy in most models will follow.

$\odot$ – Finally, if the Higgs turns out to be heavier than $\sim$800 GeV/c^2, it is no longer discoverable as particle, and the Higgs sector is strongly interacting. The programme for studying the mechanism of electroweak spontaneous symmetry breaking would consist of precision measurements of gauge boson production, e.g., the $W_L W_L$ scattering experiment at the highest energy to which the machine could be upgraded. This again should probably be $\sim$1.5 TeV. At this stage, the e$^+$e$^-$ linear collider will be the best place to measure new phenomena which may exist at such energies. Examples are the direct or indirect evidence for an extended-gauge Z', or the production of new heavy fermions if their masses are within the energy range of the collider. This highest energy question will be a topic for future workshops.

Complementarity of Hadron and e^+e^- Colliders

This point is addressed briefly here, since it touches the discussion several times in this chapter. It has been emphasized at the international workshops [1]-[11] that the pp and e$^+$e$^-$ physics programmes are complementary, and what will have been found at the LHC will influence the experimental programme at the e$^+$e$^-$ collider. Further examples of comparison of the physics potential of e$^+$e$^-$ and pp colliders are found in Refs. [17], [18], and [19], and the most thorough examination to date is contained in the DPF study [11].

These studies show that the complementarity of the e$^+$e$^-$ machine to LHC is already important enough and sufficient to justify its construction at $\sqrt{s} \simeq 0.5$ TeV, which is a necessary technological step on the way to the higher energies; afterwards this complementarity shifts to other areas with the increase in $\sqrt{s}$ of the e$^+$e$^-$ machine. For example, the properties of a light Higgs would be measured at the first phase of the machine running at the peak of the Higgs production cross section, whereas an intermediate-mass Higgs would be measured at the second phase of the machine running at the appropriate energy. Most top quark properties will be derived from running at the peak of the $t\bar{t}$ cross section around 0.4 TeV. A similar strategy would be followed for measuring the properties of the supersymmetric particles and for mapping out $\mathcal{SUSY}$ parameter space: beam energy and polarization would be tailored to the measurement in question. If the new physics, now hoped for, were not to exist, the mechanism for $\mathcal{ESB}$ would be studied in W^+W^- production at 1.5 TeV and

in precision measurements with polarized beams at lower energies.

Hence, it is the capability to optimize the different measurements by running at low or high energies, with or without polarized beams, that gives the e^+e^- collider its full physics potential and full complementarity to the hadron colliders. It is well understood [17] that the discovery reach of the LHC is matched by the e^+e^- machine at the second stage of 1 to 2 TeV, and that this match is ultimately needed for more precise measurements of any new physics found there. But the experiments at lower energy are an essential part of the entire programme, so that a starting energy of $\sqrt{s} \simeq 0.4$-0.5 TeV is fully justified.

Finally, the e^+e^- and pp programmes not only complement each other, they also overlap as well, and the crosschecks that emerge from the competing experiments will enrich the scientific understanding of the measurements.

Two Experiments, Two IRs

The reasons for needing at least two experiments are:
–scientific redundancy: particle-physics measurements must be done several times independently to ensure that the result is correct;
–complementarity: with two detectors, all requirements for e^+e^- in Tables 2.6.1 and 2.6.2 can be fulfilled;
–competition: the competition of physics ideas between several detector collaborations is an important stimulous for scientific progress;
–sociology: the constituency of particle physicists interested in e^+e^--physics is large enough for at least two collaborations.
–reliability: having at least two operational detectors will improve the overall machine-detector performance, since time lost for detector maintenance can be reduced.

Two experiments could of course co-exist in a push-pull fashion at one IR, which would mean less expensive construction costs for the collider but more expensive operating costs since the switchover time would take longer. Also, such a setup would put one experiment at a disadvantage with respect to the other.

Other advantages of having two or more IRs are:
–one of them could be equipped for the $\gamma\gamma$ and $e^-\gamma$ programmes;
–one of them could be equipped for machine development studies;
–especially attractive is the possibility discussed at LC95 of being able to switch between two IRs within a short time [20], which would clearly increase the flexibility of the facility and make it possible to serve two experiments with data in the same running period. Ideas for producing a collider facility with multiple IRs should be explored further [21].

The e^-e^-, $\gamma\gamma$, and $e^-\gamma$ colliders

These options allow complementary measurements to those of the e^+e^- collider. A few examples of standard physics and of new physics follow here, and more in Appendix B. The reactions $e^-e^- \to e^-W^-\nu$, $\gamma\gamma \to W^+W^-$, and $e^-\gamma \to W^-\nu$ provide alternate ways of measuring the trilinear gauge couplings and thus yield sensitive tests of the $\mathcal{SM}$. Also all three collider modes offer alternate ways of producing supersymmetric particles, e.g., $e^-\gamma \to \tilde{e}\tilde{\gamma}$.

The e^-e^- collider gives access to possible exotic doubly charged objects, Higgses or dileptonic bosons, and to possible discovery of a heavy Majorana neutrino. Since the e^-e^- collider requires only minor changes to the hardware of the e^+e^- machine and detector, its

programme could be pursued during the first phase of the facility if there are strong physics arguments for it at that time.

A most important option, which should be a benchmark for feasibility studies of the $\gamma\gamma$ collider (see next subsection), is to use it for direct production of the Higgs boson, which proceeds via loops with contributions from new particles as well as from $t\bar{t}$ and W^+W^-. Thus a precision measurement of $\Gamma_{\gamma\gamma\to Higgs}$ gives indirect access to new physics.

The $e^-\gamma$ collider is the best conceivable machine for measuring the quark and gluon structure of the photon.

Z^0-pole running for physics

This option is discussed in Appendix C. The physics case might be made at some time to test sensitively the internal consistency of the $\mathcal{SM}$ with precision measurements at low energy, for example if no Higgs particle has been found up to $\sqrt{s} \simeq 1$ TeV. The luminosity requirement is $\sim 5 \times 10^{31}\mathrm{cm}^{-2}\mathrm{s}^{-1}$for Z^0-pole running for precision measurements using polarized beams. Both beams should be polarized to reduce the error on $\sin^2\theta_W$ to well below ± 0.0001. For experiments measuring CP violation in the b-quark sector or B_s^0 oscillations, a luminosity of $\sim 10^{33}\mathrm{cm}^{-2}\mathrm{s}^{-1}$would be needed.

Polarized beams

For the reason just given, for disentangling the γ and Z^0 contributions to the trilinear couplings, for the $g-2$ measurement of the top quark, for $\mathcal{SUSY}$ studies, to mention a few examples, polarized beams permit qualitatively new and important measurements to be performed. The SLC/SLD experience demonstrates that this technique opens new windows to precision measurements without excessive demands on luminosity.

$\mathcal{L}(\sqrt{s})$, the luminosity spectrum

Some physics studies require the highest possible luminosity, even at the cost of a larger machine-energy spread and significant beamstrahlung. But both machine-energy spread and beamstrahlung must be kept to a minimum for the top threshold scan, for an M_{Higgs} measurement, or for precision measurements of the trilinear gauge couplings, among other things. The ideal linac will operate in both a high-luminosity mode and in a narrow machine-energy-spread mode. In the latter mode the machine-energy spread should be of order 0.2% (standard deviation) or less, and the detector for measuring $\mathcal{L}(\sqrt{s})$ will need good endcap tracking so that the luminosity spectrum can be known to a matching precision of $\pm 0.1\%$ (see last row of Table 2.6.2) [22].

Z^0-peak running for calibration

Running at the Z^0-peak would be of great help for the calibration of the detectors, but only about 3 pb^{-1} of data is enough per calibration run, of which about three per year would be needed. Thus a luminosity of $\sim 10^{31}\mathrm{cm}^{-2}\mathrm{s}^{-1}$is sufficient for this purpose.

2.6.5 IR and Detector

Issues for which the machine and detector closely interact are discussed, and quantities affecting the detector design follow in Tables 2.6.3 and 2.6.4.

The machine parameter lists from LC95 [16] were used by Daniel Schulte/DESY to derive an internally consistent set of figures for luminosity and background. That is, the same set of Monte Carlo programs was used to calculate the numbers for all machines, so that a relative comparison of conditions at the experiment due to machine effects is possible. In Chapter 1 of this report, luminosity and background figures from analytic formulae by Pisin Chen/SLAC were used. The absolute accuracy of the numbers in the tables will be the subject of further study. Those in Table 2.6.3 related to luminosity from the Monte Carlo tend to be larger than the ones from the analytic calculation, but agree to 30% or better in most cases. The figures in Table 2.6.4 related to backgrounds due to minijets are different from those of the analytic formulae because of the addition of the direct process and the once-resolved process (describing the interaction of virtual quarks or gluons from one photon with the photon from the other beam) in the Monte Carlo. By and large the Monte Carlo and analytic calculations always agree within a factor of two.

Backgrounds

The sources of background are synchrotron radiation and debris from the final quads, muon backgrounds arising from upstream sources, e^+e^- pair creation in the field of the colliding bunches, and hadron produced by collisions of real or virtual photons from beamstrahlung or initial state radiation. Synchrotron backgrounds are typically produced by particles in the beam tails which radiate photons in the latter sections of the final focus (FF) which strike the tip of the last quadrupole. These backgrounds can be controlled by scraping beam tails in the post-linac collimation section. The muon background which results from this collimation is controlled by the big bend and by a number of spoiler magnets which fill the transverse dimensions of the tunnel. The majority of e^+e^- pairs from beam-beam effects are produced at small angles to the beam axis, with a transverse momentum and angle determined by the beam size and intensity. Their angular distribution defines a so-called dead cone which must be covered by a mask. While the machine design should minimize this cone, the mask should be instrumented with an e^+e^- pair monitor, which can provide information about the size of the luminous region, and small angle bhabha (luminosity) monitor. The detailed design of the masks, detectors, the aperture of the exit quadrupoles, and the value of the beam crossing angle determine how many backscattered pairs will reach the detector. In Table 2.6.3 values for crossing angle, dead cone (for 2T magnetic field, 0.5m to mask), collimation, drift to IP, and aperture of quadrupoles are listed.

Beam parameters at the interaction point (IP) control the number of primary e^+e^- and hadron pairs produced at inherently large angles. Table 2.6.4 compares backgrounds per bunch crossing and the backgrounds for the example of a sub-detector integrating over 100ns. The number of particles ($e^\pm$) from beam-beam effects are seen in rows 6 and 9 of Table 2.6.4, and those for hadronic events produced in two-photon reactions are in rows 7,8 and 10,11. The actual backgrounds of $e^\pm$ reaching the detector are suppressed by the magnetic field; the average energy of the particles listed in rows 6 and 9 is only 100 MeV, independent of machine design. Note that the backgrounds in Table 2.6.4 are not exactly the same as those calculated by P. Chen which appear in Tables 2.1 and 3.1. This difference is due to the use of slightly different methodologies and assumptions. Also note that N in row 6 here designates individual particles and not pairs.

Vibrations

All machine designs, whether at 0.5 or 1.0 TeV, require beam stability at the sub-10 nm level to achieve their design luminosities, as can be seen in the values for the spot-height σ_y in Table 2.6.3, row 8. Ground vibration, of either seismic or cultural origin, must be controlled to well below this level at the FF. After site selection, mechanical means must be used to reduce vibrations at frequencies greater than those which can be corrected by beam-based feedback. Active devices which feedback signals measuring absolute or relative quad motion are under investigation; if successful in principle, they must be engineered into the detector environment. The passive device most frequently suggested to date is a support tube linking the quads on either side of the IP. The size and mass of such a tube, the weight of the masks and quadrupoles it must support, and the consequences to detector access must be considered. However, it would be better for the experiment if a way could be found to avoid this tube, which would add additional scattering material inside the detector volume. Detector and FF quad cooling and gas systems must be designed which do not introduce any additional vibrations.

Beam diagnostics near the IP

It is important to be able to measure the beam parameters at the IP separately for each beam at the full beam intensity. Physical wires will not survive; current designs for optical wires or interferometers will not work at wavelengths less than about 10 nm. Thus R&D to produce such devices and locate them within 20% of the distance from the IP to the first quad is needed and will require close cooperation between detector and machine physicists.

Extracted beam diagnostics

Experience from the SLC/SLD tells us that these entail an energy spectrometer, a Compton polarimeter, and a beamstrahlung photon monitor. Initial design work, as elaborated on later, should begin as soon as possible.

$\gamma\gamma$-collider implications

The laser photons must be transported to within a few centimeters of the IP for Compton backscattering and the electrons must be extracted without creating too much background. The interaction among these devices, the vertex detector, the other beam monitoring equipment, and the masks is sufficiently complicated so as to require the design of a dedicated detector for the $\gamma\gamma$ experiments at a dedicated IR. Conceptual engineering solutions have not yet begun to address these issues. Since e^-e^-, $\gamma\gamma$, and $e^-\gamma$ colliders are addressing similar physics questions to e^+e^-, it is possible that the outer detector for an e^+e^- experiment with a modified inner detector would be suitable.

Detector timing

The bunch time structure of the various designs varies from 0.67 ns (CLIC) to 1000 ns (TESLA), as seen in Table 2.6.3, row 7. Through the beam-beam interaction, each bunch crossing occuring within the time resolution of the detector may produce particles that can partially obscure a real physics event triggered by a different bunch in the train. Or, the background event may itself produce a non-physics junk trigger (as dealt with in the next section). Thus, the time resolution of the detector and the maximum tolerable trigger rate

become potentially important parameters in deciding between competing machine designs. If sub-nanosecond timing were trivial and computing power large, fast, and cheap enough, any machine bunch structure could be considered. Unfortunately, such is not the case. While sub-nanosecond timing has been achieved in various detectors, it is typically not trivial and not available in real-time. Proponents of machine designs requiring fast, high resolution detectors must begin realistic conceptual detector designs as soon as possible, or demonstrate that the backgrounds do not adversely affect their analyses. Table 2.6.4, row 11 gives a measure of the probability of having stiff particles from underlying hadronic events in a good physics event for a detector with a typical timing resolution of 100 ns. The situation degenerates beyond that described in Table 2.6.4 if the bunch spacing and crossing angle are not sufficient to prevent the interaction of incoming bunches which have passed the IP with outgoing bunches yet to arrive at the IP.

Trigger rate and Data volume

At the SLC/SLD the trigger rate and data volume can vary enormously from pulse-to-pulse. Overall trigger rates under poor conditions are much larger than can be explained by physics or simulated backgrounds. Typically they are ascribed to abnormal and atypical behavior of some part of the accelerator. While one hopes that any future collider will be immune to such problems, it is prudent to design the trigger and data aquisition with sufficient dynamic range to ride out these disturbances. Additionally, it has been found that the detector often provides some of the most useful diagnostics for the accelerator. The ability to easily correlate its data with that of the machine should be a design consideration.

All the machine designs except VLEPP incorporate multibunch operation. When the interbunch spacing is long enough to allow for a trigger decision, one can imagine schemes where the rate of the first-level trigger would be the product of the average bunch-crossing rate (Table 2.6.4, row 12) and the probability for a hadronic background event from the beam-beam interaction (Table 2.6.4, row 7). The resulting trigger rate (Table 2.6.4, row 13) can be compared, for example, with the LEP first-level triggers.

When the interbunch spacing is very short, it makes more sense to consider a simple bunch train crossing as first level trigger [4]. This would be followed by a software trigger that analyzed all data buffered into memory during the bunch train. In this model, the maximum trigger rate would be the machine repetition rate, as tabulated in Table 2.6.4 row 14. For comparison, Table 2.6.4 row 15 shows the rate for useful physics events, assuming 20pb as a rough idea of the cross section.

There are different ways to imagine the architecture for the trigger and data acquisition system as indicated above, and some combination of hardware and software triggers can be adapted to the time structure of the machine that is ultimately built. The system would consist of buffering the frontend signals in pipelines at a rate related to the instantaneous bunch-crossing rate (see *Detector timing* above) along with hardware triggers to pick out which locations in the pipeline should be transferred to memories for the last-level software trigger. Rows 12 and 13 indicate that hardware triggers can reduce by an order of magnitude the number of locations in the pipeline that have to be transferred.

Finally, a guess at the data volume can be made using row 15 (the 20pb rate). Extrapolating from LEP/SLC experience, a good event might contain a few megabytes of information [4].

Table 2.6.3 Table of some machine parameters related to IR and detector design.

	TESLA	SBLC	JLC(S)	JLC(C)	JLC(X)	NLC	VLEPP	CLIC
[Units in brackets]	Upper numbers for 0.5 TeV$\equiv\sqrt{s_0}$ machine version Lower numbers for 1.0 TeV$\equiv\sqrt{s_0}$ machine version							
1)$\mathcal{L}$ (with pinch)	6.0	3.9	4.6	9.3	5.1	6.9	9.7	1.0-4.5
$[10^{33}\mathrm{cm}^{-2}\mathrm{s}^{-1}]$	10.1	6.3		21.1	9.6	14.1		2.2-9.7
2)$\int \mathcal{L}dt/_{y=10^7 s}$	20	13	15	31	17	23	32	3-15
$\times$33%eff.$[\mathrm{fb}^{-1}]$	33	21		70	32	46		7-32
3)δ_B (due to beamstr.)	2.9	3.1	8.2	4.9	3.0	2.5	10	3.6
[avg.beam en.loss in %]	2.4	6.5		8.0	7.5	7.1		7.3
4)$\mathcal{L}$ ($\sqrt{s}>0.99\sqrt{s_0}$)	3.4	2.1	1.7	4.4	3.2	4.3	1.4	0.5-2.4
$[10^{33}\mathrm{cm}^{-2}\mathrm{s}^{-1}]$	6.4	2.2		7.7	4.4	5.9		0.8-3.6
5)Bunches/train	800	125	50	72	85	90	1	1-10
	4180	50		72	85	75		1-10
6)Trains/sec	10	50	50	150	150	180	300	2530-1210
	5	50		150	150	120		4000-1800
7)Interbunch spacing	1000ns	16ns	5.6ns	2.8ns	1.4ns	1.4ns	3.3ms	0.67ns
	200ns	10ns		2.8ns	1.4ns	1.4ns		0.67ns
8)σ_x/σ_y-spot size	1000/64	670/28	260/3.0	260/3.0	260/3.0	320/3.2	2000/4	250/7.5
[nm]	325/8	572/9		372/2.2	191/2.2	357/2.3		200/6.0
9)σ_z-spot size	1000	500	120	120	90	100	750	200
$[\mu\mathrm{m}]$	500	500		120	81	100		200
10)pb^{-1}/bunch	7.5	6.3	18.2	8.6	4.0	4.3	323	3.9-3.7
$[10^{-7}\mathrm{pb}^{-1}]$	4.8	25.2		19.5	7.5	15.7		5.5-5.3
11)Crossing angle	0	3	6.4	6.0	6.1	20	6	1
[mrad]	0	3		6.0	5.0	20		1
12)Detector dead cone	79	83	120	97	85	81	124	66
(2T.0.5m to mask)[mrad]	65	85		116	89	107		70
13)Collimation $n \times m$	12x38	7x7	6x35	6x35	6x35	10x40		6x13
$[n\sigma_x \times m\sigma_y]$								
14)ℓ^* (drift to Q01)	3.0	2.0	2.5	2.5	2.5	2.0		1.25
[m]								
15)a ($\emptyset$ aperture of Q01)	48.	8.	13.7	13.7	13.7	10.		12.
[mm]								

Table 2.6.4 Table of some machine parameters related to backgrounds.

	TESLA	SBLC	JLC(S)	JLC(C)	JLC(X)	NLC	VLEPP	CLIC
[Units in brackets]	Upper numbers for 0.5 TeV machine version Lower numbers for 1.0 TeV machine version							
1)$N_{e^\pm}$ per bunch	5.1	2.9	1.44	1.0	.63	.65	20	.8
$[10^{10}]$	.9	2.9		1.44	.62	1.1		.8
2)$\gamma\epsilon_x/\gamma\epsilon_y$	20./1.	10./.5	3.3/.045	3.3/.045	3.3/.045	5./.05	20./.075	3./.15
$[10^{-6}$ m rad]	5.2/.063	10./.1		3.3/.048	3.3/.045	5./.05		3.9/.2
3)β_x/β_y at IP	24.5/2.	22./.8	10./.1	10./.1	10./.1	10./.1	100./.1	10./.18
[mm]	20./1.	32./.8		41./.1	11./.1	25./ .1		10./.18
4)$N_{beamstr.\gamma}$per $e^\pm$	2.6	2.0	1.8	1.3	.9	.8	4.7	1.4
	1.2	2.2		1.4	1.1	1.2		1.7
5)$\langle E_{beamstr.\gamma}\rangle$	2.9	3.9	11.3	9.3	8.6	7.3	5.3	6.3
[GeV]	9.5	14.5		28.	33.	29.		22.
Backgrounds/bunch								
6)$N_{beamstr.e^\pm}$/bunch	31	18	37	15	6	6	1219	7
$\theta >$150mrad, $p_T >$20MeV/c	8	53		29	10	21		10
7)Hadr.ev. per bunch	.15	.10	.33	.13	.05	.05	6.1	.05
$E_{\gamma\gamma-c.m.s.} \geq$5GeV	.09	.60		.47	.19	.34		.13
8)Minijet ev. per bunch$[10^{-2}]$	.32/.016	.26/.014	1.9/.10	.52/.03	.16/.009	.13/.007	28/1.4	.15/.009
p_T^{min}(GeV/c)= 3.2 / 8	.41/.022	4.4/.23		5.2/.26	2.0/.10	3.1/.16		1.2/.063
Backgrounds/100ns								
9)$N_{beamstr.e^\pm}$/100ns	31	112	661	536	429	429	1219	7-70
$\theta >$150mrad, $p_T >$20MeV/c	8	530		1036	714	1500		10-100
10)Hadr.ev./100ns	.025	.16	1.3	.50	.70	.52	.63	.05-.11
per unit lumi$[10^{33}$cm^{-2}s$^{-1}]$	.009	.95		.80	1.4	1.7		.06-.13
11)Minijet ev./100ns	.003	.016	.33	.18	.11	.09	28	.002-.015
p_T^{min}=3.2GeV/c	.004	.44		1.9	1.4	2.2		.012-.12
Rates								
12)$\langle$Bunch crossing rate$\rangle$	8.	6.25	2.5	10.8	12.75	16.2	.3	2.53-12.1
[kHz]	20.9	2.5		10.8	12.75	9.		4.-18.
13)$\langle$Hadr.ev. rate$\rangle$[kHz]	1.2	.6	.8	1.4	.6	.8	1.8	.1-.6
$E_{\gamma\gamma-c.m.s.} \geq$5GeV	1.9	1.5		5.1	2.4	3.1		.5-2.3
14)Train crossing rate	10	50	50	150	150	180	300	2530-1210
[Hz]	5	50		150	150	120		4000-1800
15)1 event/20pb rate	.12	.08	.09	.18	.11	.14	.19	.02-.09
[Hz]	.20	.13		.42	.19	.28		.04-.19

2.6.6 Detector Options

To summarize the discussion up to now, the physics implications on the detector design are listed in Tables 2.6.1 and 2.6.2, and the effects of the different machine designs on the IP and detector design are given in Tables 2.6.3 and 2.6.4. Here, some performance figures of detectors used in simulations for workshops [4, 22, 23,24, 25, 26, 27, 28, 29, 30, 31, 32, 33, 34, 35, 36, 37, 40, 41, 42, 43, 44, 46] are listed in Table 2.6.5.

Earlier studies have shown that the performance of existing e^+e^- detectors would be good enough to do much of the physics in the early phase of the machine at low energy. Typical performance figures are shown in the first three columns of Table 2.6.5. For higher luminosities and/or higher energies, high performance detectors are needed, and such detectors are the subject of the last two columns. Examples given are the "JLC Detector" [4] which is being designed at KEK and the "1 TeV Detector" [44] suggested in Europe. The JLC Detector is conceived to have good hermeticity over the fullest possible solid angle, to have jet invariant mass resolution comparable with the natural widths of the $W^{\pm}$ and the Z^0, and give a lepton pair recoil mass resolution for $e^+e^- \rightarrow Z^0 H_{SM}$ comparable with the beam energy spread of ~200 MeV. The 1 TeV Detector is being designed with the demands on performance listed in Tables 2.6.1 and 2.6.2 in mind. Both detectors are large and give good performance at the higher energies of the second phase of the machine. An alternative would be a small high-field detector [37, 46]; the details of such a detector have not yet been worked out.

Table 2.6.5 Examples of detector performances used in physics studies.

	LEP/SLC-Style	ee500 1991	ee500 Typical	JLC Detector	1 TeV Detector	units
Tracking $\frac{\delta p_t}{p_t^2} = C$						
$C =$	8	5-100	10	1	2	$\times 10^{-4}$GeV/c^{-1}
E-M Calorimeter $\frac{\delta E}{\sqrt{E}} =$	0.2	0.02-0.15	0.1	0.15	0.10	$\sqrt{GeV}$
Hadronic Calorimeter $\frac{\delta E}{\sqrt{E}} =$	0.9	0.3-1.0	0.8	0.40	0.65	$\sqrt{GeV}$
Energy Flow $\frac{\delta E}{\sqrt{E}} =$	0.65	0.3-0.8	0.5	0.3	0.4	$\sqrt{GeV}$
Vertexing $\delta(IP) = A \oplus \frac{B}{p}$						
$A =$	25	5-20	10	11	10	μm
$B =$	100	50-100	50	28	50	μmGeV/c
Hermetic coverage $\lvert\cos\theta\rvert <$	0.96	0.70-0.99	0.95	0.98	0.98	

2.6.7 Tabulation of What Has Been Done

Backgrounds	
$e^{\pm}$ pairs	-ABEL runs into JLC and LEP/SLC-like detector (T.Tauchi) using EGS/GEANT (G.Punkar, D.Schulte).
	-Interface ABEL to GEANT with SLC/LEP-type detectors (M.Ronan, D.Schulte).
Synchrotron rad. from Q's	-QSR program vectors → IP (T.Tauchi) → detector using EGS(G.Punkar, D.Schulte).
Muons	-Feldman MarkII muon transport code run on NLC/JLC/TESLA beam lines → "big bend" and collimators to reduce flux (L.Keller, Y.Namito, M.Sachwitz, J.Schreiber).
Programs	
Beam-beam effects with $e^{\pm}$ pair creation	ABEL (K.Yokoya, P.Chen, T.Tauchi)
	MACPAR+TRACKIT (S.Ritter, D.Schulte)
	GUINEA PIG (D.Schulte)
	RBEAM with no pairs (L.Wood, O.Napoly, P.Pierini, D.Schulte)
Minijets	Minijet (P.Chen, T.Barklow)
	GUINEA PIG (D.Schulte)
	MINIJET (A.Miyamoto, H.Hayashii)
Synchrotron rad.	MQRAD (T.Morimoto, T.Tauchi)
	SLAC QSR (S.Hertzbach)
Muons	MU-CARLO (G.Feldman, S.Rokni)
	MUON89 (W.R.Nelson) - analytic calculation
Vibrations	
Ground measurements	done at SLAC,DESY,KEK,CERN, Finland and Sazare(Japan).
Support tube	design and calculations (SLAC, KEK, DESY)
Beam spot size (nm)	
	Laser interferometer (T.Shintake)
	$e^{\pm}$ pair monitors (T.Tauchi, P.Chen)
	Beamstrahlung photon monitor (D.Schulte)
	IP-BPM (T.Shintake)
	Nanometer RF BPM (S. Hartman)

2.6.8 Other Things Left to Do

Vibrations

Measurements of Ground Motion

Current measurements of ground motion have concentrated on the frequency dependence of the displacement power spectrum and the normalized correlation function relating the coherence of motion between two detectors separated by a given distance. We now understand that the quantity most useful as input to the calculation of tolerances for a given linac or final focus lattice is the power spectum $S(f,k)$ as a function of both frequency f and wave number k, measured in units of 1/distance. This function contains all spatial and temporal correlations. Current tolerance estimates use semi-empirical formulae to relate frequency and wave number.

$S(f,k)$ should be measured at a quiet, a moderate, and a noisy site, tabulated, and made generally available. The emphasis should not be on supporting one particular site over another, but on pointing out the sensitivity of each machine design to the problem. Currently the devices used for these seismic measurements compare two absolute measurements of motion. Arrays of devices which can accurately measure the *differences* in motion may need to be developed.

Additionally, as most of the power in seismic events is carried within one wavelength of the surface in so-called Raleigh waves, the general dependence of $S(f,k)$ as a function of depth should be made. Moreover, the tunnel itself may serve to influence the propagation of waves impinging on it from an otherwise homogeneous material. Studies, whether by simulation or measurement, of how this may affect the overall problem of ground motion should be carried out.

Engineering of Supports

Supports for magnets, rf structures, and the detector should be designed which do not amplify the effects of seismic or cultural noise. The concept of the support tube linking both ends of the final focus needs to be more adequately developed. Insufficient engineering has been done to indicate what the size and mass of such a tube must be to provide stability against relative motion of both sides of the FF quads. If indeed necessary it would limit access, add mass, and, if not carefully supported, it could translate low frequency seismic noise to the higher frequencies of its normal modes where it would be more difficult to control with feedback.

Active and Passive Vibration Suppression

Tests which attempt to feedback seismic signals to piezoceramic actuators in a closed feedback loop have begun at SLAC, KEK, and DESY. Early results show a factor of three reduction in rms jitter in the 1-10 Hz frequency range. More work to develop systems with higher attenuation is necessary. This may require the development of devices to measure the exact quantity of interest for beam stability. For example, using a geophone to measure the motion of a magnet might be less desirable than measuring the change in field that the beam sees as a result of such motion. If correlated motion between two magnets is driving luminosity loss, then perhaps devices which accurately measure the relative motion of the two magnets need to be developed. One would not feel confident until at least a factor of ten safety margin exists in the frequency range not covered by beam-based feedback.

Engineering efforts for structure or magnet mounts might include passive damping if such a system did not compromise the long term stability of the machine alignment. Investigations into elastic materials or the effects of trenches to isolate structures from shallow ground waves of high frequency may be in order.

Beam-Based Feedback as a Vibration Suppression Tool

Current estimates of the efficacity of beam based techniques to control vibrations are based on models of the SLC feedback system extrapolated to the bunch frequency of the new machines. Estimates based on actual SLC performance should be carried out.

Analysis of the Spent Beam

Beamstrahlung at the IP will shift the mean energy and introduce a large energy spread when the beams are in collision. When the beams are not in collision they will have their full energy and narrow width. Beam dump devices such as the energy spectrometer and Compton polarimeter must be built in such a way as to be able to make measurements under both conditions. Already at SLC, the beamstrahlung photon background makes these measurements difficult. Designs which can handle the increased photon background of the higher energy colliders must be developed. Depolarization of the electron beam due to the spin-flip (Sokolov-Ternov) effect in the field of the opposing beam is expected to be about 0.4% at 0.5 TeV and go up to about 5% at 1 TeV. A system of pre- and post-collision polarimeters may be required to understand the polarization completely.

Conceptual designs exist for using the distribution of electron pairs produced by the beam-beam interaction as a diagnostic tool. The practical design of detectors which can survive the radiation environment and readout in the multibunch environment of the machines should be developed.

Background Studies

Studies which incorporate the tracking of secondary particles from beam-beam interaction pairs into vertex detectors have begun. More elaborate simulations which model realistic detectors, and which allow events from the physics generators to be overlaid, must also begin. Discussions of machine design would be facilitated if these simulations were in some sense generic. That is, machine design comparisons will be more meaningful if the simulations use a single model detector and physics generator, a common program to calculate the beam-beam backgrounds, and a mutually agreed upon benchmark physics process.

2.6.9 Summary and Recommendations

One concludes from the discussion on Tables 2.6.1 and 2.6.2 above and in the Appendices that:

$\odot$ – the lowest energy of the machine should overlap with the highest energy of LEP so that no e^+e^- "discovery/measurement gap" exists;

$\odot$ – the first stage of the collider should be $\sqrt{s} \simeq 0.5$ TeV, which opens much of the physics potential listed in Tables 2.6.1 and 2.6.2, allows precision measurements of the $\mathcal{SM}$ and perhaps discovery of the Higgs and/or $\mathcal{SUSY}$ and provides a physics programme complementary to hadron colliders;

$\odot$ – the machine design should include an upgrade path to $\sqrt{s} \simeq 1$ - 2 TeV in order to match the discovery reach of LHC, to discover/measure any new physics in this energy regime, and to study $\mathcal{ESB}$ in the heavy Higgs case;

$\odot$ – the luminosity required is $\int \mathcal{L}dt$ up to 100fb^{-1}/year for precision measurements;

$\odot$ – polarized beams open new physics windows and are necessary: polarized e^- are essential, polarized e^+ will improve the power of this technique; and

$\odot$ – Z^0-peak running with polarized beams offers the possibility for sensitive new tests of the internal consistency of the $\mathcal{SM}$.

The series of physics milestones between LEP energies and $\sqrt{s} \simeq 1$ TeV show that a convincing physics case can be made for commissioning the machine at lower luminosity

(10^{33}cm^{-2}s^{-1}) and a c.m.s. energy of 0.3 to 0.4 TeV before reaching the first stage energy of $\sqrt{s} \simeq 0.4$ to 0.5 TeV. The combination of experiments with polarized beams and attainment of the design luminosity (a few $\times$ 10^{33}cm^{-2}s^{-1}) would round out a physics programme that would span several years. The second stage will continue with a step-wise energy increase up to $\sqrt{s} \simeq 1$ - 2 TeV. Both stages contain important ingredients of the complementarity and competition to the hadron colliders.

How the increase to 1 TeV or higher is realized is a question generating considerable discussion and leading to several options: increase the accelerating gradient, increase the length of the machine, change the technology, or a combination of these. The final design report for the 0.5 TeV machine should include a viable strategy for such an energy increase, which of course could change after the experience with the first-stage running is gained.

In the event that no light Higgs boson has already been found before the linear collider is built, then the decision to build the $\gamma\gamma$ option can be left until after the physics results have been extracted from the 0.5 TeV e^+e^- running – as can decisions about energy upgrades or running at the Z^0-pole. The modifications needed for the e^-e^- collider seem to be modest, so that this running could follow at any time the physics case warrants it.

The detectors are more challenging that those for LEP/SLC, though easier than for hadron colliders. There seems to be no critical aspect of the detectors which would tell us that any one of the machine designs would preclude achieving the physics goals set forth. For the hardware, larger beam spots make mechanical problems easier to solve but high repetition rates favoring the efficacy of feedback systems may offset the disadvantages of designs with small beam spots. For the physics analyses, a larger bunch-crossing time reduces the effects of underlying events. The backgrounds for the different machines are similar and will be larger than at LEP, but not so large as to spoil the cleanliness of e^+e^- experimentation as experienced in the past.

Considerable R&D work related to IR issues must be done, as discussed in subsection 6 above; it is mainly related to elimination of vibrations and to a better understanding of backgrounds.

2.6.10 Appendices

A. The e^+e^- Linear Collider Experimentation

Tables 2.6.1 and 2.6.2 of the subsection on main e^+e^- physics topics serve as a guide to the interplay between physics requirements, machine parameters and detector performance for the e^+e^- collider. In this appendix some details of the reasoning leading to those tables are discussed.

The list of physics topics and their implications is the result of many international workshops on e^+e^- physics beyond LEP2 – La Thuile [1], SLAC [2], Snowmass [3], Japan [4, 13], Europe [5, 9, 10, 12], Finland [6], the USA [7, 11], Hawaii [8], among others – and from the workshops on the machine technology: LC88 at SLAC, LC90 at KEK, LC91 in Protvino, LC92 [14] in Garmisch-Partenkirchen, LC93 [15] at SLAC, and LC95 at KEK [16].

A.1 Overview

Examples of the main **e^+e^- physics goals** cited in Tables 2.6.1 and 2.6.2 are:

• Higgs bosons: discovery and exploration of Higgs bosons (via Higgs-strahlung and gauge-

boson-fusion) and of associated production in the case of the minimal $\mathcal{SUSY}$ model ($\mathcal{MSSM}$); measurement of the spin-parity quantum numbers and of the branching ratios in order to test the theory (e.g., to distinguish between $\mathcal{SM}$ and $\mathcal{MSSM}$ Higgses).
• W_LW_L-scattering: in the heavy Higgs scenario, study the mechanism for $\mathcal{ESB}$ through measurement of W_LW_L-scattering at the highest possible energy if no light Higgs is found.
• Supersymmetry: search for signals of charginos, neutralinos, sleptons, as well as of squarks and gluinos; if discovered, extraction of the mass spectrum, the widths and the couplings; measurement of the $\mathcal{SUSY}$-model parameters to understand the mechanism for supersymmetry breaking.
• Extended-gauge models: discovery limits for new gauge bosons and new matter particles.
• Gauge bosons: measurement of the trilinear couplings, of the quadrilinear couplings; unfolding the γ and Z^0 couplings with polarized-beam experiments.
• Top quark: measurement of M_{top} at and above threshold, of the top quark magnetic and electric dipole moments, of its decay properties, of the Yukawa coupling, and of rare decays.
• Quantumchromodynamics: measurement of $\alpha_s(s)$, many studies of the hadronic final state.
• Two-virtual-photon collisions: systematic study of QPM-QCD ("minijet") phenomenology; measurement of the photon structure function $F_2^\gamma(x,Q^2)$, and of inclusive resonances and heavy-flavor production.

The global **machine** aspects of interest listed in Tables 2.6.1 and 2.6.2 are: luminosity, $\sqrt{s} \equiv$ c.m.s. energy, $\mathcal{L}(\sqrt{s})$ spread, and beam polarization. In this evaluation one assumes that both beams are polarized. Narrow $\mathcal{L}(\sqrt{s})$ means that the energy spread from the machine must be small ($\sigma \simeq \mathcal{O}(0.2\%)$) and the luminosity spectrum well-measured (to the $\pm 0.1\%$ level).

The **detector** perfomance has the following general breakdown in Tables 2.6.1 and 2.6.2: hermetic coverage, tracking ($\frac{\delta p_t}{p_t^2}$), calorimetry ($\frac{\delta E}{\sqrt{E}}$), three diminsional (3-D) granularity of the subdetectors, charged lepton identification (and sign determination), vertex tagging, and π/K identification. Table 2.6.5 lists the performance used in physics simulations for the international workshops [4, 22, 23, 24, 25, 26, 27, 28, 29, 30, 31, 32, 33, 34, 35, 36, 37, 40, 41, 42, 43, 44, 46].

A.2 The Evaluations in Tables 2.6.1 and 2.6.2

The basis for the $\star$-ratings, which are being continually updated, is illustrated with a few examples.

• The Higgs boson

In the $\mathcal{SM}$ there exists a single CP-even scalar boson H_{SM}. In the $\mathcal{MSSM}$ the physical spectrum consists of three neutral bosons, the CP-even h^0 and H^0 and the CP-odd A^0, and a pair of charged bosons $H^\pm$. The searches for these particles have been simulated in quite some detail using the performance of existing detectors [23, 26, 32, 35, 40, 49], and the discovery with such detectors is straightforward in the light-Higgs scenarios studied up to now (i.e., for Higgs masses up to about 350 GeV/c^2 at $\sqrt{s} \simeq 0.5$ TeV). Vertex tagging improves the significance of the signals considerably and is thus rated highly, in particular if $M_{Higgs} \simeq M_{Z^0}$[32]. Excellent tracking improves the M_{Higgs} determination [4]. Hermeticity is

needed to identify decays with large missing energy and therefore might help to distinguish between $\mathcal{SM}$ and $\mathcal{MSSM}$ since the $\mathcal{MSSM}$ Higgses can possibly decay invisibly. While light Higgses can be discovered with detectors of a performance similar to LEP and SLC detectors, the measurement of a heavier Higgs at higher $\sqrt{s}$ requires a detector with improved resolution as indicated in Table 2.6.5.

High luminosity is needed to measure the Higgs branching ratios [35]. A higher c.m.s. energy and luminosity are required in case the $\mathcal{SM}$ Higgs is heavy; the H_{SM} could be discovered up to a mass of $M_{\phi^0} \simeq 800$ GeV/c^2 [36]. Higher luminosity and $\sqrt{s}$ are also needed if the world is supersymmetric, since then the Higgs masses range from light (h^0) to possibly very heavy (H^0,A^0) and the charged Higgs ($H^{\pm}$) may also be heavy. In addition to Higgs-strahlung, the neutral $\mathcal{SUSY}$ Higgses are produced in association and the charged Higgs is pair-produced.

As stated earlier, already at $\sqrt{s} \simeq 0.3$ TeV, the e^+e^- linear collider is unique in being able to cover all presently known $\mathcal{SUSY}$ Higgs models and, more generally, theories involving multi-Higgs doublets and singlets.

• W_LW_L scattering

If $M_{Higgs}$is larger than ~800 GeV/c^2, the Higgs is strongly interacting and no longer discoverable as particle, and the programme for understanding the mechanism of electroweak spontaneous symmetry breaking would consist of precision measurements of gauge boson production, the W_LW_L-scattering experiment 28, 43], at the highest energy to which the machine could be upgraded, which should be at least 1.5 TeV.

• Supersymmetry

The lightest supersymmetric particle (LSP) is often assummed to be the lightest neutralino $\tilde{\chi}_1^0$ and stable. It is weakly interacting and frequently an end-product in reactions producing supersymmetric particles. Thus topologies involving $\mathcal{SUSY}$ particles are often characterized by missing energy, so that hermeticity of the detector is essential for these measurements. On the machine side, beam polarization will help for the searches, since for example *slepton* production is enhanced while the W^+W^- background is supressed. If $\mathcal{SUSY}$ is discovered, beam polarization becomes a very important tool for measuring its properties [33], and very good three-dimensional granularity of the detector makes the studies of the complicated final states more tractable. In many $\mathcal{SUSY}$ models, the non-colored states (chargino $\tilde{\chi}_j^{\pm}$, neutralino $\tilde{\chi}_i^0$,slepton $\tilde{\ell}$) are light and might be produced at the 0.5 TeV phase of the machine, while the colored states (squark $\tilde{q}$, gluino $\tilde{g}$) tend to be heavy so that higher energies would be needed to study them.

• Extended gauge models

Extended gauge models almost always require higher energies, higher luminosities, and the best possible detectors. If a Z' exists, or new heavy fermions, the linear collider is ideally suited to investigate these objects. For these studies the highest energy of the e^+e^- collider should be realized, $\sqrt{s} \simeq 2$ TeV, and the discovery reach of the LHC will be exceeded by virtual Z' production in e^+e^-[11].

• The electroweak gauge bosons

The golden channel for the measurement of anomalous $W^{\pm}$ couplings ($WWV, V = \gamma, Z^0$) [28, 31] is $e^+e^- \rightarrow W^+W^- \rightarrow \ell\nu\bar{q}q'$. Detector aspects for the measurement of anomalous $W^{\pm}$ couplings are discussed in Ref. [41]. Hermeticity is important because of the energetic neutrino in the final state. The LEP/SLC-type detectors are adequate for extracting the couplings at $\sqrt{s} \simeq 0.5$ TeV [28], but detectors as studied for JLC [4] and for 1 TeV [44] improve the small-angle tracking performance, which is valuable due to the forward-peaking of the production angular distribution. These detectors allow good tracking down to $|\cos\theta| < 0.98$ for the helicity analyses. At higher energies, the improved tracking performance is necessary.

A well-measured luminosity spectrum, polarized beams, high luminosity and higher energy are important machine aspects. The error in measuring the trilinear gauge couplings decreases roughly as $1/s$, so that higher energies are preferable [28] for this measurement, along with the corresponding increase in luminosity. Beam polarization is of great help in disentangling the γ and Z^0 couplings.

• The top quark

The study of the top quark is one of the central research topics at the linear collider [30]. The demands on the collider performance will be different for the two energy regions in which top-quark studies will be done: at the threshold of $t\bar{t}$ production and at the maximum energy of the collider. In both cases the majority of $t\bar{t}$ events will have a characteristic six-jet structure coming from the prompt decay of each t-quark into a b-quark and a W-boson. Monte Carlo studies show that these events will be efficiently separated from backgrounds.

The measurement of the top mass in the *threshold region* is particularly exacting. The $t\bar{t}$-threshold scan will be a distinct and important part of the early programme of the collider's first phase, and it is important that the linac design be capable of operating in the required low-momentum-bite, low-beamstrahlung mode at around 0.35 TeV, for which the machine parameters may need reoptimization. Thus one needs to know what beamstrahlung spectrum a luminosity of $10^{33} cm^{-2} s^{-1}$ and a machine energy spread of $\sigma \simeq 0.2\%$ would yield. Equally important for the accuracy with which the top mass can be determined is the precision measurement of the luminosity spectrum $\mathcal{L}(\sqrt{s})$ to an accuracy of $\pm 10^{-3}$. This requires good tracking in the endcap region of the detector [22], as indicated in the last row of Table 2.6.2 top quark mass, so that a precision of better than ± 500 MeV/c^2 can confidently be predicted from a 10 fb^{-1} scan. This provides a crucial extra input to the fits of the standard model parameters which can be used to constrain the Higgs boson mass. In this case, the light Higgs boson mass can be restricted to ≤ 500 GeV/c^2 (90% CL) [53].

For top-quark studies *above threshold*, where $t\bar{t}$ events will be produced at about the same rate as $\mu^+\mu^-$ events, the collider can operate in its highest luminosity mode, producing of the order of 10,000 well reconstructed $t\bar{t}$ events for analysis of angular distributions and decay-modes, allowing new precision measurements of parameters of the $\mathcal{SM}$ and opening new windows on its possible breakdown or extension. Examples listed in Table 2.6.2 are the measurements of the top anomalous magnetic $(g-2)$ and electric dipole moments, of its decay $(V \pm A)$ structure, of searches for rare decay modes such as $t \rightarrow H^+b$ and $t \rightarrow \tilde{t}\tilde{\chi}_1^0$, and of the Yukawa coupling. The measurements tend to require higher luminosity and energy and also beam polarization for those involving the analysis of helicity states.

A LEP/SLC-sized detector could do many of these measurements [24, 25, 30]. Hermetic coverage down to $|\cos\theta| < 0.98$ is important for forward-backward measurements of the helicity structure and for detecting rare decays involving the $\tilde{\chi}_1^0$. Good lepton I.D. is essential for studying the leptonic decays of top, for the p_{top} measurement during the threshold scan, for the helicity analyses and for the study of rare decays $t \rightarrow H^+ b$, $H^+ \rightarrow \tau^+ \nu$. The latter reaction also calls for good vertex detection, which is important for the standard $t \rightarrow W^+ b$ decay mode. For the calorimetry/energy-flow measurement, the calibration error must be below 1% to enable an uncertainty in the M_{top} measurement to less than ± 500 MeV/c^2.

• QCD

The measurement of the energy dependence of the strong coupling constant is an important measurement of the $\mathcal{SM}$, and requires the machine energy to be varied over a broad range [39]. Other QCD studies include the measurement of the general properties of hadronic final states. Mainly the tracking and calorimetry of the detector should be good but they do not have to be excellent for these studies, and the lower luminosity expected in the early operating phase of the machine is sufficient.

• Two-photon physics

Even at an e^+e^- collider there are useful event rates both from virtual photon collisions and from beamstrahlung collisions with virtual photons. The higher energy and luminosity of the linear collider will significantly enhance the precision physics done at TRISTAN and LEP - particularly studies of heavy flavour production and the determination [38] of the quark and gluon structure of the photon by measurement of hadronic $\gamma\gamma$ events with and without an observed final state electron.

B. Topics for e^-e^-, $\gamma\gamma$, and $e^-\gamma$ Collider Programmes

These programmes are in the formation stage, even though much theoretical work has been and is being done [45, 48]. The reason that clear goals which make a solid physics case are still being discussed is that these programmes will follow the 0.5 TeV e^+e^- phase of the machine. The e^-e^-, $\gamma\gamma$, and $e^-\gamma$ reactions encompass $\mathcal{SM}$ and non-$\mathcal{SM}$ physics similar to e^+e^-, and are also complementary to e^+e^- since other Feynman diagrams govern the processes. More emphasis is needed on the importance of the complementary aspects of e^-e^-, $\gamma\gamma$, and $e^-\gamma$ physics, since their exploration will come after the e^+e^- physics has been extracted from the 0.5 TeV running.

B.1 The e^-e^- Collider

Collisions of e^-e^- beams could be studied in an early phase of the machine with a normal e^+e^- interaction region and detector [48]. The only special requirement would be a second polarized electron source. The luminosity will be a factor of two or three lower than the corresponding e^+e^- luminosity since the beams will blow up rather than pinch.

Examples are

$e^-e^- \rightarrow e^- W \nu$: copious production for precision tests of the standard model;

$e^-e^- \rightarrow H^{--}$: in case of existence of an extended Higgs sector;

$e^-e^- \rightarrow X^{--}$: production of a possible dileptonic boson;

$e^-e^- \to e^-e^-$: anomalous effects in Möller scattering reveal substructure or Z' effects;
$e^-e^- \to W^-W^-$: due to the exchange of a heavy Majorana neutrino.

B.2 The $\gamma\gamma$ Collider

The reaction $\gamma\gamma \to Higgs$ can give an indirect window to new physics in a similar way that the precision LEP/SLC measurements are sensitive to the top quark and Higgs boson masses. Polarization of incoming laser light and of the electrons can be used to give a narrow energy peak on-resonance.

The most important quantity to be measured is $\Gamma_{\gamma\gamma \to Higgs}$, which could have an anomalous value without violating present knowledge, and it could be sensitive to loops of undiscovered heavy charged particles. Thus the Higgs couplings and branching ratios test for $\mathcal{SM}$, $\mathcal{MSSM}$, or extended-$\mathcal{SUSY}$ particles. One would measure, for example, $\gamma\gamma \to$Higgs$\to b\bar{b}$ or $\gamma\gamma \to$Higgs$\to Z^0Z^0$, depending on the value of M_{Higgs} up to 300 GeV/c^2 for the 0.5 TeV phase of the collider [45].

Other important examples are
$\gamma\gamma \to H^0$or A^0, which are possible for some $\mathcal{MSSM}$ scenarios,
$\gamma\gamma \to t\bar{t}$, which is favored by angular momentum over the equivalent e^+e^- channel,
$\gamma\gamma \to t\bar{t}$, which has a larger cross section than in e^+e^- production because of the coupling to the charge of the top quark, and
$\gamma\gamma \to W^+W^-$ and $W^+W^-Z^0$, for which the copious production allows for precision tests of anomalous couplings, complementary to the e^+e^- measurements.

B.3 The $e^-\gamma$ Collider

Interesting processes which this machine is ideal to study include:

Copious production of $e^-\gamma \to W^-\nu$ provides a complementary measurement of the $WW\gamma$ coupling.

The reaction $e^-\gamma \to \tilde{e}\tilde{\gamma}$ is likely to provide the lowest observable SUSY particle threshold, possibly with a cross-section as large as $\sim$10 fb [50]. Analysis is straightforward with a clear single electron signal and a mass measurement from the Jacobian peak in p_T.

Hundreds of events of the type $e^-\gamma \to \nu tb$ will be produced with 10 fb^{-1}, providing an excellent laboratory for measuring $|V_{tb}|$.

The process $e^-\gamma \to e^-$(tagged)+ hadrons will allow the study of the quark structure of the photon to lower x and higher Q^2 than by any other technique [51]. The detector will require a small-angle tagger. Polarized beams will give access to polarized structure functions. Similarly, the process $e^-\gamma \to$jets or inclusive heavy flavour will allow for the study of the gluon structure of the photon.

B.4 Extension to Energies > 1 TeV

The new particle search channels may need an extension of the energy, but an additional strong motivation will come if there is no light Higgs boson [45].

$\gamma\gamma \to WWZZ, WWWW$, with > 100 fb^{-1}: a 700 GeV/c^2 Higgs may appear as a broad final state W_LW_L resonance, or enhanced rates may be seen [47]. The strongly interacting

electroweak sector could generate a family of narrowerW_LW_L resonances at higher mass.

$e^-e^- \to \nu\nu W^-W^-$ with > 200 fb^{-1}: this experiment would give unique access to $I = 2$ resonant states for production of strong W_LW_L resonances [48].

C. Z^0-Peak Running for Physics

One of the primary goals of precision electroweak measurements is to be sensitive to the Higgs boson mass. If not performed at LEP, an e^+e^- linear collider, running at the Z^0-peak with longitudinally polarized beams and with higher luminosity than the SLC, could do excellent measurements in this field since, even if the Higgs has been discovered, it can probe sensitively the internal consistency of the $\mathcal{SM}$. This was first discussed in the JLC report [4].

At present the main limitation on the sensitivity to M_{Higgs} comes from the poor knowledge of M_{top}, but this should improve soon with new measurements from the Tevatron. From the precision on $\sin^2\theta_W$ of ± 0.0003 which should be achieved by LEP and SLC and from the accuracy on M_{top} from Fermilab of ± 5 GeV/c^2, one would be able to set a significant upper bound on the Higgs mass provided its central value is below 150 GeV/c^2, as predicted by $\mathcal{SUSY}$. In that case the upper bound would be $\sim$500 GeV/c^2 at 90% confidence level (CL), which would imply that the Higgs boson should be observed directly at future colliders, and if it is not observed, then something is wrong with the $\mathcal{SM}$. If the M_{Higgs} is lighter, i.e. $\sim$100 GeV/c^2, its mass would be known to $\pm$40-50 GeV/c^2 [53].

If the upper bound is inconclusive, for example because of measurement errors or if no light Higgs is found at the e^+e^- linear collider or at LHC, then it would seem urgent to cross-check and sharpen the indirect determinations of the Higgs mass. The linear collider can help in two ways: (1) with the accurate M_{top} measurement to ± 0.5 GeV/c^2 and (2) with a measurement of $\mathcal{A}_{LR}$ which improves on that of SLC. The latter would be possible if the accuracy of the polarization measurement can be improved. Assuming $\delta P/P \leq \pm 0.5\%$, i.e. twice as good as SLD, then with only 100pb^{-1} of data taken at the Z^0-peak, $\sin^2\theta_W$ could be measured to ± 0.0001. Thus a luminosity of $\sim 5 \times 10^{31}$cm^{-2}s^{-1} would suffice. This error on the polarization is easily achievable if e^+ polarization is available [52]. At this level of accuracy there is a new limitation due to uncertainties on $\alpha(M_Z)$ coming from poor knowledge of the hadronic cross section in e^+e^- below 10 GeV. Assuming that progress in the near future will reduce this uncertainty by a factor of two, then the Z^0-peak running would set an upper bound on the Higgs mass of, for example, 800 GeV/c^2 (90% CL) for a central value of $M_{\phi^0} \simeq 500$ GeV/c^2.

This option would thus open new avenues for attack on the $\mathcal{SM}$ via precision measurements using polarized beams with modest requirements on luminosity. Another example is the measurement of $\sin^2\theta_W$ for different flavors.

If 10^{33}cm^{-2}s^{-1} is available for Z^0-pole running, then experiments become feasible such as measuring CP violation in the b-quark sector [4], or B_s^0 oscillations [54], in case there are still open questions from experiments now in preparation.

References

[1] *Proceedings of the Workshop on Physics at Future Accelerators* (La Thuile 1987), ed. J.H. Mulvey, CERN 87-07 (1987).

[2] C. Ahn et al., *Opportunities and Requirements for Experimentation at a Very High Energy e^+e^- Collider*, SLAC-Report-329 (1988).

[3] *Proceedings of the Summer Study on High Energy Physics in the 1990s* (Snowmass, 1988), ed. S. Jensen (World Scientific, Singapore, 1989).

[4] Three Workshops on the Japan Linear Collider (1989,1990,1992) resulting in:
JLC Group, *JLC-I*, KEK Report 92-16 (1992).
The latest workshop took place in 1995.

[5] *e^+e^--Collisions at 500 GeV: The Physics Potential, Parts A and B* (Workshops at Munich, Annecy, Hamburg, 1991), ed. P.M. Zerwas, DESY 92-123A&B (1992).

[6] *Physics and Experiments with Linear Colliders, Vols. I and II*, eds. R. Orava, P. Eerola and M. Nordberg (World Scientific, Singapore, 1992).

[7] *Proceedings of the 1992 Workshops on High-Energy Physics with Colliding Beams* (Trilogy of Workshops at Yale, Wisconsin, Santa Cruz, 1992), ed. J. Rogers, SLAC-428 (1993).

[8] *Workshop on Physics and Experiments with Linear e^+e^- Colliders, Vols.I and II* (Waikoloa, Hawaii, 1993), eds. F.A. Harris, S.L. Olsen, S. Pakvasa and X. Tata (World Scientific, Singapore, 1993).

[9] *e^+e^--Collisions at 500 GeV: The Physics Potential, Part C* (Workshops at Munich, Annecy, Hamburg, 1992-1993), ed. P.M. Zerwas, DESY 93-123C (1993).

[10] *Proceedings of the Zeuthen Workshop on Elementary Particle Theory – Physics at LEP200 and Beyond* (Teupitz/Brandenburg, Germany, April 1994), eds. T. Riemann and J. Blümlein, Nucl. Phys. B (Proc. Suppl.) 37B(1994).

[11] This year (1995) the proceedings of the studies in the USA by "DPF Long Range Planning" working groups (DPF is the Division of Particles and Fields of the American Physical Society), to assess the particle-physics landscape after the cancellation of the SSC, have been completed and appear on the World Wide Web under http://www.pha.jhu.edu/cltp/.

[12] *Physics with e^+e^- Linear Colliders, Part D* (Workshops at Annecy, Gran Sasso, Hamburg, 1995), proceedings to be published as DESY 96-123D.

[13] *Proceedings of the 1995 International Linear Collider Workshop at Morioka-Appi* (Sept. 8-12, 1995), to be published.

[14] *Proceedings of LC92, the ECFA Workshop on e^+e^- Linear Colliders, Vols. I and II*, ed. R. Settles, MPI-PhE/93-14, ECFA 93-154 (1993).

[15] *Proceedings of the Fifth International Workshop on Next-Generation Linear Colliders* (LC93, SLAC, October 13-21, 1993), SLAC-436 (1993).

[16] *Proceedings of the Sixth International Workshop on Linear Colliders* (LC95, KEK, March 26-31, 1995), KEK Report, to be published.

[17] Michael E. Peskin, "Complementarity of e^+e^- and pp Colliders for the Exploration of Electroweak Symmetry Breaking", SLAC-PUB-6582 (August 1994).

[18] S.L. Glashow, *Proceedings of the LEP Summer Study*, CERN 79-01, Vol.1, p.285.

[19] P. Zerwas, Phys. Bl. 49(1993)187.

[20] P. Emma, in Ref. [6].

[21] K. Oide, in Ref. [16].

[22] M.N. Frary and D.J. Miller, in Ref. 5], p.379.

[23] P. Janot, in Ref. [5], p.107.

[24] G. Bagliesi, et.al., in Ref. [5], p.327.

[25] K. Fujii, in Ref. [6], p.203.

[26] S. Komamiya, in Ref. [6], p.277.

[27] J.-F. Grivaz, in Ref. [6], p.353.

[28] T. Barklow, in Ref. [6], p.423.

[29] David Burke, in Ref. [14], Vol. II, p.557.

[30] P. Igo-Kemeñes, in Ref. [8], p.95.

[31] A. Miyamoto, in Ref. [8], p.141. [8]

[32] P. Janot, in Ref. [8], p.192. [8]

[33] S. Orito, in Ref. [8], p. 230.
[8] T. Tsukamoto, in Ref. [8], p. 814.

[34] D.L. Borden, in Ref. [8], p.323.

[35] M.D. Hildreth, in Ref. [8], p.635.

[36] JLC Study Group (Y. Kurihara), Ref. [4], p.73, and KEK Proceedings 91-10 (Nov. 1991), p.293.

[37] P. Grosse-Wiessmann, contribution to Hawaii Workshop; cf. William W. Ash, in Ref. [8], p.402.

[38] D.J. Miller, B.W. Kennedy, J.J. Ward, and J.R. Forshaw, in Ref.[8], p.577.

[39] S. Bethke, in Ref. [8], p.687.

[40] A. Sopczak, in Ref. [9], p.121.

[41] R.W. Forty, J.B. Hansen, J.D. Hansen and R. Settles, in Ref. [9], p.235.

[42] R. Settles, for the ee500 Experimentation Working Group (G. Coignet, P. Colas, J.D. Hansen, D. Miller and R. Settles) in Ref. [9], p.591.

[43] T. Barklow, SLAC-PUB-6618 (1994).

[44] R. Settles, in Ref. [10], p.316.

[45] *Proceedings of the Gamma-Gamma Collider Workshop* (Berkeley, March 28-31, 1994), ed. A. Sessler, NIM A355(1995).

[46] F. Richard, Conventional Detectors for a Photon-Photon Collider, LAL 94-45 (June 1994).

[47] G. Jikia, in Ref. [45], p. 84.

[48] *Proceedings of the Santa Cruz Workshop on e^-e^- Collisions* (Sept. 4-5, 1995), ed. C. Heusch, to be published.

[49] P. Igo-Kemenes, in Ref. [12], to be published.

[50] D. Cline, UCLA, private communication.

[51] D. Miller, in Ref. [13], to be published.

[52] K. Flöttmann, DESY 95-064.;
K. Fujii and T. Omori, KEK Preprint 95-127.

[53] F. Richard, LAL 95-25;
P. Renton, private communication.

[54] H.-G. Moser, NIM A295(1990)435.

3 UPGRADES AND OTHER OPTIONS

3.1 Upgrades to 1 TeV c.m. and Above

In Chapters 1 and 2, we considered the linear collider designs for 500 GeV c.m. energy. This was the first charge to the Technical Review Committee. We now come to one of the additional charges which was to consider how these machines, once built, could be extended in energy to 1 TeV c.m. and possibly higher, with a luminosity reaching $10^{34} cm^{-2} s^{-1}$. The TRC has not had the time to consider this charge in the same depth as the 500 GeV c.m. case but all the designs have an upgrade path to higher energy. Tables 3.1 and 3.2 summarize the 1 TeV c.m. parameters. Here again, the background numbers have been calculated by P. Chen at SLAC. Brief paragraphs, which follow below, describe how each of the machines might be upgraded.

3.1.1 TESLA

Upgrading TESLA to higher energies and luminosity can be effected by means of a number of steps. Tables 3.1 and 3.2 show an increased luminosity and 1 TeV c.m. resulting from:

- A smaller emittance
- A smaller β_y^* and smaller spot
- More bunches per pulse (closer spacing)
- A lower charge per bunch
- A shorter bunch
- Doubling the number of klystrons, modulators and sections
- Unchanged beam power
- Reduction of the repetition rate from 10 to 5 Hz (this step may also be adopted from the beginning for the 500 GeV c.m. case)

The above conditions still keep δ_B at about the same level as for the 500 GeV c.m. design, i.e., a factor of about 3 lower than for the other machines. Cavity position tolerances in the linac are kept relaxed by lowering the bunch charge. The bunch spacing (354 ns instead of 800 ns) is reduced but still sufficient to resolve single bunch crossings. However, the option of an rf gun without a damping ring for electrons seems to be excluded for this low emittance approach.

It may be possible to reach an energy of 1.6 TeV c.m. if the cavity gradient can be increased to 40 MV/m with a Q_0 of 5×10^9 to keep rf losses within reasonable limits.

Concerning the $\gamma - \gamma$ option for TESLA, ideas exist based on the concept of generating FEL radiation from the beams at low energy and converting the intense soft photons into hard γ's by backscattering off the e^- and e^+ in the IR. This option, as well as $e^- - e^-$ and $e^- - \gamma$ collisions in TESLA require further study.

Table 3.1

Linear Colliders: Overall and Final Focus Parameters – 1 TeV (c.m.)

	TESLA	SBLC	JLC (C)	JLC (X)	NLC	VLEPP	CLIC
Initial energy (c.of .m.) (GeV)	1000	1000	1000	1000	1000	1000	1000
RF frequency of main linac (GHz)	1.3	3	5.7	11.4	11.4	14	30
Nominal Luminosity (10^{33} cm^{-2}s^{-2})†	7.48	3.25	6.4	10	10.4	17.3	1.7-7.6
Actual luminosity (10^{33} cm^{-2}s^{-2})†	12.8	6.3	6.3	9.17	14.5	13	2.20-10
Linac repetition rate (Hz)	5	50	50	150	120	300	4000-1800
No. of particles/bunch at IP (10^{10})	1.8	2.9	1.44	.7	1.1	20	.8
No. of bunches/pulse	2260	50	72	85	75	1	1-10
Bunch separation (nsec)	354	10	2.8	1.4	1.4	–	.67
Beam power/beam (MW)	16.5	5.8	4.2	6.4	7.9	4.8	2.6-11.7
Damping ring energy (GeV)	4.0	3.15	2.0	2.0	2.0	3.0	2.15
Main linac gradient, unloaded/loaded†† (MV/m)	25/25	42/36	58/47	73/58	85/63	100/91	80/78
Total two-linac length (km)	58	33	26.6	21.8	18.7	14	17.6
Total beam delivery length (km)	4	4	6	6	6.8	4	2.4
$\gamma\epsilon_x/\gamma\epsilon_y$ (m-$rad \times 10^{-8}$)	1400/6	1000/10	330/4.8	330/4.8	500/5	2000/7.5	390/20
β_x^*/β_y^* (mm)	25/0.7	32/0.8	41/0.1	10/0.1	25/0.1	200/0.1	10/0.18
σ_x^*/σ_y^* (nm) before pinch	598/6.5	572/9	372/2.2	184/2.2	360/2.3	2000/2.7	200/6.0
σ_z^* (μm)	500	500	120	90	100	750	200
Crossing Angle at IP (mrad)	0	3	6.0	6.1	20	6	1
Disruptions D_x/D_y	0.2/14	.26/16.2	.07/12.1	.1/8.9	.05/7.6	.2/165	.22/7.4
H_D	1.64	1.68	1.32	1.42	1.35	2.0	1.32
Upsilon sub-zero	.053	.06	.28	.33	.27	.12	.17
Upsilon effective	.053	.06	.29	.33	.27	.15	.18
δ_B (%)	2.5	6.5	9.6	9.0	7.4	26.6	7.7
n_γ (no. of γ's per e)	1.2	1.4	1.4	1.2	1.1	5.0	1.52
$N_{pairs}(p_T^{min}) = 20$ MeV/c, $\theta_{min} = 0.15$)	7.3	7.6	13.8	4.9	7.0	?	3.4
$N_{hadrons}$/crossing	.16	.19	.55	.19	.25	?	.13
$N_{jets} \times 10^{-2}(p_T^{min}) = 3.2$ GeV/c	.66	.80	5.3	1.9	2.3	?	.95

† For the sake of uniformity, the nominal luminosity is simply defined as $N^2/4\pi\,\sigma_x^*\,\sigma_y^*$ times the number of crossings per second, and in all cases assumes head-on collisions, no hour-glass effect and no pinch. The actual luminosity incorporates all these effects, including crossing angle where applicable. NLC calculations assume crab-crossing.

†† The loaded gradient includes the effect of single-bunch (all modes) and multibunch beam loading, assuming that the bunches ride on crest. Beam loading is based on bunch charges in the linacs, which are slightly higher than at the IP.

Table 3.2
Pre-linacs, Damping Rings and Main Linac Parameters – 1 TeV (c.m.)

	TESLA	SBLC	JLC (C)	JLC (X)	NLC	TBNLC	VLEPP	CLIC
Pre-linacs								
First stage $e\pm$ energy (GeV)	4	3.15	1.98	1.98	2	2	3.0	2.15
Second stage $e\pm$ energy (GeV)	-	-	20	10-20	10	10	–	9.0
Beam energy to make e^+ (GeV)	500,	500	10	10	6	6	150	2.15
Damping Rings								
e^+ pre-damping ring energy (GeV)	-	-	1.98	1.98	2.0	2.0	–	2.15
$e\pm$ damping ring energy (GeV)	4	3.15	1.98	1.98	2.0	2.0	3.0	2.15
Ring circumference (m)	20,000	650	321	277	223	223	160	283
Damping times (ms) (τ_x/τ_y)	20/20	3.8/3.8	3.5/4.3	4.0/5.2	4.1/4.6	4.1/4.6	1.8/2.9	10.5/10.5
Number of bunches per ring	2260	50	288	340	4×75	4×75	3	72×10
Bunch length (mm)	10	4	5	5	4.1	4.1	9.8	1.8
Extr. beam emittance, $\gamma\epsilon_x/\gamma\epsilon_y$ 10^{-6}	10/.5	10/.5	3/0.03	3/0.03	3/0.03	3/0.03	45.5/0.45	2.5/0.04
Main Linacs								
RF frequency (GHz)	1.3	3.0	5.7	11.4	11.4	11.4	14	30
Unloaded/loaded gradient†† (MV/m)	25/25	42/36	58/47	73/58	85/63	85/63	100/91	80/78
Active two-linac length (km)	40	29.4	22.2	18.2	17	17	11.6	12.8
Total two-linac length (km)	58	33	26.6	21.8	18.7	18.7	14	17.6
Total number of klystrons	1280	4904	6176	6910	9456	64†	2800	4
Total number of modulators	1280	4904	3088	6910	4728	18912†	280	NA
Klystron peak power (MW)	8	150	100	135	72	38480†	150	NA
Klystron repetition rate (Hz)	5	50	50	150	120	120	300	4000/1800
Klystron pulse length (μsec)	1300	2.8	2.4	.5	1.1	.300	.5	.0176/.0176
Pulse compression ratio	1	?	5	2	5	1	4.55	NA
Pulse compression gain	1	?	3.5	1.96	3.6	1	3.3	NA
RF pulse length at linac (μsec)	1300	2.8	.48	.23	.22	.300	.110	.0116/.0176
Number of sections	38656	5034	12352	13820	9456	9456	11200	45772
Section length (m)	1.04	6	1.8	1.31	1.8	1.8	1.0	0.280
a/λ (range if applicable)	.15	.16/.11	.16/.12	.20/.14	.22/.15	.22/.15	.14	.20
Total AC power to make rf (MW)	184	284	200	220	191	152	114	275
Wall plug → beam efficiency (%)	17.9	4.1	4.4	6.7	7.9	20	8.4	1.9/8.5

† The definitions for the TBNLC are somewhat different from the other machines. Each 300 m-long induction linac driver is counted as one klystron. There are 64 such drivers. Each has approximately 300 induction pulse power modules for reacceleration which are counted as modulators. There are two such modules per NLC accelerator section. With the rf pulse length increased to 300 ns, the number of bunches could be increased from 75 to 143, with a corresponding increase in luminosity.

†† The loaded gradient includes the effect of single-bunch (all modes) and multibunch beam loading, assuming that the bunches ride on crest. Beam loading is based on bunch charges in the linacs, which are slightly higher than at the IP.

3.1.2 SBLC

The path to 1 TeV c.m. and higher luminosity for SBLC shown in Tables 3.1 and 3.2 consists of:

- A smaller vertical emittance
- Similar β^*
- Reduced bunch separation
- Reduced number of bunches
- Reduced beam power
- Increased gradient (by a factor of 2)
- Doubling the number of klystrons and modulators
- Addition of pulse compression to enhance klystron peak power by a factor of 2

On other options, SBLC is similar to TESLA above.

3.1.3 JLC

JLC(X) has been designed from the beginning for 1 TeV c.m. energy. The upgrade from 500 GeV to 1 TeV c.m. (see Tables 3.1 and 3.2) is obtained by:

- Approximately doubling the length of the main linacs.
- Hence, doubling the number of klystrons, modulators and sections
- Keeping practically all beam parameters unchanged in the damping rings and linacs
- Doubling beam power and AC power
- Obtaining the enhanced luminosity from smaller spots via adiabatic damping

The upgrade of JLC(C) is obtained by:

- Increasing the length of the linacs by 40%
- Increasing the numbers of klystrons, modulators and sections by 40%
- Doubling the peak power of the klystrons
- Reducing the repetition rate from 150 to 50 Hz to conserve AC power
- Increasing the number of particles/bunch by 44%

- Keeping the beam power approximately constant
- Increasing β_x^* from 10 to 41 mm to keep δ_B at an acceptable level

The JLC(S) is not shown in the tables. The only reasonable way to upgrade it is to lengthen the entire complex to ≈50 km without changing the gradient because the gradient is already very high. The number of particles per bunch and the number of bunches cannot be increased because of the total beam loading and the beam loading compensation by SLED. The reduction of the beamstrahlung in this approach can be obtained only by increasing the horizontal beam size but this inevitably reduces the luminosity.

3.1.4 NLC

The NLC, similarly to JLC(X), has been designed from the beginning for a 1 TeV c.m. energy, with several upgrade paths to 1.5 TeV. The path from 500 GeV to 1 TeV c.m. (see Tables 3.1 and 3.2) could be implemented gradually or in a single step. It is obtained by:

- Increasing the two-linac length and number of accelerator sections by 20%
- Doubling the number of klystrons and modulators per unit length - 4 klystrons would then feed a single SLED-II pulse compressor
- Increasing the klystron peak power from 50 MW to 72 MW. The combination of increasing the klystron power and doubling the number of klystrons per SLED-II yields a 72% increase in accelerating gradient.
- Increasing the bunch charge correspondingly to the increase in accelerating gradient to keep the beam loading constant
- Increasing β_x^* from 10 to 25 mm to keep δ_B at an acceptable level
- Reducing the repetition rate from 180 to 120 Hz and shortening the bunch train by 16% to save AC power and contain the beam power

Details of the $\gamma - \gamma$ and other options are under design.

3.1.5 TBNLC

The TBNLC approach is another option towards the 1 TeV c.m. upgrade of the NLC. Details of the TBNLC technology have been described in Section 2.3. The path to 1 TeV c.m. with the TBA would depend on whether the NLC for 500 GeV c.m. had originally been built with conventional rf or not. If it had, the transition to a TBNLC system would require considerable changes in the layout since the tunnel would now have to include the induction linac drivers and the transfer structures. The SLED-II rf pulse compression system would no longer be needed. Referring to the TBNLC column in Table 3.2, the following equipment would have to be installed:

- 64 relativistic klystrons with their injectors, choppers, capture sections, transfer structures, afterburners and dumps
- All the X-band linac structures would have to be individually reconnected to the corresponding transfer structures
- All the equipment peripheral to the TBA would have to be installed in the klystron gallery
- The control system would have to be rebuilt for the TBA mode
- In principle, the primary e^+ and e^- beams could be very similar to the NLC beams

Conversely, if one started with a TBNLC at 500 GeV c.m., the path to 1 TeV c.m. would depend entirely on the length and configuration of the 500 GeV c.m. system already in place.

3.1.6 VLEPP

The VLEPP path from 500 GeV to 1 TeV c.m. is straightforward (see Tables 3.1 and 3.2) and simply involves:

- Doubling the length of the two linacs and the number of sections
- Doubling the number of klystrons, power supplies and power compressors
- Keeping all the beam parameters unchanged except the beam power, which is doubled
- Doubling the AC power
- Increasing the luminosity by decreasing the horizontal beam spot via adiabatic damping

$\gamma - \gamma$ and other options are under study.

3.1.7 CLIC

The CLIC upgrade path from 500 GeV to 1 TeV c.m. (see Tables 3.1 and 3.2) is obtained by:

- Doubling the length of the main and drive beam linacs, hence doubling the number of sections in both linacs
- Doubling the power of the drive beam generation systems to produce two extra drive beams, and adding isochronous loops at the ends of the main and drive beam linacs in order to inject the beams into the new ends of the linacs
- Keeping the gradient unchanged
- Increasing the number of pulses per second to 1800 Hz

- Adapting the quadrupole focusing to the new energy in the original linacs

As far as $\gamma - \gamma$ or other options are concerned, FEL's at the end of the drive beams generate soft photons which are converted to hard γ's by backscattering off the main beams.

3.2 Interaction Region for Gamma-Gamma and Gamma-Electron Collisions

This section was written by Kwan-Je Kim (mentioned here because he was not an official member of the Technical Review Committee) of LBNL, together with Valery Telnov, Deputy Chairman of the Beam Delivery working group.

3.2.1 Introduction and Motivation

In order to maximize the accessible high energy physics, it is sensible that a future linear collider, if built, should be provided with at least two interaction points (IPs): one for "normal" e^+e^- or e^-e^- collisions and a second one for γe^- and $\gamma\gamma$ collisions. High energy photons, i.e., γ rays, for these collisions are most effectively produced via Compton backscattering of focussed laser beams by the high energy electron beams of the linear collider. The high energy photon beams are then brought into collision with opposing electron and photon beam for γe^- collisions and $\gamma\gamma$ collisions, respectively. Since positrons are not necessary for this operation, the collider may be operated in the e^-e^- mode before one or both electron beams are "converted" to γ rays. With suitable laser and electron beam parameters, a luminosity of γe^- or $\gamma\gamma$ collisions comparable to that of the e^+e^- collisions can be achieved. The polarization of the high energy photons can be controlled by the polarizations of the laser and the electron beam. With high luminosity and variable polarization, the $\gamma\gamma$ and γe^- collisions at TeV energies will significantly enhance the discovery potential and analytic power of a TeV linear collider complex.

The physics opportunities for γe^- and $\gamma\gamma$ collisions are described in detail in Section 2.6. Some examples are:

1) A $\gamma\gamma$ or γe^- collider serving as a W-factory, producing $10^6 - 10^7$ W's/year, allowing a precision study of the gauge boson interactions and search for their possible anomalies;

2) A $\gamma\gamma$ collider for searching new charged particles, such as SUSY particles, leptoquarks, excited states of electrons, etc., because photons are generally more effectively coupled to these particles than electrons or positrons;

3) A $\gamma\gamma$ collider to measure the two-photon decay width of the Higgs boson, providing a glimpse of the mass scale beyond the TeV range;

4) A γe^- collider to study the photon structure functions, and others. Furthermore, e^-e^- collisions (without conversion to γ rays) are also interesting in themselves.

The idea of incorporating γe^- or $\gamma\gamma$ collisions in a future linear collider via Compton backscattering has been studied for sometime, especially by scientists from Novosibirsk.

However, the work so far has been mainly at the conceptual level, a review of which can be found in the proceedings of a recent workshop at Berkeley. More serious work on the feasibility of such collider is now under way. In the following sections we briefly review the concept, the current status, and various issues associated with the development of γe^- and $\gamma\gamma$ colliders.

3.2.2 The General Scheme

The general scheme for a $\gamma\gamma$ collider is shown in Fig. 3.2.1. Two electron beams from their respective final focus systems (FFS) are heading toward the IP. At a location a short distance (of order 1 cm) upstream from the IP, referred to hereafter as the conversion point (CP), a laser beam is focussed and Compton backscattered by the electrons, resulting in a high energy beam of photons. The photon beam follows the original electron motion with a small angular spread of order $1/\gamma$, arriving at the IP in a tight focus, where it collides with an opposing high energy photon beam similarly produced by the other electron beam.

The energy of the high energy photon depends strongly on the scattering angle, being maximum in the the original electron direction and decreasing rapidly away from this direction. Thus the spectral luminosity of the $\gamma\gamma$ collision depends strongly on the distance b between the CP and the IP. Introducing the parameter $\rho = b/\gamma\sigma_y^*$, where σ_y^* is the vertical rms electron beam size (assumed to be smaller than the horizontal size) in the absence of the CP, the spectral luminosity is broadly distributed as a function of the c.m. energy of the two photon system when $\rho \ll 1$. As ρ is increased, the low energy part of the luminosity spectrum becomes suppressed because of the larger spot size occupied by low energy photons. Thus the luminosity spectrum develops a well defined peak at the high energy end with a bandwidth of about 10% when $\rho \geq 1$. For most applications, one would choose $\rho \simeq 1$ to obtain a narrow spectrum without incurring a large luminosity reduction.

By varying the polarization of the electron and the laser beams, the polarization of the high energy photon beams can be tailored to fit the needs of a particular experiment. Controlling the polarization is also important to sharpen the spectral peak in the $\gamma\gamma$ luminosity. Because of the polarization dependence of the Compton scattering, the spectral peak present in the case $\rho \geq 1$ is significantly enhanced by choosing the helicity of the laser photons to be of the sign opposite to the helicity of the electrons.

The "spent" electron beam, following its interaction at the CP, together with the photon beam will cause background γe^- and e^-e^- events as well as producing copious beamstrahlung photons, which will further increase the backgrounds, in interaction with the other electron beam. In Fig. 3.2.1, the spent electron beam is shown to be bent away from the IP by a sweeping magnetic field. Several other ideas have been proposed to reduce unwanted background events (See Section 3.2.7).

A γe^- collider would be similar to a $\gamma\gamma$ collider discussed above, except that it would have only one CP.

3.2.3 Laser Parameters

The energy of the Compton scattered photon is a maximum when the scattered photon is in the direction of the incoming electron, i.e., in the backscattering direction. The maximum

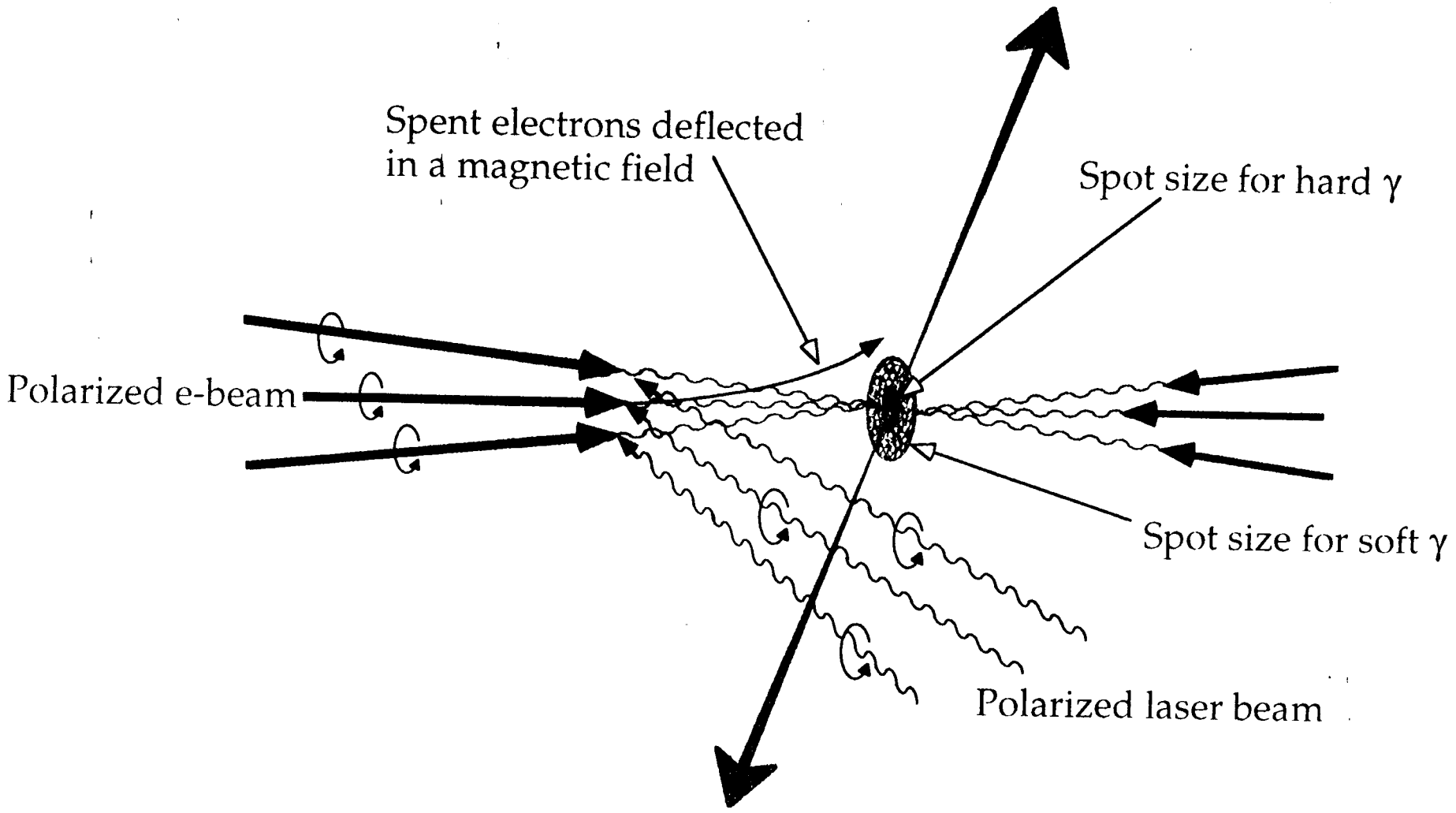

Fig.3.2.1 General schematic of a $\gamma\gamma$ collider interaction point.

energy is given by

$$\omega_m = \frac{x}{x+1} E_0,$$

where

$$x = \frac{4E_0\omega_0}{m^2c^4} \simeq 15.3 \left[\frac{E_0}{TeV}\right] \left[\frac{\omega_0}{eV}\right];$$

Here ω_0 is the energy of the laser photons and E_0 is the initial energy of the electrons. Hence, the energy of the backscattered photon increases with increasing value of the parameter x, but if x is larger than 4.8, high energy photons can be lost because of e^+e^- pair creation in collision with unscattered laser photons. Thus, the optimum value is $x = 4.8$. For $E_0 = 0.25$ TeV, this leads to a laser wavelength of about 1 μm.

The probability of the Compton backscattering per unit length is linearly proportional to the laser pulse energy A. The total "conversion" probability for high energy photons per individual electron in such a circumstance is approximately given by $k = 1 - \exp(-A/A_0)$, where A_0 is the laser pulse energy corresponding to a conversion probability of 65%. The increase in the conversion probability with a laser pulse energy larger than A_0 is relatively small, and, furthermore, is expensive because of higher laser power requirements. We shall therefore use $A = A_0$ and $k = 65\%$ for the following estimates.

The laser pulse energy A_0 is minimized when the electron pulse length l_e, the laser pulse length $c\tau$, and twice the Rayleigh length are all about the same, and is given approximately by $A_0[\mathrm{J}] \sim 15 l_e[\mathrm{cm}]$. However, the corresponding laser intensity could at times be so large that nonlinear QED effects may spoil the conversion process (such as multiphoton pair production) and reduce the high energy photon flux. For a 1 μm laser beam, these effects can be suppressed if the laser intensity remains below 1×10^{18} W/cm^2. At this limiting intensity, the laser pulse length is determined by $c\tau[\mathrm{cm}] \sim 0.2E[\mathrm{TeV}]$ and the pulse energy $A_0[\mathrm{J}] \sim 4E_0[\mathrm{TeV}]$. The required laser pulse energy and length are given by the larger of the values obtained from each of these considerations.

Versatile polarization control is crucial for a $\gamma\gamma$ or γe^- collider for physics experimentation as well as for luminosity calibration. Pulse-to-pulse switching of helicity is proposed to characterize all helicity components of the luminosities.

The laser parameters required for an optimum conversion at $x = 4.8$ may then be summarized as :

Micropulse energy	$A_0 \sim \max(15 l_e[\mathrm{cm}], 4E_0[\mathrm{TeV}])$, J
Micropulse duration	$c\tau \sim \max(l_e, 0.2E[\mathrm{TeV}])$, cm
Repetition rate	Same as electron beam pulse rate
Wavelength	$\lambda = 4.2E_0[\mathrm{TeV}]$ μm or $\omega_0 = 0.3/E_0[\mathrm{TeV}]$ eV
Spotsize	Near diffraction limited
Polarization	Fully polarized with adjustable helicity

Consequently, the laser parameters for a 500 GeV c.m. energy collider are: wavelength about 1 μm, micropulse energy about 1-3 J, and micropulse duration 1-5 ps. The peak power is therefore in the TW range. With a pulse repetition of rate of 10^4 Hz, the time averaged power of the optical beam would therefore be tens of kW. In Section 3.2.8, we discuss the technology of lasers producing the required optical beams.

Projects	$L_{\gamma\gamma}$	ϵ_x (m rad)	ϵ_y (m rad)	σ_x (m)	σ_y (m)	β_x (m)	β_y (m)
TESLA	9.2E+32	1.96E-05	1.00E-06	4.00E-07	4.50E-08	4.00E-03	9.89E-04
SBLC	4.12E+32	9.98E-06	4.79E-07	3.50E-07	2.90E-08	6.00E-03	8.58E-04
JLC	9.48E+32	3.31E-06	4.40E-08	4.50E-08	1.00E-08	3.00E-04	1.11E-03
NLC	1.11E+33	5.01E-06	5.01E-08	7.00E-08	7.00E-09	4.79E-04	4.79E-04
CLIC	4.33E+32	2.98E-06	1.49E-07	1.00E-07	8.00E-09	1.64E-03	2.10E-04
VLEPP	1.97E+33	1.96E-05	6.11E-08	5.00E-07	9.68E-09	6.25E-03	7.50E-04

Table 3.2.1 Monochromatized $\gamma\gamma$ luminosities attainable with current e^+e^- designs for E_{cm} = 500 GeV with an optimized FFS.

3.2.4 Electron Beam Parameters and $\gamma\gamma$ Luminosity

The optimization of the electron beam parameters for $\gamma\gamma$ collisions is different from that corresponding to the e^+e^- collisions. For e^+e^- collisions, the beam spot at the IP is normally designed to be flat in order to minimize the beamstrahlung effect. In $\gamma\gamma$ collisions, on the other hand, electron beams with much smaller horizontal spot size and larger number of particles per pulse are allowed, because neither beamstrahlung nor disruption play a role.

In the following, we shall be mainly concerned with the case $\rho \simeq 1$. The total $\gamma\gamma$ luminosity is then approximately given by $k^2 \simeq 0.4$ times the geometric e^-e^- luminosity. On the other hand, the most valuable part of the spectral luminosity is the peak at the high energy end of the invariant mass distribution. Not only is the photon energy high, but this region is also characterized by a high degree of polarization. This region, with an energy bandwidth of about 10%, accounts for about 20% of the total $\gamma\gamma$ luminosity, or about 10% of the geometrical e^-e^- luminosity. The "monochromatized " $\gamma\gamma$ luminosity may therefore be taken to be one-tenth of the geometric e^-e^- luminosity.

To obtain a monochromatized $\gamma\gamma$ luminosity about the same as the e^+e^- luminosity, it is therefore necessary to have a design of an e^-e^- collider with a geometric luminosity ten times larger than the e^+e^- luminosity. This is a challenging task, involving reoptimization of the whole linac-damping ring complex. However, it should be feasible to increase the geometric e^-e^- luminosity by a more modest factor, say 2 or 3, by modifying the FFS to reduce the beta functions, but keeping the other electron beam parameters the same as in the current e^+e^- designs. In doing so, proper account should be taken of the Oide effect as well as the constraint that β_x and β_y be larger than the bunch length. To implement this idea, we have used the best guesses on the minimum $\beta_x\beta_y$ products for various e^+e^- linear collider projects, as provided by experts at the corresponding laboratories, and calculated the monochromatized $\gamma\gamma$ luminosities. The results are summarized in Table 3.2.1. Note that the β_x values are much smaller than those for the current e^+e^- designs. It is seen that the monochromatized $\gamma\gamma$ luminosity is about 10^{33} $cm^{-2}s^{-1}$ or about 20% of the luminosity in e^+e^- collisions for most projects. This is already sufficient to study many interesting processes.

It should be mentioned that for many processes, the monochromaticity and a high degree of polarization are not required and the invariant mass can be measured from the final particles. In that case one can decrease the distance between the CP and the IP, obtaining

a total $\gamma\gamma$ luminosity larger by a factor 3 or 4.

As the $\gamma\gamma$ luminosity is not limited by collision effects, it is worthwhile to optimize the damping ring designs for a smaller horizontal emittance. This should result in a $\gamma\gamma$ luminosity several times larger than that obtained above.

Increasing the number of particles per bunch at a reduced pulse repetition rate will further increase the $\gamma\gamma$ luminosity. This will also relax the requirement on the average laser power, but will require a detailed re-optimization of the linac–damping ring complex.

3.2.5 FFS

As was stated in the precceding section, the value of the beta functions used in Table 3.2.1 were best guesses by experts and need to be verified through a detailed FFS design. It should be noted that, for most cases, the focussing is much stronger in the x-direction and somewhat weaker in the y-direction than is the case for the corresponding e^+e^- designs, so that β_x and β_y are similar in magnitude. An FFS producing such focussing would probably involve a final triplet, rather than a doublet, of quadrupoles. A design of an FFS for $\gamma\gamma$ collisions at the NLC is currently under way.

3.2.6 Laser Optical Path

Designing a high power optical transport system leading to a tight focus at the CP, while satisfying various constraints imposed by particle detectors, electron transport hardware, the coil arrangement for the sweeping magnet if employed, and so on, is one of the major tasks in designing a $\gamma\gamma$ collision region. Figure 3.2.2 illustrates a possible mirror arrangement for the $\gamma\gamma$ collision region of the NLC. The figure shows the inner radius of the vertex chamber surrounding the IP, the conical mask, the quadrupole holders indicated by two cylinders, the incoming electron beam path indicated by a line nearly parallel to the axis, and the outgoing, disrupted electron beam path indicated by a narrow cone emanating from the IP next to the incoming beam path. The small elliptical objects are the mirrors, the numbers indicating the path of the laser beam in time. One of the laser beam enters parallel to the axis from the right, incident on mirror 1 and deflected to mirror 2 (located at the edge of the quadrupole holder, at a symmetry point of mirror 9 on the left side), incident on mirror 3 and deflected to mirror 4. The laser beam until this point is wide. The beam is then focussed to a spot a small distance away from the top edge of mirror 6, thus avoiding it. The beam further propagates to fill mirror 5, reflected and focussed to the CP facing the incoming electron beam from the right. The laser beam further propagates and fills mirror 6, reflected and focussed now to a spot a small distance away from the bottom edge of mirror 5, thus avoiding it. The beam propagates further to mirrors 7, 8, 9, and 10, and exits to the left.

Mirror 5 has two holes, a small one for the incoming electron beam and a larger one to accomodate the 10 mr angular cone of the outgoing disrupted electron beam. The laser profile is designed so that the intensity profile incident on mirror 5 is uniform over the surface to minimize loss from the holes. An $f/10$ optics is used for focussing the laser beam to the CP, which is an optimum condition for the conversion efficiency. Mirror 6 is identical to mirror 5. This mirror arrangement is symmetric with respect to the IP.

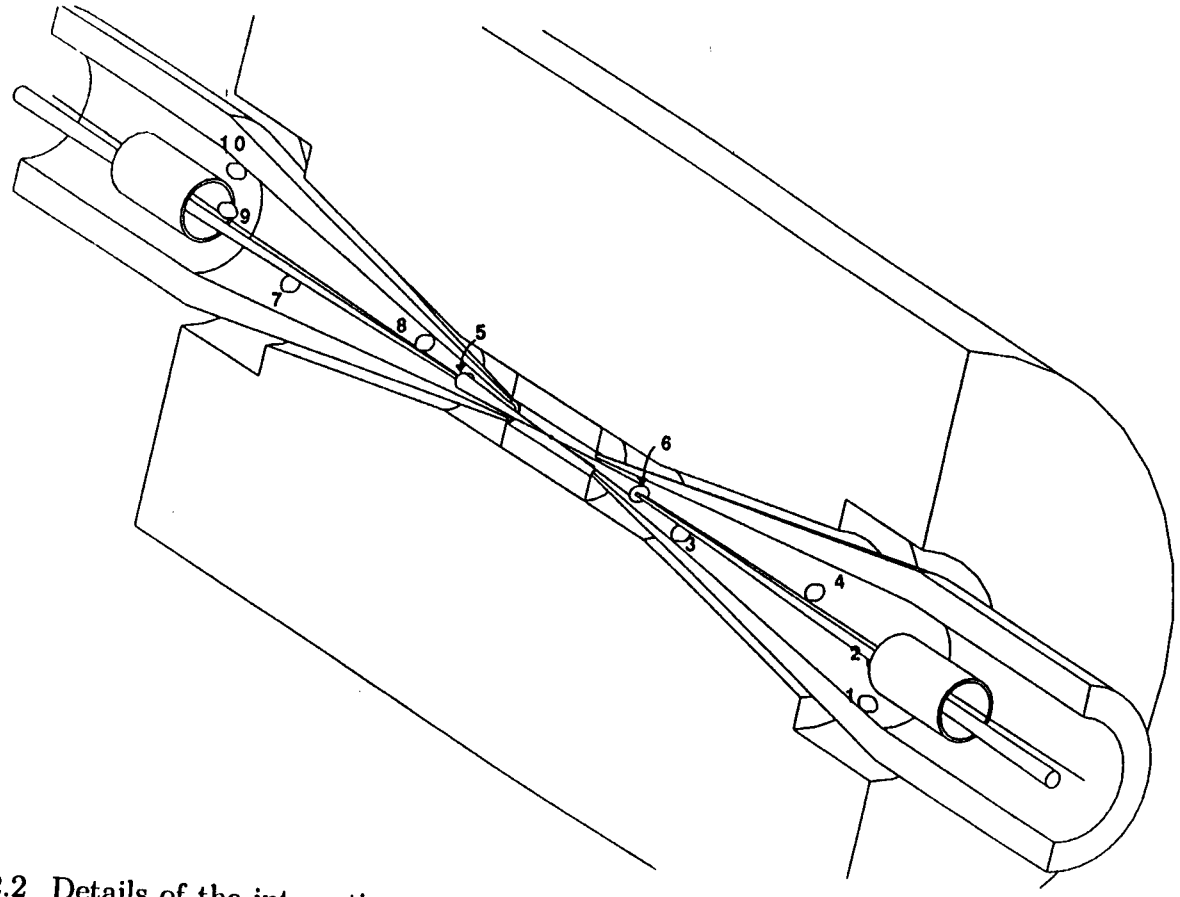

Fig.3.2.2 Details of the interaction region. The separation between the IP and CP is not apparent at the scale of this figure. The incoming laser pulse is bounced from mirror to mirror in numerical order. See Section 3.2.6 for details.

Another laser beam enters from the left following a path symmetric to the beam coming from the right, nearly overlapping the exiting beam. The exiting beam should be prevented from entering the laser amplifier.

It is assumed that the mirrors will be of dielectric material with suitable multilayer coatings developed for high power laser systems. The problems of the power loading and radiation damage need to be carefully studied in the future.

A laser path arrangement in which a laser pulse is reused several times will greatly reduce the optical power requirement. Several multipass schemes have been proposed, for example an arangement involving confocal cavity arrangement. Practical implementation of these ideas appears to be difficult in view of the tight geometry of the interaction region, and the necessity to preserve the picosecond time structure of the optical pulses.

The coil for the sweeping magnet, which is not shown in Fig.3.2.2, may still be accomodated. There are also schemes where the sweeping magnet is not employed.

3.2.7 IP Issues

The energy of individual electrons after multiple Compton backscatterings may be as low as 3% of their initial energy. Low energy electrons will be deflected up to an angle of about 10 mrad because of collisions with the opposing electron beam. The crossing angle should therefore be larger than 10 mrad plus an additional angle to clear the quadrupole face. For the NLC, the crossing angle for the $\gamma\gamma$ collision is taken to be 30 mrad. Crabbing the electron beam is therefore essential for a $\gamma\gamma$ collider. The effect of the solenoidal field on beam collisions with a large crossing angle also needs to be studied.

To obtain good monochromaticity of $\gamma\gamma$ collisions and clean $\gamma\gamma$ or γe^- events, it is desirable to sweep the spent electrons by an external magnetic field. The magnetic field should extend longitudinally to about 1-3 cm with a strength 0.5-2 T. The sweeping magnet could be either a superconducting or a pulsed magnet. It is important that the magnet present a minimum obstruction to the detector. A plasma lens to overfocus the spent electron beam has also been proposed. This scheme must inject gases to produce the plasma and also remove them from the interaction region. Another proposal is to arrange the electron beams to repel and miss each other entirely in " a heads-up " collision, in which the front ends of the electron beams before the CP are displaced by a few vertical beam sizes to stimulate beam-beam instabilities. For this scheme to work, the electron beam intensity needs to be much higher than that contemplated in most linear collider proposals. It may also be possible to mitigate the effect of the spent electron beam by introducing a small offset in the vertical direction, about one rms beam size, in the overlap of the two beams at the IP. Such an offset would have only a small effect on the $\gamma\gamma$ luminosity, while reducing the e^-e^- luminosity significantly because of the beam-beam disruption. However, the background due to $e^-\gamma$ luminosity is a serious problem of this scheme.

Developing codes which will simulate the entire complex of CP and IP physics, including multiple Compton scattering and other QED effects such as beamstrahlung, is an urgent task. Such a code has been developed at Novosibirsk and appears to work well. Another code, CAIN, is under development by the NLC group and by the JLC group. It is desirable that several codes be available so that simulation results can be cross-checked.

3.2.8 Laser Technology

As we have seen in Section 3.2.3, the optical beam for $\gamma\gamma$ or γe^- colliders consists of a sequence of TW micropulses, each a few ps long, with an average power of tens of kW. Unless multipass optics can be used in the interaction region, these are the requirements for the lasers.

Lasers with TW peak power and picosecond pulse length have been built using chirped pulse amplification and compression techniques. However, the maximum average power of these lasers is, at present, only about 10 W. On the other hand, solid state CW lasers pumped by diode arrays producing 500 W have also been built. It may be necessary to combine these two technologies, for example, by pumping a Nd-glass laser with diodes, which could in turn pump a broadband Ti:Saphire laser whose pulse can then be compressed. The main challenge would be the power handling capability, which may be solved by techniques such as a moving slab(or disk) geometry of the amplifier, phase conjugate mirrors (or adaptive optics), dielectric gratings, etc.

Free-electron lasers(FEL) are another option for photon colliders. Several schemes have been proposed based on different combinations of FEL oscillators, amplifiers, and optical switching techniques. A scheme based on the chirped pulse amplification and compression, similar to the technique used in solid state lasers but replacing the amplifier with an FEL driven by an induction linac, is another attractive option. In the particular case of CLIC, the availibility of a 3 GeV drive beam at high charge per bunch offers an interesting possibility of simple adaptation to a $\gamma\gamma$ or $\gamma e^{\pm}$ collider. The first bunch is used for polarized light amplification by an FEL in an appropriate wiggler. The amplified light is then converted into a polarized γ beam by Compton backscattering on the incoming electron beam close to the I.P.

3.2.9 Conclusions

With a relatively small incremental cost and relatively straightforward modification, the physics capability of a future e^+e^- collider can be enhanced significantly by providing $\gamma\gamma$ collisions with a monochromatized luminosity of about 10^{33} $cm^{-2}s^{-1}$ (and by a factor 3 more for γe^- collisions). A higher luminosity is feasible by re-optimizing the collider system designs. At present, lasers and the associated optics for terawatts of peak power and kilowatts of average power, suitable for $\gamma\gamma$ colliders, are being actively pursued for various other e^+e^- physics applications. Many relevant and challenging issues in $\gamma\gamma$ collider design may be investigated by a cost effective upgrade of the SLC. Therefore, with strong support from the HEP physics community, a $\gamma\gamma$ collider with the potential for fundamental physics not accessible to, and with highly desirable redundancy of the data from these e^+e^- collisions, appears to be both a tantalizing and realistic possibility.

4 EXPERIMENTS and TEST FACILITIES

This chapter gives a summary of the purpose and status of all the linear collider experiments and major test facilities currently under development all over the world. They are presented in the following order:

1. The Final Focus Test Beam (FFTB) at SLAC
2. The TESLA Test Facility (TTF) at DESY
3. The S-Band Test Facility (SBLC TF) at DESY
4. The Accelerator Test Facility (ATF) at KEK
5. The Next Linear Collider Test Facility (NLCTA) at SLAC
6. The VLEPP Test Facility (VTF) at BINP
7. The CLIC Test Facilities at CERN
8. The Relativistic Two Accelerator (RTA) Test Facility at LBNL

At the end of the chapter, Table 4.1 summarizes the work that has already been achieved and what remains to be learned at these various facilities.

4.1 The Final Focus Test Beam (FFTB) at SLAC

With the successful operation of the SLC starting in 1990, it became apparent that a TeV-scale linear collider was feasible. It also became apparent, however, that all concepts for such a collider required that beams of electrons and positrons be focused to dimensions at least one and perhaps two orders of magnitude smaller than in the SLC. A collaboration was formed to experimentally address this problem. The Final Focus Test Beam Collaboration, as it has come to be called, consists of scientists from the Budker Institute (BINP), DESY, Fermilab, KEK, LAL (Orsay), MPI (Munich), and SLAC. The collaboration designed a beam line to be installed at the end of the SLAC linac to demagnify the SLC beam by factors consistent with those needed for any TeV-scale collider. The Final Focus Test Beam (FFTB) was built from components designed and fabricated by the laboratories of the participating institutions and industries in the respective countries and brought to SLAC for installation and testing in the FFTB beam channel. Construction of the FFTB was completed in 1993, and commissioning and scientific investigation of its properties began shortly thereafter. A layout is shown in Fig. 4.1a.

Initial testing of the FFTB hardware and software took place during the Fall and Spring of 1993/1994. During the latter part of the Spring running, the SLC beam was delivered with a vertical invariant emittance of 2×10^{-6} rad-m, and was demagnified in the FFTB by a factor of $\approx$ 320 to a height of 70 nm. This result was close to the design goals of the experiment (50 nm). Experimentation with the FFTB continued in the Fall of 1994. Detailed studies of the geometric and chromatic properties of the lattice were made that revealed good agreement with the expected behavior.

Measurement of the small FFTB beam spot is a difficult challenge. Two monitors have been designed and built to do this job. One monitor built by KEK and Kawasaki Heavy

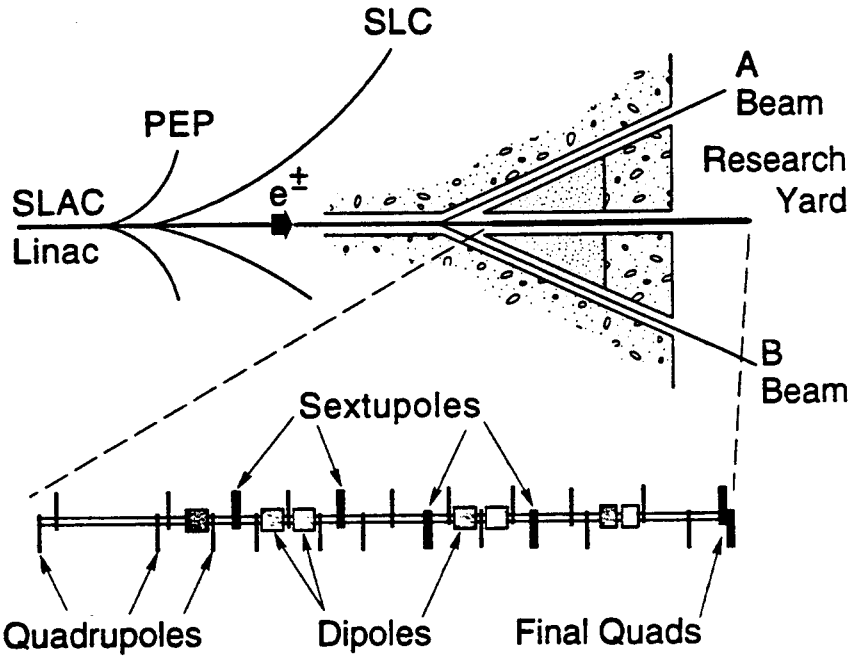

8-90 Fig. 4.1a Final Focus Test Beam layout. 6700A2

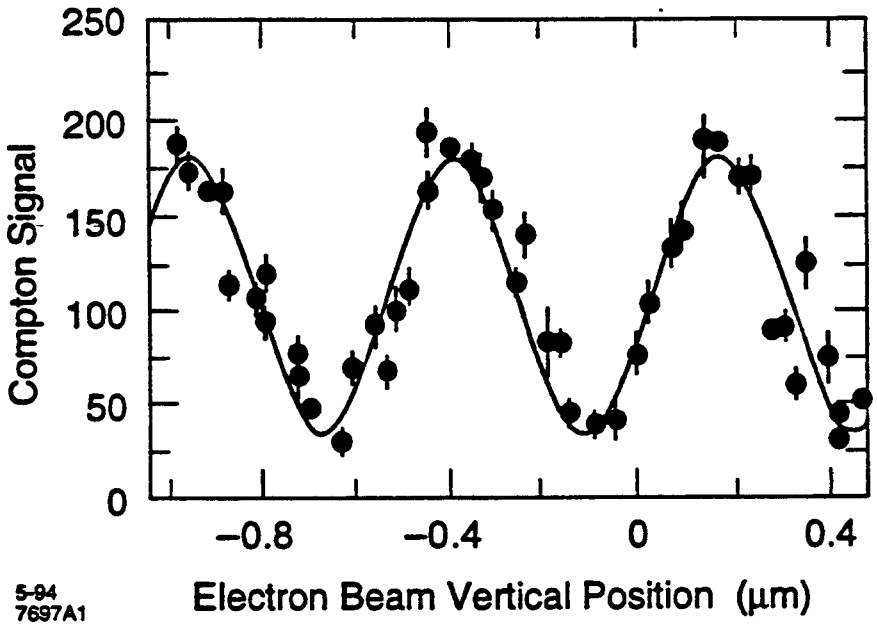

5-94
7697A1

Fig. 4.1b Measurement of vertical height of the beam at the FFTB focal point with the laser-Compton spot monitor. The observed fringe spacing agrees well with the 0.5 micron expected from the wavelength of the laser. The beam height is 73 nm in this case.

Industries uses a laser beam that is split into two parts. The resulting beams are brought back into coherent interference with each other at the beam line where an optical fringe pattern is created. The electron beam is scanned across this pattern. The resulting modulation of Compton-scattered photons is used to determine the beam size. An example of such a measurement is shown in Fig. 4.1b. A second monitor designed and built by the group at LAL (Orsay) uses the interaction of a gas azimuthally surrounds the focal point is used to detect the arrival of HE or Ar ions created in the interaction of the beam with the gas. Measurements of the flight times and azimuthal distributions of the ions are used to recreate the density and shape of the electron spot. Estimates of the beam size made by the two monitors agree well, and serve to provide confidence in the performance of the FFTB.

The FFTB Collaboration will continue to conduct experiments with the beam line over the next year or so. Further investigation of the optics of the lattice will be made, and a number of studies of the stability of the beam spot are planned. New rf beam position monitors are being constructed to allow measurement of the position of the beam centroid to a few nanometers. This system of monitors will allow studies to be made of the pulse-to-pulse motion of the beam spot, and should provide a good first look at the problems inherent to colliding nanometer-size beams.

4.2 The TESLA Test Facility (TTF) at DESY

The TESLA Test Facility (TTF) under construction at DESY (Fig. 4.2) by an international collaboration is an R&D test bed for the superconducting cavity approach to future TeV-scale linear colliders. The main body of the TTF linac will consist of four cryomodules, each containing eight 1 m long nine-cell cavities made from bulk niobium and operated at L-band frequency (1.3 GHz). The infrastructure to process and test these cavities was installed in 1993/1994. The facility includes a complex of clean rooms, an ultraclean water plant and a chemical etching installation for cavity surface preparation and cavity assembly, all under conditions of extreme cleanliness. To improve the cavity performance with respect to thermal conductivity, a firing procedure at 1400° C in an ultra-high vacuum furnace is also available. An existing cryogenic plant has been modified to cool down the cavities below 2° K and to measure them in vertical and horizontal test cryostats. The rf power for the linac will be provided by two 4.5 MW klystron-modulator systems (pulse length 2 ms). One system is also being used for a high power rf treatment to further improve cavity performance by eliminating potential sources of field emission. The whole infrastructure has been commissioned with two prototype cavities, both surpassing the TTF goal of 15 MV/m at $Q = 3\times10^9$. (The final Tesla 500 GeV c.m. machine goal is 25 MV/m at $Q = 5\times10^9$). Three additional prototype five-cell cavities have been tested at Cornell and have achieved greater than 25 MV/m at Q greater than 3×10^9.

For beam tests with the first cryomodule, a first injector will be installed in 1995 and will provide 8 mA beam current within a 800 μs long macro pulse. Bunch structure for this injector is at 216 MHz. An electrostatic gun is combined with a buncher cavity and a standard TESLA superconducting cavity preaccelerator.

A second injector based on a laser-driven rf gun combined with a bunch compressor is under development. This injector will need to operate with a bunch charge of 5×10^{10} electrons at 1 MHz bunch spacing and again a macropulse length of 800 μs.

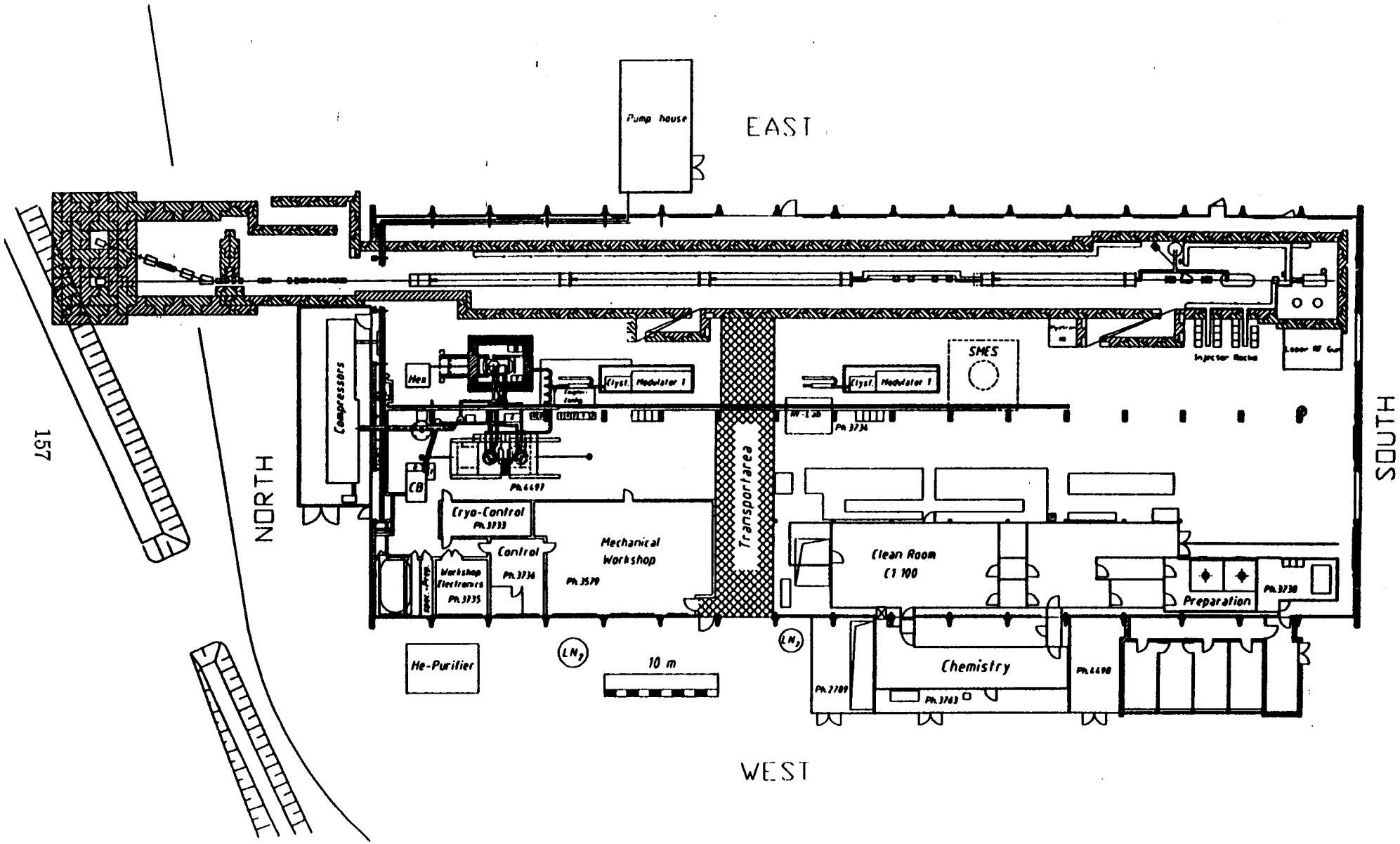

Fig. 4.2 TESLA Test Facility building.

Beam analysis areas are provided to study both injected and high energy output beams in excess of 500 MeV.

The main purpose of the test facility is to demonstrate the feasibility of superconducting technology. This includes that these test cavities can be reliably constructed to achieve gradients of 15 MV/m or greater, and that they can be successfully assembled and operated to provide the accelerated beam in the TTF linac. Experience gained in the construction will also provide information for cost estimates of the TESLA 500 GeV c.m. machine. Significant improvement over existing installations in performance/cost ratio must be demonstrated.

Specific technical issues to be addressed in the TTF beyond reliable high-gradient, high-Q operation are: low heat leak cryostats, alignment stability of the cavities and quadrupoles within the cryostat, pulsed rf operation and low level rf control, dark current, and with the second injector, HOM loss and wake field measurements. Additional studies are underway for efficient rf generation and cavity fabrication cost reduction methods.

The whole TESLA Test Facility with the high bunch charge injector and a total of four low heat leak, low cost cryostats should be operational early 1997. Tests with the first injector and the first cryomodule are planed to begin at the end of 1995.

4.3 The S-Band Linear Collider Test Facility (SBLC TF) at DESY

The S-Band Linear Collider Test Facility under construction at DESY will serve as a test bed for the necessary technical developments of a large scale 500 GeV c.m. S-band linear collider. The test facility consists of two modular units similar to those that would be installed in a linear collider tunnel (Fig. 4.3). Although S-band linear accelerator technology is well accepted and used around many laboratories, the demands placed on an S-band linear collider are not a simple extrapolation from any existing accelerator, not even the SLC at SLAC. Two main reasons lead to the decision to build and operate an S-band test accelerator at DESY.

The parameters being proposed for the linear collider technology, even if they are based on well proven and existing linacs, have been pushed to what we think are the limits which can be achieved within the next few years. Especially for the klystrons and modulators, the peak power is more than twice as high as that of the 5045 klystron being used at the SLC right now. Because the modulators and the klystrons must be fabricated in large numbers, reliable operation must be proven and the costs for production have to be estimated. A dedicated test accelerator will provide the possibility of proving the feasibility and to a certain extent the reliability of these components. In addition, an injector is being installed and commissioned which will produce the full charge bunch train with different bunch-to-bunch spacings (Fig.4.4). However, the small emittance, the bunch length and the single bunch energy spread required for the linear collider cannot be achieved. Open questions concerning the stability of a flat beam in a 15 km-long S-band linear accelerator have only been investigated by computer simulation so far. While with the SLC single bunch instabilities have been investigated experimentally in great detail, the multibunch operation required in the SBLC will lead to strong cumulative effects of the beam break-up type if the higher order modes (HOM's) are not controlled from the beginning in the design of the accelerator structure. For this purpose, HOM excitation, damping using HOM couplers and internal loads will be studied. The measurement of the HOM's through the HOM couplers will have

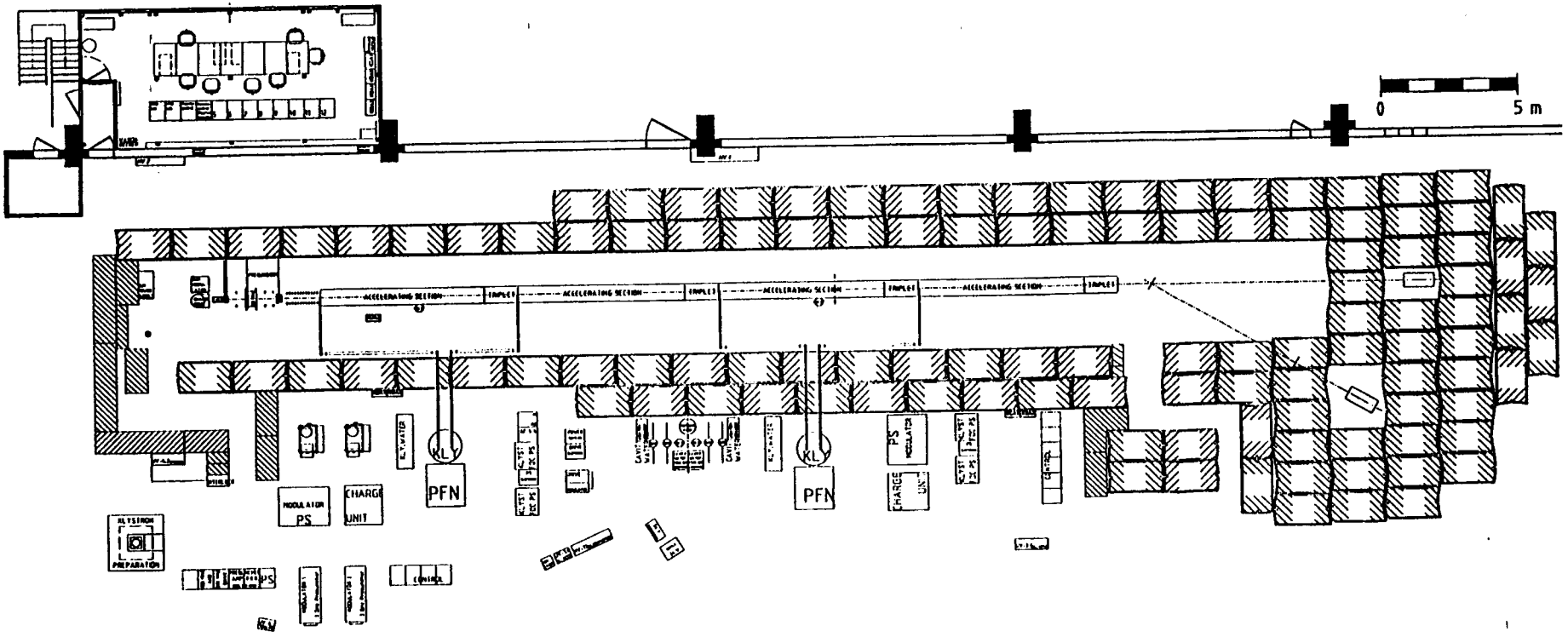

Fig. 4.3 General layout of the S-band test facility with two modules similar to that of the LC setup.

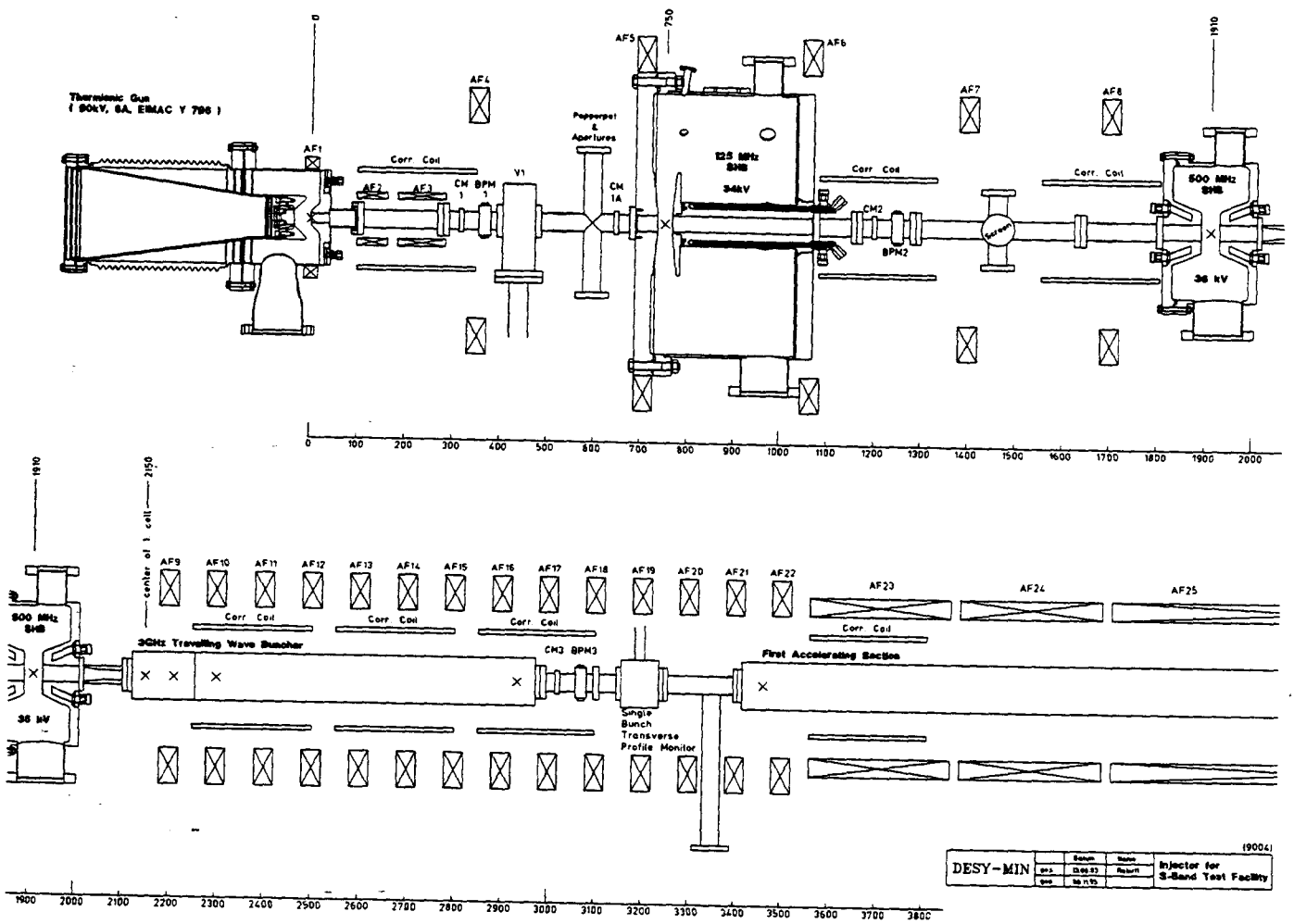

Fig. 4.4 Sketch of the injector set-up of the S-band test facility up to the injection into the first six-meter accelerator structure.

to provide the possibility of using a mechanical feedback with micromovers at two supporting positions of the accelerating structure near the front and the back end. Ground motion feedback loops, multibunch energy compensation schemes and bunch to bunch monitors will also be investigated.

While a large fraction of the injector is already being setup and tested, beam acceleration to the final energy of 450 MeV will not take place before 1997. The first klystron installed at the test facility has already been operated at 150 MW with a 3 μs pulse length and a repetition rate of 60 Hz. The first modulator is under construction while the second one is under preparation. Many components, such as the quadrupoles, beam position monitors and beam diagnostics, etc., are under construction.

4.4 The Accelerator Test Facility (ATF) at KEK

The Accelerator Test Facility (ATF) at KEK consists of three major parts: an S-band injector linac, a damping ring, and a bunch compressor (Fig. 4.5). Each part directly contributes to the development of technologies relevant to high luminosity linear colliders. The ATF will verify the feasibility of the multibunch scheme (putting many bunches in one rf pulse) in all parts from the injector to the bunch compressor. The multibunch scheme is essential to boost the rf-to-beam transfer power efficiency in the acceleration, and will be used in most designs of future linear colliders. The ATF will generate, accelerate, damp, and compress a train of 20 bunches with 2×10^{10} electrons/bunch and 2.8 ns spacing. The amount of total charge per train will be about half of the 500 GeV c.m. JLC design, but is enough to test its feasibility. The ATF has already produced some of the basic technologies for the multibunch scheme, such as a multibunch thermionic gun, a multibunch buncher, and a choke-mode S-band damped accelerating structure. The ATF will continue to help develop and test many techniques to handle the multibunch beam. One is the beam loading compensation system in the injector linac. A new idea using two rf side-bands will be applied to compensate the bunch-to-bunch energy deviation due to beam loading. A newly developed damped cavity will suppress the coupled-bunch instabilities in the damping ring. A new simultaneous injection-extraction system for the damping ring will solve the problem of transient beam loading due to multi-train operation in the damping ring. The beam loading in the bunch compressor will be compensated by a higher harmonic rf system (C-band).

The contribution of the ATF to provide a beam with an extremely small emittance is even more exciting. The goal is to achieve a normalized emittance of 5 μm horizontal and 0.03 μm vertical and a 100 μm bunch length for the multibunch beam. The small spot size at the interaction point requires small emittances and strong focusing. The damping ring is the necessary and sufficient tool to realize such a small emittance since there is no mechanism to damp the beam during acceleration in the linac. The small emittance from the damping ring will be achieved by special design of a strong focusing lattice with precise alignment of components and beam orbit control. The nonlinear behavior of the beam will have to be well understood to provide enough dynamic aperture under such strong focusing conditions. Since the beam intensity is very high because of the multibunch scheme, an unconventional design is necessary for the rf cavity and the vacuum chamber in order to reduce the impedance and maintain the small emittance. The ATF damping ring will operate at 25 Hz with 2 to 5 bunch trains, 10 to 60 bunches/train and 1 to 3×10^{10} particles/bunch. The bunch spacing will be

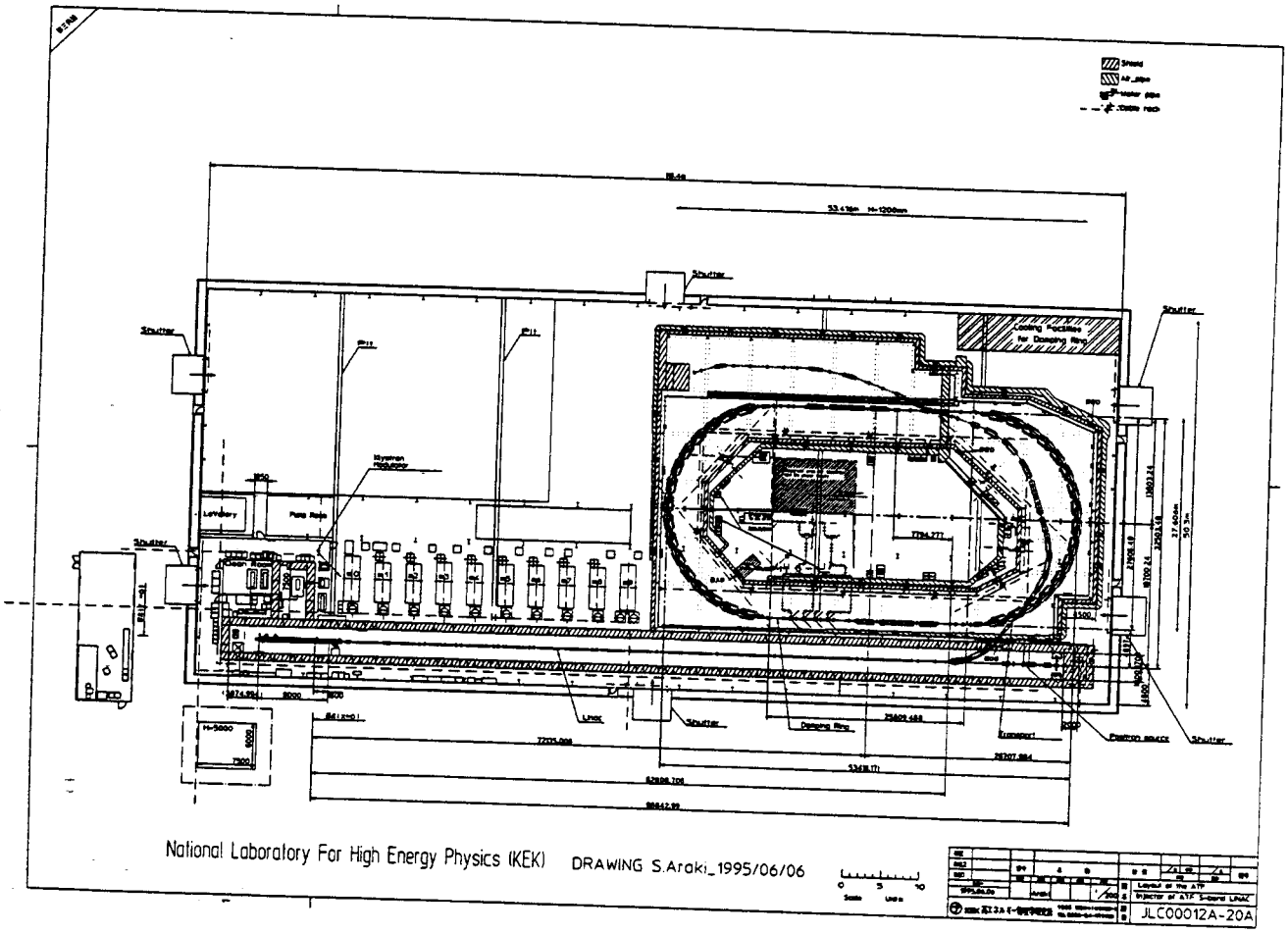

Fig. 4.5 The Accelerator Test Facility (ATF) at KEK.

2.8 ns and the train spacing 60 ns. New ideas for the multibunch small-emittance beam will also be tested in the injection/extraction system, as well as beam loading compensation and beam diagnostics. Strong focusing of the beam will inevitably require a short bunch to reduce the depth of focusing (small β-function). The short bunch will be produced by the bunch compressor. The bunch compressor will be particularly challenging since it will consist of a single stage device with a huge (1:50) compression ratio.

4.5 The Next Linear Collider Test Accelerator (NLCTA) at SLAC

The Next Linear Collider Test Accelerator (NLCTA) is a prototype high-gradient X-band linac that is being built at SLAC to integrate the new technologies of X-band rf systems and accelerator structures being developed for the NLC. The NLCTA will serve as a test bed as the design of the NLC evolves, and will provide a model upon which a reliable cost estimate for the rf system of an NLC can be based.

The NLCTA, which is 43 m long, is surrounded by concrete shielding and consists of an injector, chicane, linac and spectrometer (Fig. 4.6). The injector contains a thermionic gun, two X-band pre-bunchers, and two 0.9 m long X-band (capture and pre-accelerator) structures. It will generate a 126 ns long train of 74 MeV bunches with an average current equal to that of the NLC design. The bunch spacing will initially equal the rf wavelength, 88 ps, and will be increased to the NLC design value of 1.4 ns by upgrading the injector (the average current will remain the same).

Downstream of the injector, the beam will pass through a chicane where its transverse and longitudinal phase space will be truncated using collimators. The resulting beam will then traverse six 1.8 m long X-band accelerator structures. These structures and those in the injector will be built to suppress beam induced long-range transverse wakefields by either detuning the cell dipole mode frequencies, or by a combination of detuning and mode damping using manifolds that couple to all cells.

The six linac structures and two injector structures will initially be powered in pairs by 50 MW klystrons whose peak power will be quadrupled by SLED-II rf pulse compressors. This will result in a linac accelerator field gradient of 50 MeV/m which will be loaded to 37 MeV/m at the nominal beam current of 6.5×10^9 electrons per 1.4 ns. The klystron modulators are being designed to accommodate a future energy upgrade in which each of the 50 MW tubes will be replaced by two 75 MW tubes. The additional rf power will increase the beam energy by $\sqrt{3}$ to about 800 MeV at the end of the linac for operation with a $\sqrt{3}$ higher beam current to produce the same 25% fractional beam loading. This upgrade path parallels that planned for the NLC linac to increase its energy.

Following the linac, the bunch train will pass though the spectrometer region to a beam dump. A pulsed kicker magnet will separate the bunches vertically so that the variation in bunch-to-bunch energy can be measured from the beam profile after the spectrometer dipole magnet. For this and other measurements, devices to monitor beam size, length, position, phase and intensity will be located throughout the beam line.

An important goal of the NLCTA experimental program is to verify that rf pulse shaping can be used to offset the 25% transient beam loading in the linac accelerator structures to the desired 0.1% level. The pulse shaping will be achieved by feedback controlled amplitude and phase modulation of the klystron rf drive, and will be verified by the spectrometer energy

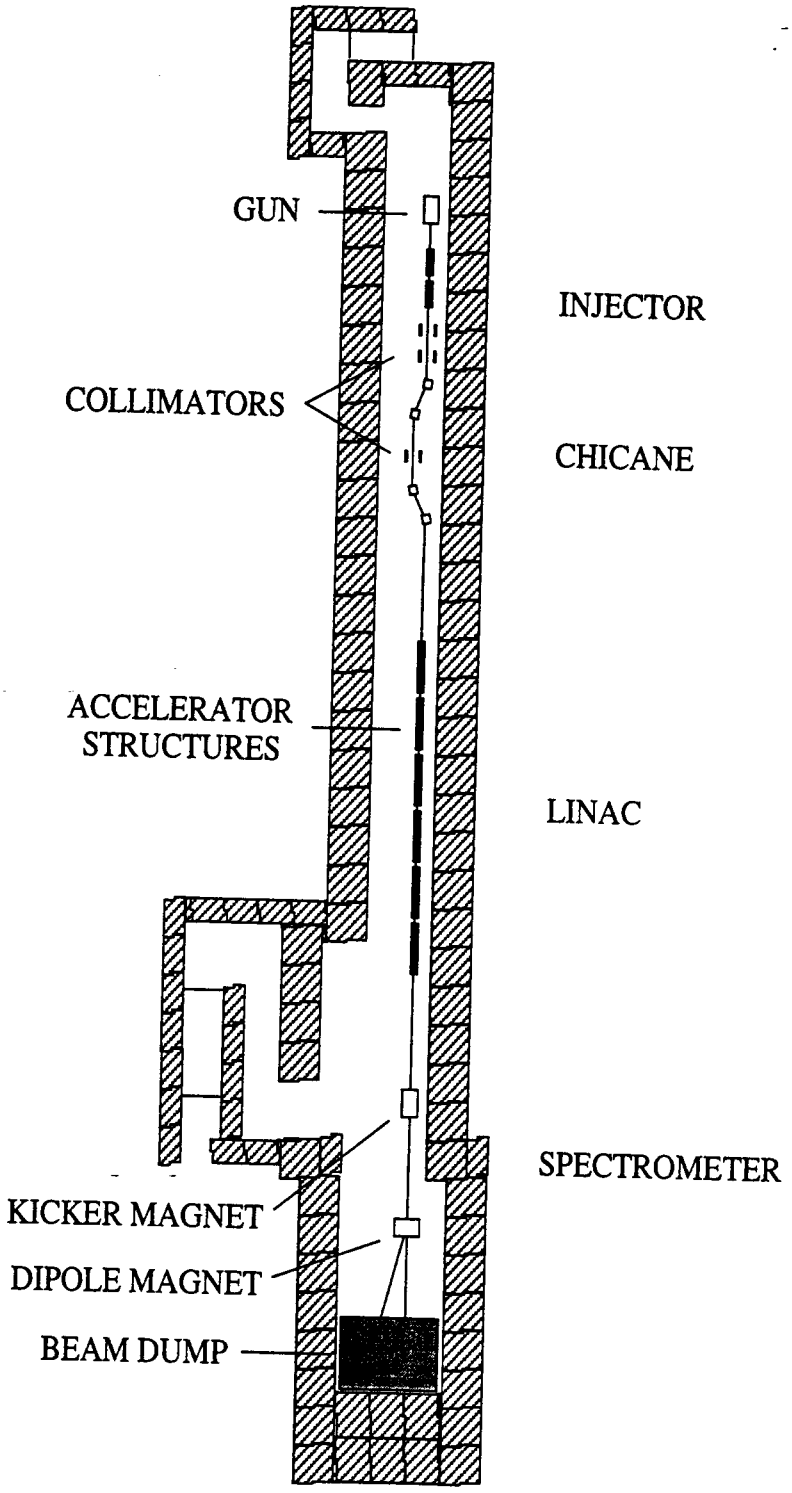

Fig. 4.6 Next Linear Collider Test Accelerator (NLCTA).

measurements. Other experiments will examine structure-emitted dark currents, transverse accelerating fields, and the effect of long-range transverse wakefields on betatron motion.

4.6 The VLEPP Test Facility (VTF) at BINP

The VLEPP Test Facility (VTF) is currently under construction in Protvino. The VTF site is a 25 m-long, 5 m-diameter tunnel contained within a 1 m thick concrete shielding wall. One of the main goals of the VTF is to test and operate an integrated VLEPP X-band linac module. This module consists of a DC high voltage system, an rf system and high-gradient accelerator structures. Also, to be tested at the VTF are the components of an adaptive feedback alignment system, thermal stabilization, electronics, etc. The VTF consists of a 200 kV injector, one DC high voltage source feeding four basic 5 m-long linac units, and a spectrometer. The first 5 m-long basic units (klystron, two pulse compressors, four accelerator sections and quads) together with the injector and the spectrometer are nearly complete and installed. During the next year, the main effort will be concentrated on studying the DC high voltage system and the klystron. The next step (1997-1998) will consist of high gradient and beam tests in the linac.

4.7 The Compact Linear Collider (CLIC) Test Facilities at CERN

4.7.1 CTF1

CERN has built and is currently operating a test facility for linear collider studies (the CLIC Test Facility or CTF) to (i) study the production of short, high charge electron bunches from laser illuminated photocathodes in rf guns, (ii) generate high power 30 GHz rf pulses by passing bunch trains through transfer cavities for testing CLIC prototype components and (iii) test beam position monitors.

The so-called CTF1 test-facility has been in a state of transition between 1994 and 1995. Fig. 4.7 shows a generic layout of the facility which includes some of the changes which took place during this period. A 3 GHz 1.5-cell rf gun equipped with a laser-driven photocathode and operating at 100 MV/m produces a bunched beam with a momentum of 4.5 MeV/c. A solenoid at the outlet of the gun provides some focusing of the beam before it is accelerated to 11 MeV/c in a 4-cell standing-wave gun-booster cavity. Final acceleration to 95 MeV/c is obtained using a 4.5 m long travelling wave section - a spare of the LEP Injector Linac (LIL) referred to as LAS. Energy is extracted from the beam by a 30 cm long travelling-wave section to provide short high power 30 GHz rf pulses. This power is in turn fed to a second identical CLIC structure to produce high accelerating gradients. The decelerated beam then either goes through a prototype 33 GHz CLIC BPM system to a dump, or is turned through 180° by bending magnets at the end of the line and re-accelerated by the second high-gradient CLIC section. The facility can be operated in either single bunch or multibunch mode at a repetition rate of 10 Hz. Multiple bunches are made by splitting the laser pulse into a train of pulses, spaced apart by 10 cm. The synchronized laser system has been optimized at the fourth harmonic (262 nm) providing a maximum energy of 0.5 mJ per

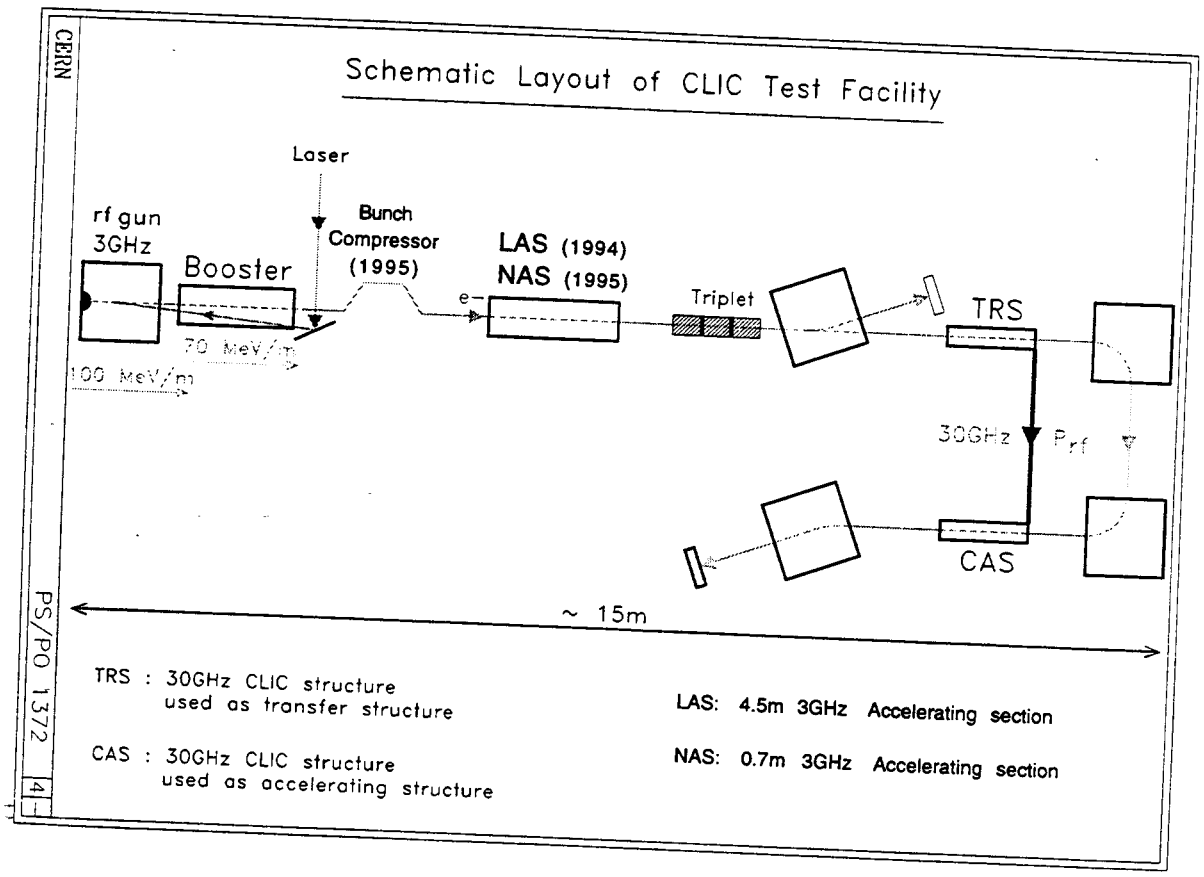

Fig. 4.7 CTF1 layout.

pulse (before splitting) and a pulse length of 8 ps FWHH. The Cs_2Te photocathodes are prepared in the laboratory and transported under vacuum and installed into the gun using a specially designed transfer system. Initial quantum efficiencies are typically 5 %, dropping to around 0.5 % after 250 beam hours. A maximum single bunch charge of 35 nC has been obtained from the gun-booster with a laser spot of about 10 mm diameter. The length of the electron bunches is measured with a streak camera using the photon beam produced by the interaction of the bunch with either a transition radiation monitor or a Cerenkov monitor. After the gun-booster cavity, the length is typically 14 ps (FWHH). Significant amounts of 30 GHz power can only be extracted from the CLIC section by using bunch trains. 76 MW has been generated by a 48 bunch train containing 160 nC at the exit of LAS and 81 nC at the exit of CAS (CLIC Accelerating Section). For this charge of 3.3 nC per bunch, the measured bunch length was $\sigma_z \approx 1$ mm. This power level corresponds to a decelerating field in the section of 124 MV/m (more than the CLIC nominal accelerating gradient). In 1994 the maximum charge which could be delivered to the power-generating structure was limited by wakefields and beam loading in LAS. By replacing this section by a much shorter (0.7 m) high gradient (60 MV/m) section (referred to as NAS), it is expected that this maximum charge limit will be more than doubled. The accelerating field in the second CLIC structure is determined from the difference between maximum and minimum energy gain of the beam as its phase with respect to the beam-induced rf accelerating field is varied. The highest re-accelerating gradient obtained to date is 104 MV/m. With the magnetic bunch compressor installed between the booster and the NAS section, a bunch of 15 ps (FWHH) at the gun exit was compressed down to 3 ps (FWHH). The measured charge was 10 nC. A new high charge 2.5-cell rf gun will be installed later on in the year.

4.7.2 CTF2

The existing CTF will be upgraded in stages during the period 1996–1998 to a two-beam test linac resembling as closely as possible the real CLIC design. The proposed layout is shown in Fig. 4.8. The drive beam train (44 bunches spaced at 10 cm) of 1 μC total charge will be generated by the new 2.5-cell rf gun driven by the existing laser and will be accelerated to 55 MeV by two new 1 m long HCS (High Charge Section) high gradient (60 MV/m) TW structures. These structures, designed to minimize both beam loading and transverse wakefield effects but also working at two slightly different frequencies will provide beam loading compensation to reduce the energy spread along the train. After passing through a magnetic bunch compressor, the bunch train is used to drive a string of CLIC transfer structures (CTS). Each CTS in turn drives two CLIC accelerating sections with 40 MW, 12 ns long, 30 GHz power pulses. The 1.3 nC probe beam simulating the CLIC main linac will be generated by the existing 1.5-cell CTF rf gun and laser and will be accelerated with the existing SAS section to 50 MeV before entering the string of 30 GHz high gradient (80 MV/m) accelerating sections. In order to minimize problems due to misalignments and at the same time to simulate the CLIC tunnel configuration as closely as possible, both 30 GHz linacs will be equipped with the CLIC support and active pre-alignment system which is now based on the stretched-wire technique.

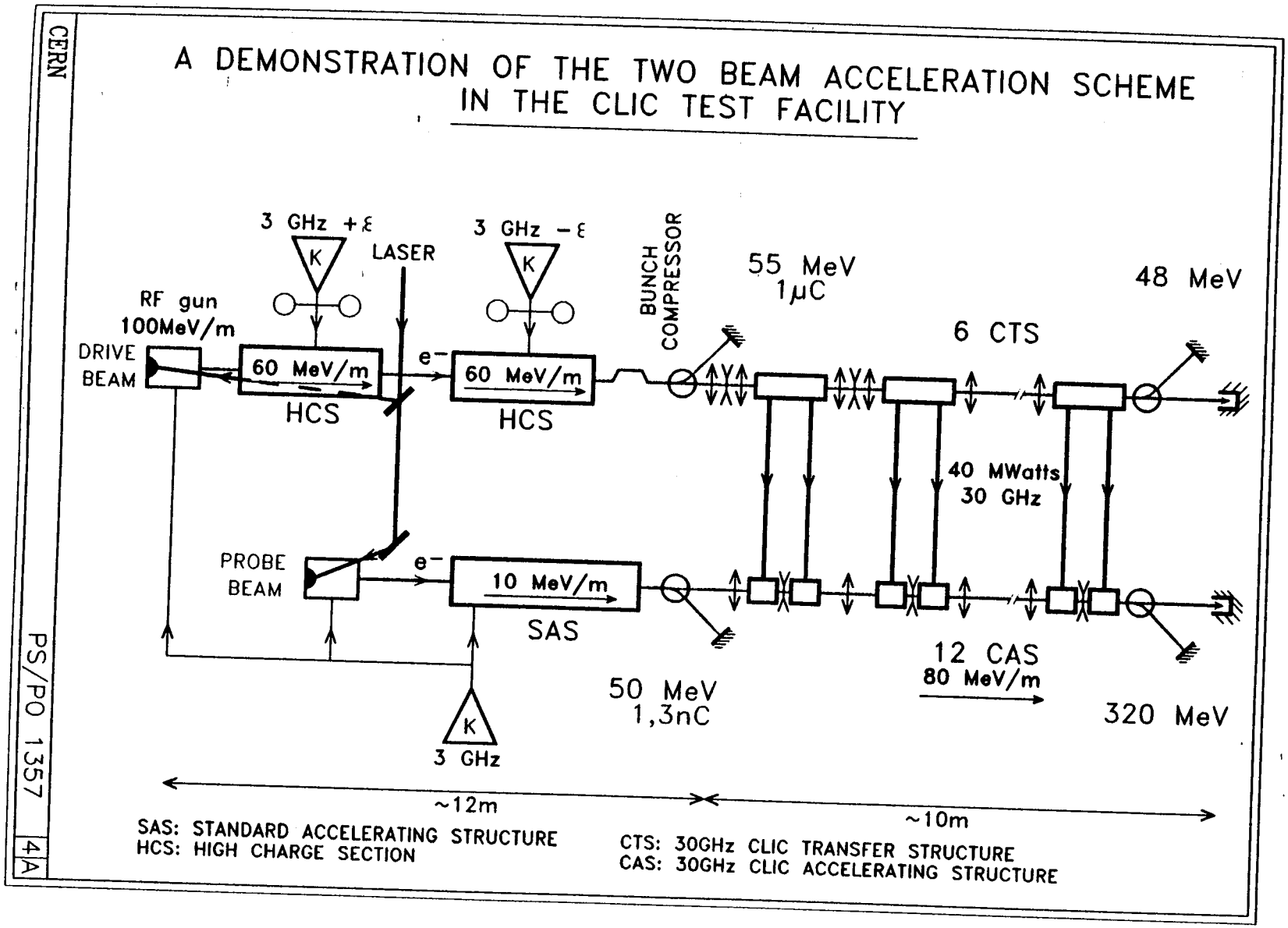

Fig. 4.8 CTF2 proposed layout.

4.7.3 CLIC Alignment Test Facility

An active alignment test facility has been built in an unused underground tunnel at CERN to study the feasibility of making controlled submicron displacements and to try out alignment systems. The structures to be aligned, dummy accelerating sections for the moment, are supported by V-blocks on 1.4 m long silicon carbide girders. The ends of two adjacent girders sit on a common platform which ensures continuity of position between units. The platforms are activated by three stepping-motor-driven precision jacks (two in the vertical plane for vertical displacement and axial rotation, and one in the horizontal plane). Movements of the set-up are monitored by linear and angular displacement transducers (0.1 micron and 10 microradian resolution respectively). A stretched wire running along the axis of the structures and passing through capacitive position transducers where the BPMs would normally be placed is used to simulate the beam. The set-up is controlled remotely from a small computer. After deliberate misalignments of 1mm, the system which is programmed for automatic alignment with respect to any of the transducers, settles back to nominal positions within <1 micron. The set-up is also being used to test a new optical pre-alignment system, developed by NIKHEF in Amsterdam, for use before injection of the beam. The image of a square-shaped red light source is focused on a light-detecting four-quadrant cell by a thin lens. Displacements of the source, lens or four-quadrant cell out of the optical axis of the instrument produce an imbalance at the detector. This system has been incorporated into the six hollow support girders of the test module and enables the relative positions of the far ends of two adjacent girders to be maintained in position with respect to the ideal straight line to <2 microns. This pre-alignment system is however unlikely to be used in CLIC because of potential radiation damage and will be replaced by a system based on stretched wires.

4.7.4 The CESTA and JINR Test Facilities

Collaborations have been set-up between CERN and the Centre d'Etudes Scientifiques et Techniques d'Aquitaine (CESTA) in Bordeaux (France) as well as with JINR at Dubna (Russia) to study an alternative scheme of drive beam generation by direct bunching at 30 GHz in an Induction Linac driven Free Electron Laser (FEL). In both laboratories, test facilities are being prepared using existing installations to the extent possible, to study and observe the quality of the bunching at a few MeV. In a later phase it is planned to use the bunched beam to generate rf power with a CLIC transfer structure.

In CESTA, the Induction Linac, LELIA, provides a 1 kA, 50 nsec electron beam at 2 MeV which is transported to a helical wiggler specially built for this purpose, where it interacts with a co-propagating 35 GHz wave delivered by a 120 kW magnetron. The beating of the electromagnetic wave and the wiggler magnetostatic field gives rise to an axial ponderomotive force and a consequent bunching of the injected pulse. The bunching, however, might be affected by longitudinal space charge forces at this particularly low energy.

In Dubna, a similar experiment is in preparation, taking advantage of the 9.5 MeV SILUND 21 Induction Linac made of seven modules of 1.5 MeV each. The detrimental effects of space charge in this case will be significantly reduced.

4.8 The Relativistic Two Accelerator (RTA) Test Facility at LBNL

Construction of the Relativistic Two Accelerator (RTA) Test Facility has begun at LBNL to study physics, engineering, and costing issues of using Relativistic Klystron Two Beam Accelerators (RK-TBA) as rf power sources for linear colliders. We use the term TBNLC to reference the proposed 1-TeV NLC upgrade using RK-TBA technology. All major components of the TBNLC rf power source will be tested at the RTA. These components include the induction gun, accelerator cells, chopper (beam modulator), pulsed power system, output structures, and the control system. However, due to fiscal constraints, the 25 m long RTA prototype will only have 8 rf output structures, with a possible upgrade to 12, instead of the 150 envisioned for the TBNLC. Also, the average beam energy in the main extraction section will be only 4 MeV instead of 10 MeV. The lower RTA beam energy requires us to place the output structures and the focusing elements at a closer spacing than in the TBNLC design. The RTA prototype output structures are located every meter and will generate 180 MW per structure. Tolerances on emittance growth and beam energy flatness are more severe in the RTA than the TBNLC. A layout of the RTA Test Facility is shown in Fig. 4.9. This facility could also be used to supply the rf power to the accelerating structures now being studied in the NLCTA Test Facility.

Important issues to be addressed by the RTA are efficiency, longitudinal beam dynamics, beam stability, emittance preservation, and rf amplitude and phase control. Efficiency can be separated into the conversion efficiency of wall plug power into beam power and beam power into rf power. A major component limiting high conversion efficiency of wall plug power into beam power is the loss in the induction cells. The induction cells will be tested with a pulsed power system appropriate for the TBNLC design. This will allow us to achieve a good estimate of the wall plug power to beam power efficiency for the TBNLC.

High conversion efficiency of beam power to rf power can only be obtained in an RK-TBA system with a large number of output structures. For the TBNLC, the number of output structures will be limited by beam stability and transport issues. The direct study of beam dynamics issues involving the beam transport through many tens of output structures will not be possible with the prototype. However, the reduced beam energy in the extraction section of the prototype will permit the observation of almost an entire synchrotron period. This will be sufficient to allow the beam to approach a steady state condition that can then be extrapolated to a full scale system with high confidence. The verification of computer simulations used to model the beam dynamics in the TBNLC will be a high priority. Beam dynamics issues related to transverse modulation, misalignment of magnetic focusing systems, and adiabatic compression, e.g. emittance growth and corkscrew motion, can be adequately studied.

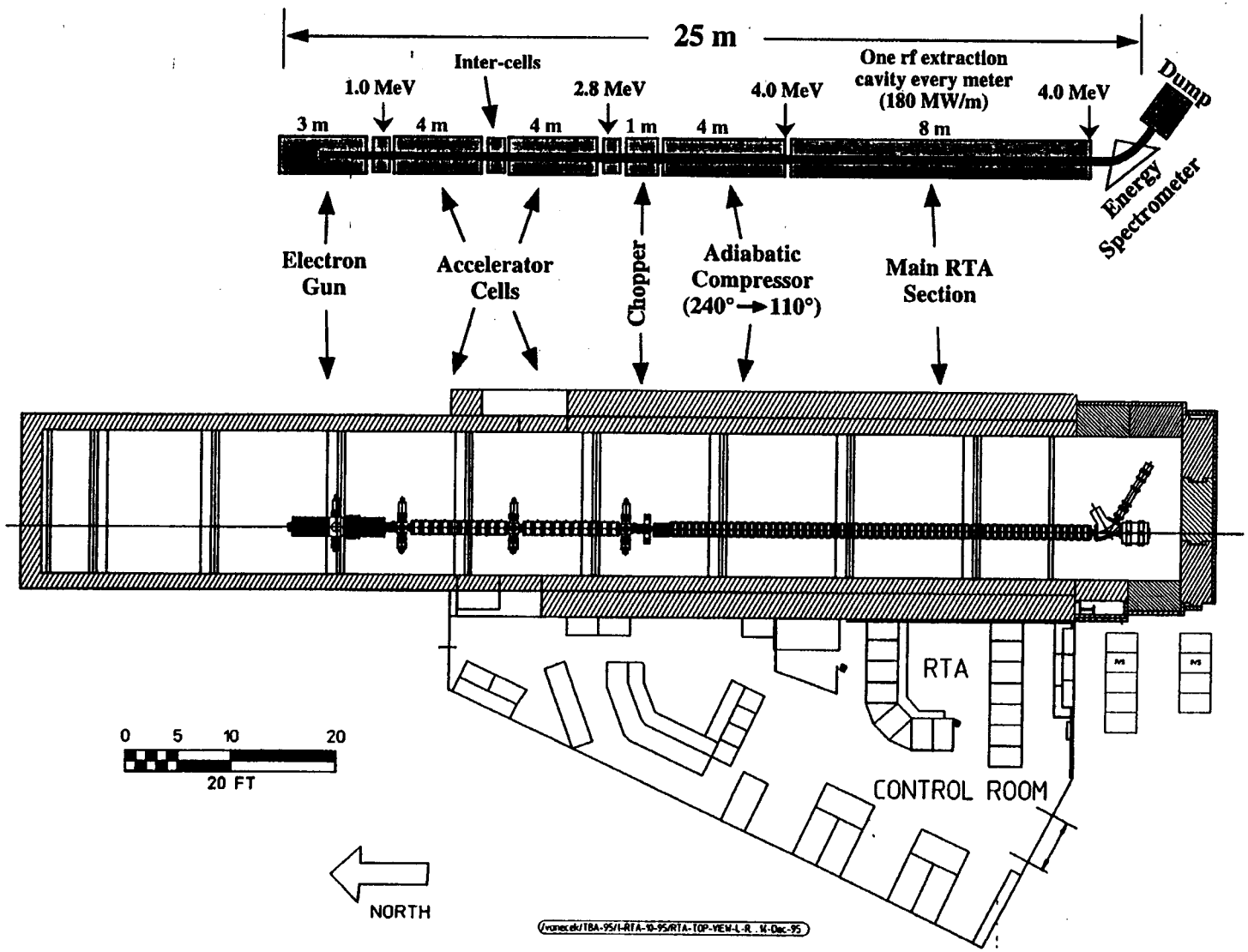

Fig. 4.9 Layout of the RTA Test Facility.

Table 4.1

PROGRESS FROM LC TEST FACILITIES (December 1995)

Facility	Constr. Start	Constr. Complete	Tested or to be Tested During Construction	Accomplished or to be Accomplished During Operation	Still to be Done	Other Things to do/ Limitations
SLAC						
FFTB	1989	1993	Alignment Stabilization (mechanical and thermal) Spot monitors BPM's	Injected beam with $\epsilon_y/\epsilon_x = 0.15/4.0(10^{-5}$m-rad) Spot demagnified by 320 to 70 nm (β_y^*=100μm) Chromatic properties verified Instrumentation and tuning Beam-based alignment developed E144 nonlinear QED observed	Finish systematic alignment and beam studies Nanometer RF-BPM's	
ASTA/ Test Lab	1992	on-going	50MW klystrons SLED II	1.8 m detuned structure tested to 67 MV/m SLED II tested to 205 MW output	50 MW PPM focused klystron SLED II tested to higher power	75 MW klystron to be developed
ASSET at SLC	1994	1997		1.8 m detuned structure wakefields verified	1.8 m damped/detuned structure wakefields to be measured	
NLCTA	1993	1997	Overall assembly of rf system	Not yet started	Injector commissioning Beam loading compensation Beam breakup tests Transverse rf field tests	Two-klystron modulator tests Injector upgrade Blumlein modulator Construction of instruments
KEK						
ATF 1.54GeV Linac & DR	1992	1996	Multibunch generation (20, 2 x 10^{10}, 2.8 ns spacing) 33 MV/m with S-band Dual-iris SLED-I S-band choke mode structure Bunch-to-bunch instrumentation Polarized electron gun	Linac loading compensation by δ-frequency Beam-based tuning in linac and DR Damping by wigglers Double kicker extraction Waveguide-damped rf cavity Multibunch beam dynamics (no. of bunches x no. of trains=10 x 5 to 60 x 2) One-stage compressor Positron source test	Final focus test Polarized rf gun Polarized positron source	X-band technologies 90-bunch trains 1.4 ns spacing Full energy positron production

Table 4.1 (continued)

PROGRESS FROM LC TEST FACILITIES (December 1995)

Facility	Constr. Start	Constr. Complete	Tested or to be Tested During Construction	Accomplished or to be Accomplished During Operation	Still to be Done	Other Things to do/ Limitations
BINP						
VLEPP 400 MeV	1992	1997	60 MW klystron 1 MV DC voltage system VPM (rf pulse comprsn.) 1 m structures 5 m submodule of VLEPP	High power test of structure High power test of VPM Alignment Super-precise BPM's Micromovers	120 MW gridded-gun klystrons with PPM focusing Feedback system	X-band technology Single bunch dynamics Cost estimates
CERN-CLIC						
CTF1	1989	1995	RF gun photocathode Laser system Short bunch measurement, 30 GHz accel. structures	Demonstration of two-beam principle Generation of 35 nC/b, 76 MW 30 GHz power No 30 GHZ breakdown up to E=125 MeV/m, $\langle E \rangle$ = 94 MeV/m in CLIC acc. section Testing 33 GHz BPM & 30 GHz transfer section Bunch compression ($10nC, \sigma_z$ = 2 psec)	Beam loading compensation Bunch compression with trains obtain 30 nC with σ_z=2ps	
CTF2	1996	1999	New 2.5 cell RF gun 3 GHz accelerating sections adapted to high charges	Not yet started	Beam loading compensation with trains Bunch compression 1 μC (48 bunches) 30 GHz reaccel. to 320 MeV Active alignment system Wakefield studies	
CESTA	1993	1997		Generation of bunched beam (1 cm spacing)		
DESY						
SBLC Test Facility 400MeV	1992	1996	Modulator I tested 150 MW klystrons I & II tested 6m sections with HOM ROBAX-ceramic support Injector design BPM's	Appropriate bunched beam generated with compression to 250 ps Quadrupole vibration feedback successful, with 12 dB attenuation between 1-20 Hz	Beam dynamics of single and multibunch (125) trains with 8, 16, 24 ns spacing (300mA)	Machine too short to study complete effects, filamentation, etc. Need RF pulse shaping to correct beam loading

Table 4.1 (continued)

PROGRESS FROM LC TEST FACILITIES (December 1995)

Facility	Constr. Start	Constr. Complete	Tested or to be Tested During Construction	Accomplished or to be Accomplished During Operation	Still to be Done	Other Things to do/ Limitations
DESY						
TESLA Test Facility 500MeV	1993	1997	Cavity gradient, Q_0 Processing steps Fabrication methods Lorentz force control Cryogenics, RF power Injector design	Not yet started	RF/Energy control Cryo heat leak, static, fundamental, HOM Alignment stability Vibration, microphonics High-charge injection Long transv. wakes, single bunch, multibunch Cavity misalignment Cryo procedures warm up/ cool down In-situ HPP Dark current, beam losses and radiation	Refine cost estimates of alternate designs for cavity fabrication High-efficiency klystron SMES Modulator TESLA design Overall cost estimates
LBNL						
RTA	1995	2002		Not yet started	Cost and efficiency issues in drive-beam generation Beam transport and BBU limits RF production and stability	Performance and efficiency of an extended system

5 PRESENT and FUTURE AREAS of COLLABORATION

5.1 Introduction

As the reader will have noted, international and interlaboratory collaboration in the field of e^+e^- linear collider R&D is rapidly becoming a way of life. It should be stated, however, that while collaborations are extremely desirable and useful because they bring together institutions with diverse specialties and resources, and people with complementary talents, forming these collaborations is not always straightforward and generally requires a great deal of effort. The funding agencies and laboratory administrators should be encouraged to lend their support to such endeavors, wherever they emerge, because in the long run they can only help the global cause.

The purpose of this chapter is to bring together in one place lists of many of the institutions currently collaborating with each other on linear collider R&D. These lists are undoubtedly incomplete but they give a glimpse of how interwoven the fabric of collaboration has become. Other opportunities for collaborations that may materialize in the future are also discussed.

5.2 List of Existing Collaborations

Institutions Collaborating with DESY on TESLA:

IHEP Academia Sinica - Beijing
Max Born Institute - Berlin
TH - Darmstadt
TU - Berlin
University of Frankfurt
TU - Dresden
FZ - Karlsruhe
GH - Wuppertal
SEFT - Helsinki
CEA - Saclay
LAL - Orsay
INP - Orsay
INFN - Frascati, Milan, Rome
University of Cracow
University of Warsaw
Polish Academy of Sciences
JINR - Dubna
IHEP - Protvino
INP - Novosibirsk
Cornell University - Ithaca
Fermilab - Batavia
UCLA - Los Angeles

Institutions Collaborating with DESY on SBLC:

TH - Darmstadt
KEK - Tsukuba
SLAC - Stanford
RWTH - Aachen
INR - Moscow
MEPhI - Moscow

Institutions Collaborating with KEK on JLC:

SLAC - Stanford
IHEP - Beijing
BINP - Novosibirsk/Protvino
Tohoku University (Laboratory of Nuclear Science) - Sendai
Tohoku Gakuin University (Faculty of Engineering) - Miyagi
University of Tokyo (Institute for Nuclear Study) - Tokyo
University of Tokyo (Nuclear Engineering Research Laboratory) - Ibaraki
Tokyo Metropolitan University (Faculty of Science) - Tokyo
Nagoya University (School of Science) - Nagoya
Kyoto University (Faculty of Science) - Kyoto

Institutions Collaborating with SLAC on FFTB:

BINP - Novosibirsk/Protvino
KEK - Tsukuba
LAL- Orsay
MPI - Munich
DESY - Hamburg
Fermilab - Batavia

Institutions Collaborating with SLAC on NLC:

LBNL - Berkeley
LLNL - Livermore
KEK - Tsukuba
Fermilab - Batavia
Stanford University Mechanical Engineering Department - Stanford

Institutions Collaborating with BINP on VLEPP:

JINR - Dubna
IHEP - Serpukhov
MEPhI - Moscow
MSU - Moscow
IM - Novosibirsk
KhPTI - Kharkov
SEFT - Helsinki
KEK - Tsukuba
SLAC - Stanford

Institutions Collaborating with CERN on CLIC:

CEBAF - Newport News
CESTA - Bordeaux
JINR - Dubna
European Network on Photocathodes and Photoinjectors
INP - Protvino
KEK - Tsukuba
LAL - Orsay
LBNL - Berkeley
MIT - Cambridge
SLAC - Stanford
University of Uppsala

There are, in addition, many people who as individuals collaborate with institutions away from their home bases.

5.3 Other Possible Future Areas of Collaboration

Listed below are other areas of possible future collaborations:

Design and experiments on electron and positron sources:

Almost all the machines will use complex high current sources capable of producing multibunch trains of polarized electrons and positrons, also polarized in certain cases. This research involves cathodes, lasers, special vacuum systems, targets, timing systems and instrumentation where mutual help is almost indispensable.

Damping rings and compressors:

This is an area where the ATF at KEK will serve the entire community. When commissioning begins, it is likely that scientists from all institutions will spend some time on that machine since the results will be important for everybody.

Linac technology:

While there is already intense collaboration on power sources, their focusing systems, pulse compressors, structures, breakdown studies, alignment, fabrication methods, this effort can only increase. For those machines where pulsed modulators are used, progress in one laboratory will be picked up everywhere else. The series of modulator workshops, of which the most recent one was held at SLAC in October 1995, is a good example of this type of cooperative work. The NLCTA, as it is completed, as well as the test facilities at DESY and CERN, will also be focal points for design integration and mutual help.

Beam dynamics:

So far, many of the discoveries regarding this topic have been experimentally tested at the SLC and the FFTB at SLAC. Also, as ideas have come from elsewhere as for example BNS damping, the SLC was used as the test bed. This will probably continue for some time, but as the other test facilities are commissioned, mutual collaboration of an experimental nature will grow at these new sites. Instrumentation such as BPMs, profile monitors, timing devices, fast kickers, laser wires, all kinds of support and alignment devices and many others

will be needed, and it will become essential to both share and divide the necessary and always insufficiently available manpower. As far as theory is concerned, most of the beam dynamicists already work together. An example where intense exchange of information is currently taking place is the whole subject of ground stability and vibrations.

Beam delivery:

What has just been mentioned for beam dynamics also counts for the beam delivery effort. Except for some differences in beam power and in the desired emittances, all the beam delivery systems are similar. Collimators, spoilers and long arrays of very stable bend and focusing magnets will have to be developed which will not differ too much from machine to machine.

Experimentation:

Section 2.6 of this report was written as an international collaboration. Since it is likely that only one or two detectors will eventually be needed, the collaboration will come together naturally as for detectors at other existing laboratories. This will be true for e^+e^- experiments as well as for $\gamma\gamma$ and all other variations. For $\gamma\gamma$ in particular, such a huge arsenal of specialized technology will have to be developed that it is inconceivable that any one laboratory could carry the burden by itself. Who will do what cannot be determined ahead of time but that coalitions will be formed is a certainty.

5.4 List of Past Linear Collider Workshops

Finally, for the record we list here the LC (machine) and LCWS (physics) workshops that have taken place in the past.

Accelerator Physics Linear Collider Workshops

Year	Workshop	Location
1988	LC88	SLAC
1990	LC90	KEK
1991	LC91	Protvino
1992	LC92	Garmisch
1993	LC93	SLAC
1995	LC95	KEK

Workshops Relevant to Particle Physics with Linear Colliders

Year	Workshop	Location
1987	SLAC Study Group	SLAC
	La Thuile CLIC Study	CLIC
1988	LCWS88	Snowmass, U.S.
1989	First JLC Workshop	KEK
1990	LCWS90	Snowmass, U.S.
	Second JLC Workshop	KEK
1991	EE500 Workshops	Saariselkä, Finland
1992	Colliding Beams Workshops	U.S.
1993	LCWS93	Waikoloa, Hawaii
1995	LCWS95	Morioka-Appi, Japan

In addition to these general workshops, there are other more specialized on-going series on rf sources, damping rings, final foci, gamma-gamma, polarization and others.

6 CONCLUSIONS

6.1 General Comments

Producing this first report of the International Linear Collider Technical Review Committee (TRC) has been a very challenging and interesting collective enterprise. Over fifty scientists from seventeen institutions participated in this international endeavor. Whenever appropriate, the names of the people making group contributions were shown near the headings of the various chapters and sections of the report. In contrast, the conclusions which appear in this last chapter were written by the TRC chairman alone, sanctioned however by the working group chairpersons before the final publication of the report.

As requested by the charge handed to our committee, we have attempted to describe, assess and compare various technical approaches towards a single goal, namely the design of a 500 GeV c.m. e^+e^- linear collider with a luminosity greater than $10^{33}cm^{-2}s^{-1}$, expandable to 1 TeV c.m. with a luminosity of $10^{34}cm^{-2}s^{-1}$. The process has no doubt been very educational for all the participants, and together with the LC workshops, it has brought an international community of scientists closer together, even if and when agreement on a particular issue could not always be reached without some lively argument or discussion.

Where do we find ourselves at this juncture in the development of e^+e^- linear colliders? A great deal of progress has been made in the last two or three years and the process of producing this report has further advanced and clarified many issues in our individual R&D efforts. It is sometimes claimed that if we all now joined forces, chose one of the five or six technical approaches being worked on, and collectively concentrated on it, we would make even faster progress towards the single goal of a Conceptual Design Report and the eventual realization of a large linear collider somewhere in the world. While this might be true, choosing one particular approach over all others at this point would involve considerable risk in case this single approach ran into difficulties or surprises, technical or financial. As it turns out, the diversity of projects and test facilities we have created somewhat spontaneously throughout the world community is a good hedge against mistakes and, through competition as well as collaboration, it is producing a broad body of knowledge that benefits all of the projects. Turning off any one of the approaches at this time would result in a collective loss. Hence, financial and technical support for all the projects should continue vigorously, at least until the various test facilities begin to bear fruit and reveal the answers for which they were conceived.

6.2 Machine Groups

If we look at all the various projects, we find that we can classify them into four groups, arranged in order of ascending main linac rf frequency:

1. TESLA
2. SBLC, JLC (S-band)
3. VLEPP, JLC(X-band), NLC (with its possible future TBNLC option)

JLC(C-band), only supported to a modest extent in Japan, could be a hedge against surprises in group (2) or (3).

Given below is a short summary of the overall characteristics of the four groups of machines and the challenges they face. One would hope that after further studies and mutual consultations, the designs of the machines in each group would coalesce.

Group 1 (1.3 GHz)

TESLA, alone in group (1), is characterized by the largest IP beam spots (commensurate with the spot measured at the FFTB, unless the repetition rate is reduced from 10 to 5 Hz and the loss in luminosity must be made up by smaller spots), most relaxed tolerances, lowest wakefields and widely spaced bunches, which can be resolved easily and between which steering can be changed. This significant advantage, however, will ultimately have to be weighed against the challenge of perfecting the necessary superconducting rf technology at an affordable cost. This technology, in all its details, must be developed to reach 25 MV/m reliably in the pulsed mode. For example, mechanical detuning due to the Lorentz force during each rf pulse must be compensated, field emission must be suppressed, and it must be shown that the alignment tolerances, though looser than for the other machines by a factor of about 5, can be attained inside the dewars. Once attained, a clear advantage of these relaxed tolerances is that short-term ground motion effects may be compensated by fast-orbit feedback and above 100 kHz will be negligible. On a longer time scale (days), the effect of drift remains to be studied and will depend on the site. The electron bunch train may be produced from a laser-driven rf gun (polarized if possible). From such a gun, the emittance may be low enough to obtain the beam spots required in the 10 Hz case without the electron damping ring. The positron bunch train is too intense to be produced by electrons impinging on a conventional target and needs to be generated by γ-conversion in a thin rotating target, a technique which is promising but has not yet been proven on an actual accelerator. The photons must be produced by passing the spent e^- beam after the IP through a wiggler or undulator. Regarding damping, the "dog bone" (or other) damping ring(s) must be designed so that it (they) can accept the long trains of bunches in a "compressed" mode. To upgrade the machine to 1 TeV c.m., the main linac gradient will have to be increased toward the fundamental Nb superconducting limit of about 50 MV/m in order to keep the length of the linacs from becoming excessive. To obtain the desired luminosity at the higher energy, the beam spots will have to be reduced but will remain a factor of three larger than those of the other machines while keeping the beamstrahlung smaller by a factor of three.

Group 2 ($\approx$3 GHz)

In group (2), SBLC and its close cousin JCL(S) benefit from the most widespread and proven technology developed at the SLC and elsewhere over many years. SBLC has the next-to-largest IP beam spots after TESLA, and relatively relaxed tolerances. On the other hand, the bunches are much more closely spaced and the accelerator structures must be designed to damp and/or detune multibunch wakefields. Residual beam-induced signals may be used to

align the structures to the beam. The main linacs for the 500 GeV c.m. case do not require other fundamental rf innovations, but with a 17.5 MV/m gradient, they will be ten times as long as the SLAC linac. Hence, efforts will have to be made to simplify the construction of klystrons, modulators, accelerator structures and other linac components to make them efficient and economical. The electron bunch train may be produced by a standard thermionic gun or a polarized laser-driven gun. The positron bunch train production is very similar to TESLA's in that it uses γ-conversion in a thin target, but the bunches are so close together that the rotating motion of the target will be negligible during the bunch train. The damping rings are not fundamentally different from those required for group (3). Compared to SBLC, JLC(S) uses smaller spots and higher gradients. For the SBLC 1 TeV c.m. option, the relative beam spot size advantage is preserved, but reaching $10^{34} cm^{-2} s^{-1}$ luminosity is very challenging. In order not to increase linac length, the number of klystrons must be doubled and SLED-I type rf pulse compressors capable of handling bunch trains with the desired bunch-to-bunch energy spread must be added. The resulting gradient then exceeds the so-called "dark current" capture gradient by a factor of 2, a problem which still needs to be examined carefully. No upgrade option to 1 TeV c.m. has been offered for JLC(S).

Group 3 ($\approx$11.4 GHz)

Group (3) lumps together JLC(X), NLC and VLEPP. Even though VLEPP is designed for 14 GHz, this frequency is not sufficiently different from JLC(X) and NLC (11.4 GHz) to put it in a separate group. For these three machines, the beam spot sizes at the IP are relatively smaller and tolerances are tighter than for S-band. However, the main linac gradients are higher and the machines are relatively shorter. At this time, JLC(X) and NLC differ from each other in their klystron peak powers, types of rf pulse compression systems, and in their numbers of modulators. They face challenges similar to the S-band machines with respect to reliable and economical mass production of components, and a way must be found to focus their klystrons with permanent magnets, or at least superconducting solenoids, to save power. The accelerator structures must be detuned and/or damped to suppress the multibunch wakefields which are more severe than at L- and S-band. VLEPP gets rid of this problem by using only one bunch per rf pulse. It has an even higher gradient and a shorter linac length, but in turn faces difficult single-bunch and background problems. The new rf technology proposed for VLEPP requires a considerable amount of R&D. The electron bunch trains for JLC(X) and NLC may be produced by thermionic or most probably laser-driven photocathode guns, and the positrons by conventional SLC-type sources, albeit of an upgraded mechanical design to take care of beam power dissipation. VLEPP may pass a 150 GeV electron beam through a helical undulator to produce polarized positrons. The damping rings for these machines have alignment tolerances a factor of 2 tighter than B-factories and must, in the case of JLC(X) and NLC, store four trains of bunches. Bunch compression is more severe than for Groups 1 and 2. To reach 1 TeV c.m., JLC(X) and VLEPP are simply doubled in length. NLC, in its conventional form, is lengthened by 20%, the number of klystrons per power unit is doubled, and the peak power per klystron goes from 50 to 72 MW. If by then, the TBNLC technology has been developed successfully and the physical layouts are compatible, the NLC could have its array of klystrons, modulators and rf pulse compressors replaced by 64 sequential induction linac driver units, each 300 meters long,

with transfer structures to supply the individual linac structures with the proper rf pulses.

Group 4 (30 GHz)

CLIC occupies a unique position in parameter space. The IP spots are similar to those in Group 3 with σ_y somewhat larger and σ_x somewhat smaller. The machine is characterized by the highest linac rf frequency, highest dark current capture field and potentially highest gradient. On the other hand, the machine requires many innovations, has the largest wakefields, and therefore the tightest fabrication and alignment tolerances. The greatest innovation is the method of generating the rf power with an intense drive beam, accelerated by LEP-type superconducting structures, which induces the power in special transfer structures. These structures play the role of the klystron output cavities in conventional machines. The problem of producing thousands of klystrons, modulators and rf pulse compressors is replaced by having to create two (or four in the 1 TeV c.m. case) high current drive beams with a bunch time structure capable of generating rectangular rf pulses at 30 GHz. The complexity of producing these drive beams and then conserving their phase space qualities along the full length of the linacs is a major challenge. An important advantage of the CLIC two-beam scheme is the absence of any active rf equipment along the length of the main accelerator, allowing all components to be housed in one tunnel. The front end of the main e^+e^- beam generation is analogous to the front end of the SLC. A number of design features of these drive and main beams remain to be elucidated, particularly for 10 bunch/pulse operation which has not yet been fully engineered but which is needed to increase the luminosity. Except for VLEPP, the length of CLIC is the shortest of all the machines. For 1 TeV c.m. energy, the linacs are simply doubled in length. Because of all these innovations which push the state-of-the-art into many new directions, it is clear that CLIC R&D will spawn a large number of technological developments which will also benefit other machines.

6.3 Common Problems and Issues

Placing the linear colliders into four separate groups emphasizes some of their fundamental differences. For more details, the reader must go back to Chapter 1 for the 500 GeV c.m. case and to Chapter 3 for the 1 TeV c.m. case and other upgrades. Chapter 2 which presented the comparative descriptions of all the sub-systems, gives summaries and conclusions for each working group. There is no reason to reproduce these here in detail but it is worthwhile to bring out some of the salient requirements which are shared by all these machines:

a) Much of the R&D on sources and injection systems is of common interest. All machines, to be competitive, will have to end up with polarized electrons. Laser-driven cathodes with the desired bunch time structure will require investments into both laser and cathode R&D. The development of rf guns capable of producing polarized electrons with low emittance, and possibly flat beams from the cathodes, would constitute a very important contribution to the entire field. Better coordinated and supported R&D would be highly desirable. The production of intense trains of positrons from photons hitting thin targets for TESLA, SBLC and VLEPP will also require a considerable development program. Finally, the design of low frequency (L- and S-band) pre-accelerators will call for new klystron as well as structure developments.

b) The requirements of pre-accelerators are closely coupled to those of the bunch compressors and damping rings. Multibunch beam loading compensation and emittance preservation permeate the design of all these sub-systems, exerting pressure on both the magnet and rf requirements. The damping rings, in addition to tight alignment tolerances, will require sophisticated kicker systems, stringent rf stability, very low impedance vacuum chambers, and broadband feedback systems similar to those designed currently for B-factories and synchrotron radiation light sources.

c) To control emittance dilution, the beam dynamics from the damping rings and compressors through the main linacs all impose tolerances, which in broad terms become tighter as a function of rf frequency, and affect the following elements:

- Quadrupole jitter and alignment
- Accelerator structure fabrication and alignment
- Beam position monitor alignment and resolution

Fortunately, remedies suggested at many institutions (BINP, SLAC, DESY, CERN, etc.) and in many cases tested on the SLC, allow one to considerably relax the quadrupole jitter tolerances and all pre-alignment tolerances (i.e., the tolerances to which these components must be aligned before the beams are turned on). Against jitter, these remedies include BNS damping or auto-phasing, and fast beam-based steering feedbacks. To relax the tolerances, the remedies consist of beam-based alignment techniques, which by iterative steps, reduce the emittance dilutions to acceptable levels. Similar techniques have been proposed for aligning the linac structures but these need further experimental verification. These techniques, which will be applied somewhat differently from machine to machine, will tend to bring the tolerances closer together. Finally, all the machines except TESLA (see remarks above) require further R&D to determine the power spectrum, correlations, and wavelengths of ground vibrations to decide what parts of the frequency spectrum may be corrected by feedback and which may have to be damped through appropriate local mechanical techniques. This R&D is proceeding at many sites around the world.

d) The so-called beam delivery sections between the ends of the main linacs and the IP currently differ somewhat from machine to machine but have many problems in common. They all consist of collimation sections, bending and matching sections, symmetrical final foci and post-IP beam lines with diagnostics and dumps. TESLA (wide-bunch spacing) and VLEPP (single bunch) do not have problems with parasitic crossing instabilities. TESLA uses head-on collisions while all the other machines have crossing angles, and in the case of SBLC and NLC some form of crab-crossing. TESLA and SBLC with larger spots may be somewhat easier to tune for collisions. TESLA with its wide-bunch spacing, and the higher repetition rate machines (JLC, NLC, VLEPP and especially CLIC) will benefit from higher sampling rates for stabilization through feedback. Materials for spoilers and absorbers require common research. At the present time, the lengths of the respective beam delivery sections differ by more than a factor of two. This is partly because they are in differing stages of design, and partly

because of differing concerns regarding the needs for orthogonal diagnostics and levels of collimation. It is likely that they will come more closely together when serious comparisons are made and one faces the decision to install tunnels from the beginning that can accommodate an ultimate upgrade to 1.5 TeV c.m. The bending angle must be such as to accommodate a layout with two IRs since it is generally recognized that such an option should be available, even if two beam lines and detectors are not necessarily installed from the beginning. The problem of ground vibrations in the final quadrupole doublets is being addressed for all machines by various stabilization and feedback methods.

e) Finally, the types of physics experimentation must be studied in great detail before any major detector design decisions can be made. A good start has been made in this report to examine and propose a physics program, and background calculations are underway, but this is only a beginning. Generic detector design is also just starting. One of the encouraging facts is that so far, the experimental physicists who have compared the various bunch structures coming from the various machines have not flagged any "show stoppers." TESLA with its very wide bunch spacing has an advantage here but the much closer bunch spacings from the other machines can also be handled. Presumably, since a choice of machine will probably not be made in the immediate future, there is still sufficient time to examine these basic questions before forging ahead with a specific detector design. Other options such as $\gamma\gamma$ and γe^- may be exploited in a second phase, with more time to develop the backscattering lasers and associated equipment such as beam pipes, mirrors, supports, and so on. Any machine that is built must be capable of also producing e^-e^- final foci with polarized electrons coming from both sides.

6.4 The Future

The broad summary of issues that has been presented here indicates that a large but fairly well defined program of work must be accomplished in the next few years. For maximum progress on the various machines, the continued use of the SLC and the FFTB, and the turn-on and thorough exploitation of the various test facilities (TTF, SBLC TF, ATF, NLCTA, VTF, CTF and RTA TF) is of crucial importance. The need for technical support and adequate funding for these facilities to allow them to produce the information for which they were built cannot be overemphasized.

Above and beyond these studies, there are some major issues that this TRC report did not have the time nor the staff to consider, but which will have to be addressed along the path to a machine selection. In this respect, the arduous turn-on and lengthy commissioning of the first and only linear collider, i.e., the SLC, has taught us a number of lessons which must not be forgotten. The next TRC report should include:

1. Procedures for turning on the machines, commissioning them and operating them
2. Maintainability, reliability and failure analysis
3. A complete chapter on instrumentation and control
4. A thorough discussion of machine protection, given the large beam powers involved

5. A chapter on radiation safety and other safety issues
6. A chapter on site considerations, including civil engineering, ground vibrations and energy expandibility
7. An analysis of cryogenic systems, where applicable
8. A chapter on utilities
9. Complete construction cost estimates
10. Operating cost estimates

As the reader can see, the next years will be extremely challenging.